Proceedings
6th International Conference on
SUSTAINABILITY IN PROCESS INDUSTRY (SPI-2022)

October 19-20, 2022

Organized By:

Department of Chemical Engineering, University of Engineering & Technology, Peshawar

&

Department of Chemical Engineering, Ghulam Ishaq Khan Institute, Swabi

Proceedings
6th International Conference on

SUSTAINABILITY IN PROCESS INDUSTRY (SPI-2022)

October 19-20, 2022

Organized By:

DEPARTMENT OF CHEMICAL ENGINEERING, UNIVERSITY OF ENGINEERING & TECHNOLOGY, PESHAWAR
AND
DEPARTMENT OF CHEMICAL ENGINEERING GHULAM ISHAQ KHAN INSTITUTE, SWABI

EDITORIAL BOARD

Prof. Dr. Muddasar Habib
Prof. Dr. Javaid Rabbani Khan
Dr. S. Naveed ul Hasan
Dr. Sajjad Hussain
Dr. Naseer Ahmed Khan

ORGANIZING COMMITTEE

Patron-in-Chief

Prof. Dr. Iftikhar Hussain
(Vice Chancellor, UET Peshawar)
Prof. Dr. Fazal Ahmad Khalid
(Rector, GIKI Swabi)

Conference Advisor

Prof. Dr. Sahar Noor
(Dean, Faculty of Mechanical, Chemical and Industrial Engineering, UET Peshawar)
Prof. Dr. Fahd Nawaz Khan
(Dean, Faculty of Materials and Chemical Engineering, GIKI Swabi)

Conference Chair

Prof. Dr. Javaid Rabbani Khan
(Chairman, Department of Chemical Engineering, GIKI)
Prof. Dr. Muddasar Habib
(Chairman, Department of Chemical Engineering, UET Peshawar)

Conference Co-Chair

Prof. Dr. Saeed Gul
(Department of Chemical Engineering, UET Peshawar)
Prof. Dr. Mohammad Younas
(Department of Chemical Engineering, UET Peshawar)

Conference Secretary
Dr. Syed Naveed ul Hasan
(Department of Chemical Engineering, UET Peshawar)

Conference Joint Secretaries
Dr. Sajjad Hussain
(Department of Chemical Engineering, GIKI Swabi)
Dr. Naseer Ahmed Khan
(Department of Chemical Engineering, UET Peshawar

Conference Organizing Committee
Dr. Syed Naveed ul Hasan
Dr. Naseer Ahmad Khan
Dr. Sajjad Hussain
Dr. Hammad Amjad Khan
Ms Ghazala Malik

Conference Steering Committee
Prof. Dr. Muddasar Habib
Dr. S. Naveed ul Hasan
Dr. Naseer Ahmed Khan
Dr. Hayat Khan
Dr. Sajjad Hussain
Fr. Hammad Amjad Khan
Dr. Manssor ul Hassan

Protocol and Registration Committee
Dr. Hayat Khan
Dr. Muhammad Usman Farooq
Dr. Irshad Ali
Dr. Asmat Ullah

Media and Publications Committee
Dr. Naseer Ahmed Khan
Dr. Nehar Ullah
Dr. Hayat Khan
Dr. Shozab Mehdi
Ms Ghazala Ali Khan

Food and Entertainment Committee

Dr. Nehar Ullah
Dr. Muazzam Paracha
Dr. Muhammad Usman Farooq

Conference Hall and Stage Committee

Dr. Naseer Ahmed Khan
Dr. Hayat Khan
Dr. Hammad Amjad Khan

Members

Prof. Dr. Iftikhar Hussain
Prof. Dr. Fazal Ahmad Khalid
Prof. Dr. Sahar Noor
Prof. Dr. Fahd Nawaz Khan
Prof. Dr. Abdul Shakoor
Prof. Dr. Misbah Ullah
Prof. Dr. Zia-ul-Haq
Prof. Dr. Farid Khan
Prof. Dr. Shahid Maqsood
Prof. Dr. Khan Shahzada
Dr. Shumaila Farooq
Ms. Ghazala Malik
Dr. Jamil Ahmad
Dr. Nehar Ullah
Dr. Imran Ahmad
Dr. Imran K Swati
Engr. Sultan Ali
Dr. Amad ullah Khan
Dr. Irshad Ali
Dr. Usman Farooq
Dr. Nasser Ahmed Khan
Dr. Muhammad Shozab Mehdi
Dr. Alam Zeb
Dr. Ali Kamran
Dr. Asmat Ullah
Dr. Muazzam Arshad Paracha

Dr. Mansoor ul Hassan
Dr. Saira Bano
Engr. Murtaza Khan

SCIENTIFIC EXPERT COMMITTEE

Prof. Dr. Javed Rabbani Khan	(GIKI, Swabi)
Prof. Dr. Rizwan A. Gul	(UET Peshawar)
Prof. Dr. Naveed Ramzan	(UET Lahore)
Prof. Dr. Siraj ul Islam	(UET Peshawar)
Prof. Dr. Khadija Qureshi	(MUET, Jamshoro)
Prof. Dr. Najma Memon	(Sind Uni, Jamshoro)
Prof. Dr. Sohail A Soomro	(MUET, Jamshoro)
Prof. Dr. Suleman Tahir	(University of Gujrat)
Prof. Dr. Afzal Khan	(UET Peshawar)
Prof. Dr. Abdul Shakoor	(UET Peshawar)
Prof. Dr. Shahid Maqsood	(UET Peshawar)
Prof. Dr. Tanveer Iqbal	(UET, Lahore, KSK)
Prof. Dr. Saima Yasin	(UET, Lahore, KSK)
Prof. Dr. Ishaq Ahmad	(UET Peshawar)
Dr. Atta Ullah	(PIEAS Islamabad)
Dr. Muhammad Najam Khan	(BUITEMS, Quetta)
Dr. Iftikhar Ahmad Salarzai	(NUST Islamabad)
Dr. Khan Muhammad	(UET Peshawar)
Dr. Muhammad Yasir Khan	(Karachi Uni, Karachi)

PREFACE

There has never been a time where the need for sustainability has been felt as profoundly as is evident from the global events of today. The global geo-political situation, emergence of new world players, decline in influence of current super powers, struggle for controlling the worlds resources, emergence of new economic blocks, utilization of resources to their optimum in today's changing world all dictate that our survival lies in a renewed strategy to use our limited resources especially in a sustainable way. Hence the new industrial, social, cultural, and environmental scenarios have to be analyzed and new strategies are to be devised so as to make our living sustainable. This need has been felt and thought after since last two decades and recognized in our Department which plays a vital role in indigenous and global research to contribute towards the sustainable development of Pakistan in the areas of vital importance such as process industries, use of natural resources, recycling, and reuse.

This international event of **"Sustainability in Process Industry (SPI-2022)**, (19-20th, Oct. 2022) hosted by the Department of Chemical Engineering, University of Engineering and Technology Peshawar in collaboration with the Department of Chemical Engineering GIKI Swabi, has been a regular bi-annual event attracting the cutting edge research from the renowned researchers of both national and international repute since its first inception in 2012. The conference has been an on-campus participating event, while in 2020 due to COVID-19, the conference was held online for the first time, and this year we are collaborating with the GIKI Swabi to expand our collaboration with the local universities.

The 1st conference on **"Sustainability in Process Industry (SPI-2012)**, was held at UET, Peshawar on March 28, 2012, 2nd on **"Sustainability in Process Industry (SPI-2014)**", on May 22, 2014, 3rd conference in this series, **"Sustainability in Process Industry (SPI 2016)"** was held on October 19-20, 2016 and 4th conference on **"Sustainability in Process Industry (SPI 2018)"** was organized on October 24-25, 2018

with the support of Higher Education Commission (HEC), Frontier Works Organization (FWO), and in collaboration with PASTIC. The 5th conference on **"Sustainability in Process Industry (SPI 2020)",** was held online on our Departments Silver Jubilee (1995-2020), utilizing indigenous resources. This year the 6th conference on **"Sustainability in Process Industry (SPI 2022)",** is going to be arranged in GIKI Swabi with collaboration of the Department of Chemical Engineering, GIKI.

Prof. Dr. Muddasar Habib
Conference Chair (UET)

Prof. Dr. Javaid Rabbani Khan
Conference Chair (GIKI)

ACKNOWLEDGEMENT

It is our great pleasure to welcome you to the SPI-2022 6th international conference of the series, “Sustainability in Process Industry (SPI-2022)”. Putting together SPI-2022 was a team effort. We greatly appreciate all the authors/researchers for providing the content of the program in the form of oral presentations and the other participants. We are also grateful to the keynote speakers from academia and various industries. These valuable talks can and will guide us to a better understanding of “Sustainability in Process Industry”.

We also thank the host organization, UET, Peshawar, GIKI Swabi and our generous sponsors PASTIC, FES and LOT without their support it would have not been possible to hold this conference.

We are grateful to all organizers, who worked hard in order to make the conference successful.

SPONSORS

PASTIC

Established in 1957 as Pakistan National Scientific & Technical Documentation Centre, (PANSDOC) by UNESCO under PCSIR, later on project was formulated and it was converted to Pakistan Scientific & Technological Information Centre (PASTIC) and transferred under the administrative control of Pakistan Science Foundation in 1973.

PASTIC is committed to serve Scientific and Technological Information needs of R&D and Industrial Community through Anticipatory and Responsive Information Services. PASTIC collects information from within the country as well as from abroad, processes and organizes the same and disseminate to its users. PASTIC is the premier organization for dissemination of Scientific and Technological Information to the citizens of Pakistan through a network of its Centers located at Islamabad, Karachi, Lahore, Peshawar, Quetta, Faisalabad and Muzaffarabad. PASTIC clients include Scientists, Researchers, Engineers, Entrepreneurs and Industry people.

PASTIC Databases (Online Products) & Services

- **Pakistan Science Abstracts (PSA):** National research published in Pakistani Journals, Conference Proceedings etc in all scientific disciplines (basic & applied Sciences excluding social sciences).
- **Union Catalogue:** Research materials (books/journals/conference proceedings/reports, etc) available in different S&T libraries of Pakistan.
- **Scientific Periodicals of Pakistan:** A handy guide of scientific periodicals published in Pakistan
- **Technology Round Up:** A bimonthly ebulletin provides latest national & international innovative S&T news/products and Industrial technology related forthcoming events.

- **R&D & Industry Information:** Universities/institutes of Pakistan; industrial challenges/problems & solutions; Pakistani commercial products/indigenous innovations; Chambers of Commerce in Pakistan; HEC established ORIC offices in universities; industries of Pakistan: Liaison between national and international industries; overseas investors of industry and commerce in Pakistan; Industrial Associations in Pakistan; Pakistan Industrial Academia Linkages.
- **Pakistan Journal of Computer & Information Systems (PJCIS): A** biannual Open Access primary Journal meant for researchers from Computer Science & Engineering, Information & Communication Technologies (ICTs), Information Systems, Library and Information Science.
- **Bibliographic/Document Supply:** Literature Search on specific topics from national/international databases (on **request**) within no time **through** PASTIC Website**.**
- **National Science Reference Library**: National Science Reference Library located at PASTIC National Centre having a collection of more than 8000 books; 900 titles of journals (300 journals regular among them) and approximately 5000 miscellaneous documents including reference material/secondary sources, conferences/seminars proceedings in S&T and R&D organizations, etc. Its main services include Reference & Referral Services; Reader Service; Internet Service, Journal Listings; Photocopying & Scanning Services
- **Reprographic Services PASTIC:** Reprographic Section has facilities for composing, designing, plate making, offset printing, binding etc. for Printing of books, Pamphlets, Brochures, Journals, Newsletters, Cards, Folders etc. These facilities are not only used for printing of PASTIC publications but are also extended to all other S&T and R&D Organizations.
- **Human Resource Development (Capacity Building)** through Seminars/Workshops /Trainings/ Exhibitions for knowledge based technological & industrial development in Pakistan for:
    - Young Researchers on Data Analysis and bibliographic citation Tools (SPSS, EndNote, Mendeley)
    - Women Entrepreneurs on e marketing and e business skills
    - Library Professionals on Library Information Management Tools & techniques (Koha, D-space etc)

- Researchers/engineers/industrialists on Patents/intellectual property (IP) rights and University Industry Partnership (UIP) for promotion of national R&D/Innovations

PASTIC is striving hard to become a leading national organization of Scientific and Technological information resources for promoting & supporting Research & Development for sustainable socio-economic development.

FES Higher Education Consultants is a leading consultancy firm providing quality education services all over Pakistan to students wishing to study abroad. FES Study Abroad Consultants was established in 2003 to provide reliable and value-added education consultancy services to students who wish to pursue further education in foreign universities with the help of our foreign study specialists.

Incorporated in 2011, LOT is a leading developing Supplier of a range of Products and Services specifically designed for the Upstream Oil and Gas Industry. Our Team of Oilfield Professionals endows us with the knowledge and ability to provide our clients with the customized Technical Solutions, along with the added benefit of strong Industry Networking all across the Middle East and North Africa Regions.

TABLE OF CONTENTS

Invited Speakers

Professor Dr. Najma Memon	(National Centre of Excellence in Analytical Chemistry, University of Sindh)
Plenary Talk on	Black Phosphorus and its Nano-composite materials for high performance supercapacitor
Professor Dr. Abdul Shakoor	(Department of Mechanical Engineering, University of Engineering and Technology Peshawar)
Plenary Talk on	Developments in bio-composites (opportunities and challenges)
Professor Dr. Tanveer Iqbal	(Department of Chemical Engineering, University of Engineering and Technology Lahore)
Invited Speaker:	Nano Mechanical Characterization of Polymeric Materials

Dr. Khurram Shahzad Baig	(Department of Chemical Engineering, Wah Engineering College)
Invited Speaker:	Sustainable Technologies
Dr. Tauseef Salma (Online)	United States of America
Invited Speaker:	Future challenges, opportunities and mitigation pathways to achieve sustainability
Dr. Erum Pervaiz	(Department of Chemical Engineering, NUST Islamabad)
Invited Speaker:	Sustainable processes
Dr. Atta Ullah	(Department of Chemical Engineering, PIEAS Islamabad)
Invited Speaker:	Modelling and simulations

Dr. Iftikhar Ahmad	(Department of Chemical Engineering, NUST Islamabad)
Invited Speaker:	CFD simulations applications and Exergy
Dr. Guichao Wang (Online)	People's Republic of China
Invited Speaker:	Modelling and simulation of floatation cell
Dr. Imran Ahmad (Online)	Energy Materials & Storage Devices Research Centre, Middle East Technical University, Ankara 06800, Türkiye.
Invited Speaker:	Vanadium based materials for electrochemical energy storage in multivalent ion batteries
Dr. Salman Naqvi	(Department of Chemical Engineering, NUST Islamabad)
Invited Speaker:	Carbon dioxide capturing

Dr. Muhammad Yasir Khan	(Department of Chemical Engineering, Karachi University)
Invited Speaker:	Current Advancements in Nanomaterials for Underground Drinking Water and Industrial Wastewater Treatment
Dr. Masroor Abro	(Department of Chemical Engineering, Mehran University of Engineering and Technology Jamshoro)
Invited Speaker:	Investigation of hydrodynamic parameters and bubble characteristics in CO2 absorption column
Dr. Sajjad Ullah	(Department of Chemistry, University of Peshawar)
Invited Speaker:	Broad Spectrum photocatalysts for environmental remediation under UV visible NIR illumination

USE OF ORGANIC AND INORGANIC PHASE CHANGE MATERIALS FOR PERSONALIZED COOLING SYSTEMS

Muhammad Amir Hamza [1, *], Rizwan Mahmood Gul [2], Muhammad Ali Kamran [3]
[123]Mechanical Engineering Department, University of Engineering and Technology Peshawar, Peshawar 25000, Pakistan
*Corresponding author **Email**: amir.hamza@uetpeshawar.edu.pk

Abstract—Human body need comfort in every situation whether to work inside or out. Heat has a huge impact on human health. In Pakistan, during hot weather, the ambient air temperature rises due to which body of human feels tired and exhausted. People working outdoors in this severe environment like policemen, students, laborers which suffers badly from this heat related issues. This problem needs serious attention and a solution to overcome this issue because environment like in summer's scorching heat issues are very often to be seen in normal day life. There are many advanced options for interior thermal comfort and they all perform well. However, there has not been much progress in terms of outdoor thermal comfort. Phase Change materials (PCM) can solve this problem because it can change its phase from solid to liquid and liquid to solid with in restricted temperature range. The wide use of PCM against heat stress for personal protection device is cooling hat and vest. PCM has the ability to store and release energy when outside temperature falls in it range. PCMs are also employed in many other industries like food, medicine, textile and also in solar energy cell. The cooling device which has PCM as a coolant is much cost effective, environment friendly and easy to use and can provide cooling for 2-3 hours with a less recharge time. If the PCM has high Latent heat and can absorb more heat than it can be used for prolong period. In this study different PCMs are explored and finally two PCMs are selected Polyethylene Glycol (PEG 600) and Glauber salt for cooling vest and cap. Their melting points comes in the range of human thermal comfort zone. Latent heat of fusion of PEG 600 and Glauber salt is 148 and 240 KJ / Kg respectively.

***Keywords*:** Phase change materials, Glauber salt, Polyethylene Glycol 600, Latent heat of fusion.

1 INTRODUCTION

Thermal comfort is the ability of an environment to maintain thermal equilibrium, or homeostasis, with the human body. This means that your surroundings should be neither too hot nor too cold for you to feel comfortable. The energy of latent heat can be stored in a medium and used whenever it is needed. Sensible heat storage (SHS) and latent heat storage (LHS) are the two methods for storing heat energy (LHS). The rise or fall in temperature of the storage substance is its sensible heat energy. Specific thermal properties of the material are directly linked to its heat capacity. Sensible Heat Storage (SHS) is rarely used since energy storage requires a large volume due to low energy density. [1] However, LHS stores energy by utilizing the phase change enthalpy of the material. Because it provides high

capacity energy storage and little temperature change due to the constant temperature provision of latent heat, latent heat storage (LHS) has a variety of uses. For latent heat storage, phase change materials (PCMs) are the best option. [2] It takes benefit of latent heat that can be absorbed or released from a material over a restricted temperature range. These materials release energy during reverse cooling process and take energy to store during heating process. Fig. 1, shows the classification of phase change materials [3]. The basic working principle of PCM can be understood from the theoretical latent heat curve for solid/liquid phase transition Fig. 2 [4]. The maximum temperature of the device is limited by the melting temperature of the PCM, due to the absorption of thermal energy from the device during phase transition [5]. The concept of employing PCMs for cooling applications has been established in several research over the recent years [6]. These previous ideas aim at encapsulating PCMs in a container or cavity that is directly in contact to a part of body. Advantages of this concept are that large amount of PCM can be used.

2 CLASSIFICATION OF PCM

There are basic three types of PCM which are classified as Organic, Inorganic and binary eutectics. Organic PCM includes Alcohols, Polyethylene glycol, esters and paraffin wax. Inorganic PCM consists of different types of salts and salt hydrates. Binary eutectics are the mixture of two compounds, these can be organic – organic, inorganic – inorganic and organic – inorganic depending on the required properties and specific characteristics.

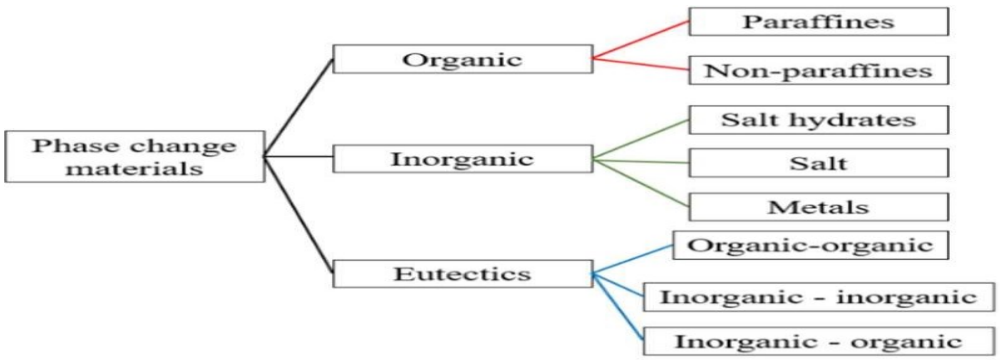

Figure-1. Classification of PCMs [3]

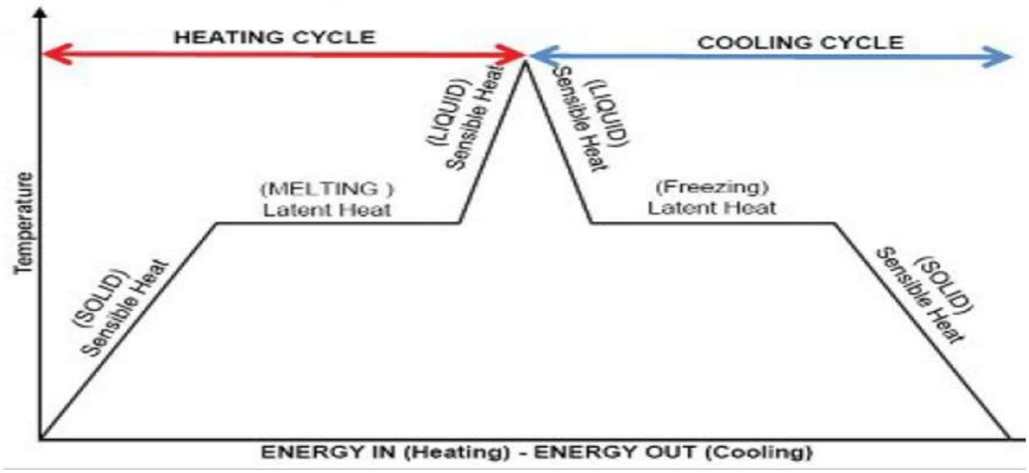

Figure-2. Thermal cycle of a PCM [4]

3 SELECTION OF PCM

The selection between the three classes of PCMs are done on the basis of non-toxicity, availability, non-flammable, cost and durability. Keeping in mind these considerations, organic and in organic PCMs become a good option on the spectrum of different types of PCMs [7]. As organic PCMs has suitable properties like feasible melting and freezing behaviour, less vapour-pressure changes and eco-friendly. In-organic PCMs has high thermal conductivity as compared to organic PCM but they have degree of super cooling and phase separation issues which can be solved by adding other salts like boron and carboxyl cellulose. Considering all the aspects for selecting material, an organic PCM namely Polyethylene glycol-600 (PEG-600) and inorganic PCM namely Glauber salt was selected. The relevant properties of PEG-600 and glauber salt are listed in Table 1 and 2.

Table 1. Relevant Properties of PEG-600 [8]

Property	**value**	**Unit**
Melting point	18- 22	Celsius
Molecular weight	600	g/mol
Latent heat of Fusion	148	kJ/Kg
Thermal conductivity	0.2040	W/m.K
Flash point	270	Celsius
Density	1.13	g/cm^3

PH	4 - 7	—

Table 2. Relevant Properties of Glauber salt [9]

Property	**value**	**Unit**
Melting point	32.2	Celsius
Molecular weight	322.20	g/mol
Latent heat of Fusion	251	kJ/Kg
Thermal conductivity	0.3	W/m.K
Flash point	330	Celsius
Density	1.464	g/cm^3
PH	7	—

4 PERSONALIZED COOLING SYSTEM

The term "personal comfort" refers to a sort of thermal comfort in which a specific location or point is thermally conditioned rather than the entire environment. For example, instead of heating the entire room to achieve thermal comfort in the winter, wear warm clothes; here, only the occupant's comfort was required, not the structure or area. A similar method is adopted for outdoor winter comfort. In the summer, we may utilize the same concept to give only cooling for the occupants rather than cooling the entire room or space, conserving electricity. Personal cooling systems have two types: passive cooling systems and active cooling systems. External power isn't required in passive systems, and they can be recharged after use. They are affordable and simple to use. They can be worn as vests, neck and head covers, and include ice, gel and phase change materials. External power is required for the circulating fluid to be pumped in active cooling systems. They cost more than passive cooling systems and have more complicated elements, but they deliver consistent cooling [10]. Passive systems include such as Gel/Ice packs, liquid circulating cooling vest, and PCM based packs. Ice and gel packs can be placed in the pockets of vests to efficiently cool the body. Gel is made up of starch, water, and other ingredients, and it has the same cooling capacity as ice. It's a low-cost system that needs to be activated in a refrigerator for 5 hours before it can be utilized. However, we know that ice can only exist at very low temperatures, up to 0°C, and that this low temperature can produce vasoconstriction, or a reduction in peripheral blood flow. Water drops that collect on the packs may come into direct contact with the skin, causing discomfort. [11] Circulating liquid systems contain miniature vapour compression system which has a reduced size and the cooling unit can be placed in a backpack. This system circulates the chilled fluid through the tube lining fitted around the body in such a way that there is a greater body-tubes contact area. The circulating liquid carries heat of the body with it and releases it in the cooling unit

outside. The system requires external power in the form of batteries which made it expensive, bulky and flammable. PCM based packs are kept inside the cooling hat and vest pocket for comfort. It totally relies on the heat absorbed during the phase change and acts as heat sink and are activated. PCM packs out perform all the other cooling devices because it can be recharged in refrigerator, ice water or the freezer. Personalized Cooling device such as cooling Vest and cap can be developed by using PCM cooling packs. [12-13] These Cooling devices can be commercially used by athletes, coal miners, labour and construction worker, traffic policemen and welders. It is easy to used and can be recharged in ice water or refrigerator within a few minutes.

5 DEVELOPMENT OF COOLING VEST AND CAP

As mentioned in the paper earlier the organic PCM PEG-600 was selected for the cooling vest and Glauber salt for cooling cap. Among the organic PCM PEG-600 had the melting temperature range i.e. 18 – 22 °C so it is directly selected while glauber salt had some degree of super cooling and phase separation issue which is resolved by adding other salts in different mixing ratio which is defined in table 3. The melting temperature is also being monitored as it reduces with the addition of other salts like boron and carboxyl cellulose. The sample 3 was selected for cooling device because it has less issue of degree of super cooling and it melting temperature also falls in human thermal comfort zone that's why it is selected for designing cooling cap.

Table 3: Chemical composition added in Glauber salt.

Sample	Na2CO3.10 H2O	NaCl	Borax	Carboxyl cellulose	Glauber salt	Melting point
01	10 wt %	2 wt %	0.5 wt %	0.5 wt %	87 wt %	30 – 32°C
02	10 wt %	5 wt %	0.5 wt %	1.5 wt %	83 wt %	27 – 29°C
03	10 wt %	5 wt %	1 wt %	1 wt %	83 wt %	24 – 27°C

For the fabrication of cooling vest and cap nylon cloth was used because of its reasonable thermal conductivity, several packs were made and kept inside the vest and cap. The vest covered the front and back side of body and cap cover the head. Total number of 8 packs were made and put inside the vest with a weight of 100 grams each and 1 pack in cap weight 85 grams having a size of 5x3 inches as shown in Fig 3. The packs need only 20 minutes to recharge in ice water or refrigerator and then can be used in device for cooling up to 1.5 hours. Although it has lower heat of fusion but are cheap, easy to use and provide safe passive cooling.

(a) (b)

Figure-3. Aluminium based encapsulated pack for cooling device (a) Organic Pcm (b) Inorganic Pcm pouch.

6 CONCLUSIONS

Personalized cooling device such as cooling vest and cap is developed by using organic and inorganic phase change materials such as PEG-600 and glauber salt. The cooling device is very effective in controlling body temperature in severe hot outdoor conditions. Its local development and use in daily life can provide a safe environment to sportsman, firefighting worker, lab workers, coal miners and security guards.

7 REFERENCES

[1] Thambidurai, M., Panchabikesan, K., N, K. and Ramalingam, V. (2015). Review on phase change material based free cooling of buildings—the way toward sustainability. Journal of Energy Storage, 4, pp.74-88.

[2] Gao, F. Wang, K. Kuklane, and I. Holmér, “PERSONAL COOLING WITH PHASE CHANGE MATERIALS,” pp. 265–267, 2011.

[3] Abhat, “Low temperature latent heat thermal energy storage: Heat storage materials,” Solar Energy, vol. 30, no. 4, pp. 313–332, 1983, doi: 10.1016/0038-092x (83)90186-x.

[4] W. R. Sutterlin, “Phase Change Materials, A Brief Comparison of Ice Packs, Salts, Paraffins, and Vegetable-derived Phase Change Materials,” Pharmoutsourcing.com, Jul. 2011.

[5] J. Maxa, A. Novikov, and M. Nowottnick, “Thermal Peak Management Using Organic Phase Change Materials for Latent Heat Storage in Electronic Applications,” Materials, vol. 11, no. 1, p. 31, Dec. 2017, doi: 10.3390/ma11010031.

[6] Ahmed, T.; Bhouri, M.; Groulx, D.; White, M.A. Passive thermal management of tablet PCs using phase change materials: Continuous operation. Int. J. Therm. Sci. 2018, 134, 101–115.

[7] Kandasamy, R.; Wang, X.-Q.; Mujumdar, A.S. Application of phase change materials in thermal management of electronics. Appl. Therm. Eng. 2007, 27, 2822–2832.
[8] Kandasamy, R.; Wang, X.-Q.; Mujumdar, A.S. Transient cooling of electronics using phase change material (PCM)-based heat sinks. Appl. Therm. Eng. 2008, 28, 1047–1057.
[9] L.Liang and X. Chen, "Preparation and Thermal Properties of Eutectic Hydrate Salt Phase Change Thermal Energy Storage Material," vol. 2018, 2018.
[10] K. Faraj, M. Khaled, J. Faraj, F. Hachem, and C. Castelain, "A review on phase change materials for thermal energy storage in buildings: Heating and hybrid applications," J. Energy Storage, vol. 33, 2021, doi: 10.1016/j.est.2020.101913.
[11] M. Ashiq, R. Francisco, and M. B. S. Kumar, "Enhancement of heat transfer in paraffin wax PCM using nano graphene composite for industrial helmets," J. Energy Storage, vol.26, no. May, p. 100982, 2019, doi: 10.1016/j.est.2019.100982.
[12] Ma, Y. Zhang, X. Chen, X. Song, and K. Tang, "Experimental Study of an Enhanced Phase Change Material of Paraffin / Expanded Graphite / Nano-Metal Particles for a Personal Cooling System," 2020.
[13] Y. C. Sezgin and M. Celik, "PCM-cap to provide thermal comfort for human head," vol. 4, no. Supply 1, pp. 2–3, 2015, doi: 10.1186/2046-7648-4-S1-A81.

EFFECTS OF VARIATION IN INDENTATION LOAD AND DWELL TIME ON THE VICKERS MICROHARDNESS OF Ti 6Al 7Nb

[1,2*]Muhammad Irfan Khan., [2]Abdul Shakoor., 2 Muhammad Usman.
[1]University of Engineering and Technology, Peshawar Pakistan
[2] CECOS University, Peshawar Pakistan
Corresponding author (M Irfan Khan): email id: irfan@cecos.edu.pk

Abstract— Biomedical alloy Ti-6Al 7Nb was taken and its Vickers Micro hardness behavior was investigated at three different loads 300 gm, 500 gm and 1000 gm and four different dwell time i-e 10s, 20s, 25s and 30s. The average VHN number for the alloy was between 350. These values for the said alloy agreed well with the reported hardness of the enamel of human molar teeth. Further, the two way ANOVA tests revealed that the dwell time had no significant effect over the hardness value therefore a dwell time of 10 seconds is sufficient. However, the hardness values showed variation with the load. Tukey tests revealed that for Ti-6Al 7Nb the difference in hardness values for 300 gm and 500 gm load at various dwell time were not statistically significant, however the hardness values for both the loads differed than that of 1000 gm applied load. The traditional Meyer's law was used to analyze the load dependence of the hardness and it pointed positively towards the indentation size effect for both the alloys.

Keywords— Biomedical Alloys, Vickers micro hardness, Dwell time, Indentation size effect, Mayer's law

1. INTRODUCTION

The number of older people is increasing at highest rate ever recorded and due to this; there is an unprecedented demand for biomedical implants that are safe and more effective[1] Increase in such demands has resulted in extensive research activities to develop suitable biomaterial. The most important criteria, for a biomaterial, is its harmonious coexistence with the surrounding bones and tissues, known as the physiological environment, and hence should have no negative influence on one another [2][3][4]. Additionally, the role of the surface properties of the biomaterial is also detrimental in its final acceptance or rejection in the body [5][6].

Furthermore, there are a number of other aspects to be investigated prior to characterize any material as biomedical material; one of them is the mechanical stability. It means that the material has to be strong enough to bear the load of the structure and thus ensure graft reliability or in other words, the material has to be mechanically sound [7][8][9] [10][11]..

A variety of materials have been investigated to comply with the demands of the biomedical industry among which Ti and Ti-based alloys stand out as the most appropriate biomaterials used hitherto[12][13][14][15]. This is mainly because of the balanced set of desirable properties like high specific strength, flexibility, withstanding the effects of body fluids[16]. For decades, Ti-6Al 4V has remained the most suitable option for the manufacturing of biomedical devices. However, hike in biomedical applications demands has prompted the development of new alloys such as Ti-6Al 7Nb [17][18].

To further improve the performance and application of these alloys a great deal of research activities have been carried out to investigate their mechanical behavior.

One effective way to define the mechanical behavior of materials in relation to its microstructure is micro hardness, and it proves to be an important parameter [19]. When it comes to complex mechanical loading e.g dental application the information provided by the micro hardness tests becomes even more critical [14], Hardness is one of the most important parameters when it comes to finding the suitability of a biomaterial for clinical use, further, it has a positive effect on the resistance to mechanical degradation. Less abrasion of implants is witnessed for higher hardness of the material used. [20][21]

Many efforts have been made to study the mechanical behavior of titanium alloys using micro indentation technique. However, the knowledge related to the effects of the variation in indentation load and dwell time of high specific strength alloys like titanium is limited. Further, no considerable information is available about the precise set of the experimental parameters for the indentation tests of these alloys as biomaterials.

2. METHODOLOGY

The standard Ti-6Al 7Nb alloy was produced by the GfE-Metalle and Materialien GmbH in Nuremberg, Germany. After 2× vacuum arc re-melting (VAR), the alloy was forged from a

diameter of approximately 200 mm to 50 mm in the two-phase field followed by air cooling, stress-relief annealing and stripping.

Three round samples having 50 mm diameter were cut from the billet of the alloy. Surface damage was removed mechanically by grinding with 2400 and 4000 grit, and then polishing on 6, 3 and 1 μm diamond lap wheels. The samples where thus polished to a mirror finish consequently ready for the indents.

For micro Vickers indentation, HVS-100 was used. The procedure adopted was strictly according to the user manual provided by the manufacturer. Using a Vickers diamond indenter each sample was impressed with a load of 300, 500 and 1000 grams for a dwell time of 10, 20, 25 and 30 seconds. Each test was repeated 4 times, therefore, every sample was subjected to 48 indents. Each time after the load removal, the length of the two diagonals of the indent was measured using an optical microscope. Subsequently the indenter, using the following equation, calculated the hardness number automatically.

$$HVN = 1842\ (F/d^2) \qquad (1)$$

Where F represents the force in grams and “d” is the diagonal length in micrometers. [22]

After micro indentation tests, data corresponding to each experimental condition were averaged and the differences in the hardness values were compared using two way analysis of variance (2-Way ANOVA) proceeded by a Tukey test.

3. RESULTS AND DISCUSSION

The results of the micro-Vickers hardness tests of Ti-6Al 7Nb are presented in Fig 1. The variation in average HVN number is from 290 to 340.

The outcome of 2-Way ANOVA is presented in Table-I. The ANOVA revealed statistically significat variance at different load for the alloys under consideration. While the variance at different dwell time did not fell in the significant category. The results of the Tukey tests, presented in Table-II, revealed that for Ti-6Al 7Nb the difference in hardness values for 300gm and 500gm load at various dwell time were not statistically significantly, while the hardness values for both the loads differed than that of 1000 gm applied load.

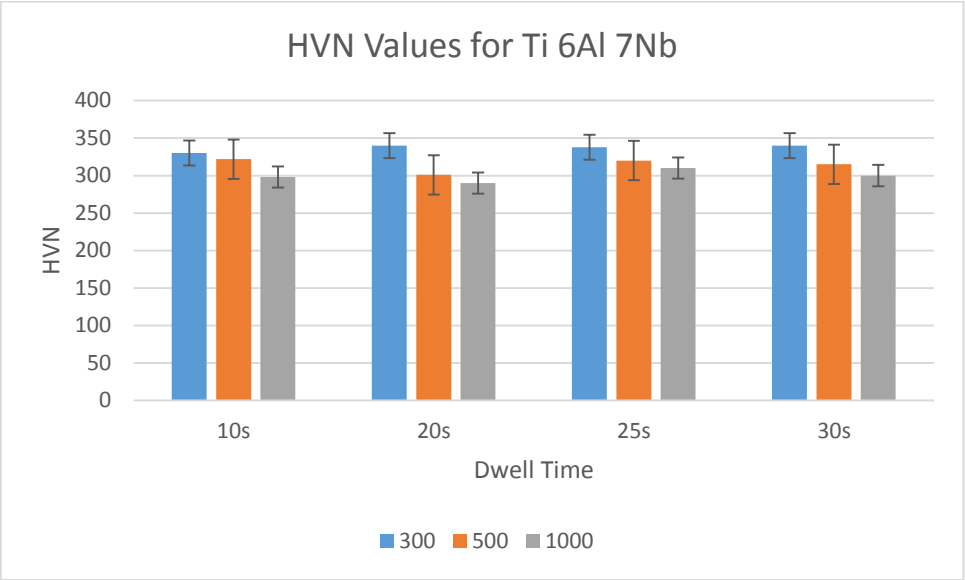

Fig. 1. Average Vickers Hardness Values for Ti-6Al 7Nb

Table I. Analysis of Variance for the Vickers Micro Hardness Test Ti 6Al 7Nb

Two Way ANOVA			
Ti-Alloy	**Source**	**F**	**P**
Ti-67	Load	12.807*	0.0059*
	DT	0.897	0.516
*The mean difference is significant at the P <0.05 level			

Regardless of the variations in the applied load and dwell time the VHN value for the alloy under discussion in this work is in accordance with those reported by [16] [13] . It is also worth mentioning that the range of VHN hardness of the enamel of human molar teeth reported in literature is also in similar range [23][24][25].

Some variation in the standard deviation of this study was observed, the same was reported by [26][27]. A number of factors can produce such variation for example preparation process of specimen, reading errors in diagonal length and variation in chemical composition [28][29].

The phenomena in which the micro-indentation results depend upon the indentation size is called indentation size effect (ISE) [22]. Further, established that along normal ISE, which usually involves a decrease in Microhardness with increase in indentation load, there are also cases where increase in Microhardness is recorded with increase in indentation load, it is known as reverse ISE. [24][30][28]

Table II: Results of Tukey Vickers Vickers Micro Hardness Test of Ti 6Al 7Nb

Tukey Test			
Ti-Alloys	(I) Load	(J) Load	P
Ti-67	300	500	0.897
		1000	0.0079*
	500	300	0.830
		1000	0.011*
	1000	300	0.0079*
		500	0.0109
*. The mean difference is significant at the P <0.05 level.			

It can be observed from Fig.1 that the Micro Vickers hardness results for the given alloy have shown normal ISE. Such behavior is also reported by [20][26].

Various factors contribute to ISE. The first is the accuracy of hardness measurement procedure along with the impact of indenter geometry on hardness. The second factor to ISE effect is related to the properties of the material under consideration [31]–[33]. According to [32], [34] the elastic recovery after indenter removal and the elastic-plastic deformation beneath the indenter tip also contributes to ISE. Pile-up or sink-in around the indentation area also leads to over or underestimation of hardness values.

To elaborate the ISE behavior of various materials a number of models are reported in the literature relating the applied indentation load to the diagonal length of the indenter.

One such model is the Meyer's law [35], it is the most common explanation used in literature for ISE. This involves the direct relation of the intrinsic structural factors of the material under consideration. In this method the experimental data is fitted according to the aforementioned law that relates the applied load to the resulting indentation diagonal length as per the following equation

$$P = Ad^n$$

$$P = logA + nlogd$$

Where P is the indentation load and is the diagonal length while A is the material constant and *n* is the Mayer's index (or work-hardening coefficient).

From the above relations it is clear that the value of HVN will increase with increase in P when n is greater than 2 and HVN will decrease with increase in P when n is less than 2. Further,

the value of '*n*' is less than 2 for hard materials and more than 2 for soft ones [36][37]. In this work, the value of n for Ti-6Al 7Nb is 1.56 (Fig-2).

4. CONCLUSION

The conclusion of this work was that the alloy under consideration have similar hardness properties to the enamel of human teeth and have great potential to be used as biometerial in the respective application[14][17][24]. Further, the variation in dwell time had no significant effect on the HVN for the same load and therefore a dwell time of 10 seconds will suffice for satisfactory results. However, the HVN values were effected by indentation load.

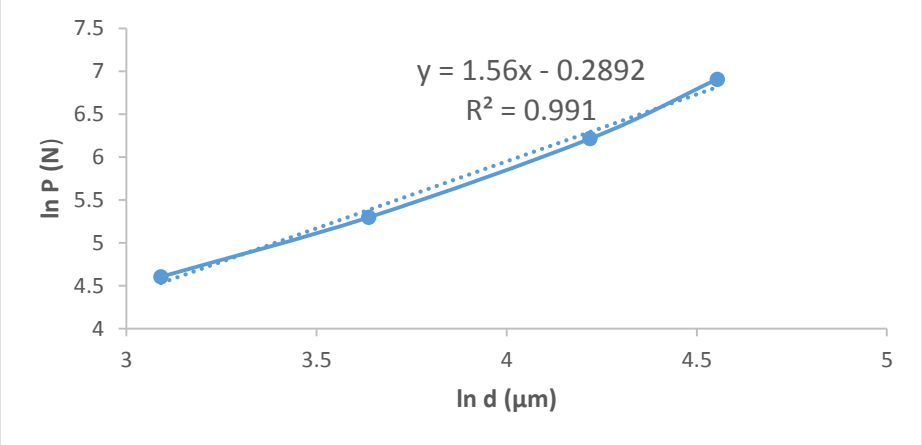

Fig. 2. Indentation load versus indentation diagonal depth for Ti-67

As a future work analytical models and finite element analysis tools can be used to develop models that could predict values of HVN for various loading conditions. Further models like Proportional specimen resistance (PSR) and Hays-Kedall model can be employed to further study the effect of load on HVN number.

5. REFERENCES

[1] K. Prasad *et al.*, "Metallic biomaterials: Current challenges and opportunities," *Materials (Basel).*, vol. 10, no. 8, 2017, doi: 10.3390/ma10080884.

[2] R. Agarwal and A. J. García, "Biomaterial strategies for engineering implants for enhanced osseointegration and bone repair," *Adv. Drug Deliv. Rev.*, vol. 94, pp. 53–62, 2015, doi: 10.1016/j.addr.2015.03.013.

[3] Q. L. Ma *et al.*, "Improved implant osseointegration of a nanostructured titanium surface via mediation of macrophage polarization," *Biomaterials*, vol. 35, no. 37, pp. 9853–9867, 2014, doi: 10.1016/j.biomaterials.2014.08.025.

[4] C. von Wilmowsky, T. Moest, E. Nkenke, F. Stelzle, and K. A. Schlegel, "Implants in bone: Part II. Research on implant osseointegration: Material testing, mechanical testing, imaging and histoanalytical methods," *Oral Maxillofac. Surg.*, vol. 18, no. 4, pp. 355–372, 2014, doi: 10.1007/s10006-013-0397-2.

[5] C. Rungsiyakull, Q. Li, G. Sun, W. Li, and M. V. Swain, “Surface morphology optimization for osseointegration of coated implants,” *Biomaterials*, vol. 31, no. 27, pp. 7196–7204, 2010, doi: 10.1016/j.biomaterials.2010.05.077.

[6] X. Liu, P. K. Chu, and C. Ding, “Surface modification of titanium, titanium alloys, and related materials for biomedical applications,” *Mater. Sci. Eng. R Reports*, vol. 47, no. 3–4, pp. 49–121, 2004, doi: 10.1016/j.mser.2004.11.001.

[7] M. Omidi *et al.*, *Characterization of biomaterials*. Elsevier Ltd, 2017.

[8] K. Camila and L. De Souza, “Biomaterials Characterization for Orthopedic Orthoses : a Systematic Review Biomaterials Characterization for Orthopedic Orthoses : a Systematic Review Corresponding author : De Souza KCL , Phd Student in Biotechnology at Northeast Network of Biotechnolog,” no. January, 2019.

[9] R. K. Roeder, *Mechanical Characterization of Biomaterials*. 2013.

[10] H. J. Rack and J. I. Qazi, “Titanium alloys for biomedical applications,” *Mater. Sci. Eng. C*, vol. 26, no. 8, pp. 1269–1277, 2006, doi: 10.1016/j.msec.2005.08.032.

[11] J. Walker, S. Shadanbaz, T. B. F. Woodfield, M. P. Staiger, and G. J. Dias, “Magnesium biomaterials for orthopedic application: A review from a biological perspective,” *J. Biomed. Mater. Res. - Part B Appl. Biomater.*, vol. 102, no. 6, pp. 1316–1331, 2014, doi: 10.1002/jbm.b.33113.

[12] S. Issue and T. Biomaterials, “Special Issue : Ti-Based Biomaterials : Synthesis ,” pp. 10–14, 2020.

[13] A. M. Khorasani, M. Goldberg, E. H. Doeven, and G. Littlefair, “Titanium in biomedical applications—properties and fabrication: A review,” *J. Biomater. Tissue Eng.*, vol. 5, no. 8, pp. 593–619, 2015, doi: 10.1166/jbt.2015.1361.

[14] P. Gubbi and T. Wojtisek, *The role of titanium in implant dentistry*, vol. 1. Elsevier Inc., 2018.

[15] C. N. Elias, D. J. Fernandes, F. M. De Souza, E. D. S. Monteiro, and R. S. De Biasi, “Mechanical and clinical properties of titanium and titanium-based alloys (Ti G2, Ti G4 cold worked nanostructured and Ti G5) for biomedical applications,” *J. Mater. Res. Technol.*, vol. 8, no. 1, pp. 1060–1069, 2019, doi: 10.1016/j.jmrt.2018.07.016.

[16] M. J. Donachie, “Titanium: A Technical Guide, 2nd Edition,” *October*, p. 128, 2000.

[17] M. Niinomi, “Mechanical biocompatibilities of titanium alloys for biomedical applications,” *J. Mech. Behav. Biomed. Mater.*, vol. 1, no. 1, pp. 30–42, 2008, doi: 10.1016/j.jmbbm.2007.07.001.

[18] M. Özcan and C. Hämmerle, “Titanium as a reconstruction and implant material in dentistry: Advantages and pitfalls,” *Materials (Basel).*, vol. 5, no. 9, pp. 1528–1545, 2012, doi: 10.3390/ma5091528.

[19] K. P. Sanosh, A. Balakrishnan, L. Francis, and T. N. Kim, “Vickers and Knoop Micro-hardness Behavior of Coarse- and Ultrafine-grained Titanium,” *J. Mater. Sci. Technol.*, vol. 26, no. 10, pp. 904–907, 2010, doi: 10.1016/S1005-0302(10)60145-4.

[20] J. Cai, F. Li, T. Liu, and B. Chen, “Microindentation study of Ti – 6Al – 4V alloy,” vol. 32, pp. 2756–2762, 2011, doi: 10.1016/j.matdes.2011.01.003.

[21] D. Micro and V. Hardness, “HVS-1000DN,” pp. 7–9.

[22] E. Broitman, “Indentation Hardness Measurements at Macro-, Micro-, and Nanoscale: A Critical

Overview," *Tribol. Lett.*, vol. 65, no. 1, 2017, doi: 10.1007/s11249-016-0805-5.

[23] M. J. Donachie, *Titanium - A Techincal Guide*, vol. 99, no. 5. 2000.

[24] C. Chuenarrom, P. Benjakul, and P. Daosodsai, "Effect of Indentation Load and Time on Knoop and Vickers Microhardness Tests for Enamel and Dentin," vol. 12, no. 4, pp. 473–476, 2009.

[25] S. A. Shahdad, J. F. McCabe, S. Bull, S. Rusby, and R. W. Wassell, "Hardness measured with traditional Vickers and Martens hardness methods," *Dent. Mater.*, vol. 23, no. 9, pp. 1079–1085, 2007, doi: 10.1016/j.dental.2006.10.001.

[26] G. Elias and P. Henriques, "Vickers Hardness of Cast Commercially Pure Titanium and Ti-6Al-4V Alloy Submitted to Heat Treatments," vol. 17, pp. 126–129, 2006.

[27] M. Kuruvilla, T. S. Srivatsan, M. Petraroli, and L. Park, "An investigation of microstructure, hardness, tensile behaviour of a titanium alloy: Role of orientation," *S¯adhan¯a*, vol. 33, no. 3, pp. 235–250, 2008, doi: 10.1007/s12046-008-0017-2.

[28] L. Fuguo, L. Jinghui, C. Bo, W. Chengpeng, and W. Lei, "Size Effects at Dwell Stage of Micro-Indentation for Pure Aluminum," *Rare Met. Mater. Eng.*, vol. 43, no. 12, pp. 2931–2936, 2014, doi: 10.1016/S1875-5372(15)60036-4.

[29] R. A. Tarefder, M. Asce, H. Faisal, and S. M. Asce, "Effects of Dwell Time and Loading Rate on the Nanoindentation Behavior of Asphaltic Materials," vol. 3, no. 2, pp. 17–23, 2013, doi: 10.1061/(ASCE)NM.2153-5477.0000054.

[30] L. E. Murr *et al.*, "Microstructure and mechanical behavior of Ti-6Al-4V produced by rapid-layer manufacturing, for biomedical applications," *J. Mech. Behav. Biomed. Mater.*, vol. 2, no. 1, pp. 20–32, 2009, doi: 10.1016/j.jmbbm.2008.05.004.

[31] K. Sangwal, "On the reverse indentation size effect and microhardness measurement of solids," *Mater. Chem. Phys.*, vol. 63, no. 2, pp. 145–152, 2000, doi: 10.1016/S0254-0584(99)00216-3.

[32] J. G. Swadener, E. P. George, and G. M. Pharr, "The correlation of the indentation size effect measured with indenters of various shapes," *J. Mech. Phys. Solids*, vol. 50, no. 4, pp. 681–694, 2002, doi: 10.1016/S0022-5096(01)00103-X.

[33] G. M. Pharr, E. G. Herbert, and Y. Gao, "The indentation size effect: A critical examination of experimental observations and mechanistic interpretations," *Annu. Rev. Mater. Res.*, vol. 40, pp. 271–292, 2010, doi: 10.1146/annurev-matsci-070909-104456.

[34] W. W. Gerberich, N. I. Tymiak, J. C. Grunlan, M. F. Horstemeyer, and M. I. Baskes, "Interpretations of indentation size effects," *J. Appl. Mech. Trans. ASME*, vol. 69, no. 4, pp. 433–442, 2002, doi: 10.1115/1.1469004.

[35] N. Budiarsa, A. Norbury, X. Su, G. Bradley, and X. Ren, "Analysis of indentation size effect of vickers hardness tests of steels," *Adv. Mater. Res.*, vol. 652–654, pp. 1307–1310, 2013, doi: 10.4028/www.scientific.net/AMR.652-654.1307.

[36] O. Sahin, O. Uzun, U. Kolemen, and N. Ucar, "Vickers microindentation hardness studies of β -Sn single crystals," vol. 58, pp. 197–204, 2007, doi: 10.1016/j.matchar.2006.04.023.

[37] J. Petrík, "On the Load Dependence of Micro-Hardness Measurements: Analysis of Data by Different Models and Evaluation of Measurement Errors," *Arch. Metall. Mater.*, vol. 61, no. 4, pp. 1819–1824, 2016, doi: 10.1515/amm-2016-0294.

Synthesis & Characterization of Polyester Based Heat Resistant Tiles

Muhammad Hayat[1,*], Syed Nasir Shah[2], Bilal Islam[3], Zaka Ansar[3], Usman Khan[3], Haseeb Ullah[1], Asad Meer[1]
[1]Department of Mechanical Engineering, Faculty of Mechanical and Aeronautical Engineering, University of Engineering and Technology Taxila, Taxila 47080 Rawalpindi, Pakistan
[2]Department of Energy Engineering, Faculty of Mechanical and Aeronautical Engineering, University of Engineering and Technology Taxila, Taxila 47080 Rawalpindi, Pakistan
[3]National Center for Physics, 44000 Islamabad, Pakistan
[*]Corresponding Author Email: rhayat785@gmail.com

Abstract— Polyesters are used in several applications regarding manufacturing of electrical and mechanical parts of different machineries. Due to its low thermal conductivity, polyester was used to make heat insulation tiles. Curing process was used to increase hardness of polyester. In the curing process, Methyl Ethyl Ketone Peroxide (MEKP) was used as a hardener and Cobalt naphthenate (CN) as an accelerator. The parameters which affected the curing process was temperature, amount of hardener and concentration of accelerator. Curing time was found to be dependent on these parameters. Different temperatures (Range 40°C -160°C) were applied during curing of polyester and curing kinetics was observed. Temperature reading of surface of sample and temperature reading of device. Testing of different samples was done through X-ray crystallography (XRD) and Fourier-transform infrared spectroscopy (FTIR). After testing of specific samples for this research, the optimum temperature for curing of polyester was found to be 110°C.

Keywords— Polyester; Heat insulation tiles; curing kinetics; Composite

1. INTRODUCTION

Curing process was used during which a chemical reaction (such as polymerization) or physical action (such as evaporation) takes place, resulting in a harder, tougher or more stable linkage (such as an adhesive bond) or substance. Polyester resins provide some advantages because of their large range of mechanical properties, low cost, good corrosion resistance and low weight [1]. The different analysis methods revealed that the cure kinetics of unsaturated polyester is complex because many reaction processes occur simultaneously. The chemical reaction took place in three steps, it is comprised of initiation, propagation and termination steps [2]. In the initiation stage, the initiator decomposes chemically, forming free radicals. In the propagation or polymerization stage, these radicals can react easily with styrene or with polyester [3].

In the curing process of polyester, Methyl Ethyl Ketone peroxide (MEKP) was used as a hardener and Cobalt Cobalt naphthenate (CN) is used as an accelerator. Curing is necessary to make polyester hard and to utilize it in manufacturing of desired parts and components of mechanical and electrical machineries [4]. At the beginning of this process, polyester was a liquid consisting of a large number of short polymer chains [5]. However, this chemical

configuration was energetically inconvenient so that the molecules cross-link to each other, thus causing the gradual transformation of the liquid into the solid material [6]. At the last phase, the polyester behaved as viscoelastic solid.

This research of cure kinetics reveals the cure behavior of the polyester resin, the various stages of the curing process and the characteristics of each stage. This knowledge can be used to develop optimal curing technology. The influence of resin curing agents, catalysts, fillers and additives are researched and analyzed. Through the kinetic parameters, a relationship between the curing rate and degree of cure with time and temperature are established. Curing kinetics of the polyester resin was found to be a function of temperature and catalyst concentration.

2. METHODOLOGY

At different temperature readings, curing time was monitored. All readings of the temperature range (40°C -160°C) were taken carefully with two specific temperatures i.e. temperature reading of surface of sample and temperature reading of device [7]. Samples were made in different beakers with specific concentrations of polyester resin, Methyl Ethyl Ketone peroxide (MEKP) and Cobalt. Readings were taken out after every 5 minutes.

For sample preparation, Beakers having weight of 35 grams were used in which polyester resin was poured and then the limited concentration of hardener and accelerator was mixed. After mixing each substituent, the weight of beaker was noted. Then the sample was kept for curing at different temperatures on the curing device that was hot plate [8]. The samples made at various temperatures were used for manufacturing of heat insulation tiles.

During the sample preparation, limited amount of Methyl Ethyl Ketone peroxide (MEKP) and Cobalt was used to avoid excess of formation of radicals to achieve proper curing. During the experiment, it was found that at high temperatures, curing of polyester occur quickly and vice versa [1]. Through X-ray crystallography (XRD) and Fourier-transform infrared spectroscopy (FTIR) testing revealed the degree of crystallinity and amount of absorption.

Through testing results it was revealed that most suitable temperature would be 110°C for curing as below this temperature pre-mature curing occurred. Above this temperature value, curing was quickly but it affected the physical and chemical properties of polyester [2].

3. RESULTS AND DISCUSSION

A. FT-IR

Fourier Transform infrared spectroscopy (FTIR) peaks manifest the presence of polyester, MEKP (methyl ethyl ketone per-oxide) after comparing it with the literature. The wave number also resembles with the obtained values of the literature. As a result, the peaks of Polyester will appear. The peak at 709 cm^{-1} (Fig. 1) is caused by a typical polytrimethylene ring seen in polyester [9]. The absorption bands at 2000 cm^{-1} are caused by the C-H groups in the benzene ring's out-of-plane bending vibration.

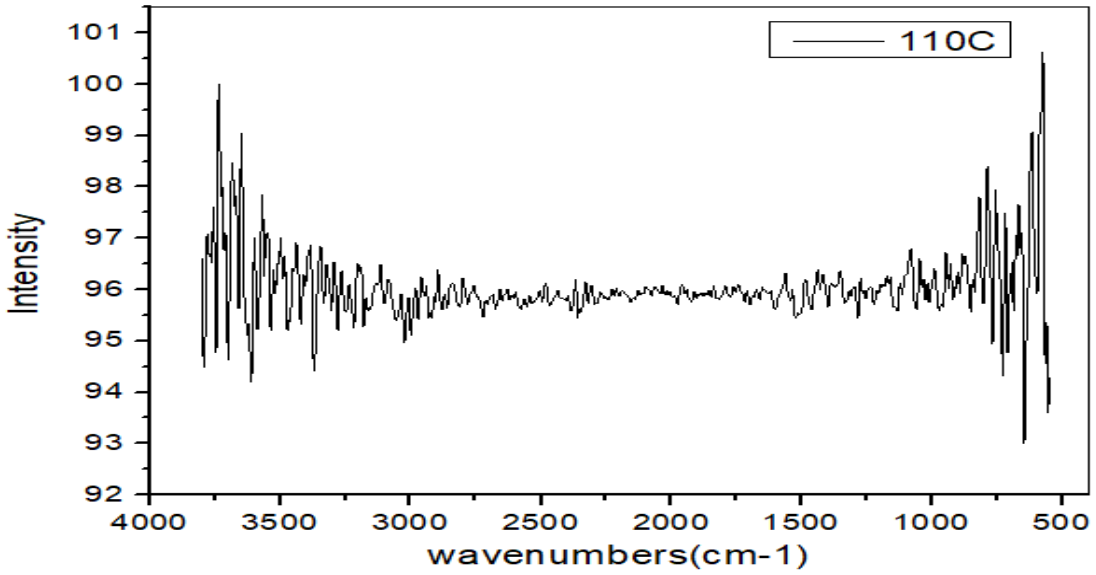

Fig. 1. FTIR Analysis of Polyester at 110°C

B. XRD

X-ray diffraction of the prepared composite depicts amorphous nature of the synthesized sample. This is because polyester is amorphous in nature. The peaks resembles with the peaks obtained in the literature. The polymer shows sharp peaks at 2θ values 9°, 22°, 25°, 50°, 62° and 74° in Fig. 2 which indicate its amorphous nature. The position (2θ), shape, and intensity of the polyester characteristic peak can be utilized to assess the degree of intercalation or exfoliation. A successful dispersion of polyester is seen when a peak disappears or moves by two. Its XRD curve no longer displays the large peak typical of polyester, and the intensity of its peak features has also lessened. The peak at 2° = 22° is sharper and the peaks at higher 2 have disappeared.

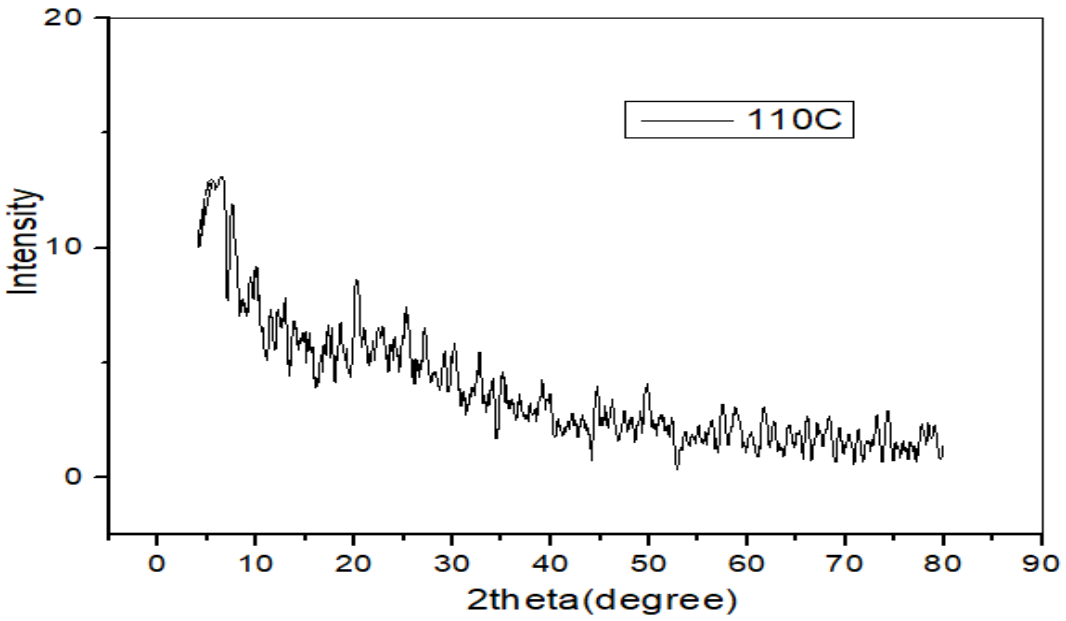

Fig. 2. XRD of Polyester at 110 °C

4. CONCLUSION

Polyester based heat resistant tiles were made through curing process. The samples were prepared with use of specific hardener and accelerator at different temperatures. Temperature range was kept (40-160)°C and curing kinetics was observed. The parameters which affected the curing process was temperature and concentration of substituents. Through XRD and FTIR testing, optimum temperature of 110°C was found for curing.

5. REFERENCES

[1] S. Islam, M. N. Arbab, A. Nawaz, B. Islam, S. Bibi, and I. Hussain, "Appropriate Polymer Selection for Insulation of High Voltage Ignition Coils by Combination of Material Index Determination and Novel Heuristical Approach," *Transactions of the Indian Institute of Metals,* vol. 74, pp. 1387-1396, 2021.

[2] A. Nawaz, B. Islam, M. S. Khattak, L. Ali, U. Saleem, A. Ullah*, et al.*, "Polyester Usage in Manufacturing of Electrical and Mechanical Products and Assemblies," 2018.

[3] M. A. Vargas, K. Sachsenheimer, and G. Guthausen, "In-situ investigations of the curing of a polyester resin," *Polymer Testing,* vol. 31, pp. 127-135, 2012.

[4] G. V. Salmoria, C. H. Ahrens, V. E. Beal, A. T. N. Pires, and V. Soldi, "Evaluation of post-curing and laser manufacturing parameters on the properties of SOMOS 7110 photosensitive resin used in stereolithography," *Materials & Design,* vol. 30, pp. 758-763, 2009.

[5] M. A. Munawar, D. W. Schubert, S. M. Khan, N. Gull, A. Islam, M. A. U. Rehman*, et al.*, "A Case Study: Particulate-Filled Polyester Hybrid Laminated Composites," 2018.

[6] B. Dholakiya, "Unsaturated Polyester Resin for Specialty Applications," 2012.

[7] D. A. A. A. Razak, "Mathematical Model For Autoclave Curing Of Unsaturated Polyester Based Composite Materials," *Tikrit Journal of Eng. Sciences,* vol. 17, p. 10, March, 2010 2010.

[8] E. Kicko-Walczak and G. Rymarz, "Flame-Retardant Unsaturated Polyester Resins: An Overview of Past and Recent Developments," 2018.

[9] X. Zhang, D. Miao, X. Ning, M. Cai, Y. Tian, H. Zhao*, et al.*, "The stability study of copper sputtered polyester fabrics in synthetic perspiration," *Vacuum,* vol. 164, pp. 205-211, 2019.

Coating Copper Substrate with Polyester Coating and Its Corrosion Analysis for Heat Exchanger Based Applications

[1*]Haseeb Ullah, [2]Syed Nasir Shah, [3]Bilal Islam, [3]Zainab Zafar, [1]Muhammad Hayat, [1]Asad Meer
[1]Department of Mechanical Engineering, Faculty of Mechanical and Aeronautical Engineering, University of Engineering and Technology Taxila, Taxila 47080 Rawalpindi, Pakistan
[2]Department of Energy Engineering, Faculty of Mechanical and Aeronautical Engineering, University of Engineering and Technology Taxila, Taxila 47080 Rawalpindi, Pakistan
[3]National Center for Physics, 44000 Islamabad, Pakistan
[*]Corresponding Author Email: engrhaseeb929@gmail.com

Abstract— Copper is provided a uniform coating of polyester using the dip-coating method to increase its ability to resist corrosion in the presence of sodium chloride solution. One substantial difference between the two substrates would be through Fourier Transform infrared spectroscopy (FTIR), which discovered a uniform and crack-free Polyester coating on a Copper substrate whereas an electrochemical corrosion test on the uncoated sample clarified a cracked texture covered in thick corrosion layers. However, by covering the corrosive pits, a higher concentration of sea water (NaCl Solution) significantly impacted the surface morphology. The electrochemical corrosion test was used to examine the homogeneous coating's resistance to corrosion on a copper substrate that had been coated with polyester. When the corrosion rate of the coated sample was slightly shifted towards the anodic direction, it resulted in a better protection efficiency (PE) when compared to the corrosion performance of a polyester coated copper substrate in a NaCl medium.
Keywords— Polyester; Copper; corrosion performance.

1. INTRODUCTION

Metal heat exchangers are a standard component of petrochemical and automobile production facilities [1] and fixing the issue is crucial since production-related corrosion reduces the heat exchanger's durability. Coating is an essential component of metal heat exchangers because it protects against corrosion and increases thermal conductivity [2], To eliminate the drawbacks caused by corrosion, an effective anti-corrosion coating with high thermal conductivity and strong heat resilience must be developed and applied to metal heat exchangers for long-term usage.

Copper oxide (cuprite) deposits on the inner tube walls have darkened due to corrosion. Cuprite facilitates oxygen diffusion, which speeds up the corrosion process. The mechanism is dangerous because corrosion damage to the mechanism's components may not be evident to the naked eye. As a result, refrigerant may leak from the copper tubing. The heat exchanger has failed, and contamination is probable as a result [3].

Recent research has shown that adding even a trace amount of potent additives to the matrix of a polymer-based composite may substantially increase its thermal, mechanical, and barrier properties [4]. Throughout the enhancing process, the matrix's intrinsic compactness, beauty, density, and anti-aging qualities are all intact. Inorganic-organic Materials with a variety of beneficial qualities, including as dirt adhesion resistance and abrasion, specific barrier characteristics, optical flexibility, and antibacterial activity, may be developed using hybrid polymers, which are nanocomposites with a hybrid structure [5].

In this research, a copper-resistive coating have made and placed in close proximity to salt water. On a copper substrate, a homogenous polyester coating is applied using a dip coating procedure, and after that we examined at how corrosion behaved in sea water. Electrochemical corrosive testing was used to find out how well the polyester covering kept the copper heat exchanger coils from rusting, in order to clarify the mechanism of corrosion resistance. The coating's chemical composition was analyzed using FTIR.

2. METHODOLOGY

C. SAMPLE PREPARATION

Cubic pieces of Cu (10 mm x 10 mm x 5 mm) were machined and supplied as substrates. The specimens were hand polished with 100-1800 grit sandpaper and cleaned with deionized water prior to coating. The substrates were agitated continuously in acetone to remove any remaining grease before being rinsed in deionized water and air-dried for an hour at room temperature. Commercial polyester purchased from Sohail Chemicals was used in this study without any pretreatment.

D. COATING OF POLYESTER ON COPPER

Polyester layers were dipped coated onto copper surfaces. The dipping procedure used fifteen milliliters of polyester fluid. For five minutes, the polyester solution was agitated at 350 rpm. The substrate was removed after one minute in a room temperature polyester solution, and a symmetrical layer was produced on it. The substrates were heated for 30 minutes at 80°C after coating to settle the Polyester layer and smooth out the Cu.

E. CHARACTERIZATION OF POLYESTER COATING ON CU SUBSTRATE

Each final composite sample was assessed in the infrared spectrum range 400-4000 cm^{-1} using a JASCO FT-IR spectrometer.

F. ELECTROCHEMICAL CORROSION TEST

The Gamry framework device MULTECHEM SERIES G750 (Warminster, PA, USA) was used to conduct electrochemical corrosion investigation of Cu with Polyester-coated surfaces in 0.6 M NaCl solution. All experiments were carried out at room temperature in a 3-electrode corrosion cell. The active electrode was a 1 cm^2 scouring sample, whereas the reference and counter electrodes were saturated calomel and graphite, respectively. The corrosive NaCl solution was made using deionized water. With an anticipated range of -500 mV to +300 mV against corrosion rate, polarization measurements were done after 60 minutes in the test electrolyte at a scan rate of 1 mV/s.

The protection efficiency *(P.E)* was calculated using the measured i_{corr} values from the following equation [6].

$$P.E = \frac{\left(i_{corr} - i_{corr(c)}\right)}{i_{corr}} \times 100 \qquad (1)$$

The corrosion current density rates in the presence and absence of the coating are i_{corr} and $i_{corr(c)}$, respectively.

3. RESULTS AND DISCUSSION

G. FT-IR

The FT-IR spectra of uncoated and coated Cu samples are shown in Fig. 1. As seen by the blue line, copper reflected the vast majority of infrared light and produced no discernible peaks before being coated with polyester. In the presence of a polyester solution, copper responded by adhering to its surface [7], So, the peaks of polyester will show up on the FT-IR graph (Red Line). The vibration of an aromatic ring, such as those found in polyester, causes the peak at 1108 cm^{-1}. When the polyester primer is fully cured at 80°C, the resulting ATR-FTIR spectra include a sharp peak at around 2358 cm^{-1} [8], seen in Fig. 1. A relatively wide peak occurred at a height of 3750 cm^{-1}, it is possible to identify OH functional groups, which is important for evaluating the presence of binders that play a role in adhesion and cross-linking activities inside samples [9]. The FT-IR analysis confirmed that polyester was employed as a coating for copper.

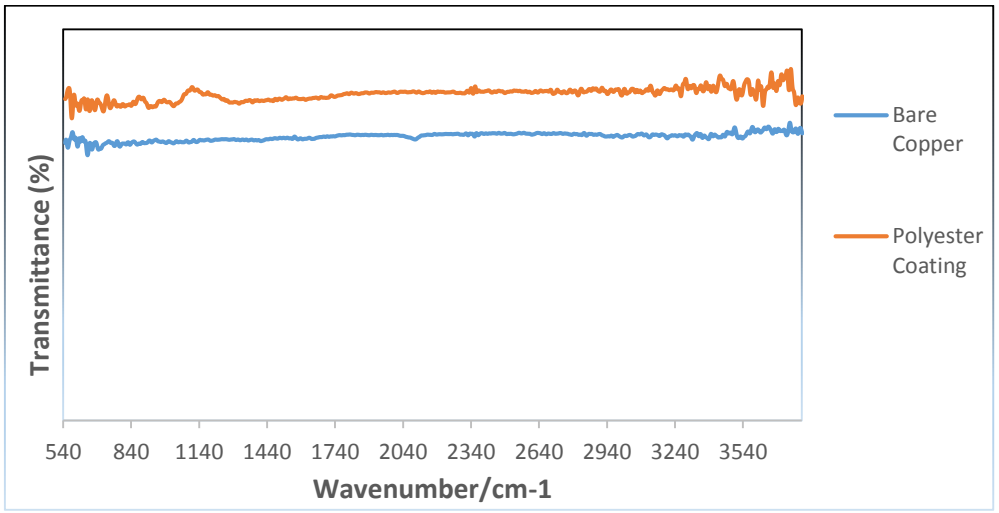

Fig. 1. ATR-FTIR spectra of bare Cu and Polyester-coated Cu Substrates.

H. Corrosion Measurement

The Gamry framework software was used to calculate E_{corr} and I_{corr} values (MULTECHEM SERIES G550). Both an untreated Cu sample and a polyester-coated Cu sample were submerged in 0.6 M NaCl solution for 30 minutes before undergoing an electrochemical corrosion test. Fig. 2 depicts potentiodynamic polarization curves recorded in NaCl solution for untreated Cu and polyester-coated samples. Bare Cu has exceptionally poor corrosion resistance, as measured by the average E_{corr}, and I_{corr} values of 489.147 mV and 60.78 A/cm^2 [10]. E_{corr} values of 247.0 mV, and I_{corr} values of 0.163 A/cm^2 were recorded for the polyester-coated substrate when tested in 0.6 M NaCl. After an electrochemical test in NaCl medium,

the shielded surface of the substrate that had some superficial holes or corrosive pitting was found to be more durable than the top of the exposed substrate that had extensive corrosive layers. Table 1 displays the results of an electrochemical analysis of a corrosion test conducted in NaCl solution.

Fig. 2 depicts the potentiodynamic polarization curves of Cu and polyester-coated samples in NaCl solution.

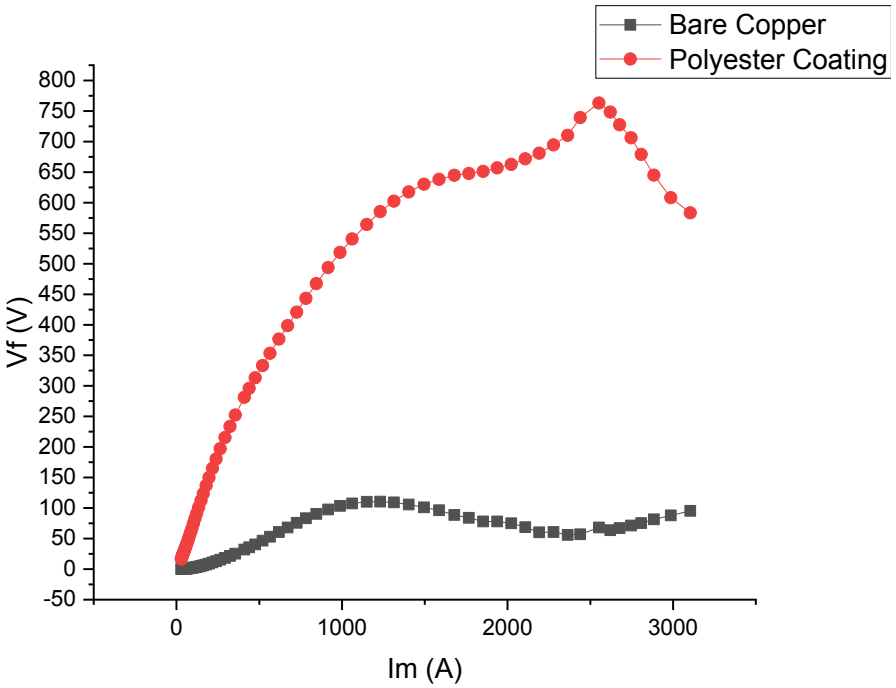

Fig. 2. Potentiodynamic Polarization Curve of Cu and Polyester coating in NaCl.

TABLE I: ELECTROCHEMICAL DATA OF CU AND POLYESTER COATING IN NaCl

Specimen	NaCl Concentration	E_{corr} (mV)	I_{corr} (μA/cm^2)
Cupper	0.6 M	-489.147	60.78
Polyester Coating	0.6 M	-247.0	0.163

4. CONCLUSION

The dip coating method was used to apply a homogeneous Polyester coating over a Cu substrate. The FT-IR analysis confirmed that polyester was employed as a coating for copper and shows high peaks than bare copper substrate. In a 0.6 M NaCl solution at room

temperature, a copper substrate covered with polyester had 99.73% Protection Efficiency (P.E). The copper's polyester coating prevented corrosion better. Polyester coatings increased corrosion resistance in NaCl by reducing corrosion potential and current. Polyester coating is promising for industrial corrosion resistance.

5. REFERENCES

[1] Z. Guan, "Study of high temperature anti-corrosion coating on heat exchanger," *PhD, South China University of Technology,* 2010.

[2] L. Jing, J. Liang, and L. Yeming, "High-thermal conductive coating used on metal heat exchanger," *Chinese Journal of Chemical Engineering,* vol. 22, pp. 596-601 %@ 1004-9541, 2014.

[3] M. M. Lachowicz, "A metallographic case study of formicary corrosion in heat exchanger copper tubes," *Engineering Failure Analysis,* vol. 111, p. 104502, 2020.

[4] S. B. Chaudhari, A. A. Mandot, and B. H. Patel, "Functionalized nano-finishing to textiles using Ag nano-colloids," *Melliand international,* vol. 15, pp. 214-216, 2009.

[5] S. Amberg-Schwab and D. Ulrikeweber, "Functional coating systems for paper," *International Textile Bulletin,* vol. 50, pp. 28-31, 2004.

[6] M. Shabani-Nooshabadi, M. Mollahoseiny, and Y. Jafari, "Electropolymerized coatings of polyaniline on copper by using the galvanostatic method and their corrosion protection performance in HCl medium," *Surface and Interface Analysis,* vol. 46, pp. 472-479 %@ 0142-2421, 2014.

[7] X. Zhang, D. Miao, X. Ning, M. Cai, Y. Tian, H. Zhao*, et al.*, "The stability study of copper sputtered polyester fabrics in synthetic perspiration," *Vacuum,* vol. 164, pp. 205-211, 2019.

[8] L. I. Fockaert, S. Pletincx, D. Ganzinga-Jurg, B. Boelen, T. Hauffman, H. Terryn*, et al.*, "Chemisorption of polyester coatings on zirconium-based conversion coated multi-metal substrates and their stability in aqueous environment," *Applied Surface Science,* vol. 508, p. 144771, 2020.

[9] N. A. M. N. K. Ramesh*, S. Ramesh, B. Vengadaesvaran, A. K. Arof, "Studies on Electrochemical Properties and FTIR analysis of Epoxy Polyester Hybrid Coating System," *International Journal of ELECTROCHEMICAL SCIENCE,* vol. 8, p. 11, 2013.

[10] W. Akram, A. Farhan Rafique, N. Maqsood, A. Khan, S. Badshah, and R. U. Khan, "Characterization of PTFE Film on 316L Stainless Steel Deposited through Spin Coating and Its Anticorrosion Performance in Multi Acidic Mediums," *Materials (Basel),* vol. 13, Jan 14 2020.

Thermal Characterization and Performance Analysis of Epoxy-based Composite and its Application on Steam Pipes

Asad Meer [a*], Syed Nasir Shah [b], Bilal Islam [c], Zaka Ansar[c], Usman Khan[c],,
Haseeb Ullah[a],, Muhammad Hayat[a],

[a*]Department of Mechanical Engineering, Faculty of Mechanical and Aeronautical Engineering, University of Engineering & Technology Taxila, Taxila 47080 Rawalpindi, Pakistan

[b]Department of Energy Engineering, Faculty of Mechanical and Aeronautical Engineering, University of Engineering and Technology Taxila, Taxila 47080 Rawalpindi, Pakistan

[c]National Center for Physics (NCP), Quaid.i.Azam University Campus, Islamabad 44000, Pakistan

Corresponding Author: Asad Meer (Email: masad9187@gmail.com)

Abstract—Currently process industries are facing excessive problem of corrosion, wear and tear, toughness, and strength degradation in various metal/alloy-based pipes. In this work, an alternative approach has been adopted in effort to fix the issue with two phase composite pipes i.e., glass fiber and epoxy resin. Two phased composite was synthesized after mixing epoxy & hardener (Amine) in a ratio of 2:1. Curing of these samples was conducted at 100, 140, and 160℃. In this synchronized thermal and mechanical study, Thermal Gravimetric Analysis (TGA), X-rays diffraction (XRD), Fourier Transfer Infrared Spectroscopy (FTIR), Hoop strength tests were performed. FTIR manifested the

presence of (O-H) group, Amine (N-H) and epoxide. Optimal degradation, hoop strength and burst pressure was recorded for a sample cured at 140℃.

Keywords: Two phased composite, Glass Fiber, Epoxy Resin, Curing, Optimum Temperature

1. INTRODUCTION

In current times, Epoxy resins are extensively utilized for various applications ranging from synthesis of composites to effective coatings. They are primarily used in microelectronics, UV-cured electronic adhesives, and generator encapsulations[1]. Epoxy resins are the primary ingredient in structural adhesives used in shipbuilding, wind turbine blade manufacturing, automotive or aerospace applications. This is because of their robust mechanical properties, excellent adhesiveness to various surfaces, better heat insulation and chemical stability[2]. In process industries, the use of metallic pipes leads to drastic effects because of spontaneous electrochemical reaction called corrosion[3]. For instance, product quality, effect on feed flow rate (blockages tends to create because of corrosive layer on the surface)[4].

Many fluids, including natural gas, pressurized gases, chemicals, crude oil, are conveyed through these composite[5]. Á. Pomázi, and A. Toldy [6], synthesized fiber-epoxy resin composite for its application in aircraft and aerospace industry as a flame retardant. By reacting polyethylene glycol and DGEBA epoxy resin, C. Yang and Z. G. Yang [7]. Fabricated epoxy resin and applied for ink-jet printing purpose by using UV light for curing of epoxy resin. For use in the packaging of opto-electronic devices, N. Gao, W. Liu, Z. Yan, and Z. Wang [8]. However, our work is focused on synthesis of epoxy resin composite with fiber glass for its application in insulated steam pipes, which was not performed in the literature; hence significance progress was required in this regard. The objective of current work is to replace conventional metallic pipes with epoxy resin incorporated with fiber glass in significant ratio to minimize the above-mentioned risks in industries.

2. MATERIAL AND METHOD

2.1 Material

In this research, general purpose Epoxy resin was purchased from Gujranwala polymer industry Ltd (Pakistan). Composite material was manufactured of epoxy resin mixed with (2:1) hardener Amin. Reinforcement of glass fiber was obtained from (Ransal Fiber Glass Engineering, Pakistan) mixed with epoxy resin to design the pipe.

2.2 Sample preparation

Composite sample was prepared in a Teflon beaker commercially available in Pakistan. In the startup Epoxy Resin (2:1) and Glass fiber (165 gm/m^2) was mixed (with the help of stirrer) in an appropriate ratio. Afterwards, all composite samples were cured on hotplate at various temperatures (100-160)^{0}C. Composite pipe was design through filament winding process with

the help of numeric control machine. Five layers of glass fiber were wind on the mandrel through hoop winding. Additionally, composite sample was cured in an oven at best curing temperature 140^0C for three hours. In the end sample was take out from the oven and separate from the mandrel.

2.3 *Characterization*

X-rays diffraction of specimens was performed with an intensity of 10-20°. FTIR of epoxy composites were analyzed with a range of wavenumbers from 400-4000cm^{-1}.

3. RESULTS AND DISCUSSION

3.1 *. X-rays Diffraction (XRD)*

The fabricated epoxy composite samples were analyzed by using XRD, and the assessment is shown in fig.1 (a) and (b). XRD graphs describe dominant amorphous band at 2θ values from 10-20^0. Additionally, epoxy composites cured at various temperatures did not show any variation in the peaks which is confirm by[9].

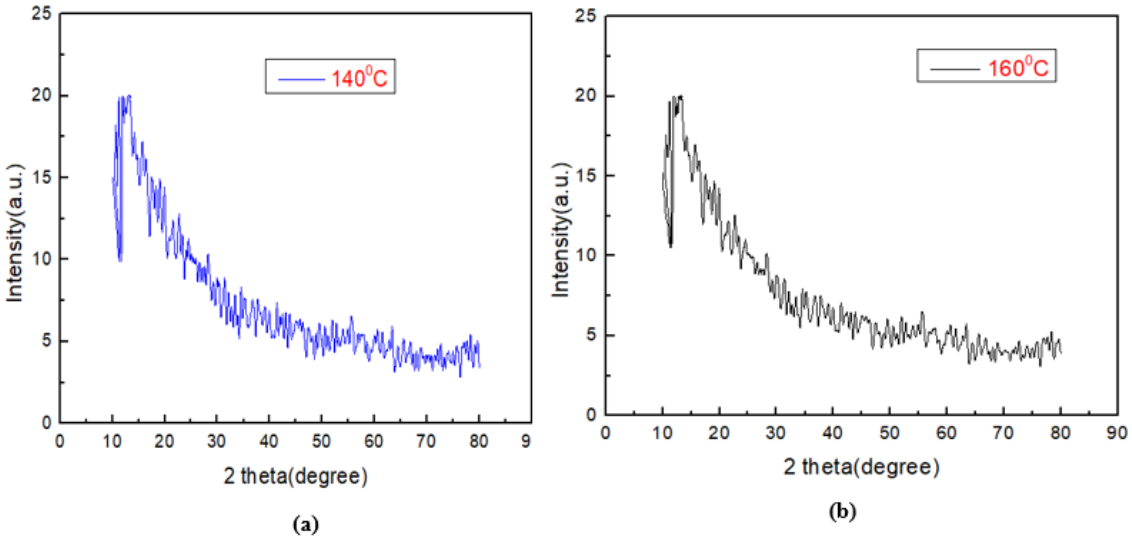

Fig.1. XRD analysis of (a) 140°C (b) 160°C cured specimens

3.2. Fourier Transform Infrared Spectroscopy (FTIR)

FTIR was performed on all samples of epoxy based composite at various temperature from (100-160)^{0}C as shown in fig.2 (a), (b), and (c). IR spectrum confirmed the peaks of stretching hydroxyl (O-H) group between 3200 to 3600 cm-1 have broad peaks on (3457, 3484, and 3492) cm-1. Second band was found at (2151, 2152, and 2128) cm-1 that attributed to the amine curing agent. Next peak represented the C-O-C at (1047, 1041, and 1028) cm-1. Finally bands of Glass fiber and epoxy were observed at (971, 968, 977) cm-1 and (850, 840, 835) cm-1 respectively. According to I. J. Fernandesa, R. V. Santos, E. C. A. Dos Santos, T. L. A. C. Rocha, N. S. D. Junior, and C. A. M. Moraes [10] that hydroxyl (O-H) group lying between

(3200-3600) cm-1 and epoxy ranges (860-950) cm-1, hence it confirms our peaks as well. Afterward, D. Mamalis, T. Flanagan, and C. M. Ó Brádaigh[11] manifested the same range of bands amine (RNH3) that we have obtained.

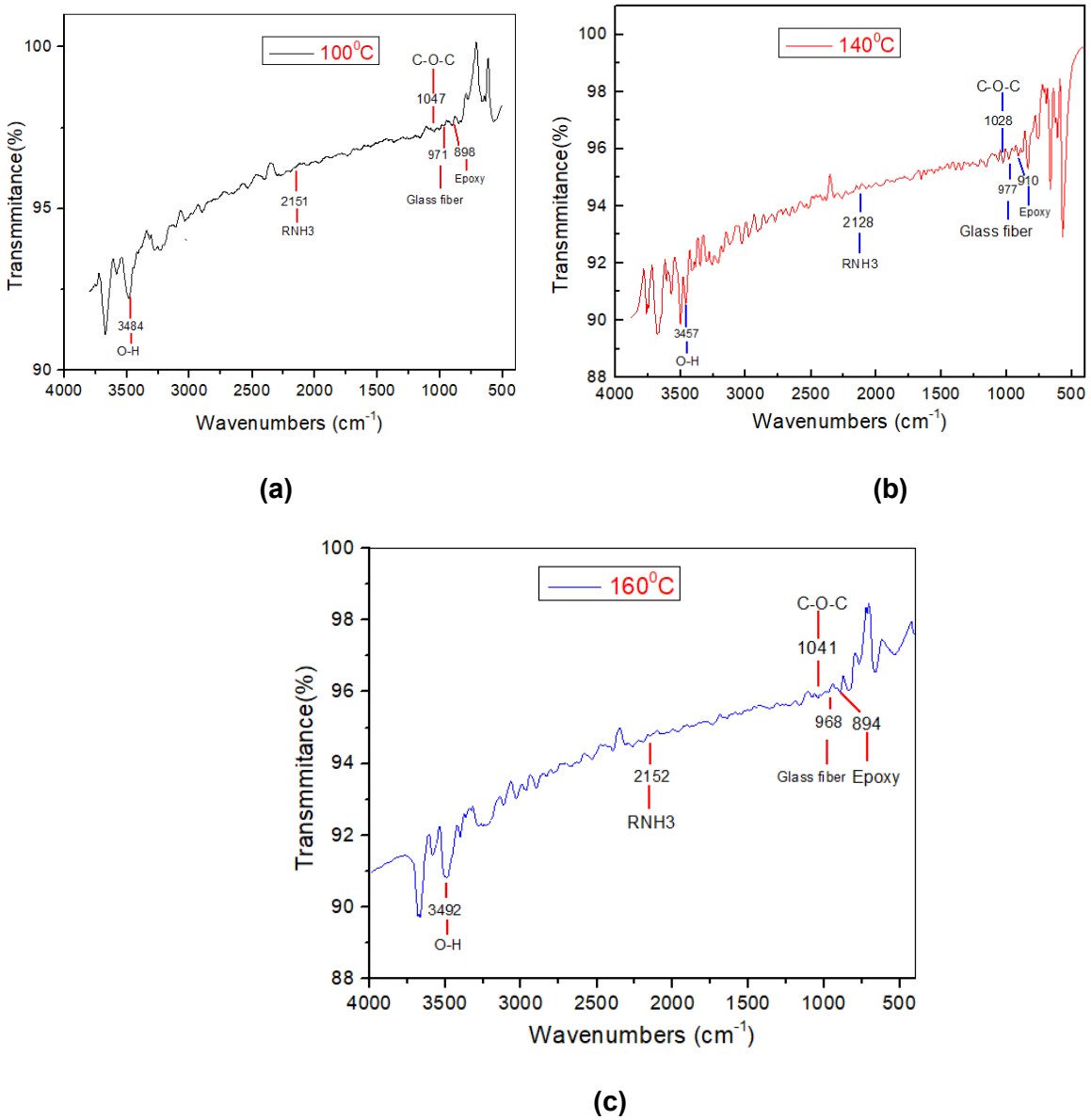

Fig. 2. FTIR analysis (a) 100, (b) 140, and (c) 160°C cured specimens

4. THERMAL AND MECHANICAL CHARACTERIZATION

Thermal characteristics were analyzed with Thermogravimetric Analysis (TGA). Furthermore, for mechanical characterization hoop strength and burst pressure were calculated.

4.1 Thermogravimetric Analysis(TGA)

TGA assessment of all the composites of epoxy resin is represented in fig.3. Decomposition of weight loss express in two steps. In 1st step initial degradation temperature was observed at (100-350)^{0}C and weight loss was around (76, 75, and 71) wt. % for all samples at various curing temperature (140, 100, and 160)^{0}C respectively. Whereas, in the next step the weight loss decline to (11.29, 7.22, and 4.81) wt. % for all samples accordingly. It can be clearly seen that all other samples (100, 140)^{0}C, the % weight loss were around 10% but for 160^{0}C cured specimen it was at 4.8% [12][13].

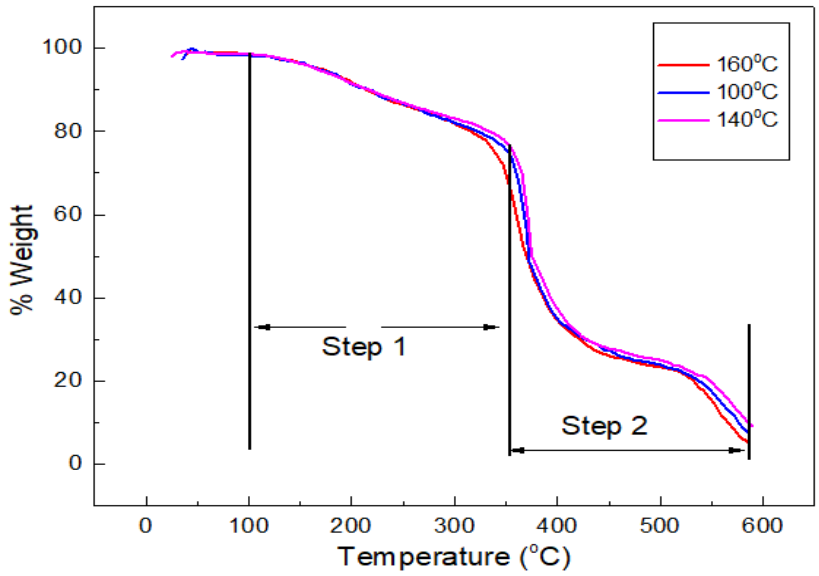

Fig. 3. TGA analysis of specimens

4.2 *Hoop Strength and burst pressure*

According to ASTM D2290[14], hoop strength were determined for experimental and theoretical both at various curing temperature for all specimens and shown in fig.4 (a) and highest values for hoop strength appeared at 140°C specimens

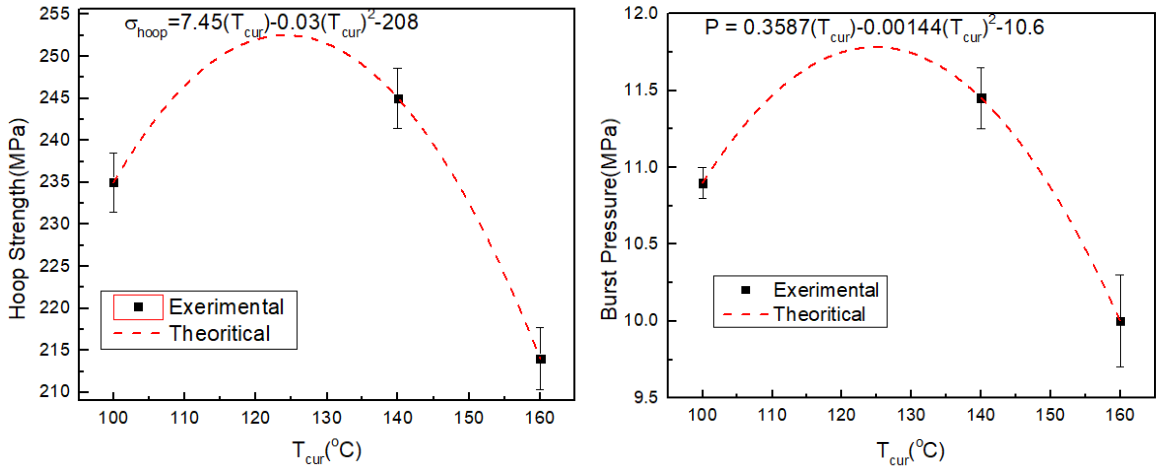

(a) **(b)**

Fig. 4(a) Hoop strength and (b) Burst pressure of cured specimens

Burst pressure were calculated theoretically for all samples from "(1)"[15] at various curing temperature.

$$S = \frac{P(d+t)}{2t} \qquad (1)$$

Whereas, S = hoop strength of specimens, P = burst pressure of specimens, d = diameter of specimens, and t = thickness of specimens. Maximum burst pressure allocated at 140°C as well and shown in fig.4 (b).

5. CONCLUSION

According to results, successful formation of ester linkages was established by characterizations i.e., FTIR and XRD. Whereas, it clearly shows that optimum curing has been achieved at 140°C. Calculated values of highest hoop strength and burst pressure further validated the optimum temperature of 140°C. Furthermore, at this curing temperature thermal stability has increased at optimally cured specimen when compared with other specimens. Therefore, it is recommended for steam pipe application.

6. ACKNOWLEDGMENT

We are very thankful to **Dr. Syed Nasir Shah** and **Dr.Bilal Islam** for their support and guidance in this research.

7. REFERENCES

[1] F. L. Jin, X. Li, and S. J. Park, "Synthesis and application of epoxy resins: A review," *J. Ind. Eng. Chem.*, vol. 29, pp. 1–11, 2015, doi: 10.1016/j.jiec.2015.03.026.

[2] Z. H. S. S, S. C. R, and A. K. L, "Investigation of compressive properties of 3D fiber reinforced polymeric

(FRP) composites through combined end and shear loading," *J. Mech. Eng. Res.*, vol. 7, no. 4, pp. 34–48, 2015, doi: 10.5897/jmer2015.0354.

[3] H. Venzlaff *et al.*, "Accelerated cathodic reaction in microbial corrosion of iron due to direct electron uptake by sulfate-reducing bacteria," *Corros. Sci.*, vol. 66, pp. 88–96, 2013, doi: 10.1016/j.corsci.2012.09.006.

[4] R. Javaherdashti, "How corrosion affects industry and life," *Anti-Corrosion Methods Mater.*, vol. 47, no. 1, pp. 30–34, 2000, doi: 10.1108/00035590010310003.

[5] O. S. David-West, D. H. Nash, and W. M. Banks, "An experimental study of damage accumulation in balanced CFRP laminates due to repeated impact," *Compos. Struct.*, vol. 83, no. 3, pp. 247–258, 2008, doi: 10.1016/j.compstruct.2007.04.015.

[6] Á. Pomázi and A. Toldy, "Development of fire retardant epoxy-based gelcoats for carbon fibre reinforced epoxy resin composites," *Prog. Org. Coatings*, vol. 151, 2021, doi: 10.1016/j.porgcoat.2020.106015.

[7] C. Yang and Z. G. Yang, "Synthesis of low viscosity, fast UV curing solder resist based on epoxy resin for ink-jet printing," *J. Appl. Polym. Sci.*, vol. 129, no. 1, pp. 187–192, 2013, doi: 10.1002/app.38738.

[8] N. Gao, W. Liu, Z. Yan, and Z. Wang, "Synthesis and properties of transparent cycloaliphatic epoxy-silicone resins for opto-electronic devices packaging," *Opt. Mater. (Amst).*, vol. 35, no. 3, pp. 567–575, 2013, doi: 10.1016/j.optmat.2012.10.023.

[9] H. Alhumade, H. Rezk, A. M. Nassef, and M. Al-Dhaifallah, "Fuzzy Logic Based-Modeling and Parameter Optimization for Improving the Corrosion Protection of Stainless Steel 304 by Epoxy-Graphene Composite," *IEEE Access*, vol. 7, no. July, pp. 100899–100909, 2019, doi: 10.1109/ACCESS.2019.2930902.

[10] I. J. Fernandesa, R. V. Santos, E. C. A. Dos Santos, T. L. A. C. Rocha, N. S. D. Junior, and C. A. M. Moraes, "Replacement of commercial silica by rice husk ash in epoxy composites: A comparative analysis," *Mater. Res.*, vol. 21, no. 3, 2018, doi: 10.1590/1980-5373-MR-2016-0562.

[11] D. Mamalis, T. Flanagan, and C. M. Ó Brádaigh, "Effect of fibre straightness and sizing in carbon fibre reinforced powder epoxy composites," *Compos. Part A Appl. Sci. Manuf.*, vol. 110, no. April, pp. 93–105, 2018, doi: 10.1016/j.compositesa.2018.04.013.

[12] N. Hameed, P. A. Sreekumar, B. Francis, W. Yang, and S. Thomas, "Morphology, dynamic mechanical and thermal studies on poly(styrene-co-acrylonitrile) modified epoxy resin/glass fibre composites," *Compos. Part A Appl. Sci. Manuf.*, vol. 38, no. 12, pp. 2422–2432, 2007, doi: 10.1016/j.compositesa.2007.08.009.

[13] P. Gañan, S. Garbizu, R. Llano-Ponte, and I. Mondragon, "Surface modification of sisal fibers: Effects on the mechanical and thermal properties of their epoxy composites," *Polym. Compos.*, vol. 26, no. 2, pp. 121–127, 2005, doi: 10.1002/pc.20083.

[14] ASTM, "D 2290 - Standard Test Method for Apparent Hoop Tensile Strength of Plastic or Reinforced Plastic Pipe by Split Disk Method," *An Am. Natl. Stand.*, vol. D 2290-00, pp. 1–5, 2003.

[15] T. Üstün, V. Eskizeybek, and A. Avci, "Enhanced fatigue performances of hybrid nanoreinforced filament wound carbon/epoxy composite pipes," *Compos. Struct.*, vol. 150, pp. 124–131, 2016, doi: 10.1016/j.compstruct.2016.05.012.

Performance evaluation of MXenes Used for Removal of Heavy Metals from Aqueous Stream

Muhammad Ilyas[1*], Mansoor Ul Hassan Shah [1], Mohammad Younas[1], Waheed Ur Rehman[2]
[1]Department of Chemical Engineering, University of Engineering and Technology, Peshawar
[2]Pakistan Council of Scientific and Industrial Research (PCSIR), Peshawar
[1*]Muhammad Ilyas
Email: milyas.che@uetpeshawar.edu.pk

Abstract—The use of 2D metal carbides, nitrides and carbonitrides (MXenes) in the treatment of heavy metals is becoming more and more widespread. MXenes have strong chemical compatibility, greater thermal stability, outstanding surface adjustable chemical compatibility, large surface area and biodegradable features. The oxidizing functional groups and accessible active binding sites of MXene nanoparticles make them a special adsorbent for eliminating heavy metals from waste-water because of their distinctive layered structure. Batch-mode investigations were carried out to ascertain the impact of several factors such as contact duration, adsorbent dosage, sample pH, temperature and initial concentration of polluted water on the adsorption of Lead (II). Using batch adsorption with optimum conditions, including pH is 10.0, adsorbent dosage is 0.01 g/ 50mL, contaminated water concentration is 100 mgL^{-1}, temperature is 298.15 K, agitation, and contact duration of 45 minutes, MXene was able to removed Lead (II) with a maximum removal rate of 96.3%. The adsorption capacity of MXene for elimination of lead (II) was 481.5 mg/g. Therefore, it can be said that MXene is a suitable adsorbent for remediation of Lead (II) metal ions from waste-water.

Keywords: 2D materials, Adsorption, Heavy Metals, MXene, Water Purification.

1. INTRODUCTION

Many factors can cause water contamination. The industrial waste and sewage from municipalities that are dumped into the rivers are the most polluting of them. Industrial waste can take many different forms, such as restaurant trash, soil and sand, brick and cement, scrap metals, rubbish, oil, solvents, chemicals, weed grass and trees, timber and scrap lumber, and other wastes [1]. Water contamination is a result of industrial waste water from manufacturing and chemical activities. Chemical substances that are distinct and easy to identify are typically present in industrial effluent [2,3].

The toxicity, mobility, and lack of biodegradability make heavy metals ions a significant global water hazard [4]. Arsenic, chromium, cadmium, nickel, selenium, mercury, zinc lead, and copper are heavy metal ions that are frequently detected in industrial and drinkable water [5]. High lead exposure levels can harm the kidneys and the brain in addition to causing anemia and weakness. Due to the fact that Pb may penetrate the placental barrier, pregnant women who are exposed to it also expose their unborn child. Different classical methods like chemical precipitation, flocculation & coagulation, solvent extraction, reverse osmosis, and many others are used to remediate these toxic metals from waste water. But these methods have some

draw backs like, lower efficiency, excess use of chemicals, weak selectivity, lower capacity and incomplete removal of pollutants etc. [6]. Adsorption is one of the most simple, efficient, and cost-effective procedures for waste-water treatment among the several water purifications processes [7]. Therefore, the removal of heavy metals ions needs the requirements of novel adsorbent which are feasible.

A growing amount of research has been done on 2D materials as a result of the discovery of graphene and its extraordinary features [8]. A recent addition to the two-dimensional material family is MXene. MXene was discovered in 2011 by Drexel institute [9,10]. MXenes are two-dimensional transition metal carbides, nitrides, and carbonitrides. General Formula of MXene is $M_{n+1}X_nT_z$ (n = 1–3) where M represent early d-block transition metals, X stands for C or N, T represents the surface termination groups like (fluoride, oxide, chloride, hydroxyl), and z, denotes the number of attached surface functionalities. [1,11]. MXenes structure are shown in **Fig. *1.1***. MXenes have tremendous characteristics like greater surface area, active metallic sides, bio- compatibility, substantial metallic conductance and many others make them an excellent choice for removing of heavy metallic ions from waste water treatment [12].

In this research, the elimination of Lead (II) ions on MXenes are carried out. The key objective of this study is to synthesis of MXenes from MAX phase by selective etching. Similarly, adsorption capacity and removal efficiency of MXenes were checked for remediation of Lead (II) ions from aqueous stream.

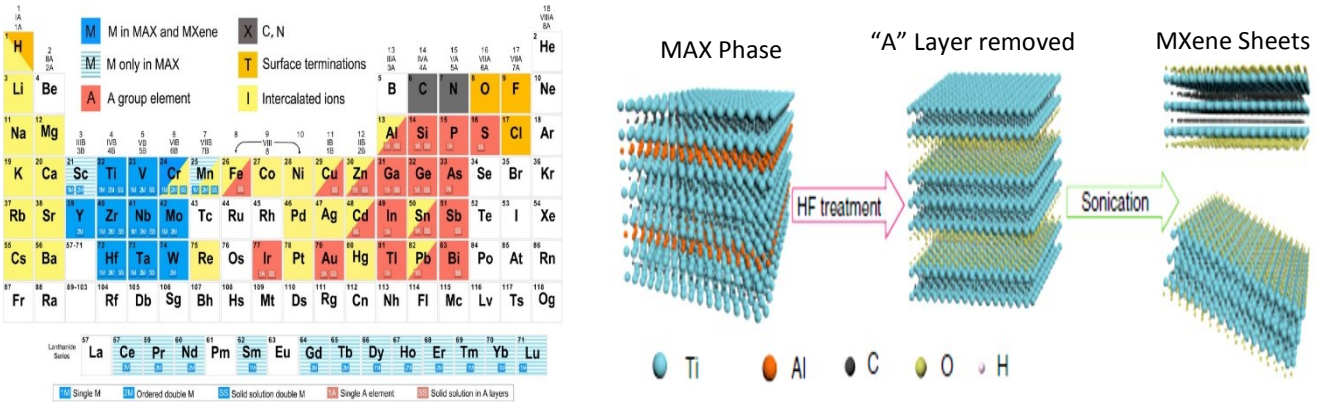

Fig. 1.1 Structure of MXene

2. METHODOLOGY

1.1 Materials

MAX Phase are purchased form Laizhou Kai Kai Ceramic Materials Co., Ltd., P.R. China. Metallic salt (Lead Nitrate), HCl, and NaOH, and DI water are brought form Haq Chemicals Ltd., Peshawar.

1.2 Synthesis of MXene

By using selective etching, MXenes are synthesized from MAX Phase. MAX phase [13–15]. Slowly add MAX phase in hydrofluoric acid (HF) in course time of 6 minutes to avoid excess bubbling and start the stirring. The reaction is proceeded for 5 hours. The HF would remove the “A” layer from MAX phase. After completion of reaction centrifuge the MXene to remove the supernatant liquids. Redisperse the MXene with deionized water (DI) to decrease the pH. Washing is carried out to remove the acid and gain the natural pH. Dry the MXene powder at 353.15 K in vacuum drier for 20 hours. For delamination of MXene, dimethyl sulfoxide (DMSO) is used. Stirrer the mixture for 12 hours to exfoliate the MXene sheets. Again, washing step is carried out to obtain the natural pH. After centrifugation, the MXene powders is dried at 393.15 for 24 hours. Sonication with argon gas was carried out for 6 hours to intercalate the particles. At last, the centrifugation was done to remove unexfoliated particles. Now the MXenes are ready for removal of heavy metals ions. MXene synthesis procedure and research methodology was shown in Figure 2..

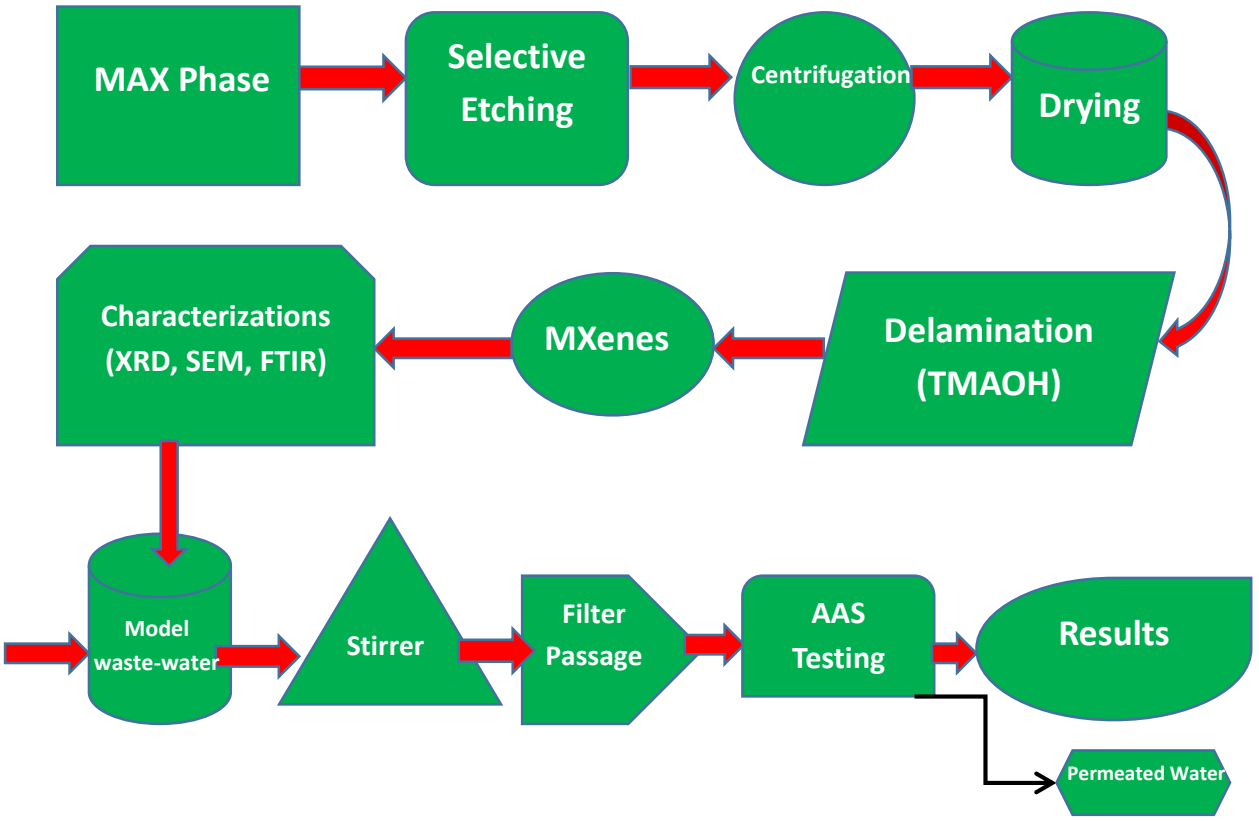

Figure 2.1 Research Methodology

1.3 Preparation of model waste water

By dissolving 1.598 g of Lead Nitrate in one Liter of de-ionized water, a 1000 mg/L concentrated standard synthetic lead contaminated wastewater was produced. A homogeneous Pb (II) contaminated water solution was produced after the system was stirred for a predetermined amount of time to completely dissolve the hazardous salt. The pH of the solution was kept at its natural pH value (6.0). The concentration of stock solution was diluted for rest of experiments.

1.4 Adsorption capacity

Batch adsorption studies was carried out. After optimizing the parameters, the adsorption capacity of MXene (481.5 mg/g) was achieved for elimination of Lead (II) from model waste water. MXene have high metallic conductivity due to which the heavy metals ions are strongly attached on the vacant sites of MXene. MXenes have large surface area. The entire surface is utilized in the adsorption process which enhance the capacity.

1.5 Removal Efficiency

In current study the removal efficiency of MXenes (96.3 %) was determined for Lead (II). The functional groups attached with the structure of MXene have greater affinity towards heavy metals ions. There is strong interaction between the adsorbent and adsorbate. That's why greater removal efficiency was achieved.

3. CONCLUSIONS

The two-dimensional (2D) transition metal carbide (MXenes) are successfully synthesized in this work. The developed MXenes are applied for removal of Lead (II) ions from an aqueous solution. MXene has a strong capacity for adsorbing lead (II) ions because of the substantial surface area and quantity of negatively surface functional groups. Similarly, MXenes showed higher effective elimination for remediation of lead (II). Hence, MXene is an ideal candidate for elimination of Lead (II) from waste-water.

4. REFERENCES

[1] K. Rasool, R.P. Pandey, P.A. Rasheed, S. Buczek, Y. Gogotsi, K.A. Mahmoud, Water treatment and environmental remediation applications of two- dimensional metal carbides (MXenes), Mater. Today. xxx (2019).

[2] Q. Wang, Z. Yang, Industrial water pollution, water environment treatment, and health risks in China, Environ. Pollut. 218 (2016) 358–365.

[3] M. Alcaraz, A. Calbet, M Sc Pl O E –, (2014).

[4] X. Xie, C. Chen, N. Zhang, Z.R. Tang, J. Jiang, Y.J. Xu, Microstructure and surface control of MXene films for water purification, Nat. Sustain. 2 (2019) 856–862.

[5] A.M. Nasir, P.S. Goh, M.S. Abdullah, B.C. Ng, A.F. Ismail, Adsorptive nanocomposite membranes for heavy metal remediation: Recent progresses and challenges, Chemosphere. 232 (2019) 96–112.

[6] A.K. Fard, T. Rhadfi, G. McKay, Y. Manawi, V. Kochkodan, O.S. Lee, M.A. Atieh, Two-dimensional mxene for efficient arsenic removal from aqueous solutions: Experimental and molecular dynamics simulation, Desalin. Water Treat. 211 (2021) 280–295.

[7] N.B. Singh, G. Nagpal, S. Agrawal, Rachna, Water purification by using Adsorbents: A Review, Environ. Technol. Innov. 11 (2018) 187–240.

[8] M. Ghidiu, M.R. Lukatskaya, M.Q. Zhao, Y. Gogotsi, M.W. Barsoum, Conductive two-dimensional titanium carbide "clay" with high volumetric capacitance, Nature. 516 (2015) 78–81.

[9] A.R. Khan, S.M. Husnain, F. Shahzad, S. Mujtaba-Ul-Hassan, M. Mehmood, J. Ahmad, M.T. Mehran, S. Rahman, Two-dimensional transition metal carbide (Ti3C2 T x) as an efficient adsorbent to remove cesium (Cs+), Dalt. Trans. 48 (2019) 11803–11812.

[10] Y. Tang, C. Yang, W. Que, A novel two-dimensional accordion-like titanium carbide (MXene) for adsorption of Cr(VI) from aqueous solution, J. Adv. Dielectr. 8 (2018).

[11] D. Xu, Z. Li, L. Li, J. Wang, Insights into the Photothermal Conversion of 2D MXene Nanomaterials : Synthesis , Mechanism , and Applications, 2000712 (2020).

[12] B.M. Jun, N. Her, C.M. Park, Y. Yoon, Effective removal of Pb(ii) from synthetic wastewater using Ti3C2T: X MXene, Environ. Sci. Water Res. Technol. 6 (2020) 173–180.

[13] B.M. Jun, J. Heo, N. Taheri-Qazvini, C.M. Park, Y. Yoon, Adsorption of selected dyes on Ti3C2Tx MXene and Al-based metal-organic framework, Ceram. Int. 46 (2020) 2960–2968.

[14] R. Chen, Y. Cheng, P. Wang, Q. Wang, Z. Yang, C. Tang, S. Xiang, S. Luo, S. Huang, C. Su, Y. Wang, Facile synthesis of a sandwiched Ti3C2Tx MXene/nZVI/fungal hypha nanofiber hybrid membrane for enhanced removal of Be(II) from Be(NH2)2 complexing solutions, Chem. Eng. J. 421 (2021) 129682.

[15] Z.H. Zhang, J.Y. Xu, X.L. Yang, MXene/sodium alginate gel beads for adsorption of methylene blue, Mater. Chem. Phys. 260 (2021) 124123.

Comparative study of CO_2 absorption performance of different frothing agents by process simulation

[1]*Muhammad Idress, [1]Sikandar Almani, [2]Masroor Abro.
Department of Chemical Engineering, Mehran UET Jamhsoro, Sindh, Pakistan
Corresponding author: idreesmuhammad441@gmail.com

Abstract— Continuous increase in the global warming resulting from emission of greenhouse gases, has been a serious challenge faced by the modern world. CO_2 is the major component among all greenhouse gases, which has touched the atmospheric concentration of 421 ppm in 2022. In this study, CO_2 capture performance of Na_2CO_3 mixed with different frothing agents (tri-ethylene glycol-butyl ether, diethylene-glycol diethyl ether, 1-hexanol, 1-octanol and 1-pentanol) at different molar concentration has been investigated and compared numerically using Aspen Plus software. Additionally, the effects of temperature and flowrate of liquid on absorption capacity of Na_2CO_3 were studied. The obtained results suggested that, absorption rate of dilute sodium carbonate was increased from 41% to 99.9% after the addition of frothing agents. Absorption capacity of Na_2CO_3 was decreased with increasing temperature.

Keywords— Absorption, Aspen Plus, CO_2, Frothing agents, Na_2CO_3.

1. INTRODUCTION

The rapid increase in global warming and crises of energy are two significant problems faced by modern world. Global warming is due to greenhouse gases and CO_2 is a main contributor

of greenhouse gases. Therefore, to reduce the CO_2 emissions, researchers have been trying hard to find out best possible alternatives such as use of renewable energy instead of fossil fuels [1]. The energy sector and production industries are the main responsible for increasing the concentration of greenhouse gases in atmosphere due to use of fossil fuels such as coal, for the production of electricity in power plants [2]. According to NOAA's Mauna Loa Atmospheric Baseline, CO_2 concentration in atmosphere was about 421 ppm in May 2022, 50% higher than pre-industrial levels.

Till now, several CO_2 capture technologies have been developed and investigated, to reduce the concentration of greenhouse gases in atmosphere, such as chemical absorption, physical absorption, adsorption, membrane separation, and cryogenics. Among all these technologies, absorption in a solvent has attracted the attention of scientists, researchers and industrialists especially in post combustion CO_2 capture system due to its various advantages such as having greater CO_2 absorption efficiency up to 99.9, this technology also adoptable at very low pressure conditions, easier recyclability of agents, eco-friendliness, absorbent availability and having ability to produce high purity up to 99% of CO_2 [3].

CO_2 absorption performance strongly depends upon choice of absorbents either in pure form or their mixture. Various chemical absorbents are investigated having ability to capture CO_2, such as amines, alkalis, ionic liquids ILs, amino acid salts and carbonate based absorbent [4]. Amine based absorbent have higher CO_2 capture ability but causing high corrosion in equipment and having high regeneration energy. Sodium carbonate is an ideal absorbent for CO_2 absorption system due to non-volatile, non-hazardous and non-corrosive in nature and having ability to capture multi-pollutant (CO_2, SOx and NOx) from flue gas [5] . However, the rate of physical mass transfer affects the CO_2 absorption rate in aqueous sodium carbonate solution. Consequently, enhancing the mass transfer kinetics with the addition of frothing agent can increase the CO_2 absorption efficiency of aqueous sodium carbonate solution. [6]. Use of a frothing agent in combination with basic sorbents could enhance the overall effectiveness of process under mild operating conditions since it alters the physical properties of basic sorbents which kinetically favors the absorption without changing their chemical structures. Frothing agents increase surface area by decreasing the bubble size that ultimately increases the mass transfer [7].

In this research, five frothing agents such as tri-ethylene glycol butyl ether (Poly-glycol), diethylene glycol diethyl ether (Poly-glycol), 1-pentanol, 1-hexanol and 1-octanol were used to check the performance of sodium carbonate (Na_2CO_3) for capturing carbon dioxide (CO_2) from flue gas and sensitivity of different operating parameters on removal efficiency were also investigated.

2. METHODOLOGY

2.1 MODEL DEVELOPMENT

Flowsheet designing for chemical process, simulation and process modeling plays an important role. Aspen Plus V11 simulator software is used in this study to estimate the overall material and energy balances for various flowsheet configuration for the mixture of aqueous sodium carbonate and frothing agent to capture CO_2 from flue gases. 0.1 Molar solution of sodium carbonate in combination with variable mole fraction of frothing agent in the range of 0.01 to 0.1 molar fraction is taken. Flue gas composition used in this study is given in Table 1.

TABLE I: COMPOSITION OF FLUE GAS

Parameter	Volume percent (%)
CO2	16
Air	84

All the parametric investigation were performed in the open loop model to identify the optimum operating conditions. The process models is created based on the initial column specification and operating parameters (Pressure, Temperature, Flowrate and Concentration) reported by [7]. Column specifications for the converging of model are given in Table 2.

The process models is created by using ELEC-NRTL thermodynamic model, equilibrium and kinetic data are selected from previously published literature. [8]

$$\ln(k) = \alpha i + \frac{bi}{T} + ciln(T) + diT \quad \rightarrow ELEC\ NRTL\ equation\ (1)$$

Where;

Ki is temperature dependent equilibrium constant

ai, bi, ci,di activity coefficient of species i

TABLE 2: COLUMN SPECIFICATION

Parameter	Specification
Column type	Packed bed
Packing material	Poly-propylene Pall rings
Packing dimension	1.2 cm * 1.2 cm
Packed bed height	121.92 cm
Height of the column	274.3 cm
Diameter	10.16 cm

In CO_2 capture system flue gases enters from bottom of the column while sorbent in combination with frothing agents enters from top of the column. Absorption process take place at packed bed section, mass transfer occur from gas phase to liquid phase. After absorption sweet gas exit out from top of the column and rich carbonate solution exit from bottom of the column.

The systematic diagram is shown in fig. 1.

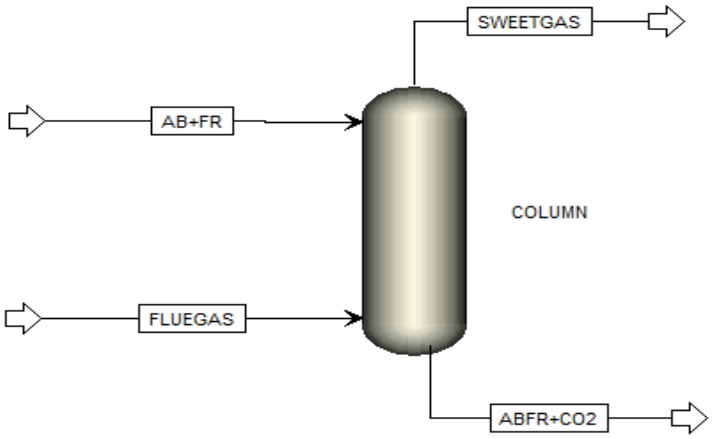

Fig. 1. Process flow diagram for CO_2 absorption system.

3. RESULTS AND DISCUSSION

3.1 Effect of Frothing agent mole fraction on CO_2 removal efficiency:

In this research, five frothing agents such as tri-ethylene glycol butyl ether (poly-glycol), diethylene glycol diethyl ether (poly-glycol), 1-pentanol, 1-hexanol and 1-octanol at different mole fraction (0.01 to 0.1) in combination with main sorbent used to check the effect on CO_2 removal efficiency. Table 3 shows the inlet operating conditions for the simulation of CO_2 scrubbing process were selected from previously published work [7].

TABLE 3: INLET OPERATING PARAMETERS FOR CO_2 CAPTURE SYSTEM

Parameter	Value
Temperature of flue-gas	31 °C
Pressure of flue-gas	101.3 KPa
Flowrate of flue-gas	1.74 lit/min
Sorbent temperature	38.5 °C
Sorbent pressure	101.3 KPa
Sorbent flowrate	7.5 lit/min

Figure 2 shows the performance of various frothing agents at different mole fraction. CO_2 removal efficiency increases as mole fraction of frothing agent increases. *Tri-ethylene glycol butyl ether and 1-Octanol* gave maximum CO_2 removal efficiency of 99.9% at 0.02 and 0.03 mole fraction. Di-ethylene glycol diethyl ether gave 99.8% of CO_2 removal efficiency at 0.05 mole fraction. Similarly, 1-Hexanol and 1-Pentanol gave 98% and 95% at 0.07 and 0.1 mole fraction respectively.

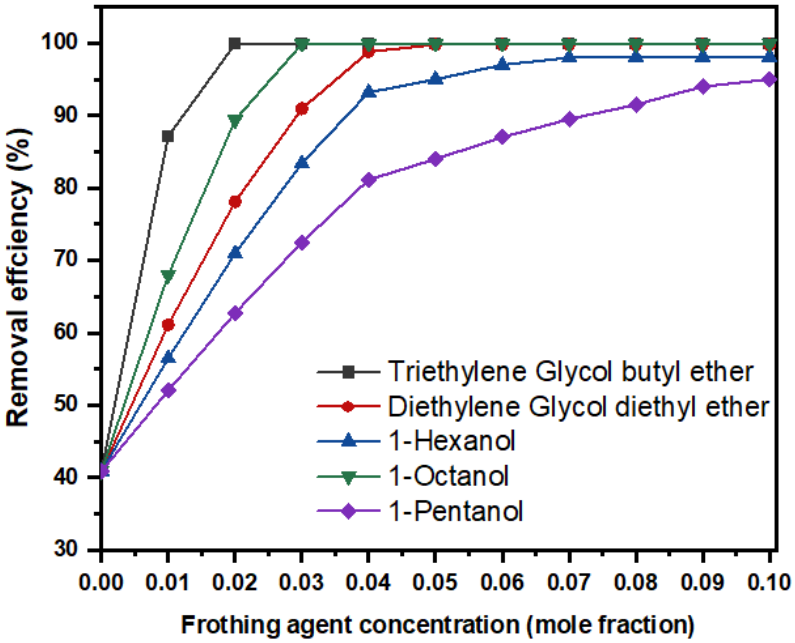

Fig. 2. Effect of frothing agent mole fraction on CO_2 removal efficiency.

I. Effect of sorbent temperature on CO_2 removal efficiency

Effect of temperature on CO_2 removal efficiency was investigated in the range of 35 °C to 65 °C. All other operating parameters (sorbent flowrate, pressure, flue gas flowrate and concentration) were remain constant. Fig 3 shows the effect of temperature on CO_2 removal efficiency. Results shows that as the temperature of sorbent increased, the CO_2 removal efficiency is decreased.

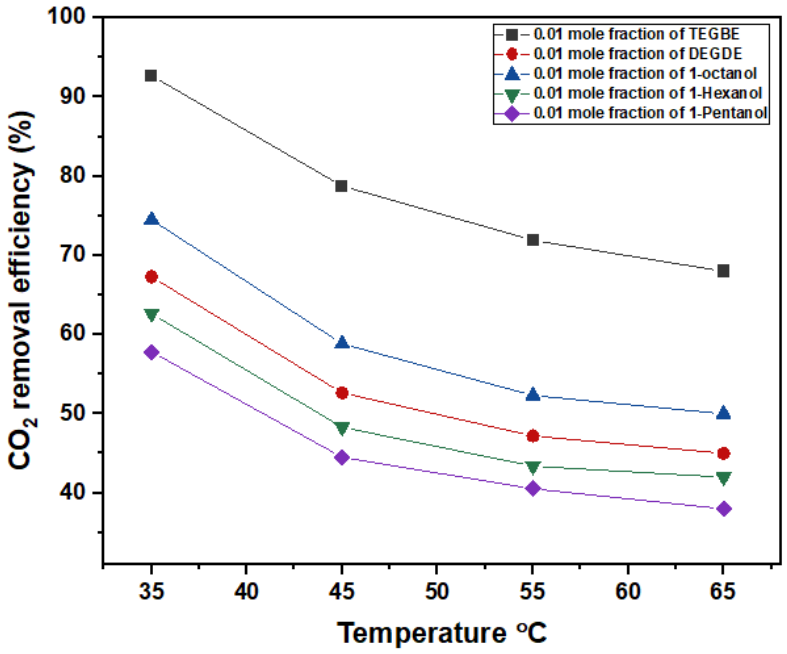

Fig. 3. Effect of temperature on CO_2 removal efficiency

1) Abbreviations and Acronyms

AB: Absorbent, FR: Frothing agent, TEGBE: Tri-ethylene glycol butyl ether, DEGDE: Di-ethylene glycol diethyl ether, CO_2: Carbon dioxide, Na_2CO_3: Sodium carbonate KPa: Kilo Pascal, lit/min: Litter/minute

2) Equations

The following equation is used to compute the CO_2 removal efficiency.

$$CO_2\ removal\ efficiency = \frac{Xi - Xf}{Xi} \times 100$$

Where Xi in the mole fraction of CO_2 in inlet flue gas stream and Xf is the mole fraction of CO_2 in sweet gas stream.

3) Other Recommendations

By this research, it has drawn that sodium carbonate used as an absorbent for CO_2 capture system because it shown excellent CO_2 efficiency in combination with frothing agents, it is easily available material at very low cost and having non corrosive in nature and low regeneration energy. More extensive work is required to capture other pollutants such as SOx

and NOx from flue gases. This present study can be used to replace other costly absorbents for CO_2 capture system.

4. CONCLUSION

CO_2 removal efficiency was investigated for different frothing agents combined with main sorbent. Effects of mole fraction and operating conditions were studied.
Following conclusions are drawn from this work;

- Increment in the CO_2 absorption efficiency was observed is a function frothing agent's mole fraction.
- Out of five frothing agents, Tri-ethylene glycol butyl ether and 1-Octanol have shown removal efficiency of 99.9%, which is maximum attainable efficiency.
- Effect of temperature on CO_2 removal efficiency was also investigated in the range of 35 °C to 65 °C. It was concluded that the CO_2 removal efficiency decreased with rising temperature.
- Effect of sorbent flowrate on CO_2 removal efficiency was investigated in the range of 5 to 10 L/min. rising trend between CO_2 removal efficiency and sorbent flowrate was observed.

ACKNOWLEDGMENT

I am very grateful to my research project supervisor **Dr. Masroor Ahmed Abro** and my co-supervisor, **Dr. Sikandar M. Almani** for their important contributions to my entire research project. They offer me a variety of assistance, resources, and their knowledge to help me get through any challenges I encountered while working on my ME project. They assisted me in refining and utilizing my thoughts across the board for my research.

5. REFERENCES

[1] T. Zhang, W. Zhang, R. Yang, Y. Liu, and M. Jafari, "CO 2 capture and storage monitoring based on remote sensing techniques : A review," *J. Clean. Prod.*, vol. 281, p. 124409, 2021.

[2] C. Dinca, N. Slavu, C. C. Cormoş, and A. Badea, "CO2 capture from syngas generated by a biomass gasification power plant with chemical absorption process," *Energy*, vol. 149, pp. 925–936, 2018.

[3] S. Yew, W. Chai, L. H. Ngu, B. S. How, and F. Engineering, "Review of carbon capture absorbents for CO 2 utilization," vol. 34, pp. 1–34, 2022.

[1] [4] P. Madejski, K. Chmiel, N. Subramanian, and T. Kus, “Methods and Techniques for CO 2 Capture : Review of Potential,” *Energies*, vol. 15, p. 887, 2022.

[5] S. Valluri and S. K. Kawatra, “Simultaneous removal of CO 2 , NO x and SO x using single stage absorption column,” *J. Environ. Sci.*, vol. 103, no. x, pp. 279–287, 2021.

[6] B. P. Spigarelli and S. K. Kawatra, “Opportunities and challenges in carbon dioxide capture,” *Biochem. Pharmacol.*, vol. 1, pp. 69–87, 2013.

[7] S. Valluri and S. K. Kawatra, “Use of frothers to improve the absorption efficiency of dilute sodium carbonate slurry for post combustion CO 2 capture,” vol. 212, no. August 2020, 2021.

[8] S. Masoudi, P. S. Fennell, and N. Mac, “International Journal of Greenhouse Gas Control A parametric study of CO 2 capture from gas- fi red power plants using monoethanolamine (MEA),” *Int. J. Greenh. Gas Control*, vol. 63, no. May, pp. 321–328, 2017.

Studying the effects of utilizing Pet Coke and Carbon Powder as an Alternative Fuel in Cement Kiln

Hina Sarwar[1*], Naveed ul Hasan Syed[2]
[1-2] Department of Chemical Engineering, University of Engineering and Technology Peshawar
[*]Corresponding author (lead presenter): Hina Sarwar (hinasarwar.che@uetpeshawar.edu.pk)

Abstract—The development of construction industry has certainly increased the demand of cement production and usage. On the other hand, cement manufacturing is considered as an energy intensive process in which the fuel demand is very high. Furthermore, the fuel crisis and fuel prices hike at national and international level is an alarming situation for the sustainable future of these industries. Therefore, researchers and industrialists are trying to find alternative fuel for cement industry which should be economically viable and cleaner solution. The main objective of this research work is to utilize Pet Coke and Carbon Powder as an alternate fuel in kiln of a cement industry and determine their effects on the product cost. In this study, up to 20% Pet coke and carbon powder are burnt in the cement kiln along with imported coal. The results showed that both alternative fuels increased carbon monoxide (CO) formation due to low volatile matters. Moreover, the particulate matters (PM) increased while using pet coke in comparison to the imported coal. It was found that the fuel cost reduced by using pet coke and carbon powder, however, the environmental pollution was increased.

Keywords: Cement industry, Carbon Powder, Fuel economy, Environment, Pet Coke

1. INTRODUCTION

One of the industries that uses the most energy is the cement industry. Sintering the cement clinker consumes the majority of the energy needed to produce cement. Hard coal, lignite, petroleum coke, and, to a minor extent, heavy fuel oil, are traditionally employed as the main energy sources. But there has been a rise in the usage of alternative fuels as an outcome of

changes in the legal and economic structure [1].

Cement manufacturers all over the world also employ alternative fuels as a source of energy. These fuels are typically made from a combination of municipal, industrial, and hazardous wastes. Solid or liquid alternative fuels are both used in the cement industry. Depending on the kind of components and the amount of organic material they contain, they must have an acceptable chemical content [2].

The solid waste product that remains after all of the valuable liquid and gaseous components of crude oil have been extracted is known as petroleum coke (petcoke). The calorific value, sulphur content, and volatile content of petcoke are all high. Low volatile concentrations result in poor fuel combustion, and high sulphur contents cause a number of issues with kiln operation. Petcock is used extensively in the cement industry, but because of the difficulties involved, it could not be employed entirely in the kiln and pre-calciner without change to the current system [3].

When gaseous or liquid hydrocarbons are partially burned or thermally decomposed under controlled circumstances, Carbon Powder is created, which is pure elemental carbon in the form of colloidal particles. It has a black exterior and takes the form of a finely ground pellet or powder. It relates to specific surface area, particle size, structure, conductivity, and colour qualities and is employed in tyres, rubber, plastic goods, printing inks, and coatings. In the rubber sector, Carbon Powder is used in over 90% of cases [4].

The specific objective of this study is to i) utilize Pet coke and carbon powder as an alternative fuel in cement industry ii) exploring the effects of utilizing alternative fuels on fuel cost and emissions of cement industry. This study is closely related to the practical needs of using alternative fuels and provides some important insights for saving fuel cost and emissions related to cement production.

2. METHODOLGY

i. Pet Coke and Carbon Powder Analysis

Pet coke consignment came from foreign country. Carbon Powder came from local supplier. The chemical composition of imported coal, Pet coke and carbon powder is shown in Table 1. Pet coke and carbon powder contains more carbon contents and sulphur contents than imported coal.

Table 1: The Chemical composition of the Imported Coal, Pet coke and Carbon Powder

S.No	Description	Imported Coal	Pet Coke	Carbon Powder
1	Carbon (%)	70.94	86.62	74.46
2	Hydrogen (%)	4.22	3.90	4.50
3	Nitrogen (%)	1.74	1.61	8.22
4	Sulphur (%)	0.79	5.24	3.23
5	Oxygen (%)	3.85	1.69	10.00
6	Ash (%)	18.46	0.94	16.03

Table 2 show the Net Calorific Value (NCV), Flash points, Fire points and densities of both used transformer oil and imported coal. Due to high carbon contents, Pet coke and Carbon Powder has higher calorific value than imported coal. Calorific value is determined through bomb calorimeter at plant laboratory.

Table 2: The Properties of the Imported Coal, Pet coke and Carbon Powder

S.No	Description	Imported Coal	Pet Coke	Carbon Powder
1	Net Calorific Value (Kcal/Kg)	5943	7436	6315
2	Flash Point (°C)	420	550	535
3	Fire Point (°C)	520	595	578
4	Density (kg/m3)	1720	2210	863

ii. Pet Coke and Carbon Powder Incineration in Kiln

Coal burning system used for burning of coal in kiln through main burner is used for Pet coke incineration. Special type of burner used in cement industry is Duolfex burner which fires rotary kilns with pulverized coal, oil and natural gas. Pet coke is burnt in Kiln at temperature of about 1400°C and 3.0% oxygen with imported coal separately. Three trials of pet coke were done at substitution rate of 10%, 15% and 20% along with imported coal. The same process is repeated for Carbon Powder utilization at 10%, 15% and 20% substitution with imported coal.

iii. Stack Emission Monitoring

Stack gas monitoring was done at the time of burning of pet coke and Carbon Powder to study effect on environment with the help of flue gas analyzer. Flue gas analyzer used for stack emission monitoring.

3. RESULTS AND DISCUSSION

i. Economic Effects of Pet coke and Carbon Powder

In order to assess the economic benefits of Pet Coke utilization, an economic model proposed by [5] has been used. Pet Coke is utilized at ratios of 10%, 15% and 20%.

The below are the parameters of cement plant in which experimentation taken place:

a) Daily kiln production quantity is 7000 T/day (24 h)
b) Number of total operating hours is 5880 h/year @ 67% run factor.
c) Daily imported coal consumption is 860 ton/ day, which equals 35.83 kg/hr.
d) Total energy consumption is 730 kcal/kg.cl.
e) Total energy consumption for the clinker stage is 26 kWh/t.
f) The calorific value of imported coal equals 5943 kcal/kg.
g) 1 ton of imported coal costs 236 USD (41,667 PKR).
h) The calorific value of Pet Coke equals 7436 kcal/kg.

Below are the calculations of fuel cost determination:

Total heat required for production of 7000 T/day clinker

= 7000 T/day × 730 kcal/kg.cl × 1000 $= 5.11 \times 10^9$ kcal

Heat required for 20% substitution of Pet Coke:

= 0.20 × 5.11 × 10^9 kcal = 1.02 × 10^9 kcal

Quantity required for 20% substitution of Pet Coke

= 1.02 × 10^9 kcal/ 7436 kcal/kg / 1000 = 137 T

Total cost for 137 T Pet Coke per hour is

= 137 T × 225.17 USD/T = 30,948 USD = 5.45 × 10^6 PKR

Fuel cost per ton of clinker for 20% Pet Coke is:
= 30,948 USD/7000 T = 4.42 USD/T.cl. = 779.75 PKR/T.cl.

Similarly, fuel cost for 80% imported coal is:

= 1.63 × 10^5 USD/7000 T = 23.22 USD/T.cl. = 4095 PKR/T.cl.

Total fuel cost with 20% Pet Coke and 80% imported coal is:

= 4.42 USD/T.cl. + 23.22 USD/T.cl. = 27.64 USD/T.cl. = 4874 PKR/T.cl

Fuel cost for 100% imported coal utilization is:

= 2.03 × 10^5 USD/7000 T = 29.02 USD/T.cl. = 5118 PKR/T.cl.

Saving of fuel cost by using 20% Pet Coke is:

= 29.02 USD/T.cl. - 27.64 USD/T.cl. = 1.38 USD/T.cl. = 244 PKR/T.cl

Table 3 shows the comparison of fuel cost and net savings per day while using 10%, 15 % and 20 % Pet Coke along with imported coal. Comparison shows that while using 20% Pet Coke with 80% imported coal, saving of 243 PKR per ton of clinker can be achieved. This will lead to saving of almost 1.7 million per day.

Table 3: Saving of fuel cost by using Pet Coke

Parameters	**Unit**	**100% Imported Coal**	**10% Pet Coke**	**15% Pet Coke**	**20% Pet Coke**
Pet Coke substitution	%	0	10	15	20
Imported Coal substitution	%	100	90	85	80
Pet Coke consumption	T/h	0	69	103	137
Imported coal consumption	T/h	860	774	731	688
Fuel cost Pet Coke	USD/T.cl.	0	2.21	3.32	4.42
	PKR/T.cl.	0	390	585	780
Fuel cost Imported coal	USD/T.cl.	29.02	26.12	24.67	23.22
	PKR/T.cl.	5118	4606	4350	4095
Net Savings (per T.cl.)	USD/T.cl.	0	0.69	1.04	1.38
	PKR/T.cl.	0	122	183	243
Net Savings (per Day)	USD/Day	0	4,847	7,270	9,654
	PKR/Day	0	854,864	1,282,296	1,702,728

Table 4 shows the comparison of fuel cost and net savings per day while using 10%, 15 % and 20 % Carbon Powder along with imported coal. Comparison shows that while using 20% Carbon Powder with 80% imported coal, saving of 711 PKR per ton of clinker can be achieved. This will lead to saving of almost 5 million per day.

Table 4: Saving of fuel cost by using Carbon Powder

Parameters	**Unit**	**100% Imported Coal**	**10% CP**	**15% CP**	**20% CP**
Carbon Powder substitution	%	0	10	15	20
Imported Coal substitution	%	100	90	85	80
Carbon Powder consumption	T/h	0	81	121	162
Imported coal consumption	T/h	860	774	731	688
Fuel cost Carbon Powder	USD/T.cl.	0	0.88	1.33	1.77
	PKR/T.cl.	0	156	234	312
Fuel cost Imported coal	USD/T.cl.	29.02	26.12	24.67	23.22
	PKR/T.cl.	5118	4606	4350	4095
Net Savings (per T.cl.)	USD/T.cl.	0	2.02	3.02	4.03
	PKR/T.cl.	0	356	534	711
Net Savings (per Day)	USD/Day	0	14,106	21,159	28,212
	PKR/Day	0	2,491,601	3,737,401	4,976,202

Figure 1 shows that carbon powder utilizations result in more saving as compared to pet coke

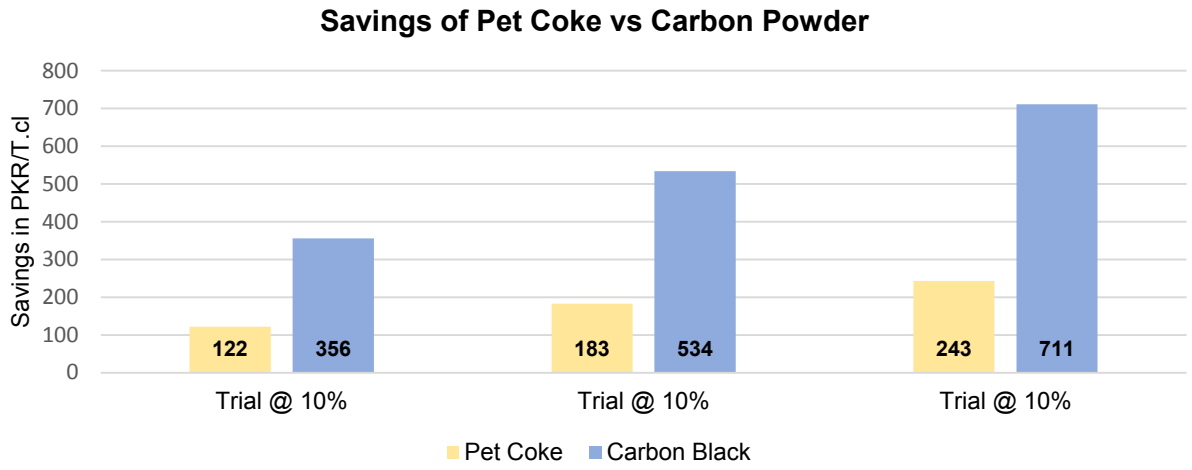

Figure 1: Savings of Pet Coke and Carbon Powder

ii. Environmental impacts of Pet coke and Carbon Powder

According to Punjab Environmental Quality Standards for Industrial Gaseous Emissions by Environmental Protection department in Pakistan, particulate matter (PM), carbon monoxide, sulphur oxides were monitored during incineration of alternative fuels and their results are shown in Table 5.

Table 5: Stack Emissions of Pet Coke and Carbon Powder

Parameters	Unit	PEQS Limits	Imported Coal @ 100%	Trial 1 @ 10% Pet coke	Trial 2 @ 15% Pet coke	Trial 3 @ 20% Pet coke	Trial 1 @ 10% CB	Trial 2 @ 15% CB	Trial 3 @ 20% CB
Particulate matter (PM)	mg/Nm^3	300	38	45	56	65	42	48	54
Carbon Monoxide (CO)	mg/Nm^3	800	480	524	538	560	505	520	535
Oxides of Nitrogen (NO_x)	mg/Nm^3	1200	540	530	535	545	555	575	593
Sulphur Oxides (SO_x)	mg/Nm^3	1700	180	230	255	269	196	225	248

Results show that particulate matter, carbon monoxide and sulphur dioxide increase more with the increase in utilization percentage of pet coke as compared to Carbon Powder. However, NO_x increases more in case of carbon as compared to pet coke due to high percentage of nitrogen in Carbon Powder.

Figures 2 and 3 show that both pet coke and Carbon Powder emissions are greater than that of imported coal. Due to high sulphur contents in pet coke its SO_x emissions are higher.

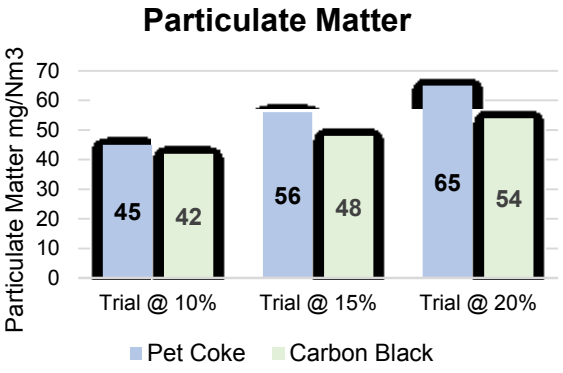

Figure 2: Particulate Matter Emission

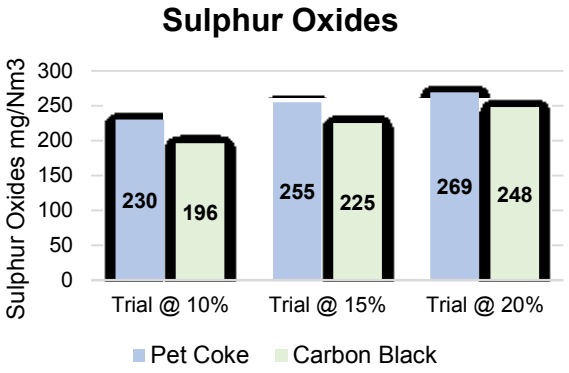

Figure 3: Sulphur Oxides Emission

iii. Carbon Dioxide Emissions

Carbon dioxide emissions standard is not given by Environmental Protection department in Pakistan. To calculate carbon dioxide emissions, method used by [6] is used.

The emission factors for fuel combustion are taken from IPCC 2006 Guidelines, where the default emission factors of CO_2 for coal, Pet Coke and Carbon Powder are 94,600,97,500 and 99,160 kg/TJ respectively. To calculate emission factor for utilized fuel, given emission factor for fuel type is multiplied by actual lower heating value of fuel as per given formula

Corrected CO_2 = Default EF_{CO2} of fuel (kg CO_2/ TJ) × Average heat value of fuel (kJ/kg)

a. Corrected CO_2 for Coal:

= 94,600 kg CO_2/TJ Coal × 24,866 kJ/kg Coal × 10^{-9}

= 2.35 kg CO_2/kg Coal

b. Corrected CO_2 for Pet Coke:

= 97,500 kg CO_2/TJ Pet Coke × 31,112 kJ/kg Pet Coke × 10^{-9}

= 3.03 kg CO_2/kg Pet Coke

c. Corrected CO_2 for Carbon Powder:

= 99,160 kg CO_2/TJ Carbon Powder × 26,422 kJ/kg Carbon Powder × 10^{-9}

= 2.62 kg CO_2/kg Carbon Powder

Carbon dioxide emission is more in case of Pet Coke and Carbon Powder due to high carbon content as compared to imported coal.

4. CONCLUSION

From the above experiment it can be concluded that Pet coke and Carbon powder can be incinerated in cement Kiln with saving in fuel cost. However, emissions like particulate matter, CO, NO_x and CO_2 increases with increase in utilization of Pet coke and Carbon powder. Emissions are more prominent in case of pet coke due to its high sulphur and carbon contents. However, the emissions are still below than EPA standards limit. So, both fuels can be used in kiln and result in saving of fuel cost. Carbon powder is more cost-effective fuel as compared to pet coke due to its less price per ton.

5. ACKNOWLEDGMENT

First and foremost, praises and thanks to Allah, the Almighty, the Most Gracious, and the Most Merciful for His blessing given to me during my research study and in completing this conference paper.

I would like to express my sincere gratitude to my advisor Professor Syed Naveed ul Hassan for his continuous support and guidance in research and writing. Then, I will thank my university for giving me this opportunity to write this conference paper.

6. REFERENCES

[1] Schmidt, Mario, Hannes Spieth, Christian Haubach, and Christian Kühne. "Alternative fuel for the cement industry." In 100 Pioneers in Efficient Resource Management, pp. 506-509. Springer Spektrum, Berlin, Heidelberg, 2019.

[2] Chatziaras, N., C. S. Psomopoulos, and N. J. Themelis. "Use of alternative fuels in cement industry." In Proceedings of the 12th International Conference on Protection and Restoration of the Environment, vol. 1, pp. 521-529. ISBN, 2014.

[3] Olmeda, Javier, MI Sánchez De Rojas, Moisés Frías, Shane Donatello, and C. R. Cheeseman. "Effect of petroleum (pet) coke addition on the density and thermal conductivity of cement pastes and mortars." Fuel 107 (2013): 138-146.

[4] International Carbon Powder Association. "Carbon Powder User's Guide, Safety, Health, & Environmental Information." International Carbon Powder association (2004).

[5] Hemidat, Safwat, Motasem Saidan, Salam Al-Zu'bi, Mahmoud Irshidat, Abdallah Nassour, and Michael Nelles. "Potential utilization of RDF as an alternative fuel to be used in cement industry in Jordan." Sustainability 11, no. 20 (2019): 5819.

[6] Shan, Yuli, Zhu Liu, and Dabo Guan. "CO_2 emissions from China's lime industry." Applied energy 166 (2016): 245-252.

Enhancing efficiency and stability of non-toxic Pb-free $MASnBr_3$ PSC with $CuAlO_2$ as inorganic p-type semiconductor by using 1D-SCAPS.

Khalid Afridi[1*], Muhammad Noman[1], Shayan Tariq Jan[1]
[1]U.S.-Pakistan Center for Advanced Studies in Energy, University of Engineering & Technology, Peshawar, Pakistan
khalidafridi.uspcase@uetpeshawar.edu.pk

***Abstract*—**Organic-Inorganic metal halide perovskite solar cells device has (PSC) fascinated researcher attention from all over the world. A non-toxic Sn-based PSC has similar photo electronic properties to that of lead based PSC. In this report work the structure consist of C_{60} as electron transport material (ETM) and $CuAlO_2$ as hole transport material (HTM) with lead free non-toxic $MASnBr_3$ as perovskite active layer. A numerical modeling of $MASnBr_3$ PSC has been investigated by utilizing 1D SCAPS simulation software. Investigation of the most important parameter such as thickness of each layers has been optimized to advance the stability and enhance the power conversion efficiency of the device. The inverted arrangement ITO/$CuAlO_2$/$MASnBr_3$/C_{60}/Al exhibit maximum PCE 16.34%, FF 89.19%, V_{OC} 1.49 V and J_{SC} 12.29 mA/cm^2 with 400 nm of absorber thickness. The device has shown a good thermal stability.

Keywords—1D-SCAPS, fullerene C_{60}, $MASnBr_3$, perovskite solar cell, stability

1. INTRODUCTION

In photovoltaic technology perovskite solar cell (PSC) has developed one of the most capable device with power conversion efficiency (PCE) of greater than 25% [1]. While stability and toxicity are the most serious factor, which is the hurdled towards industrialization [2]. However organic-inorganic metal halide perovskite is non-toxic such as Sn- based Pb free PSC is used instead of toxic lead perovskite device [3]. The active layer of the structure consists of ABX_3, where A is an organic methyl ammonium (MA) or formamidinium (FA), B is inorganic cation such as (Pb^+ or Sn^+) and X represent halogen ions (I^-, Br^-, or Cl^-) [4]. The PCE of the perovskite has been improved from 3.8% in 2009 to 22.1% in 2016 [5]-[6]. It is found that $MASnBr_3$ is highly stable and efficient perovskite [7]. Spiro-OMeTAD is the material that is extensively used for HTM and TiO_2 for ETM, while they are unstable material [8]. Therefor inorganic p-type semiconductor such as $CuAlO_2$ has shown good stability and are highly transparent [9]. The n-type organic material C_{60} has been studied as the best ETM candidate for good presentation of the device [10].

2. DEVICE STRUCTURE AND METHODOLOGY

The inverted planar p-i-n design of perovskite solar cell (PSC) is presented in Fig.1. which consist of three layer i.e. ETL, active layer and HTL. These layers are stacked to each other. The performance of the device is analyzed by using 1D-SCAPS simulation software. The equation used for numerical analysis in the calculation of the output result in the software is based on Poisson's eq and continuity eq (1) which are given below;

$$\nabla^2\Psi = \frac{q}{\varepsilon}(n - p + N_A + N_D)(1)$$

Where N_A and N_D represent (acceptor and donor) concentration; ψ denote electrostatic potential. Continuity equation for semiconductor is given by eq (2) and (3);

$$\nabla . J_n - q\frac{\partial n}{\partial t} = +qR\ (2)$$

$$\nabla . J_p - q\frac{\partial p}{\partial t} = -qR\ (3)$$

Where J_n and J_p are current densities for electron and holes; R denote carrier recombination rate.

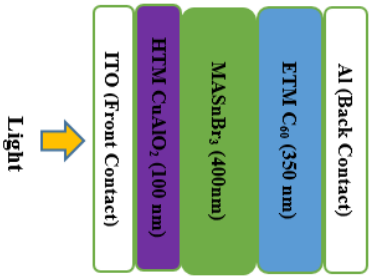

Fig.1. General Design of inverted p-i-n Perovskite Solar cell

3. RESULTS AND DISCUSSION

a. Thickness Optimization of Active layer ($MASnBr_3$), HTM and ETM

The thickness of active layer and charge transport layer (CTL) play a vital part in the presentation of the device efficiency. Parameter of the device were used from TABLE.1. At start the active layer thickness is simulated from 50 (nm) to 750 (nm) with step of 50 (nm) keeping the other parameter of the device constant. In Fig.1. (a), (c) & (d) it is shown that up to 400 nm PCE, V_{OC}, J_{SC} was increased which indicate that up to certain thickness the generation of charge is increased while beyond that thickness the drop of all parameter is due to rise in recombination rate. while in Fig.1. (b) FF increased till 200 nm and beyond it start decreasing is because of increase in charge pathway resistance [11]. The optimized value is used for the analysis of CTL thicknesses and their results are displayed in Fig. 3 show effect of HTM thickness with 100 nm enhanced value and Fig. 4 of ETM giving the best performance with 350 nm.

TABLE I: INPUT PARAMETER FOR HTL, ETL AND ABSORBER LAYER [12],[13],[14].

	$CuAlO_2$	C_{60}	$MASnBr_3$
Bandgap E_g (eV)	3.46	1.70	2.15
Electron affinity X (eV)	2.50	3.90	3.39
Dielectric permittivity ε_r (relative)	60.00	4.20	8.2
CB effective density of state N_C ($1/cm^3$)	1×10^{18}	1×10^{18}	1×10^{18}
VB effective density of state N_V ($1/cm^3$)	1×10^{18}	1×10^{18}	1×10^{18}
Electron mobility μ_n (cm^2/Vs)	2.00	8.00×10^{-2}	1.6

Hole mobility μ (cm^2/Vs)	8.60	3.50×10^{-3}	1.6
shallow uniform donor density N_D	0	1×10^{18}	0
shallow uniform acceptor density N_A	1×10^{18}	0	1×10^{17}
Defect density N_t	1×10^{14}	1×10^{14}	1×10^{15}

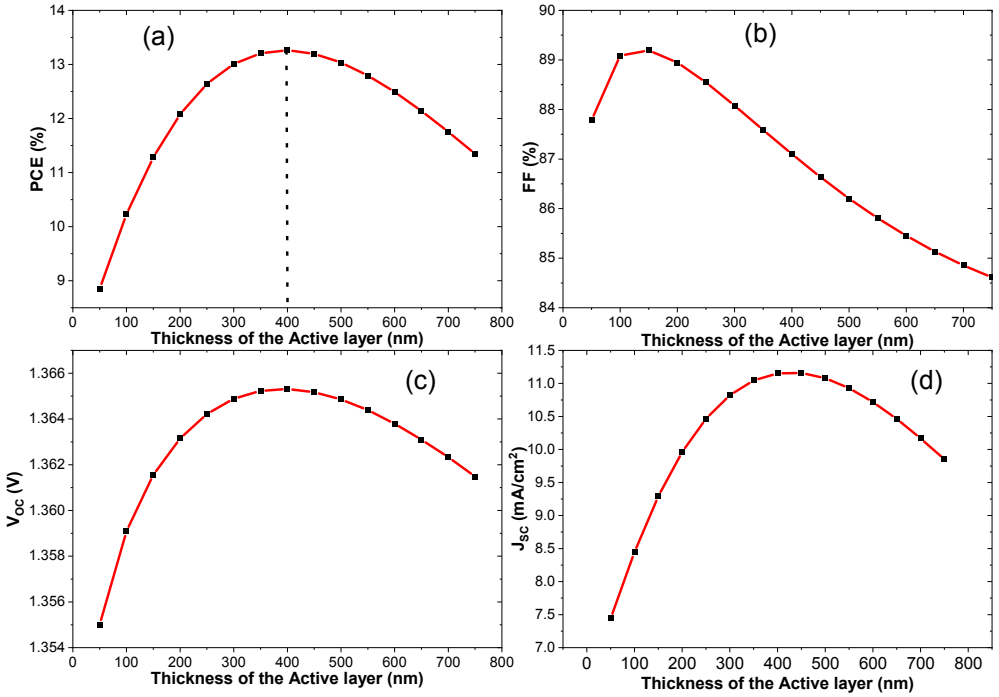

Fig.2.Effect of Active layer thickness on (a) PCE (b) FF (c) V_{OC} (d) J_{SC} .

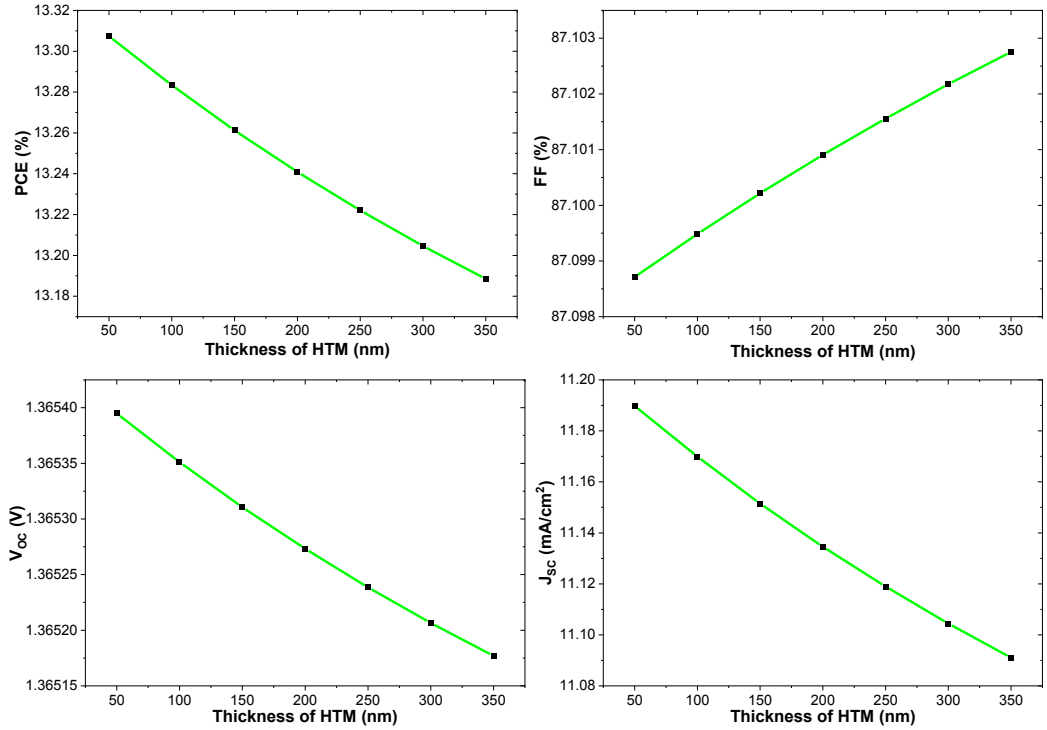

Fig.3.Effect of HTL thickness on (a) PCE (b) FF (c) V_{OC} (d) J_{SC}.

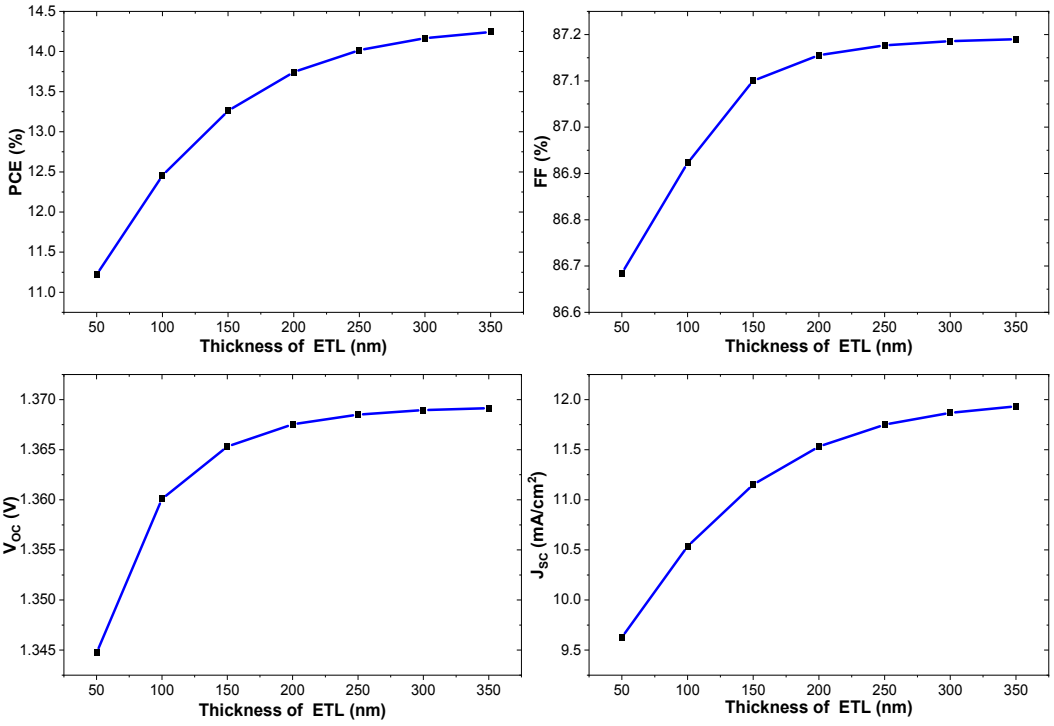

Fig.4.Influence of ETM thickness on (a) PCE (b) FF (c) V_{OC} (d) J_{SC}.

B. J-V Curve and External Quantum Efficiency EQE of Optimized Structure

To know the effect of quantum efficiency when different wavelength of photon incident on the device. It is varied starting with 300 nm to 900 nm. The EQE graph is shown Fig.5. (a) which reveals that the photon of shorter wavelength (350nm to 550nm) is

absorbed with external quantum efficiency EQE of more than 80% beyond that the EQE drop drastically due to low energy photon. The J-V characteristics of the improved configuration of perovskite device is shown in Fig.5. (b) wheres the J_{sc} is 11.16% and V_{OC} is 1.38 V with PCE of 16.38%.

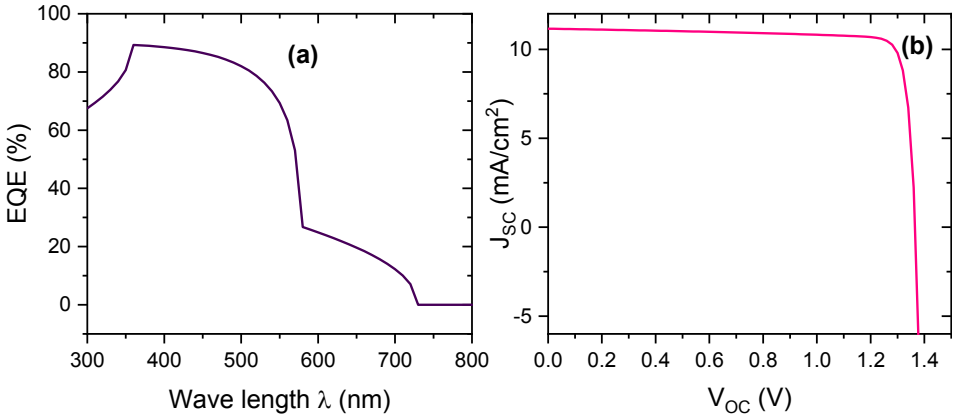

Fig.5. (a) Different wavelength photon effect on EQE (b) J-V Characteristics

4. CONCLUSION

A comprehensive analysis simulation of the lead free perovskite device is examined by using 1D-SCAPS. The stability of the device has been enhanced with efficient output by optimization of thickness of each layer. The high transparency of the inorganic copper based HTM $CuAlO_2$ due to its wide bandgap (3.46 eV) which has improved the efficiency. If $MASnBr_3$ with a wide bandgap of 2.15eV is replaced with narrow bandgap $MASnI_3$ of 1.3 eV. the conversion efficiency of the device can be further enhanced due to its high absorption property having similar optoelectronic properties to Pb-based perovskite.

5. REFERENCES

[1] E. M. Younes, A. Gurung, B. Bahrami, E. M. El-Maghraby, and Q. Qiao, “Enhancing efficiency and stability of inverted structure perovskite solar cells with fullerene C60 doped PC61BM electron transport layer,” *Carbon N. Y.*, vol. 180, pp. 226–236, 2021, doi: 10.1016/j.carbon.2021.05.008.

[2] A. K. Jena, A. Kulkarni, and T. Miyasaka, “Halide Perovskite Photovoltaics: Background, Status, and Future Prospects,” *Chem. Rev.*, vol. 119, no. 5, pp. 3036–3103, 2019, doi: 10.1021/acs.chemrev.8b00539.

[3] L. Hao *et al.*, “A tin-based perovskite solar cell with an inverted hole-free transport layer to achieve high energy conversion efficiency by SCAPS device simulation,” *Opt. Quantum Electron.*, vol. 53, no. 9, pp. 1–17, 2021, doi: 10.1007/s11082-021-03175-5.

[4] D. Jayan K. and V. Sebastian, “Comparative Study on the Performance of Different Lead-Based and Lead-Free Perovskite Solar Cells,” *Adv. Theory Simulations*, vol. 4, no. 5, pp. 1–11, 2021, doi: 10.1002/adts.202100027.

[5] A. Kojima, K. Teshima, Y. Shirai, and T. Miyasaka, “Organometal halide perovskites as visible-light sensitizers for photovoltaic cells,” *J. Am. Chem. Soc.*, vol. 131, no. 17, pp. 6050–6051, 2009, doi: 10.1021/ja809598r.

[6] U. Mandadapu, S. V. Vedanayakam, K. Thyagarajan, M. R. Reddy, and B. J. Babu, “Design and simulation of high efficiency tin halide perovskite solar cell,” *Int. J. Renew. Energy Res.*, vol. 7, no. 4, pp. 1604–1612, 2017.

[7] S. Islam, K. Sobayel, A. Al-kahtani, M. A. Islam, and G. Muhammad, “Defect Study and Modelling of SnX3-Based Perovskite Solar Cells with SCAPS-1D,” 2021.

[8] A. K. Singh, S. Srivastava, A. Mahapatra, J. K. Baral, and B. Pradhan, “Performance optimization of lead free-MASnI3 based solar cell with 27% efficiency by numerical simulation,” *Opt. Mater. (Amst).*, vol. 117, no. May, p. 111193, 2021, doi: 10.1016/j.optmat.2021.111193.

[9] M. Shasti and A. Mortezaali, “Numerical Study of Cu2O, SrCu2O2, and CuAlO2 as Hole-Transport Materials for Application in Perovskite Solar Cells,” *Phys. Status Solidi Appl. Mater. Sci.*, vol. 216, no. 18, 2019, doi: 10.1002/pssa.201900337.

[10] A. Hima and N. Lakhdar, “Enhancement of efficiency and stability of CH3NH3GeI3 solar cells with CuSbS2,” *Opt. Mater. (Amst).*, vol. 99, no. November 2019, p. 109607, 2020, doi: 10.1016/j.optmat.2019.109607.

[11] I. Alam and M. A. Ashraf, “Effect of different device parameters on tin-based perovskite solar cell coupled with In2S3 electron transport layer and CuSCN and Spiro-OMeTAD alternative hole transport layers for high-efficiency performance,” *Energy Sources, Part A Recover. Util. Environ. Eff.*, vol. 00, no. 00, pp. 1–17, 2020, doi: 10.1080/15567036.2020.1820628.

[12] Q. J. and P. M. Yongjin Gan, Xueguang Bi, Yucheng Liu, Binyi Qin, Qingliu Li, “Using Cell Capacitance Simulator,” *Energies*, 2020.

[13] F. Igbari, M. Li, Y. Hu, Z. K. Wang, and L. S. Liao, “A room-temperature CuAlO2 hole interfacial layer for efficient and stable planar perovskite solar cells,” *J. Mater. Chem. A*, vol. 4, no. 4, pp. 1326–1335, 2015, doi: 10.1039/c5ta07957h.

[14] X. Liu *et al.*, “Novel efficient C60-based inverted perovskite solar cells with negligible hysteresis,” *Electrochim. Acta*, vol. 288, pp. 115–125, 2018, doi: 10.1016/j.electacta.2018.09.004.

Utilization of Potato and Wheat Waste for Starch Synthesis along with Kinetic Study

[1]Author, Sundus Khushnood., [1]*Second-Author, Dr. Javaid Rabbani Khan.,
[2]Third Author, Dr. Abdul Qadeer Malik
[1]umerbinyasir1991@gmail.com, Ghulam Ishaq Khan Institute, Topi, Swabi, Pakistan
[2] National University of Engineering Science and Technology , Islamabad, Pakistan
Corresponding author (Sundus Khushnood): umerbinyasir1991@gmail.com

Abstract—Mankind has explored the natural resources of earth without limits, including extraction of raw material for industry. The planet's capacity to absorb and convert the waste , resulting from modern life, seems to be inexhaustible. Situation has become a matter of great concern with the exponential increase in the population of planet. Consequently, waste production will increase by many folds. To counter this, alternatives such as substitution of conventional plastics for biodegradables are being studied. So, the main focus during the present work was the utilization of solid potato and wheat waste into biodegradable product such as starch, having various applications. For extraction of starch from waste potato and wheat, hydrothermal pretreatment was performed due to its high conversion efficiency and then compared it with the synthetic starch. Furthermore, kinetics of different starch were also carried out indicating that potato starch was the most suitable candidate and it follows the first order kinetics.

Key Words: Biodegradable, Hydrothermal Pretreatment, , Kinetics, Starch,

1. INTRODUCTION

The natural resources of earth are being discovered by mankind deprived of constraints, and regarding this, extract raw material for industry. The planet's capacity to absorb and convert the waste, caused due to modernism appeared to be boundless. This alarming condition has become a piece of great attention, with the exponential increase in the population of planet[1].Consequently, waste production will increase by many folds. To counter this, alternatives such as replacement of conservative plastics to eco-friendly one are being studied[2]. Among these, substances like starches has the ability to replace synthetic polymer in plastic industries because of low cost, biodegradability ,non-toxicity and availably[3, 4]. Edible and non-edible substances are largely composed of starch, which is a simple carbohydrate taken from the natural resources of agriculture. It has replaced the constituents of fossil fuel and is used as good natural resource because of it's biodegradable and renewable nature. Potato and wheat starch are two main sources of starch that constitutes around more then 50% of starch content. Since About 10 % of total wheat and 18 % of potato production was lost every year due to flood, fog, and heat stress. Utilization of this waste is an efficient strategy to reduce the stress of pollution. Hence this area is explored by employing the method of hydrothermal pretreatment for starch extraction.

2. METHODOLOGY

In this section details about the experimental setup is provided. Materials used were potatoe, wheat (for starch extraction), water as solvent and ambient temperature and pressure.Fig.1. shows schematic of starch extraction.

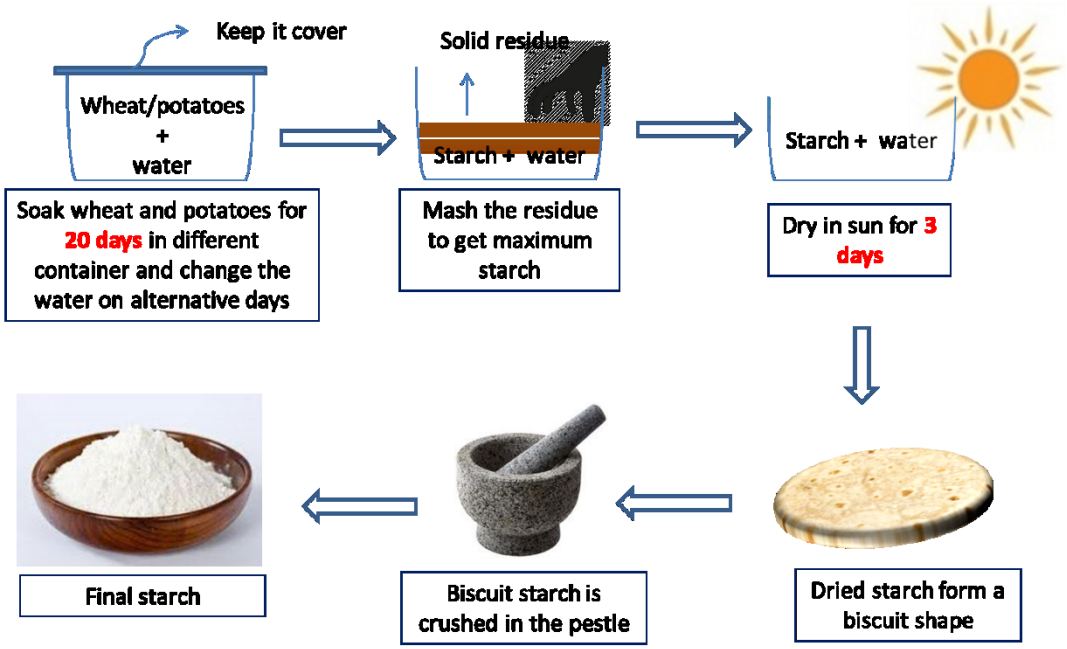

Fig. 2. Schematic of starch extraction using hydrothermal pretraetment method

3. RESULTS AND DISCUSSIONS

Extracted potato and wheat starch was characterized using FTIR, EDX, viscocity. For kinetic study U.V visible was also carried out at room temperature.

3.1. FTIR Results

FTIR of potato, wheat, hybrid and original starch are given in Fig.2. performed by FTIR equipment model Spectrum 100 (Perkin Elmer) . Strong and broad FTIR peaks of starches were observed at 3400cm^{-1} owing to the presence of OH group in the amylose chain. Peak intensity at 2931cm^{-1} and 1600 cm^{-1} is because of the presence of methyl and carbonyl groups in the starch chain. Peaks at 1430cm^{-1} and 900cm^{-1} is attributed to “crystalline” and “amorphous” structure of starch , respectively. The intensity of peak at 1157cm^{-1} is due to the presence of C-O-C bond in starch molecule. Moreover, the splitting of band at 996cm^{-1} and 1017cm^{-1} is correlated to a change from native to gelatinized form of the starch. The results were very much similar to the literature cited[5, 6].

3.2. EDX Analysis

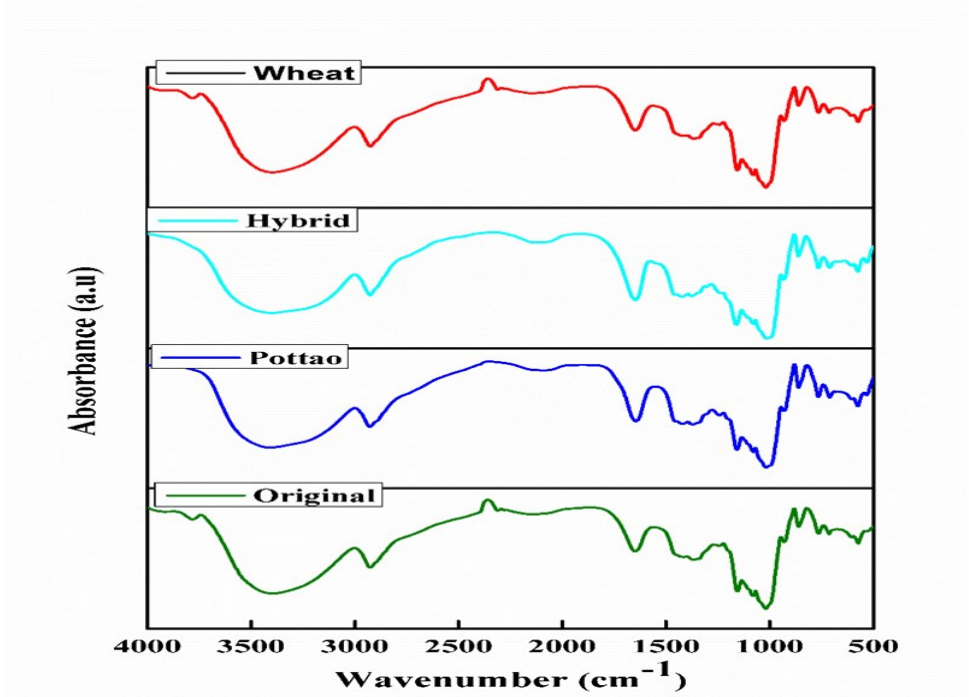

Fig. 3. FTIR of different starches

Different types of starch when analyzed through EDX confirms the elemental and relative proportion of both carbon and oxygen .Hydrogen can not be analyzed as it is the lightest element and beyond the resolution capacity of equipment present. Some impurities might also be there in starches as they are extracted. Furthermore, pictorial display of EDS is shown in Fig. 3.

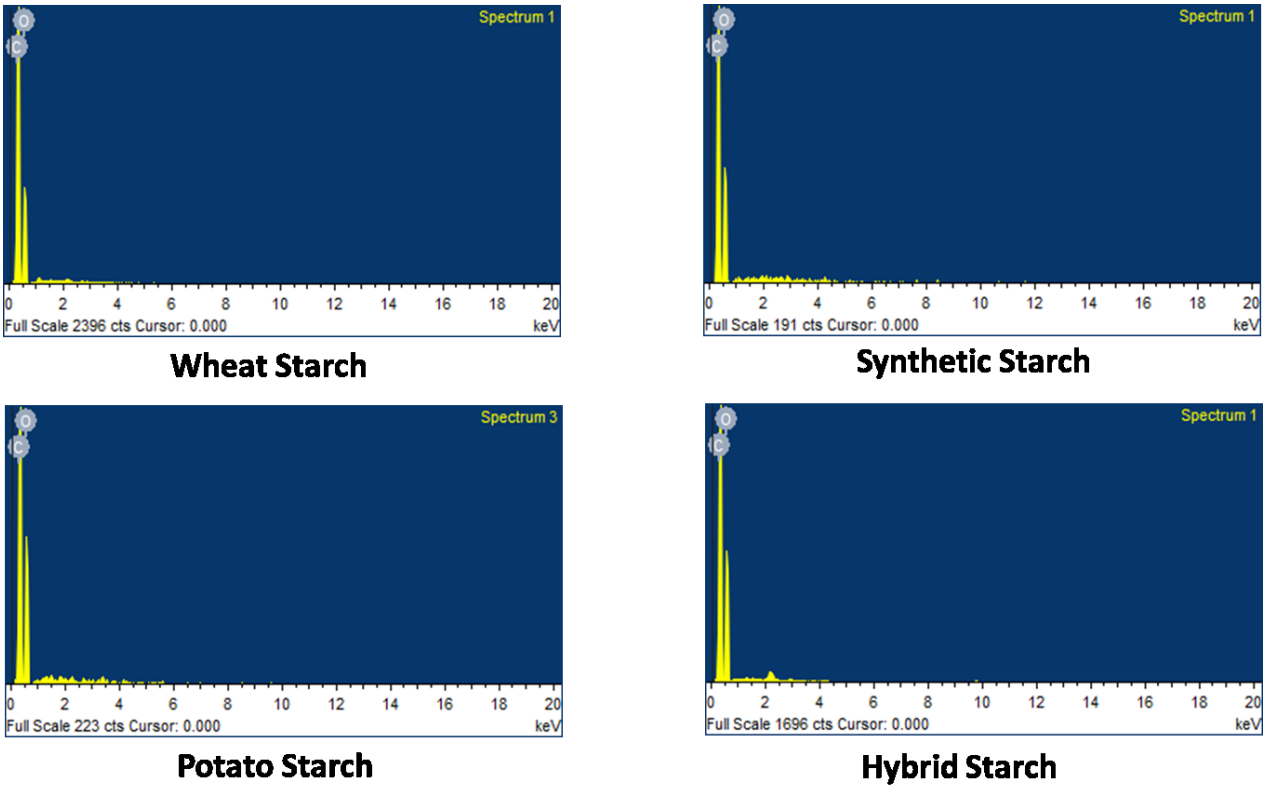

Fig. 4. EDX Analysis of Different Starches

3.3. Viscosity Measurement

Viscosity is being measured by using equipment Visco meter of model DV-E, DV 11+Pr0 of Brook Field present in SCME lab. Table 4.2 show the viscosity of different extracted and hybrid starch. Viscocity of wheat starch is lower compared to potato starch. This is because of the presence of phosphorous linkages, present in tuber unlike that of cereals[7].Hybrid starch has the viscosity comparable to each of the wheat, potato and synthetic starch.

Table 3. Viscosity of different starches

S. No	Material	Viscosity (Cp)
1	Synthetic Starch	118.4
2	Wheat Starch	32.39
3	Potato Starch	95.46
4	Hybrid Starch	75.24

3.4. U.V Results

UV spectroscopy is being measured at room temperature of 27°C using the equipment UV visible spectrophotometer model,UV-1900 present in SCME lab. UV of extracted, hybrid and original starches at room temperature show the absorbance peak at λ_{max} of about 215°C[8].Slight variation is there in case of potato and wheat starch.Fig.4. shows the UV spectrum of different starches at room temperature.

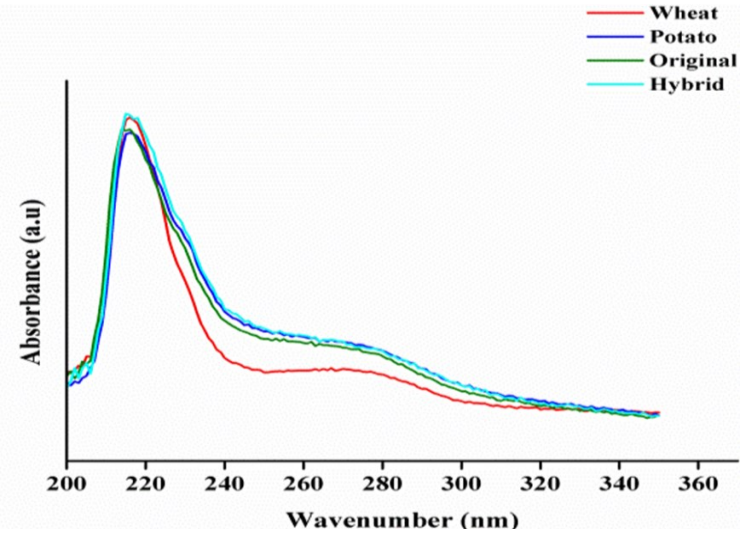

Figure 5 U.V of different starches

3.5. Kinetic Study

Kinetic study was also conducted by interpretating the U.V results of different starches. It is clear from the table that potato starch follows first order kinetics more precisely then wheat and other hybrid starch.

Table 4: First order kinetics of different starches

Samples	K (min^{-1})	R^2
Synthetic Starch	.0043	.98
Potato	.0047	.97
Wheat	.0018	.96
Hybrid	.0038	.94

4. CONCLUSION:

- Waste utilization was carried out effectively
- Hydrothermal pretreatment method was employed for starch synthesis

- Results of extracted starch were comparable to synthetic starch
- Kinetic models were being applied successfully after interpretation of U.V analysis.

5. REFERENCES

1. Akovali, G., et al., Frontiers in the science and technology of polymer recycling. Vol. 351. 2013: Springer Science & Business Media.
2. Sotero, A.P., Plásticos biodegradáveis trazem melhoria ambiental. Jornal de Plásticos, , 2000: p. 1017/1018.
3. Fajardo, P., Martins, J. T., Fuci˜nos, C., Pastrana, L., Teixeira, J. A., & Vicente, A. A., Evaluation of a chitosan-based edible film as carrier of natamycin toimprove the storability of Saloio cheese. Journal of Food Engineering 2010. **4**: p. 349–356.
4. Simkovic, I., Unexplored possibilities of all-polysaccharide composites. Carbohydrate Polymers, 2013. **2**: p. 697-715.
5. Buléon, A., et al., Starch granules: structure and biosynthesis. International Journal of Biological Macromolecules, 1998. **23**(2): p. 85-112.
6. Taherzadeh, M. and K. Karimi, Pretreatment of Lignocellulosic Wastes to Improve Ethanol and Biogas Production: A Review. International Journal of Molecular Sciences, 2008. **9**(9): p. 1621.
7. Jan, R., et al., Pasting and Thermal Properties of Starch Extracted from Chenopodium Album Grain. 2013.
8. Bajer, D., H. Kaczmarek, and K. Bajer, The structure and properties of different types of starch exposed to UV radiation: A comparative study. Carbohydrate Polymers, 2013. **98**(1): p. 477-482.

Effective separation of dye from wastewater using Ionic liquid

[1]Saeed ur Rahman, [1]*Mansoor Ul Hassan Shah
[1]14pwche0895@uetpeshawar.edu.pk, University of Engineering and Technology Peshawar, Pakistan
[2]University of Engineering and technology Peshawar, Pakistan.
mansoorshah@uetpeshawar.edu.pk

Abstract—Disposal of dye-containing wastewater which is mainly derived from textile industries is more disastrous and need significant attention. Therefore, environmental benign treatment process needs to be develop for elimination of such pollutants from wastewater. This work aimed to evaluate the application of the hydrophobic ionic liquid, trihexyltetradecylphosphoniumchloride ([PC6C6C6C14][Cl] used for the removal of tartrazine dye from aqueous solution. The results revealed that [PC6C6C6C14][Cl] have the potential to adsorbed tartrazine dye from aqueous solution with adsorption capacity of (150 mg/g). Furthermore, the removal efficiency of the [PC6C6C6C14][Cl] was also evaluated and it was observed that [PC6C6C6C14][Cl] have the capability to remove more than 90% tartrazine dye from aqueous solution. Overall, the result presented in this study depicted that ILs have the potential to replace the conventional toxic adsorbents used for the removal of toxic dyes.

***Keywords*:** Adsorption capacity, Ionic Liquid, Hydrophobic IL, tartrazine dye, toxic dyes,

1. INTRODUCTION

Over the past decades, water faces unprecedented challenges due to human activities such as industrialization, deforestation and urbanization. However, disposal of dye-containing wastewater which is mainly derived from textile industry, food production, leather factory, pharmaceutical, paper and pulp industries which are more disastrous, and pose a serious threat toward many living organisms. Further, sources of these dyes pollutants are depicted in Fig 1. The presence of dyes acts as barrier to light, temperature and oxidizers, which retard photosynthesis and eventually affect aquatic life-cycle [1]. Furthermore, numerous of these dyes are toxic, carcinogenic, mutagenic and having low bio-degradability [2]. For Example Tartrazine an azo dye is most commonly used in drugs, cosmetics, syrups, food additive and capsules shells. However this dye is typically toxic in nature and difficult to identify its presence due to high solubility in water. The presence of this dye in high concentration can cause human diseases such as lupus, cancer in thyroid, asthma, migraines, hyperactivity, eczema, and also cause infertility [3]. Therefore, industrial effluents containing azo dyes needs significant attention before disposal into water bodies.

To cope up this issue various traditional techniques were employed including chemical, physical and biological methods such as decomposition with microbes, ozonation process, coagulation method, flocculation method, decolorization with photo-catalytic, adsorption and sono-chemical method. However, each of these methods in separation has merits and disadvantages which include high cost, low efficiency, long treatment time, chemical additives usage, and secondary pollutant production [3]. Adsorption method is highly effective among these techniques owing to numerous advantages such as least capital cost, flexibility, ease operation and negligible waste generation. High adsorption capacity, effective surface area, adsorbent pore volume and pore size, chemical firmness, more selectivity for various dyes, reusability, ease regeneration and low cost are consider as Ideal properties of an adsorbent [4]. Synthetic adsorbents such as metal organic frameworks, polymers, clays, activated carbon, bio adsorption and biomass has been extensively used due to its commercial and natural availability. However, high cost, slower adsorption rates, dependency on pH and blockage problems are core issues [5]. Hence development of a competent, effective, economical and reusable novel adsorbent is required to remove toxic chemicals and dyes from aqueous media by implementing sustainable approach.

Ionic liquids (ILs) are recently considered as an effective alternative for treating dyeing

wastewater as it contain organic cations along with combination of inorganic or organic anions. Furthermore, due to its remarkable and fascinated properties such as its stability at high temperature, negligible vapor pressure, low melting point and simply reusability recently attracted high interest [6].

Therefore, in this research work hydrophobic ionic liquid, trihexyltetradecylphosphoniumchloride ([PC6C6C6C14][Cl] utilized for the extraction of tartrazine dye from aqueous media. In this study adsorption capacity, removal efficiency and comparison with other ILs are quoted.

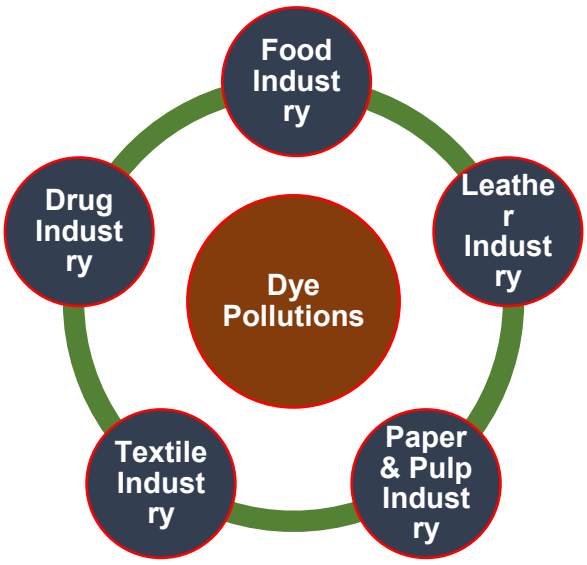

Figure 1: Principle Substrates of various dyes pollutants.

2. METHODOLOGY

MATERIALS

All materials used in experimentations including dye material and solvents were used without any further processing and of analytical grade. The phosphonium based ILs [PC6C6C6C14][Cl] MW = 519.31 g/mol, was kindly provided by Ionic liquid laboratories of Queen's University (QUILL), located at Belfast UK with purity ≥ 95.0% (NMR). Tartrazine which is also branded as Acid Yellow 23 an anionic dye, $C_{16}H_9N_4Na_3O_9S_2$, having a MW 534.4 g/mol depicted in Fig 2 were purchased from local market in Pakistan. Then preparation of standard solution of the dye by mixing required quantity of dye and pure distilled water. Then various

standard solutions of 50 mg/L to 250 mg/L obtained by diluting the stock solution with distilled water.

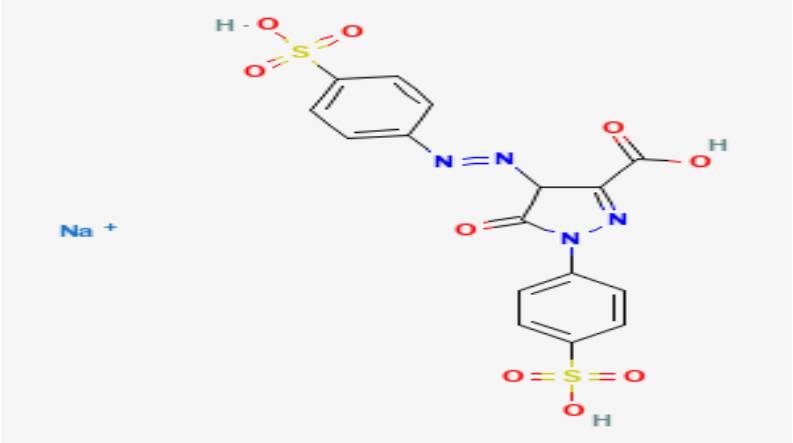

Figure 2 Detailed Molecular structure of Tartrazine dye (anionic)

3. RESULTS AND DISCUSSION

Adsorption experiments were performed to evaluate removal efficiency (E%) and adsorption capacity Qe (mg/g) and to compare it performance with other traditional and novel adsorbent used for Tartrazine dye removal.

J. Adsorption Capacity

Extraction of Tartrazine dye with the IL, trihexyltetradecylphosphoniumchloride [PC6C6C6C14][Cl] were studied in batch adsorption to evaluate adsorption capacity. For Adsorption studies 100 ml of Tartrazine dye solution, from prepared stock solution was put in beakers having various concentrations such as 50, 100, 150, 200 and 250 mg/L. Then injection of IL ranging from 100 to 160 mg into all prepared standard dye solution carried out. Further 100 mL of dye solution having desired initial concentration and adsorbent at pH of 7, and at temperature of 318 K agitated at 180 rpm for various time intervals.

After complete phase separation, then Cary-50 UV Spectrophotometer at wavelength 199 nm (λ_{max}) used to analyze the supernatant in order to find out the final concentration of the anionic dye Tartrazine adsorbed from waste water solution onto the adsorbent.

The adsorption capacity Qe (mg/g) at time (t) find out by using following equation respectively.

$$Qe = \frac{(Ci - Ct)V}{m}$$

Where Ci (mg/L) and Ct (mg/L) are the initial concentration and the final concentration at time t (min) of the dye (mg/L) respectively, weigh of ionic liquid are denoted with m (g) and dye solution volume with V (mL).

As per calculation from above equation, adsorption capacity of the dye is obtained as 150 mg/g with 250 mg/L dye concentration initially and 0.1 g dosage of IL at pH 7 and 25 min contact time for completion of adsorption process.

K. Removal Efficiency

The removal efficiency of IL in is also a very important parameter to evaluate the performance of adsorbents for pollutant removal. Therefore the removal efficiency (E %) of [PC6C6C6C14][Cl] adsorbent was investigated by using following equation.

$$E(\%) = \frac{Ci - Ct}{Ci} \times 100$$

Where Ci (mg/L) and Ct (mg/L) are the initial concentration and final concentration at time t (min) of the dye (mg/L) respectively and removal efficiency represented with E(%)

As per calculation from above equation, percent removal of the dye is obtained as 90% mg/g with 250 mg/L of dye concentration initially and 0.1 g dosage of IL at pH 7 and 25 min contact time for completion of adsorption process.

Results clearly shown that, the uptake of Tartrazine by ILs from aqueous phase is a significantly a very fast process and the adsorption equilibrium is reached within first 15 min. Then no significant change observed in extraction efficiency with further increase in contact time. It show that due to presence of various functional groups at the external surface of Ionic Liquid (IL) at beginning of adsorption process, leads to electrostatic attraction forces the molecules of dye used and surface of the adsorbent.

L. Comparison with other adsorbents

The comparison of adsorption capacities and removal efficiency of Tartrazine dye in this study with various adsorbents such as Nigerian soil, saw dust, rice husk and commercial activated carbon reported in the detailed literature and show in Table 1. It was found that [PC6C6C6C14][Cl], are effective, economical, have great potential, and advanced adsorbent

for the remediation and treatment of noxious dye pollutant from dye containing wastewater. Hence, the current research study suggest and open new doors for the applications hydrophobic phosphonium based ILs for tartrazine removal from dye containing wastewater.

Table 1
Comparison of adsorption capacities of Tartrazine dye onto different types of adsorbents

Adsorbents	Initial concentration (mg/L)	pH	Time (min)	Dose (g)	Qe (mg/g)	Reference
Rice husk	5	2	120	0.1	1.24	[8]
Commercial activated carbon	5	2	60	0.1	3.32	[8]
Saw dust	15	3	70	0.1	4.71	[2]
Nigerian Soil	50	2	120	0.05	83.33	[3]
[PC6C6C6C14][Cl]	250	7	25	0.1	150	This study

4. CONCLUSION

In this study trihexyltetradecylphosphoniumchloride was found to have a higher extraction efficiency of tartrazine as compared to other novel absorbents in the literature and can therefore be used as a substitute of traditional adsorbents for extraction of the noxious dye tartrazine from dye containing water solution. [PC6C6C6C14][Cl] IL can be utilized and studies as “green adsorbent” for extraction of different types of anionic dyes from waste water which contain dye as pollutant. Further, detail studies need to be carried out for other anionic dye and their removal percentage to be investigated by using the same IL used in this research work.

ACKNOWLEDGMENT

The author gratefully acknowledges efforts and ideas of research supervisor Dr. Mansoor ul Hassan Shah for fruitful discussions. I am very thankful for continuous support and encouraging me to pursue this innovative idea for study. Further I acknowledge the Laboratory assistances and other facilities provided by the Fatima Fert, Lahore. I also thankful to Fatima Fert laboratory section management, staff and lab technicians for their continuous working with me. It has been a good pleasure time for me to work with such enthusiastic, positive and technical staff. Finally I thank my fellow Mr. Muhammad Bilal Khattak for moral support and cooperation throughout support.

5. REFERENCES

[1] Z. Al-Qodah, W.K. Lafi, Z. Al-Anber, M. Al-Shannag, A. Harahsheh, Adsorption of methylene blue by acid and heat treated diatomaceous silica, Desalination. 217 (2007) 212–224. https://doi.org/10.1016/J.DESAL.2007.03.003.

[2] S. Banerjee, M.C. Chattopadhyaya, Adsorption characteristics for the removal of a toxic dye, tartrazine from aqueous solutions by a low cost agricultural by-product, Arab. J. Chem. 10 (2017) S1629–S1638. https://doi.org/10.1016/J.ARABJC.2013.06.005.

[3] M.O. Dawodu, K.G. Akpomie, Evaluating the potential of a Nigerian soil as an adsorbent for tartrazine dye: Isotherm, kinetic and thermodynamic studies, Alexandria Eng. J. 55 (2016) 3211–3218. https://doi.org/10.1016/J.AEJ.2016.08.008.

[4] M. Makrygianni, Z.G. Lada, A. Manousou, C.A. Aggelopoulos, V. Deimede, Removal of anionic dyes from aqueous solution by novel pyrrolidinium-based Polymeric Ionic Liquid (PIL) as adsorbent: Investigation of the adsorption kinetics, equilibrium isotherms and the adsorption mechanisms involved, J. Environ. Chem. Eng. 7 (2019) 103163. https://doi.org/10.1016/J.JECE.2019.103163.

[5] A.A. Hassan, M. Sajid, A. Tanimu, I. Abdulazeez, K. Alhooshani, Removal of methylene blue and rose bengal dyes from aqueous solutions using 1-naphthylammonium tetrachloroferrate (III), J. Mol. Liq. 322 (2021) 114966. https://doi.org/10.1016/J.MOLLIQ.2020.114966.

[6] H. Karimi-Maleh, S. Ranjbari, B. Tanhaei, A. Ayati, Y. Orooji, M. Alizadeh, F. Karimi, S. Salmanpour, J. Rouhi, M. Sillanpää, F. Sen, Novel 1-butyl-3-methylimidazolium bromide impregnated chitosan hydrogel beads nanostructure as an efficient nanobio-adsorbent for cationic dye removal: Kinetic study, Environ. Res. 195 (2021) 110809. https://doi.org/10.1016/J.ENVRES.2021.110809.

[7] K.G. Akpomie, F.A. Dawodu, Efficient abstraction of Ni(II) and Mn(II) ions from solution onto an alkaline modified montmorillonite, J. Taibah. Univ. Sci. 8 (2014) 343–356.

[8] Khader, E.H., Mohammed, T.J. and Albayati, T.M., 2021. Comparative performance between rice husk and granular activated carbon for the removal of azo tartrazine dye from aqueous solution. Desalin Water Treat, 229, pp.372-383.

Optimization of waste to energy and useful products conversion technologies for processing of municipal solid waste: A case study of Pakistan

[1]Hira Amin, [1]Muhammad Muqaddam Javaid, [2]Muhammad Rizwan, [1*]Muhammad Zaman, [3]Salman Raza Naqvi, [1]Khurram Shehzad,
[1]hiraa.amin50@gmail.com, Department of Chemical Engineering, Pakistan Institute of Engineering and Applied Sciences (PIEAS), Lehtrar Road, P.O. Nilore, 45650, Islamabad, Pakistan
[2]University of Bahrain, Bahrain
[3]National University of Sciences and Technology (NUST), Pakistan
Corresponding author (Muhammad Zaman, PhD): zaman@pieas.edu.pk

Abstract— Burgeoning municipal solid waste (MSW) generation and concern about inadequate energy resources have drawn worldwide attention to waste to energy (WtE) technologies that provide valuable products or electricity while reducing reliance on fuels and materials produced from fossil sources. For this purpose, this research problem identifies the WtE technologies (thermochemical, biochemical, and transesterification), electricity generation from landfills, and recycling of the recyclable constituents of MSW and employs the combination of these technologies in the superstructure. A mixed integer nonlinear programming (MINLP) model is developed to find out the promising technology under the objective function of profit. The findings of the study reveal that recycling followed by the composting process is the ideal path for treating MSW and it is according to the waste management hierarchy as well.

Keywords— Mathematical modeling, municipal solid waste, optimization, MINLP, Waste to Energy.

1. INTRODUCTION

The world's increasing population demands more energy. Consequently, the amount of municipal solid waste (MSW) is escalating at an alarming rate. Approximately 2 billion tons of MSW are produced worldwide each year, but only about 33% of that amount is collected by municipalities [1]. MSW is mainly a mixture of food waste, wood waste, paper, plastic, glass, metal, and textile. MSW discharges pollutants into the environment, contributing to climate change and negatively affecting both human and environmental health [2]. The problems arising from MSW direct the researchers to find a sustainable solution. Waste to energy (WtE) technologies are being utilized in many countries.

The conversion technologies are thermochemical (incineration, gasification, pyrolysis), biochemical (composting, anaerobic digestion), and physicochemical (trans-esterification) [3]. The abbreviations and acronyms used in the current study are mentioned before the acknowledgement section.

In the treatment of MSW, both environmental and economic factors are important. Most researchers have worked on both. A model was formulated by Minas et al. (2013) for the Greek state by doing nonlinear mathematical modeling for WtE technologies (INC, COMP, AD, LAF). According to the conclusion of the study, there was a trade-off between cost and the greenhouse effect [4]. The location of waste transfer sections affects the cost objective function. In both the mixed and segregated waste contexts, Pradeep et al. (2019) proposed a strategy for determining waste transfer station locations that was cost-effective [5]. Arsalan et al. (2022) developed a MINLP model for the designing of MSW treatment system. The model was solved under the objective functions of environmental and economic aspects. The study consists of WtE technologies employed in different scenarios [6].

Although, numerous studies in the context of MSW to energy processing and optimization of MSW management systems are available. This research problem deals with WtE technologies and additionally incorporates the trans-esterification process for the case study of one of the cities of Pakistan, Lahore, by developing a generic and detailed mathematical model.

2. METHODOLOGY

This research problem is comprised of 4 steps, describing the milestones of this research study as shown in Fig. *1*.

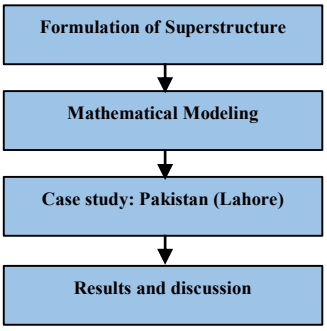

Fig. 1. Methodology framework for the current work

M. Problem statement

This research problem deals with finding a sustainable and optimal way of processing MSW and producing valuable commodities as well as energy from the treatment of MSW. Superstructure based optimization is performed by developing a MINLP model and solving it in GAMS. WtE technologies are incorporated in the superstructure to identify economically optimal technology.

N. Superstructure's formulation

The superstructure is the description of MSW treatment stages and technologies to process it. The proposed superstructure is composed of technologies i.e., recycling, composting, anaerobic digestion, incineration, pyrolysis, gasification, plasma arc gasification, trans-esterification, and landfills. The processing stages are raw material, segregation & recycling, treatment, and products. The superstructure is displayed in Fig. *2*.

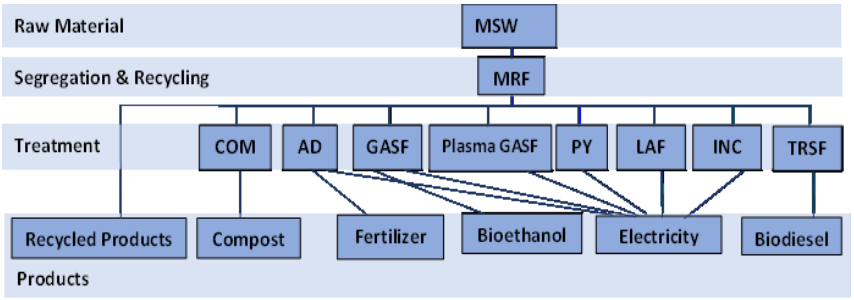

Fig. 2. Proposed superstructure for the MSW treatment

O. Mathematical Model

The mathematical model consists of the objective function (i.e., profit) and mass balance constraints. The objective is the maximization of net profit. Indices c, t, and s represent the components of MSW, technologies, and stages of treatment of MSW, respectively. Binary variable $x_{t,s}$is the decision variable. The selection of technology makes binary variable 1 and 0 otherwise. Equation (1) represents the selection of technology. *Fig. 3* represents the flow of MSW in stage s.

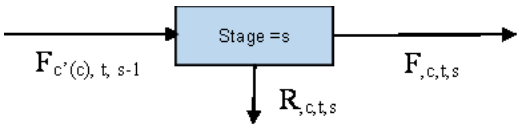

Fig. 3. Flow of MSW coming out of previous stage s-1 to stage s

[redacted] *(1)*

Equation (2) represents the composition of MSW at inlet stage 1.

$$Fh_{c,1,1} = \varphi_c \quad (2)$$

Equations (3) and (4) represent the flow of MSW $Fh_{c,t,s}$, and waste in residue stream $Rh_{c,t,s}$.

$$F_{c,s} = \sum_{t \in T} x_{t,s}.Fh_{c,t,s} \quad (3)$$

$$R_{c,s} = \sum_{t \in T} x_{t,s}.Rh_{c,t,s} \quad (4)$$

Equation (5) shows the allocation of MSW components coming from previous stage s-1 to the stage s and technology t. $\alpha_{c,t,s}$ represents the allocation of components.

$$Fh^{in}{}_{c,t,s} = \alpha_{c,t,s}.F_{c'(c),\,s-1} \quad (5)$$

Equation (6) represents the flow of the waste coming out of the technology t of stage s. $\sigma_{c,t,s}$ represents consumption and $\beta_{c,t,s}$ represents yield coefficient.

$$Fh^{out}{}_{c,t,s} = Fh_{c,t,s}{}^{in} + \sum_{c' \in C}\left(\beta_{c'(c),t,s}.Fh_{c,t,s}{}^{in}\right) - \sigma_{c,t,s}.Fh_{c,t,s}{}^{in} \quad (6)$$

Equation (7) represents the separation of the residue stream from the processed stream.

$$Fh_{c,t,s} = Fh^{out}{}_{c,t,s} - Rh_{c,t,s} \quad (7)$$

Equation (8) represents the splitting of waste and $\omega_{c,t,s}$ is the split factor.

$$Rh_{c,t,s} = \omega_{c,t,s}.Fh^{out}{}_{c,t,s} \quad (8)$$

Equation (9) is the objective function.

$$Profit = Product\ Sales - O\&M\ Cost - Capital\ cost \quad (9)$$

Equations (10,11,12,13) calculate the product sales prices ($Price_c$), operating & maintenance ($OM_{t,s}$) and capital costs ($CapitalCost$), respectively.

$$Product\ sales = \sum_{c \in C}\left(Price_c.F_{c,4}\right) \quad (10)$$

$$O\&M\ cost = \sum_{c \in C}\sum_{t \in T}\sum_{s \in S}\left(OM_{t,s}.\ x_{t,s}.Fh^{in}{}_{c,t,s}\right) \quad (11)$$

$$CapitalCost = \sum_{s \in S}\sum_{t \in T}\left(CapitalCost_{t,s}.x_{t,s}\right) \quad (12)$$

Terms $DesiredCapacity_{t,s}$, $Capacity^{base}{}_{t,s}$, and $M\&SI$ represent desired capacity, base capacity, and Marshall & Swift cost index.

[redacted] *(13)*

Equation (14) calculates ACCR i.e., annualized capital charged ratio. M is the project life taken to be 20 years and IR is the interest rate i.e., 15%.

$$ACCR = (IR.(1+IR)^{M}) / ((1+IR)^{M} - 1) \quad (14)$$

P. Software

General Algebraic Modeling System (GAMS) is used here to solve the MINLP mathematical model. Data is stored in Microsoft Excel and loaded into GAMS via GAMS Data Exchange (GDX) files.

3. CASE STUDY: PAKISTAN

According to current estimates, Pakistan produces 30 million metric tons of MSW per year [7]. Hence, the proposed methodology is applied to the waste composition of Lahore, a famous city in Pakistan. The waste composition of Lahore is shown in *Table 5*. Further information related to costs incurred, selling prices and yield may be furnished upon request.

Table 5. Composition of MSW in percentage for Lahore city [7]

Components	Food waste	Paper	Plastic	Glass	Metal	Wood	Textile	Misc.
Composition (%)	56.3	3.2	10.6	0.7	0.1	6.1	9.2	13.8

4. RESULTS AND DISCUSSION

100 tons of MSW is processed. The proposed methodology obtained for the handling of MSW is the recycling of MSW and introducing the rest of the waste into composting technology. Composting is a famous and commonly employed technology for treating the MSW. The optimal path shown in

*Fig. **4*** is according to the MSW management's framework i.e., reducing, re-using, recycling the waste, treating the MSW by recovering energy or obtaining useful products, and ultimately disposal. Table *6*. displays the optimization results. The recycled materials (19.8 tons) obtained after recycling have product values that contribute positively to the maximization of the net profit (7141$). Selected technology for processing waste is composting which provides compost (33.4 tons) as the final product.

5. CONCLUSION

In the current study, a MINLP model was employed to construct the most effective MSW treatment approach for transforming waste into valuable commodities and/or electricity. The economic feasibility of MSW processing is shown by the results of optimization. This effective system promotes MSW recycling and waste to composting as a practical solution for MSW handling because it yields a maximum profit of $7141 per 100 tons of MSW treated.

Table 6. Results obtained for 100 tons of MSW

Recycled Products (tons)					Selected Technology	Product (tons)		Profit ($)
RPR	RP	RG	RM	RT				
2.9	7.9	0.6	0.05	8.3	Composting	Compost	33.4	7141

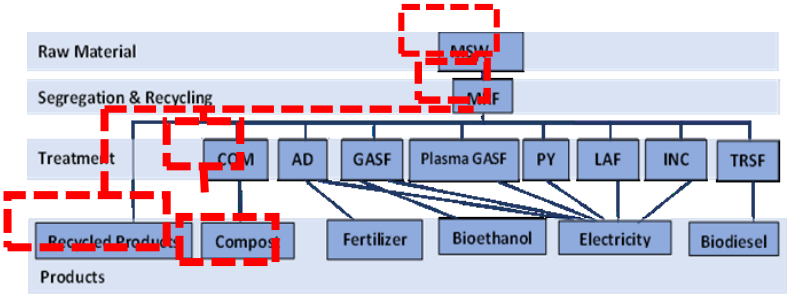

Fig. 4. Result of optimization illustrated in the superstructure

ABBREVIATIONS & ACRONYMS

AD	Anaerobic Digestion	***MRF***	Material Recycling Facility	***RP***	Recycled Plastic
COMP	Composting	***MILP***	Mixed Integer Linear Programming	***RPR***	Recycled Paper
GASF	Gasification	***MINLP***	Mixed Integer nonlinear Programming	***RT***	Recycled Textile

INC	Incineration	***PY***	Pyrolysis	***TRSF***	Trans-esterification
LAF	Landfills	***RG***	Recycled Glass	**GDX**	GAMS Data Exchange
MSW	Municipal Solid Waste	***RM***	Recycled Metal		

6. ACKNOWLEDGMENT

This research study was fully supported by Pakistan Institute of Engineering and Applied Sciences (PIEAS), Islamabad.

7. REFERENCES

[1] J. Aleluia and P. Ferrão, "Characterization of urban waste management practices in developing Asian countries: A new analytical framework based on waste characteristics and urban dimension," *Waste Manag.*, vol. 58, pp. 415–429, Dec. 2016, doi: 10.1016/J.WASMAN.2016.05.008.

[2] S. Khan, R. Anjum, S. T. Raza, N. Ahmed Bazai, and M. Ihtisham, "Technologies for municipal solid waste management: Current status, challenges, and future perspectives," *Chemosphere*, vol. 288, p. 132403, Feb. 2022, doi: 10.1016/J.CHEMOSPHERE.2021.132403.

[3] S. Varjani *et al.*, "Sustainable management of municipal solid waste through waste-to-energy technologies," *Bioresour. Technol.*, vol. 355, no. February, 2022, doi: 10.1016/j.biortech.2022.127247.

[4] M. Minoglou and D. Komilis, "Optimizing the treatment and disposal of municipal solid wastes using mathematical programming - A case study in a Greek region," *Resour. Conserv. Recycl.*, vol. 80, no. 1, pp. 46–57, 2013, doi: 10.1016/J.RESCONREC.2013.08.004.

[5] P. Rathore and S. P. Sarmah, "Modeling transfer station locations considering source separation of solid waste in urban centers: A case study of Bilaspur city, India," *J. Clean. Prod.*, vol. 211, pp. 44–60, Feb. 2019, doi: 10.1016/J.JCLEPRO.2018.11.100.

[6] A. Yousefloo and R. Babazadeh, "Designing an integrated municipal solid waste management network: A case study," *J. Clean. Prod.*, vol. 244, p. 118824, Jan. 2020, doi: 10.1016/J.JCLEPRO.2019.118824.

[7] A. development Bank, *Solid Waste Management Sector in Pakistan*, vol. 01, no. March.2021.[Online].Available:https://www.adb.org/sites/default/files/publication/784421/solid-waste-management-pakistan-road-map.pdf

Unplasticized polyvinyl chloride (UPVC) pipe industry of Pakistan: few suggestions to improve the finishing and the strength of the pipes while reducing the production cost

[1]Hamza Ahmad., [1]*Bilal Ahmad., [2]Sheharyar Khan., [2]Hammad Ismail. & [3]Naseer Ahmed Khan.
[1]hamzaah7090@gmail.com,
[2] University of Engineering & Technology Peshawar, Pakistan.
Corresponding author: naseerahmedkhan@uetpeshawar.edu.pk

Abstract— Polyvinyl chloride (PVC) resin is polymerized to produce a variety of plastic materials. Worldwide about 40 million tons of different PVC products are produced annually. Unplasticized Polyvinyl chloride (UPVC) are rigid plastics prepared from the polymerization of the same PVC resin. In Pakistan, UPVC pipes are very commonly used as sewer and water pipes. Our industries use calcium carbonate (CaCO3) mineral as a filler during the polymerization of the resin.

Filler replaces some part of the expensive PVC resin and thus decreases the cost. On the other hand, if the concentration of calcium carbonate(CaCO3) increases from 10 PHR the net weight (specific gravity) of the pipes increases. Moreover, if added than a certain concentration the produce pipes may not retain the required mechanical strength. The handling of the viscous polymerized mixture is difficult and creates difficulties in processing. In short, the addition of calcium carbonate reduces the overall cost but it adversely affects the specific gravity and other mechanical properties.

Our study was about the possible fillers having less effect on the specific gravity and can improve the smoothness of UPVC pipes at a minimum cost. We propose a mix of organic (corn starch) and inorganic (aluminum trihydride) fillers. Organic fillers have less weight (specific gravity) and are usually cheap. Polyethylene wax (lubricant) will improve the smoothness and overall finishing quality of the pipe. The use of these types of lubricants facilitates in flowing processing and increases the chances of uniformity in the polymerized chains.

Keywords— Calcium carbonate (CaCO3), organic fillers, parts per hundred rubber (PHR), Unplasticized Polyvinyl chloride (UPVC).

1. INTRODUCTION

Polyvinyl chloride (PVC) is the 3rd most widely used thermoplastic polymer. It is one of the most valuable products in the chemical industry. The production of PVC is 40 million each year. There are two basic forms of PVC, these are rigid (U-PVC) and flexible. PVC is used in window frames, drainage pipes, water services pipes, medical devices, wire insulation, automotive interiors, and construction materials. U-PVC pipes are usually recognized as pressure pipelines and they are most commonly used in the agriculture, chemical, and construction industries. There is only one difference between PVC and U-PVC, PVC contains BPA (Bisphenol A) and phthalates, which are two plasticizers that make it more flexible. When they are added to PVC it makes it unsuitable for transporting water for drinking while U-PVC pipes are widely used for drinking purposes.

Fillers are cheap materials that are used in U-PVC pipes by replacing some volume of

expensive materials that reduce the cost of U-PVC pipes. They are solid additives, different from materials of plastics in composition and structure, which are added to polymers to improve properties such as tensile and compressive strength, toughness, thermal stability, and other properties. They may be organic or inorganic. The inorganic fillers that are used as fillers are calcium carbonate, clays, barium sulfate, fine powders of some metals, etc. These inorganic fillers have some limitations of use due to greater specific gravity. The organic fillers are classified by their low specific gravity. Organic fillers include Banana Pseudo stem, Kenaf, wood floor, eggshell, and different edible starches. [1]

The inorganic filler Calcium Carbonate is used for the reason that it improves processing characteristics, mechanical properties, and electrical properties (due to better moisture resistance) and it also reduces the absorption of minor additives. By using Calcium Carbonate as a filler it increases the impact strength but it also increases the specific gravity. The filler Calcium carbonate can reduce the cost of the sample formulation of the pipe but it has an adverse effect on the specific gravity of the pipe. Reducing the particle size of calcium carbonate led to a small decrease in the tensile strength but improve the impact energy, the storage modulus, and the fracture toughness.[2]

Due to the lack of petroleum and to reduce the dependency on fossil fuel products, the interest of the people increases in renewable materials like kenaf fiber. Including the kenaf in the formulation provide some cost reduction to the world of plastic industry and agro-based industry. We can enhance mechanical properties such as tensile strength.[3]

By using the Banana Pseudo stem (filler) the dynamic properties such as the storage modulus and damping behavior increase. The storage modulus increases with increasing BPS content in the sample.[4]

Improving the thermal insulation of the windows have great importance. Using small-size fillers such as aerogels to make polymeric nano-composite windows can improve thermal insulation, mechanical properties, and acoustic parameters. Aerogels are highly porous materials having very low density (<0.05 g/cm3) and high surface area. The sound velocity in aerogels is less compared to the air, they prevent acoustical activity up to a great instant. We can conclude that by using silica aerogel as a filler in U-PVC the thermal insulation and acoustic properties increase [5].

2. METHODOLOGY

There are many types of low-cost and readily available organic and inorganic fillers compounded with PVC resins to make UPVC pipes. Most commonly calcium carbonate is used as a filler in UPVC pipes. We planned to make a blend of the organic and inorganic filler such as corn starch and aluminum trihydrate were used in different proportions along with the PVC resin. The size of corn starch granules is more uniform ranging from 15 to 25 μm. Corn starch has a low specific gravity of 1.45. Aluminum trihydrate (ATH) is an important inorganic filler and has a specific gravity of 2.42. It suggests a wide range of physical properties such it gives low oil absorption, moderate water absorption, and enhanced hardness as well as other mechanical properties. Its particle size is about 45 μm and it is also used as a flame retardant and smoke suppression hence reducing the extra cost of using a flame retardant. Along with these two fillers, a barium-cadmium liquid stabilizer is used as a heat stabilizer. It is a good stabilizer and lead-free. Since the dispersion of corn starch in PVC matrix is difficult, it was treated with stearic acid for easy dispersion and to avoid its decomposition with time. To improve the physical appearance and smoothness of pipe the Polyethylene wax was used and it also reduces the shear and heat losses during processing as it acts as a good lubricant and gives a good finishing to UPVC pipes

Different properties such as tensile strength, tear strength, shore hardness, specific gravity, water absorption, etc. were studied and also compared with the results of using conventional calcium carbonate as a filler. So the combination of organic and inorganic filler was used in different proportions to obtain a low specific gravity and improve the other properties.

Q. Experimental work

First of all the required amount of filler was added to the PVC resin, stabilizer, and other additives in a mixer. At the bottom of the mixer, a high-speed propeller was used to insure proper mixing. It was mixed for 15 to 20 min. The mixture was properly blended to ensure the desired properties and to improve processibility and stability. Then the mixture was melted under the compression of the screw and the temperature of the barrel in an extruder. The temperature of the barrel was set at 200-210 °C. The volatile matter evolved in a considerable amount during the extrusion process. The pipe was given a proper shape by a die at the end of the extruder and the pipe was cooled in the sizing operation. The water in cooling tanks was used to cool the pipes and to make unbent pipes. Finally, pipes were cut as per standard length in a cutting machine. The processing of the mixture was made easier due to the use of

polyethylene wax as a lubricant. Also, the finishing and smoothness of pipes were enhanced due to the use of lubricant.

The following formulation was used for the preparation of UPVC Pipes.

PVC - 100, Barium Cadmium Liquid Stabilizer - 3, Polyethylene wax - 1, Filler - 30, and Calcium Stearate - 1 PHR .

Different composition of corn starch and aluminum trihydrate was used to obtain different results and to analyze the better results. The pipes were tested for different physical and mechanical properties. It was observed that good mechanical properties were achieved when 15 PHR of corn starch and 15 PHR of Aluminum Trihydrate were used.

3. RESULTS AND DISCUSSION

The use of an inorganic filler with PVC resin for making UPVC pipes to improve the physical, mechanical and thermal properties of the pipes is quite common nowadays. There are many inorganic fillers used but calcium carbonate is mostly used as filler to improve the properties but it has some limitations such as it increases the specific gravity of the final product and the viscosity of the mixture increases which leads to processing problems. Due to the natural hardness of the inorganic fillers, the processing equipment has been worn out. The results obtained by using 8 PHR of calcium carbonate as a filler are shown in table 1. If we increase the concentration beyond 8 PHR it increases the specific gravity of pipes. So, it is recommended to use a low concentration of calcium carbonate to achieve low specific gravity but it increases the final cost of the pipes.

TABLE I: RESULTS OF USING CALCIUM CARBONATE AS A FILLER.

Properties	Values
Specific gravity	1.45
Tensile strength (kg/cm^2)	250
Tear strength (kg/cm)	58
Elongation (%)	150
Water absorption (%)	0.28
Shore hardness	110

It is therefore more advantageous to use an organic filler in UPVC pipes. Organic fillers are known for their low specific gravity such as corn starch (1.4). Due to the organic nature of PVC, the dispersion of these organic fillers is easy in the polymer matrix. Most edible starches such as corn starch are commonly used as organic fillers. These edible starches have a low cost. To use these organic fillers in commercial products, we must know the characteristics of these fillers, their behavior when used with polymers, and the problems that must be faced during their processing. As we know that these organic fillers are decomposed by insects and microorganisms. To avoid this decomposition, these fillers must be coated with calcium stearate so that the pipes are protected and their service life is not affected.

In the comparative study of using corn starch and calcium carbonate as a filler, it was observed that corn starch gives a low specific gravity and water absorption but the mechanical properties such as tensile strength were reduced. As well as corn starch shows easier processing as compared to calcium carbonate. The better performance of corn starch is due to its low specific gravity and uniform grain size which ranges from 15 to 25 μm.

Aluminum trihydrate (ATH) is an inorganic filler having specific gravity (2.42) and a particle size of more than 45 μm. ATH has a hardness comparable to calcium carbonate, shows moderate water absorption, and is non-toxic. It is also used as a flame retardant. It has a gelatinous nature and can be used in combination with organic fillers. The mechanical properties of UPVC pipes can be improved by using ATH as a filler. The result obtained by using a blend of corn starch and ATH in different compositions was better as shown in table 2.

The mechanical properties were improved as well as the specific gravity and water absorption were reduced. Different results were obtained from different concentrations of filler. Among them when the corn starch/ATH combination (15:15) was used, the result was the best. The specific gravity was reduced to 1.31 and also the mechanical properties were improved as compared to the use of calcium carbonate as a filler.

The use of Polyethylene wax improves the physical appearance of the pipes such as smoothness and surface finishing and facilitates easy processing.

TABLE 2: FORMULATION: PVC - 100, BARIUM CADMIUM LIQUID STABILIZER - 3, POLYETHYLENE WAX - 1, FILLER - 30, AND CALCIUM STEARATE - 1 PHR.

Filler (PHR)	Specific gravity	Tensile strength (kg/cm^2)	Tear strength (kg/cm)	Elongation (%)	Water absorption (%)	Shore hardness
Corn starch	1.32	203	62	198	0.26	85
ATH	1.45	267	98	210	0.06	136
Corn starch (18) + ATH (12)	1.35	195	75	270	0.13	115
Corn starch (15) + ATH (15)	1.31	280	78	290	0.04	121

4. CONCLUSION

From the above results, it can be concluded that organic fillers such as corn starch can be used as a filler for UPVC pipes, after treating it with stearic acid and it gives a low specific gravity to the pipes. When a blend of organic filler (corn starch) and inorganic filler(ATH) is used it results in low specific gravity, and low water absorption and improves the mechanical properties of the pipes. The best results can be obtained by using a corn starch/ATH combination (15:15).

The cost of UPVC pipes can also be reduced because corn starch and aluminum trihydride have low costs and they can be used in high concentrations as compared to calcium carbonate. In the case of calcium carbonate, a total of 8 PHR can be used to fill the volume of the PVC resin but in the case of alternate fillers (corn starch and aluminum trihydride), a total of 30 PHR can be used to fill the PVC resin. So, the cost of the final UPVC pipe can be reduced because a high volume of expensive PVC resin can be replaced with filler.

Physical appearance such as internal and external smoothness, polishing, and surface finishing can also be enhanced with the use of polyethylene wax. With the internal smoothness, the flow in the pipe experience less turbulency. Heat losses are common during extrusion but in order to facilitate easy processing, lubricants such as polyethylene wax can be used which mitigates the heat losses, resulting in increased production.

ACKNOWLEDGMENT

The author wishes to thank Dr. Naseer Ahmed Khan of the University of Engineering & Technology, Peshawar for their assistance, and support and for providing all the facilities in preparing this paper.

5. REFERENCES

[2] M. M. Zurale, and S. J. Bhide, “Properties of fillers and reinforcing fibers, ” *Mechanics of Composite Materials*, Vol. 34, No. 5, 1998.

[3] J. S. Falcone, ”Fillers,” in *Kirk-Othmer Encyclopedia of Chemical Technology*, 4th ed. Vol 10, M. Howe-Grant, Ed. New York: John Wiley & Sons, 1992, pp. 169-175.

[4] M. F. Abdrahman and E. S. Zainudin, “Properties of kenaf filled unplasticized polyvinyl chloride composites,” in *Key Engineering Materials*, vol. 471–472. Switzerland: Trans Tech Publications, 2011, pp. 507–512.

[5] E. S. Zainudin, S. M. Sapuan, K. Abdan, and M. T. M. Mohamad, “Dynamic mechanical behavior of banana-pseudostem-filled unplasticized polyvinyl chloride composites,” *Polymers & Polymer Composites*, Vol. 17, No. 1, 2009.

[6] N. Eskandari, S. Motahari, Z. Atoufi, G. Hashemi Motlagh, and M. Najafi, “Thermal, mechanical, and acoustic properties of silica-aerogel/UPVC composites,” *Journal of Applied Polymer Science*, vol. 134, No. 14, Apr. 2017.

Evaluation of Co-torrefaction performance of risk husk and coffee bean ground blends for bio-solid production

Abdul Waheed[1], Salman Raza Naqvi[1*],
[1]School of Chemical and Material Engineering, National University of Science & Technology, Islamabad, Pakistan
***Correspondence:** salman.raza@scme.nust.edu.pk

Abstract— Co-torrefaction was performed on rice husk (RH), coffee bean ground (CBG) and their various blending ratio such as CBG:RH (25:75%), CBG:RH (50:50%), CBG:RH (75:25%), CBG 100%, and RH 100% as well as the impact of temperature were studied. The co-torrefaction experiments were performed using a laboratory scale tube furnace varying temperature from 200 °C- 300 °C. Because of increased temperature the carbon content raised from 55.1% to 69.2%. Also show improved calorific value of 30835.13 Kj/kg. In addition, the high carbon content and better fuel properties were found for CBG 100% and blending ratio of CBG:RH (75:25%) at 300 °C for 60 min as a bio-solid production of 65.2%. This research found that co-torrefaction improves CBG, RH, and their blends as bio-solid fuel for energy applications.

Keywords— Rice husk, Coffee bean ground, Co-Torrefaction, Bio-solid, Blending ratio.

1. INTRODUCTION

The demand of clean energy is needed to support modern lifestyle, especially in developing nations, where standard of living is improving [1]. Due to depleting supplies and environmental damage, fossil fuels can't meet energy demand. Renewable, clean, and sustainable energy will be a strategic goal [2]. Wind, solar, hydropower, and biomass are renewable energy alternatives [3] in which biomass promoted itself as a renewable energy option by promising carbon neutrality, renewability, eco-friendliness, widespread availability, and conversion technology [4]. Coffee is currently one of the most commonly traded commodities, with annual global consumption topping 12 million kg [5]. rice producing nations in the world, with an annual output of more than 11000 million Kg [6]. Rice husk (RH) and coffee bean ground (CBG) are abundant feedstock for energy generation across the world.

There are different barriers to use biomass. Because of high moisture and low energy density cause this difficulty. The pretreatment of biomass includes drying, blending material, and torrefaction. Drying lowers biomass moisture, and mixing enhances calorific value. Torrefaction have a potential to produce bio-solid. Torrefaction is a thermochemical process that produces solid fuel at 200-300 °C in an inert atmosphere. Torrefaction improves the energy and mass density, ignitability, grindability, moisture content, heating value, and hydrophobicity of biomass.

Co-torrefaction of lignocellulose biomass (sugarcane bagasse) and non-lignocellulose biomass (sewage sludge)has also been studied [7], hemicellulose, cellulose, lignin, xylose, and glucose [8] to improve its solid-fuel characteristics. CBG and RH co-torrefaction has not been studied before. Therefore, an in-depth knowledge of co-torrefaction of CBG and RH is required to analyze its fuel properties.

In this research, CBG and RH are co-torrefied from 0% to 100%. Various blending ratios were also evaluated at 200-300 °C. Comparing elemental composition of CBG and RH before and after co-torrefaction. We used a bomb calorimeter to find the calorific value of torrefied, un-torrefied biomass with various blended ratios.

2. METHODOLOGY

R. Experimental setup for co-torrefaction

The experimental setup of co-torrefaction is done. 3-4g of CBG and RH samples are placed in a ceramic crucible and placed in a quartz tube (OD=60 mm 0.5 mm (2.36"), ID=55 mm 0.5 mm (2.17"), length 1000 mm (40")) in the furnace. The furnace heats at 10 °C/min while a variable area flow meter (Rotameter) maintains a 50mL/min nitrogen flow to provide an inert environment. The K-type thermocouple on the furnace is carefully adjusted to maintain 200–300°C. The experiment is done three times for accuracy.

S. Characterization of biomass and torrefied biomass

The ultimate analysis of CBG and RH blends was done using ASTM D7291-96 (LECO CHNS 932) [9]. The elemental analyzer measures C, H, O, N, and S content of CBG, RH, and their blends [10].

To identify calorific value of CBG, RH, and their blends, we used a bomb calorimeter type Parr 6200 [11] Standard oxygen-burning of the sample. Thermometers monitor temperature increase to compute heat released [11].

3. RESULTS AND DISCUSSIONS

A. Ultimate analysis

Fig. 1 shows that when temperature rises, CBG, RH, and blends' chemical compositions changes. As temperature rises, carbon content rises, according to the data. Fig. 1(a) CBG (100%) at 300 °C has 69.24% carbon while CBG:RH (75:25) has 65.24%.

The results for hydrogen in CBG and RH vary as shown in Fig. 1(b). Hydrogen diminishes with rise in temperature. Fig. 1(c) express that increase RH in sample rises oxygen content. While blend of CBG:RH (75:25%), the oxygen concentration is 18.14% at 300 °C, which is the lowest among blending ratios. Fig. 1(d) shows variances this is due to CBG 100% oxygen content drops quickly. Severe temperature zone causes strong depolymerization, polymerization, and dehydration. Decrease in nitrogen increases the heating value of co-torrefied samples. Furthermore nitrogen produces NO_x during combustion. Fig. 2(a) shows that temperature affects nitrogen content. Fig. 2(b) depicts that sulphur content decreases with increase in temperature. High-sulfur bio-solids may create toxic gaseous emissions, corrosion, or acid rain.

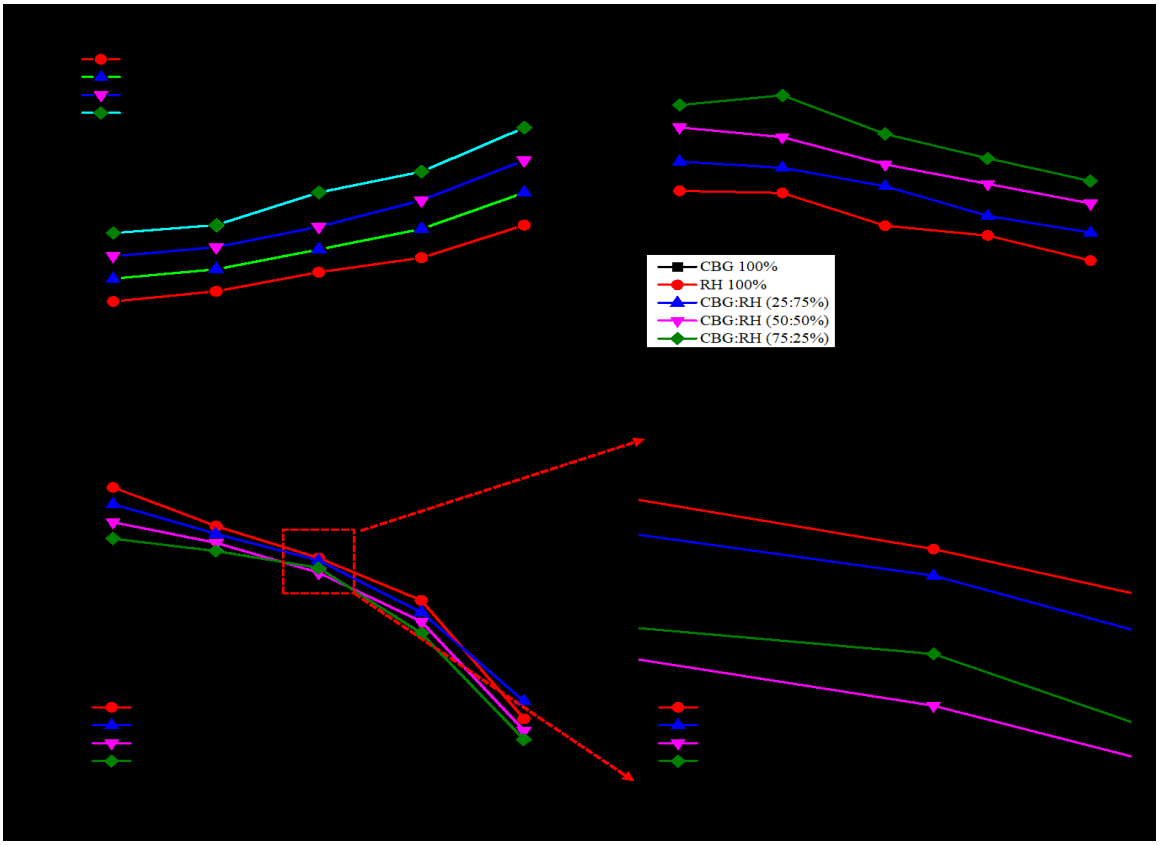

Fig. 1, Impact of temperture on ultimate analysis of co-torrefied biomass (a) Carbon content (b) Hydrogen content (c) Oxygen (d) Oxygen content at 250 °C.

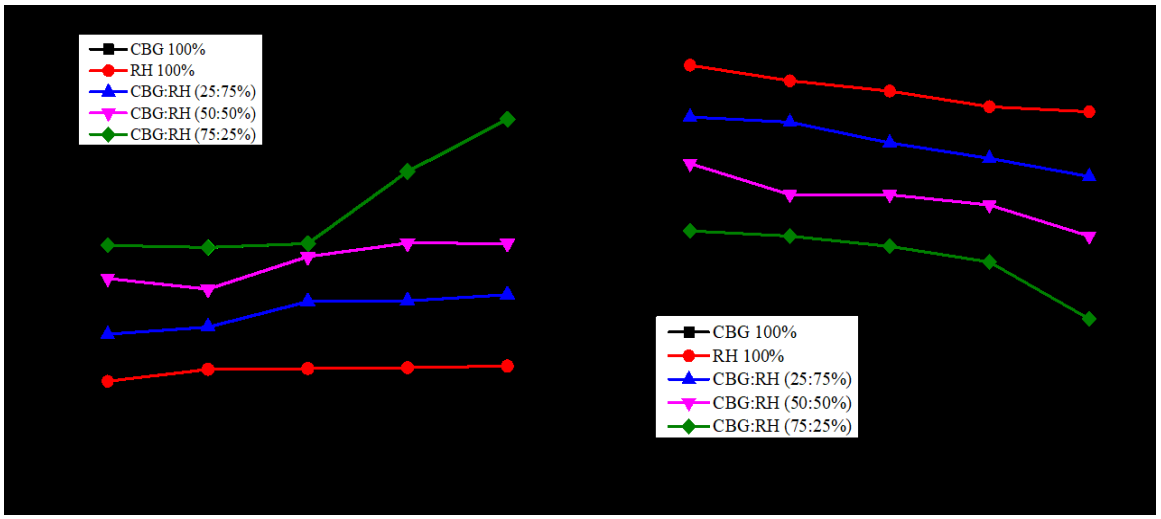

Fig. 2, Impact of temperture on ultimate analysis of co-torrefied biomass (a) Nitrogen (b) Sulphur content.

B. Fuel characteristics of biomass blends and torrefied biomass

Table. 1 shows that co-torrefaction temperature increases biomass calorific value. CBG 100% and CBH:RH (75:25%) at 300 °C have a significant calorific value. Torrefying biomass at 250 °C, 275 °C, and 300 °C causes greater thermal breakdown and volatile release, increasing bio-solid's heating value. CBH:RH (75:25%) has the highest heating value at 300 °C, as indicated in Table. 1.

Table. 1, Calorific value of un-torrefied and torrefied biomass.

Biomass	Temp (˚C)	CV of torrefied biomass (Kj/kg)
CBG 100%		23144.66
CBG 100%	200	23655.74
CBG 100%	225	23846.77
CBG 100%	250	24848.40
CBG 100%	275	28182.95
CBG 100%	300	30835.13
RH 100%		16870.83
RH 100%	200	17407.29

RH 100%	225	17750.72
RH 100%	250	18071.60
RH 100%	275	18123.78
RH 100%	300	19121.42
CBG: RH (25:75%)		18070.50
CBG: RH (25:75%)	200	18408.64
CBG: RH (25:75%)	225	18953.46
CBG: RH (25:75%)	250	19053.50
CBG: RH (25:75%)	275	21146.23
CBG: RH (25:75%)	300	23600.53
CBG: RH (50:50%)		20908.65
CBG: RH (50:50%)	200	20996.87
CBG: RH (50:50%)	225	21893.13
CBG: RH (50:50%)	250	22466.45
CBG: RH (50:50%)	275	22286.03
CBG: RH (50:50%)	300	23684.79
CBG: RH (75:25%)		22170.87
CBG: RH (75:25%)	200	22497.08
CBG: RH (75:25%)	225	22935.13
CBG: RH (75:25%)	250	23836.62
CBG: RH (75:25%)	275	25525.67
CBG: RH (75:25%)	300	25893.73

4. CONCLUSIONS

The co-torrefaction of CBG, RH has been established. Optimal blending ratio CBG:RH (75:25%) at 300 °C express high carbon content (65.24%) and low oxygen content (18.14%). That means excellent bio-solid has a high carbon and low oxygen content. In co-torrefaction, hemicellulose and lignin are partly depolymerized. The Calorific value shows that CBG 100% and CBH: RH (75:25%) at 300 °C is the optimal co-torrefied biomass. This study provides

fundamental statistics for researchers and commercial organizations interested in converting CBG and RH to bio-solid fuel.

5. REFERENCES

[1] S. R. Naqvi, S. Jamshaid, M. Naqvi, W. Farooq, M. B. K. Niazi, Z. Aman*, et al.*, "Potential of biomass for bioenergy in Pakistan based on present case and future perspectives," *Renewable and Sustainable Energy Reviews,* vol. 81, pp. 1247-1258, 2018.

[2] A. Al-Rumaihi, M. Shahbaz, G. McKay, H. Mackey, and T. Al-Ansari, "A review of pyrolysis technologies and feedstock: A blending approach for plastic and biomass towards optimum biochar yield," *Renewable and Sustainable Energy Reviews,* vol. 167, p. 112715, 2022/10/01/ 2022.

[3] R. Mehdi, N. Raza, S. R. Naqvi, A. H. Khoja, M. T. Mehran, M. Farooq*, et al.*, "A comparative assessment of solid fuel pellets production from torrefied agro-residues and their blends," *Journal of Analytical and Applied Pyrolysis,* vol. 156, p. 105125, 2021.

[4] S. Ge, S. Y. Foong, N. L. Ma, R. K. Liew, W. A. W. Mahari, C. Xia*, et al.*, "Vacuum pyrolysis incorporating microwave heating and base mixture modification: an integrated approach to transform biowaste into eco-friendly bioenergy products," *Renewable and Sustainable Energy Reviews,* vol. 127, p. 109871, 2020.

[5] S. J. Fain, M. Quiñones, N. L. Álvarez-Berríos, I. K. Parés-Ramos, and W. A. Gould, "Climate change and coffee: assessing vulnerability by modeling future climate suitability in the Caribbean island of Puerto Rico," *Climatic Change,* vol. 146, pp. 175-186, 2018.

[6] L. A. Silva, I. F. S. dos Santos, G. de Oliveira Machado, G. L. Tiago Filho, and R. M. Barros, "Rice husk energy production in Brazil: An economic and energy extensive analysis," *Journal of Cleaner Production,* vol. 290, p. 125188, 2021.

[7] N.-Y. Zheng, M. Lee, Y.-L. Lin, and B. Samannan, "Microwave-assisted wet co-torrefaction of food sludge and lignocellulose biowaste for biochar production and nutrient recovery," *Process Safety and Environmental Protection,* vol. 144, pp. 273-283, 2020.

[8] W.-H. Chen and P.-C. Kuo, "Torrefaction and co-torrefaction characterization of hemicellulose, cellulose and lignin as well as torrefaction of some basic constituents in biomass," *Energy,* vol. 36, pp. 803-811, 2011.

[9] S. A. Y. Shah, M. Zeeshan, M. Z. Farooq, N. Ahmed, and N. Iqbal, "Co-pyrolysis of cotton stalk and waste tire with a focus on liquid yield quantity and quality," *Renewable Energy,* vol. 130, pp. 238-244, 2019/01/01/ 2019.

[10] M. Danish, M. Naqvi, U. Farooq, and S. Naqvi, "Characterization of South Asian agricultural residues for potential utilization in future 'energy mix'," *Energy Procedia,* vol. 75, pp. 2974-2980, 2015.

[11] N. Hamzah, M. Zandi, K. Tokimatsu, and K. Yoshikawa, "Wood Biomass Pellet Characterization for Solid Fuel Production in Power Generation," vol. 3, 05/10 2018.

Carbon dioxide absorption for gaseous fuel up-gradation application

Nadeem Shah[a*], Muazzam Arshad[a]

a Department of Chemical Engineering, Faculty of Mechanical, Chemical & Industrial Engineering, University of Engineering & Technology, Peshawar, KPK, Pakistan.

Abstract—Renewable energy is currently the world's leading interest area. Biogas is being given significant attention regarding its production, purification and upgradation for it to be used as a renewable fuel supplement for the generation of energy. Biogas is a rich source, due to the presence of high contents of methane. The composition of biogas is methane (50-70%) and impurities like carbon dioxide (30-50%), sulphur oxide, water and other trace components (1%). The presence of these impurities makes it difficult to use biogas directly, as it reduces the gas heating value, causes operational problems for equipment and restricts its applications. It is necessary to upgrade biogas by removing carbon dioxide content to be used for required purposes. Different methods are used for

biogas upgrading, such as cryogenic separation, membrane separation, adsorption and absorption. The method used for upgrading biogas in this work is chemical absorption using a novel solvent for small-scale applications. This utilizes a solvent that has the ability to effectively remove carbon dioxide from the biogas mixture. Several previous pieces of research studied different types of solvents such as amine-based solvents, organic solvents, solvent blends and ionic liquids. Amine solvents such as MEA have been long used for carbon dioxide removal from natural gas but due to certain limitations are not applicable for small-scale applications. The solvent used in this work aims to achieve effective carbon dioxide absorption, a high absorption rate, greater absorption capacity and the possibilities for improvement by providing a more environmentally friendly operation.

Keywords: Biogas, biogas upgradation, CO_2 absorption, solvent blend.

1. INTRODUCTION

The world focuses on energy production from renewable sources at large with specific technology being explored and implemented such as solar energy, wind energy, hydropower, geothermal, biofuel and biomass. The use of natural gas at a high rate is leading to a lack in the amount of its capacity. Biomass is a significant and alternate source of energy supply for biogas production. After biogas is captured from biomass, it produces heat and electricity, which can be used in engines, micro turbines, and fuel cells. Biogas can also be upgraded into biomethane. This upgradation of biogas also known as renewable natural gas or RNG. The upgraded biogas can be injected into natural gas pipelines or used as a vehicle fuel. Currently, 2,200 operating biogas production systems in the United States across all 50 states, and has the capacity to install over 13,500 new systems. Produced and stored biogas can provide a renewable, clean, and a good source of base load power in place of coal or natural gas. Similar to natural gas, biogas can also be used as a source of peak power that can be rapidly ramped up. Using stored biogas limits the amount of methane released into the atmosphere and reduces dependence on fossil fuels.

Renewable natural gas or Biogas which is also named Biomethane is formed by a process termed anaerobic digestion in which large organic molecules are broken down into small organic molecules of the feedstock's in the absence of oxygen with the help of chemicals and microorganisms. There are various types of wastes from which biogas are produced such as wastes from landfills, livestock operations, wastewater treatment plants and other sources The composition of biogas mainly depends on the nature of wastes collected from different sources and various sectors. Due to the different nature of wastes, their composition is different having

methane content (50-70%), carbon dioxide (30-50%) and other traces of gases such as hydrogen sulphide (0-10000 ppm), VOCs &VFAs (0-1000 ppm), Siloxanes (0-50 ppm) and ammonia in small traces.

The biogas produced present impurities mentioned need purification for biomethane production. The production of biomethane mainly poses two major steps. The cleaning process, in which traces of hydrogen sulphide, ammonia, and water vapours, etc. are removed and the Upgradation process, in which carbon dioxide is removed to improve the biomethane contents. Depending upon the up gradation process various methods are used to upgrade biogas but in these methods, the Chemical absorption process offers the best results on a small-scale operation by using appropriate solvents such as small-scale equipment requirements. Different chemicals can be used for CO_2 capture through chemical absorption, such as organic solvents, ammonia, amines and potassium carbonate, sodium hydroxide, and potassium hydroxide. Favourable properties of commercial absorbent for carbon dioxide separation from a gas stream(biogas) include high absorption capacity, high absorption rate CO_2, high thermal and chemical stability, low regeneration energy requirements, low vapour pressure, low molecular weight, low viscosity and low corrosion rates.

In this work, the absorption of CO_2 in a solution of aqueous NaOH at different concentrations is carried out at constant pressure of 10 psi to analyse the efficiency of NaOH as a solvent for absorption of CO_2.

2. Methodology

Our research methodology has to investigate the suitability of Sodium hydroxide solution for CO_2 captured. It involves the preparation of a molar solution of sodium hydroxide used of known molarity and pouring it into the absorption tank. After this, we will connect the absorption tank inlet for gas to the CO_2 cylinder pipe and start operation by maintaining the tank pressure within the desired range through the control valve fitted on the cylinder tank. After 15 to 20 minutes of operation, we take different samples of known volume from the tank through the sample collection valve. Then we will start the Analysis of the sample with a known amount of HCL in the titration flask for CO_2 absorption.

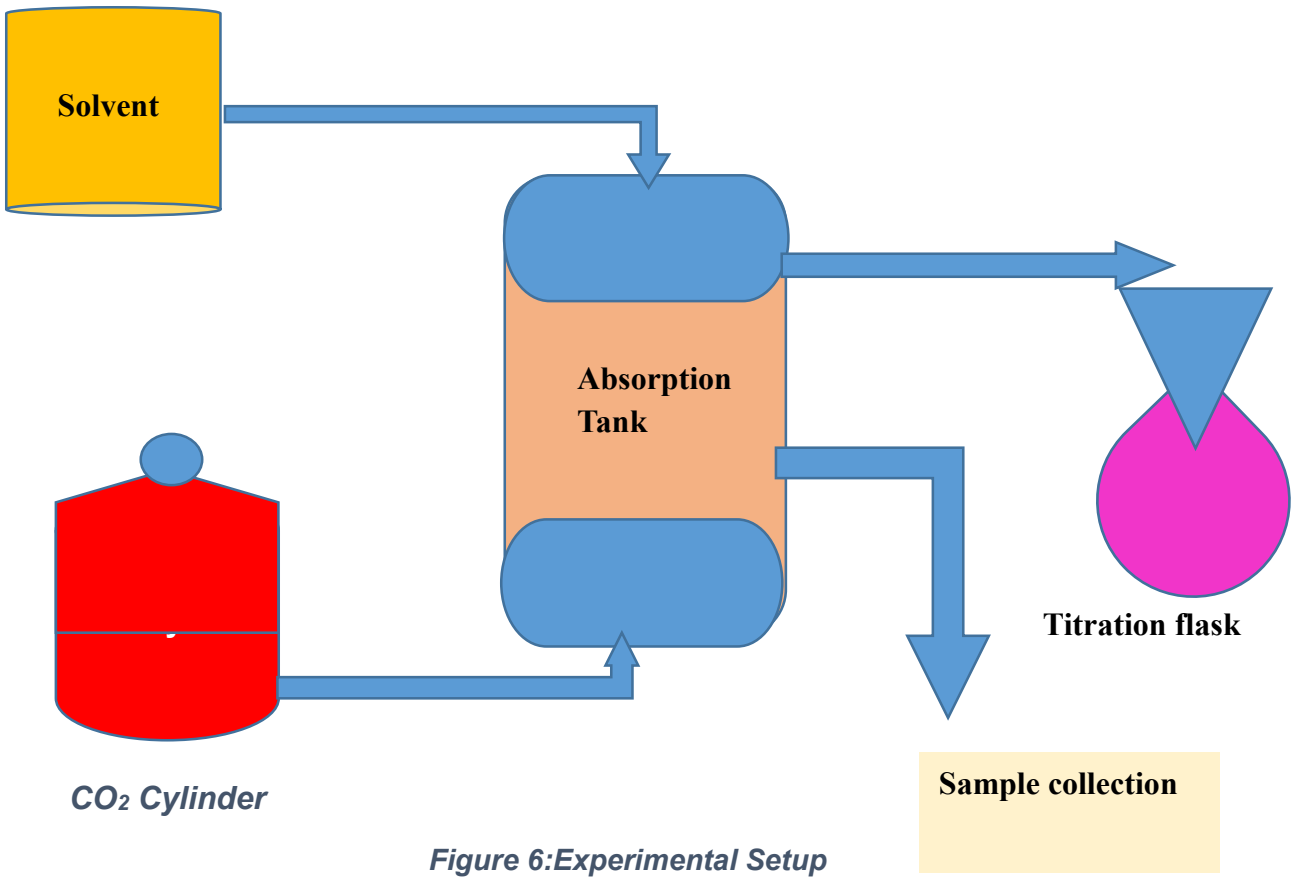

Figure 6:Experimental Setup

3. Result and discussion

Carbon dioxide concentration has been analyzed before and after treatment with Sodium hydroxide solution with different concentrations. Reading of Carbon dioxide absorption in different concentrations shows significant results. It shows that Sodium hydroxide solution has a great capacity for Carbon dioxide absorption at different concentrations. Fig. 2 shows the Carbon dioxide reading after purification under different concentrations of sodium hydroxide solution.

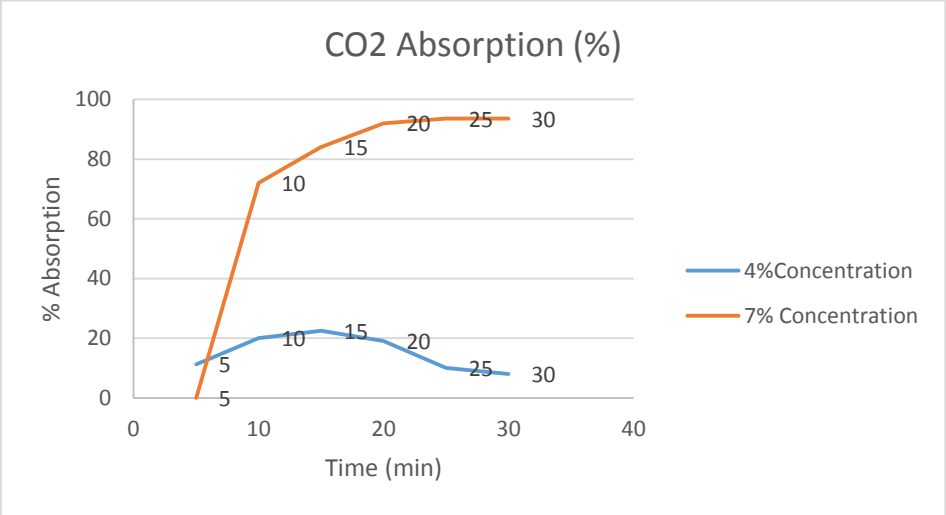

Figure 7: CO_2 composition after treatment at two different sodium hydroxide concentrations

The given data from the graph shows that for 4 % Concentration of NaOH solution absorption of CO_2 occurs from 0 to 15 minutes and after that desorption starts. Similarly, for 7% concentration solution of NaOH absorption starts from 0 to 20 minutes and after 20 minutes it shows steady state operation. It means that increase in NaOH concentration from 4% to 7 % increases CO_2 absorption capacity.

4. Conclusion

The experimental study shows that the concentration of solution plays an important role in CO_2 removal efficiency. When the concentration of absorbent increased, the CO_2 removal would be increased and we will obtain high efficiency. The results also indicated that the highest performance of sodium hydroxide solution as an absorbent is when the concentration of the solution used is at 7% (w/v)

5. References:

[1] Ideas. Insights. Sustainable Solutions (https://www.eesi.org/papers/view/fact-)
sheet- biogas converting-waste-to-energy (Accessed date: 16-8-2022)

[2] D. Deublein and A. Steinhauser, Biogas from waste and renewable resources. Weinheim, Germany: Wiley, (2008).

[3]O.I. Maile[a*], E. Muzenda[a,b], H. Tesfagiorgis[c] "Chemical Absorption of Carbon Dioxide in Bio Gas Purification" International conference on sustainable materials processing and manufacturing, SMPM 2017, 23-25 January, Kruger National Park.

[4] E. Ryckebosch, H. Vervaeren and M. Drouillon, "Techniques for transformation of biogas to biomethane", Biomass and Bioenergy, 35(5), pp.1633–1645(2011).

[5] H. Oechsner, S.K. Khanal, M. Taherzadeh, Advances in biogas research and application, Bioresour. Technol. 178 (2015) 177.

[6] D. Divya, L.R. Gopinath, P. Merlin Christy, A review on current aspects and diverse prospects for enhancing biogas production in sustainable means, Renew. Sust. Energy. Rev. 42 (2015) 690–699.

[7] N. Korres, P. O 'Kiely, J.A.H. Benzie, J.S. West, Bioenergy production by anaerobic digestion: using agricultural biomass and organic wastes, Routledge, 2013.

EFFECTS OF DIFFERENT MEDIUM ON THE CORROSION OF CRUDE OIL STORAGE TANK BOTTOM PLATE AND REMEDIAL ACTIONS FOR ITS LIFE ENHANCEMENT

Muhammad Usman[1], Abdul Shakoor[1], Muhammad Irfan Khan[1,2]
[1] University of Engineering and Technology Peshawar, [2] CECOS University of IT and Emerging Sciences Peshawar
[1] muhammad.usman@ogdcl.com

Abstract- Every industry in the world is experiencing a huge problem with corrosion, which is the degradation of materials to their atomic components, but the petrochemical industry is particularly affected. Crude storage tanks play a crucial role in the petrochemical process since they keep everything functioning properly. Storage tanks are extremely vulnerable to corrosion because of the aqueous environment, which could lead the petrochemical industry to significant financial loss. Corrosion in the bottom plates of storage tanks for crude oil and refined products is directly related to water present in the crude that is transported with the products, whether in suspended or condensed form.

The extracted crude oil from wells after processing is kept in a storage tank for 24 to 72 hours before being transported. Crude contains microorganisms as well as salt, sand, carbonates, and chlorides. Produced water accumulates in the tank's bottom all year long. During the settling process, slugs progressively accumulate in the tank's bottom and corrode the bottom plate.

This study's objectives were to assess the underlying the effect various corrosive media including crude, produced water, and solution (crude represented 80% of corrosion and produced water 20%) by using weight loss methods on the corrosion of crude storage tank's bottom plate. Additionally, the application and analysis of various corrosion control measures, such as corrosion inhibitor (oil base, water base), and fiber reinforcement polymer (FRP) coatings, are the main goals of this study. The findings demonstrated that FRP coating, as opposed to corrosion inhibitors, reduced the specimen's rate of corrosion. By using FRP coating, the bottom plate's corrosion rate was decreased by 93 (%).

Keywords: Corrosion, Corrosion inhibitor, Crude, FRP coating, Produced Water.

1. INTRODUCTION

The petroleum industry is subject to a variety of caustic environments. Some of these are particular to this industry. Therefore, it is convenient to combine all of these situations. The petroleum industry encounters corrosion problems in at least three key areas: production, shipping, and storage, as well as refinery activities. [1]. A crude oil storage tank, which is also widely used in the oilfield, storage and transportation, oil refining, chemical, and other industries, has served as the major storage facility for crude oil. The failure of crude oil storage tanks is influenced by various design and production levels, operational and medium circumstances, external surroundings, inspection and maintenance conditions, as well as operating and medium factors [2]. As the petroleum and chemical industries grow swiftly,

storage tanks play a bigger role in the storage of crude oil and its derivatives. The interior of the tank is susceptible to corrosion, particularly near the bottom. The thickness of the tank's bottom is decreased by corrosion coming from the top and bottom, or "soil side."[3]. Failures of tanks used for storage can be attributed to a variety of causes, such as human error, poor or inadequate maintenance, wall thickness loss due to corrosion, vapour ignition, excessive pressure, or natural disasters. Early tank failure have been most frequently attributed to corrosion on flooring.[4]. Corrosion is the irreversible degradation of a metal's surface in a corrosive environment caused on by chemical reactions that change a pure metal into its chemically more stable form, such as sulphides, oxides, hydroxides, etc. Any form of corrosive environment, such as a solid, liquid, or gas, may exist. [5]. Due to material deterioration, maintaining the integrity of equipment in the industry may be challenging. The consequences of corrosion on the oil and gas industry have a big impact on the unproductive time (NPT) that is lost from exploration to production, which is 20–30% of the total.[6]. The most hazardous and uncontrollable method of tank construction deterioration is metal corrosion. Depending on the levels of exposure to the corrosive elements of petroleum products, corrosive damage to the internal surface of tanks is separated into three zones: the roof, the bottom, and the lower belt. Inspections carried out after petroleum products were kept in them reveal that tanks' bottoms and lower region are particularly vulnerable to corrosion [7]. The US loses over $276 billion a year as a result of metallic corrosion. One third of the corrosion-related costs ($100 billion) might be avoided by using corrosion-resistant materials and implementing cutting-edge corrosion control technology.[8]. One method used to reduce corrosion in the petroleum industry is corrosion inhibitors. [9]. Corrosion inhibitors have been successfully used for many years. The use of corrosion inhibitors is the most common and frequently the most economical method of preventing corrosion in carbon steel.[10]. Storage tanks and components deteriorate mostly as a result of corrosion. Tank corrosion control and prevention are consequently of paramount importance for efficient plant economics and safety. The bottom layer of this tank is typically referred to as bottom sediment and water. The most important method of preventing corrosion is painting and lacquering tank surfaces. It probably makes up around half of the total cost of anti-corrosion procedures. [11].

2. METHODOLOGY

Weight loss method is used to investigate the effects of three different types of medium i.e crude, produced water and solution (80% crude & 20% produced water) on the corrosion of crude oil storage tank bottom plate and also the effect of different remedies i.e oil & water base corrosion inhibitor and fiber reinforcement polymer (FRP) on the corrosion rate.

Low carbon steel plate Grade Ss400 is utilized for crude storage tank bottom plate. Total 18 numbers of sample size (L=2cm, W=1.5cm & T=1cm) were prepared. The entire samples surface finish through abrasive paper of 60, 120, 240, 400, 600, 800, 1000 & 1200 grit. Drill a hole of size 0.34cm in the weight loss sample to hang in different medium. Carried out the FRP coating of 03 numbers of weight loss method. Resin Malkiens AD555-04 and Emulsion mate used for FRP coating of samples.

Three types of corrosive medium i.e crude, produced water and solution (crude 80% & produced water 20%) was used to investigate the effects of these medium on the corrosion rate of storage tank bottom plate. Also different types i.e corrosion inhibitor water & oil base were added in different concentration in these corrosive medium to check the effect of these

remedies on the corrosion rate of specimens. Also the effect of FRP coating on the corrosion rate of specimens in these three medium was investigated. The crude and produced water as shown in table 1 & 2 respectively were used as a medium.

TABLE 1: CRUDE ANALYSIS

Test Method	Test Parameters	Test Result
D-1298	Specific Gravity 60/60°F	0.8116
D-1298	API Gravity 60/60°F	42086
D-4294	Total Sulphur Content, wt%	0.032
D-96	BS&W vol%	<0.05
D-95	Water Content by D&S Vol%	<0.05
D-3230	Salt Content, lbs/1000bbl	Nil
D-445	Kinematic Viscosity at 40°C,cSt	2.13
D-97	Pour Point, °C	+18
D-189	Con Carbon Residue (CCR), wt%	0.837
D-323	Reid Vapor Pressure @37.8°C,psi	4.8
USB-97	Calorific Value (Gross), Btu/lb	19808

TABLE 2: PRODUCED WATER ANALYSIS

Properties	PH	Calcium	Magnesium	Sodium	Potassium	Chloride	Sulfate	Iron	Strontium	Bicarbonate
Value	7.5	970 ppm	136 Ppm	145 ppm	190 ppm	88380 ppm	2030 ppm	2.36 ppm	97.50 ppm	1342 ppm

3. RESULT AND DISCUSSION

Weight loss used to investigate the effect of different medium on the corrosion of crude storage tank bottom plate and also the effects of different remedies on the corrosion rate.

It is conventional method used to calculate the corrosion rate in different medium by calculating the weight loss in different interval of time. Weight the 12 numbers of specimens of weight loss through digital balance upto three decimal to record the initial weight. Tie each specimen with thread and hang in bottle of 250ml containing 225ml of crude, produced water and solution (80% crude and 20% produced water).
The weight of each sample was recorded at interval of 600hr, 1800hr & 5400hr. Each sample cleaned according the method ASTM G1 before calculating the weight. The corrosion rates calculated by using the formula (1) are listed in table 3.

$$(C.R) = \frac{W(g) * K}{\rho(g/cm^3) * A(cm^2) * T(hr)} \qquad (1)$$

Where (C.R) corrosion rate, (W) weight loss, ρ density of alloy, (A) exposed area, (T) total exposed time and the constant K=3.45x10^6 as area is in cm^2 can be varied to calculate the corrosion rate in mils/year(mpy).

TABLE 3: CORROSION RATE AT DIFFERENT INTERVAL OF TIME

Sample ID	Medium	Corrosion Rate(mpy) at 600hr	Corrosion Rate(mpy) at 1800hr	Corrosion Rate(mpy) at 5400hr	Percentage (%) Fluctuation
01	Crude	0.979	1.430	1.879	-

02	Crude +10ppm C.I oil Base	0.583	1.133	1.546	18
03	Crude + 10ppm C.I Water Base	1.223	1.698	2.060	-10
04	Crude (FRP Coated)	0.019	0.044	0.089	95
05	Water	4.308	6.160	9.255	-
06	Water+10ppm C.I oil Base	1.692	2.903	4.020	57
07	Water+ 10ppm C.I Water Base	1.103	2.010	2.759	70
08	Water (FRP Coated)	0.294	0.450	0.666	93
09	Solution (Crude80% + Water20%)	1.329	2.095	3.314	-
10	Solution (Crude80% + Water20%)+ 10ppm C.I Oil Base	1.078	1.687	3.037	8
11	Solution (Crude80% + Water20%)+ 10ppm C.I Water	0.831	1.373	2.228	33
12	Solution (Crude80% + Water20%) (FRP Coated)	0.157	0.229	0.326	90

The maximum corrosion rate is recorded in produced water followed by solution and least in crude is depicted in table 3. Also it is observed that corrosion rate is increasing with time in the same corrosive medium.

From the table 3 it is depicted that in crude corrosion rate is decrease by 18% by adding 10ppm corrosion inhibitor oil base while corrosion rate increase 10% by adding 10ppm corrosion inhibitor water base and 95% reduction calculated in FRP coated sample.

In produced water corrosion rate is decrease 57% by adding 10ppm corrosion inhibitor oil base and 70% reduction calculated by adding 10ppm corrosion inhibitor water base. In FRP coated sample 93% reduction observed.

In solution 8% reduction in corrosion rate observed by adding 10ppm corrosion inhibitor oil base and 33% reduction by adding 10ppm water base corrosion inhibitor. The 90% reduction observed in FRP coated sample.

4. CONCLUSION

From the above study it is concluded that the main corrosive medium for crude storage tank bottom plate corrosion is produced water as maximum corrosion calculated. The best remedy to reduce corrosion among these three is FRP coating as maximum corrosion reduction i.e 90% and above observed in the entire corrosive medium. From the results it is concluded that oil and water base corrosion inhibitor depend on the corrosive medium, the water base corrosion inhibitor is good for produced water as compared to oil base corrosion inhibitor and oil base corrosion inhibitor is good for crude. To achieve the good result both the inhibitor to be used with proper dosage and proper time. As produced water remain in the storage tank throughout the years it can be minimized but cannot be eliminated 100%, therefore the main medium which effect the bottom plate is produced water and FRP is the best remedy as 95% reduction is calculated in corrosion rate.

5. REFERENCES

1. Prabha, S.S., et al., Corrosion problems in petroleum industry and their solution. Eur. Chem. Bull, 2014. **3**(3): p. 300-307.
2. Luo, F.-W., R. Ran, and L. Wang, Study on corrosion law of large crude oil storage tank floor and risk-based inspection and maintenance technology. Corrosion Science and Technology, 2020. **19**(2): p. 66-74.
3. Martinez, S., Estimating internal corrosion rate and internal inspection interval of aboveground hydrocarbon storage tanks. Goriva i maziva: časopis za tribologiju, tehniku podmazivanja i primjenu tekućih i plinovitih goriva i inžinjerstvo izgaranja, 2013. **52**(2): p. 134-143.

4. Cirimello, P.G., et al., A major leak in a crude oil tank: Predictable and unexpected root causes. Engineering Failure Analysis, 2019. **100**: p. 456-469.
5. Harsimran, S., K. Santosh, and K. Rakesh, Overview of corrosion and its control: A critical review. Proc. Eng. Sci, 2021. **3**: p. 13-24.
6. Nagalakshmi, T. and A. Sivasakthi, Corrosion Control, Prevention and Mitigation in Oil & Gas Industry. International Journal of Innovative Technology and Exploring Engineering (IJITEE), 2019. **9**(2): p. 1568-1572.
7. Sultanbekov, R. and M. Nazarova. The influence of total sediment of petroleum products on the corrosiveness of the metal of the tanks during storage. in E3S Web of Conferences. 2019. EDP Sciences.
8. Miksic, B.A., et al., Storage tank protection using volatile corrosion inhibitors. Materials performance, 2006. **45**(6): p. 34.
9. Tamalmani, K. and H. Husin, Review on corrosion inhibitors for oil and gas corrosion issues. Applied Sciences, 2020. **10**(10): p. 3389.
10. Oberndorfer, M., K. Thayer, and W. Havlik. Corrosion control in the oil and gas production-5 successful case histories. in CORROSION 2007. 2007. OnePetro.
11. Gibril, M.M., M.R. El-Jazwi, and F.M. Shuaeib. Recent advances in protective coating of crude oil storage tanks. in Proceedings of the 6th Libyan Corrosion Conference. 2007.

Numerical Modelling of Formamidinium-Tin-Iodide Based Solar Cell using Scaps-1D

Muhammad Ismail[1*], Muhammad Noman[1,] Shayan Tariq Jan[1],
[1] U.S.-Pakistan Center for Advanced Studies in Energy, University of Engineering & Technology, Peshawar, Pakistan
[*]mismailmarwat.uspcase @uetpeshawar.edu.pk

Abstract—Photovoltaic technologies have shown great development over recent years, especially perovskite solar cells (PSCs). Methyl Ammonium Lead Tri-Iodide ($MAPbI_3$) based PSCs gained attention because of their impressive Power Conversion efficiencies (PCE). However, the presence of thermally unstable Methyl Ammonium (MA) Cation and toxicity of lead (Pb) limits its progress towards future commercialization. FA (Formamidinium) and Sn (Tin) have emerged as good alternatives for MA and Pb. $FASnI_3$ is more thermally stable and nontoxic but lower in PCE than $MAPbI_3$. In this work, $FASnI_3$ is numerically modeled in SCAPS-1D software. To enhance the performance of FA-PSC, copper and carbon charge transport layers are used. To improve electric conduction CuI is used as HTL (Hole Transport Layer) while to improve thermal conduction PCBM (phenyl-C61-butyric acid methyl ester) is used as ETL (electron Transport Layer). For further performance improvement, the optimized thickness for each active layer (Absorber, PCBM, and CuI) is identified and the effect of thickness on parameters like Voc, Jsc, FF, and PCE is observed. Thickness optimization showed phenomenal results in terms of an increase in PCE from 16.6% to 19.45 %. Moreover, the effect of the charge transport layer (CuI and PCBM) on the absorption bandgap alignment electric field intensity are also been analyzed and studied in detail in this paper.

Key Words: Perovskite, Nontoxic, $FASnI_3$, SCAPS, Optimization

1. INTRODUCTION

Organic-inorganic halide perovskites are widely used as absorber layers because of their unique optoelectrical properties[1]. Lead-based perovskite materials with the structure of $APbX_3$ ("A" being the monovalent cations such as FA or MA and X being the halogens) are known for their higher efficiencies[2][3]. However, Pb being non-eco-friendly uplifts the concerns about its commercialization. Many nontoxic metals such as Sn, Ge, Bi, Sb, and Cu have been reported as potential replacements for lead[4]. In this study Sn is used instead of lead and FA(Formamidinium) is used as a monovalent cation to tackle these issues. Studies show that $FASnI_3$ exhibits more thermal stability as compared to $MASnI_3$[5][6]. $FASnI_3$ with the narrow band gap of 1.41ev is used as an absorber along with highly conductive CuI (Copper Iodide) as the hole transport layer and PCBM (Phenyl-C61-butyric acid methyl ester) as Electron Transport Layer. The p-i-n type structure is proposed for the above-mentioned materials because of the higher band gap of the hole transport layer and literature shows that p-i-n structures show less hysteresis current values and simple fabrication[7].

A. Simulation Tool and Device Architecture:

SCAPS is a simulation tool widely used for analyzing the device performance of various thin film solar cells technologies by using three important equations i.e., Poisson's equation (Eq.1) continuity equation (Eq.2 and Eq.3), and drift-diffusion equations (Eq.4 and Eq.5).

$$\frac{\partial^2 \varphi}{\partial x^2} = \frac{q}{\varepsilon}(n - p) \quad (1)$$

$$\frac{\partial n}{\partial t} = \frac{1}{q}\frac{\partial J_n}{\partial x} + \mathrm{G} - \mathrm{R}, \frac{\partial p}{\partial t} = -\frac{1}{q}\frac{\partial J_p}{\partial x} + \mathrm{G} - \mathrm{R} \quad (2,3)$$

$$J_n = \mathrm{q}D_n \frac{\partial_n}{\partial_x} - \mathrm{q}\mu_n \mathrm{n}\frac{\partial_\varphi}{\partial_x}, J_p = \mathrm{q}D_p \frac{\partial_p}{\partial_x} - \mathrm{q}\mu_p \mathrm{p}\frac{\partial_\varphi}{\partial_x} \quad (4,5)$$

The basic proposed inverted (p-i-n) structure is shown in Fig. 1. In an inverted structure, the TCO (Transparent Conductive Oxide) is the top layer followed by HTL, Absorber Layer ETL, and Metal Electrode. TCO is a conductive material with a low absorption coefficient acting as an anode. ITO (Indium Tin Oxide) is mostly preferred as a TCO in inverted structures. Al is used as a back contact metal acting as a cathode.

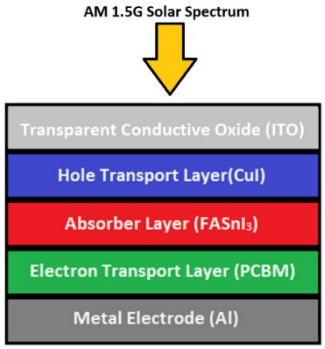

Fig. 1. Proposed P-I-N inverted structure.

The complete PSC structure ITO/CuI/$FASnI_3$/PCBM/Al is simulated through SCAPs. All the material parameters mentioned in Table 1 are taken from multiple works of literature [8][9][6]. At front and back contact ITO and Al were used with the work function of 5eV and 4.2eV respectively. Interface with defects density of 10^{10} cm^{-1} is incorporated at HTL/Absorber and ETL/Absorber interface with the single energetic distribution. The defect density for the $FASnI_3$ absorber layer is kept at 10^{15} cm^{-1} for all the simulations with Gaussian energetic distribution while for the charge transport layers (PCBM and CuI) defects density is kept at 10^{14} cm^{-1}. All simulations are performed in 1.5G solar radiation under STC.

TABLE 1: Material Parameters of Solar Cells.

Parameters	Thickness (nm)	E_g (eV)	Electron Affinity (eV)	Dielectric Permittivity	μ_n (cm^2/Vs)	μ_p (cm^2/Vs)	Total Defect Density (cm^{-3})
$FASnI_3$	350	1.41	3.52	8.2	22	22	1E+15
CUI	150	2.98	2.1	6.5	1.69×10^{-4}	1.69×10^{-4}	1E+14
PCBM	150	2	3.9	4	10^{-2}	10^{-2}	1E+14

Based on the parameters mentioned in the table the numerical modeling was performed for ITO/CuI/$FASnI_3$/PCBM/Al. Based on simulation results Voc=0.87V, Jsc=28.7mA/cm^2, FF= 83.22, PCE= 16.6% were achieved. IV and QE curves are shown in Fig. 2. QE is the ratio of current generated in response to incident photons of a particular wavelength. Fig. 2(b) shows that the cell works best in the range of 450-800 nm which is most of the visible region after that

the QE falls drastically. The QE of the cell can be improved by thickness and doping optimization[10].

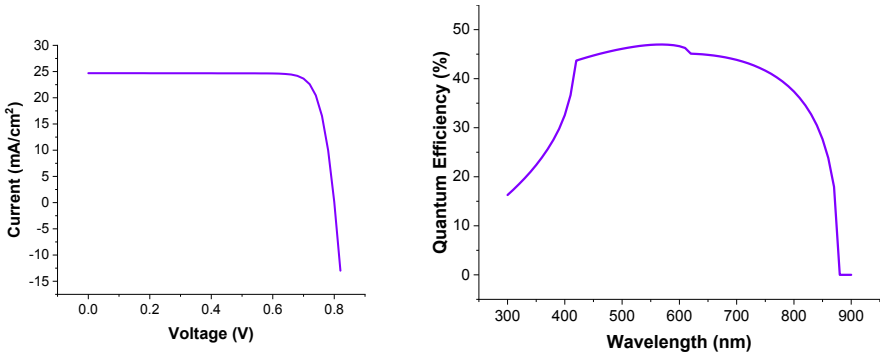

Fig. 2. (a)IV curve and (b) QE curve for simulated cell.

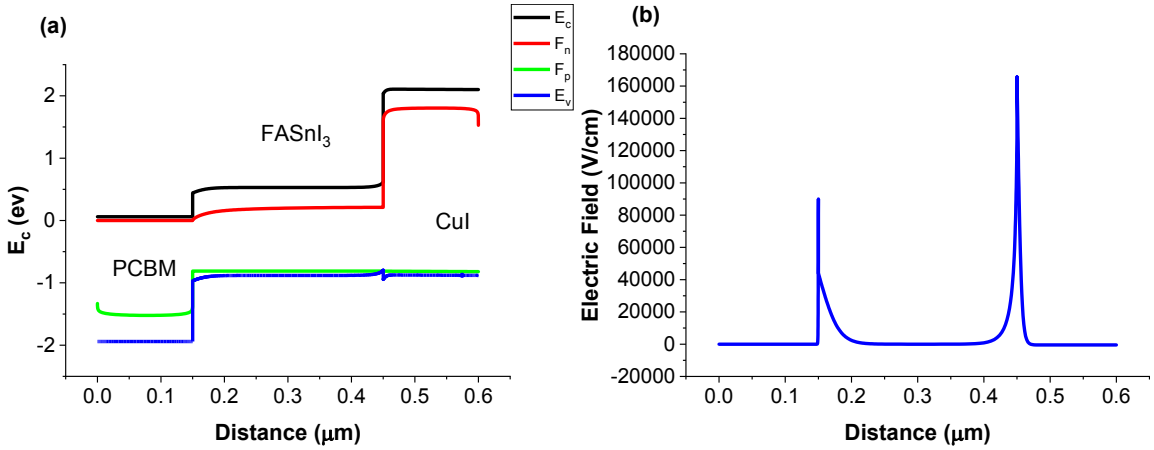

Fig. 3. (a) Band Alignment of simulated PSC (b) Electric Field at interfaces

Band alignment plays a very significant part in improving the performance of the solar cell. The VBO and CBO at $FASnI_3$/CuI and $FASnI_3$/PCBM interfaces are responsible for electron and hole transport from the absorber to the corresponding charge transport layers. Narrow CBO (Conduction Band Offset) and VBO (Valence Band Offset) at Absorber/ETL and Absorber/HTL interfaces respectively are required for the smooth transport of electrons and holes which can be seen in Fig. 3. The significance of band alignment can be related to the surge in an electric field at interfaces shown in Fig. 3(b). The electric field is created as a result of fermi level difference at interfaces ($\Delta E_F = qVoc$) facilitating the charge transport, reducing recombination, and blocking the unwanted charges at the respective interfaces[11][12].

2. RESULTS AND DISCUSSION

1. Influence of Perovskite Absorber ETL and HTL thickness:

The response of solar cells towards the solar spectrum is greatly dependent upon the absorber thickness. To investigate the impact of thickness on the output of solar cells the thickness is increased from 0.05μm to 1.5 μm and the results are shown in Fig. 4. The increase in absorber thickness increases the capability of solar cells to absorb a greater number of photons as a result of which more electron-hole pairs are produced. This in turn improves the current density as can be seen in Fig. 4(b). This results in more charge carriers reaching the respective electrodes which enhances the Voc and PCE [13]. Due to more charge carriers being produced, recombination also increases, reducing the F.F. It can be observed that after the thickness of 0.7μm the saturation in performance is observed and after 0.85μm the cell performance drops. The drop in cell performance at higher thickness is because the perovskite thickness exceeds the carrier diffusion length of charge carriers and recombination accelerates. The optimized thickness for the $FASnI_3$ layer is found to be 0.7μm.

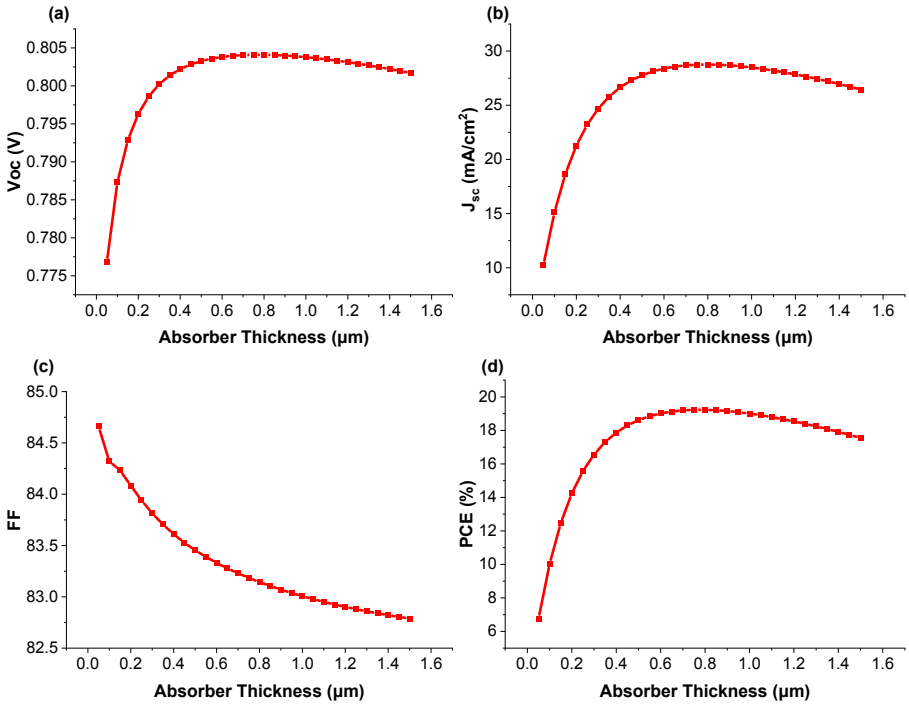

Fig. 4. Influence of Absorber Layer Thickness Variation on (a) V_{oc} (b) J_{sc} (c) FF (d) PCE.

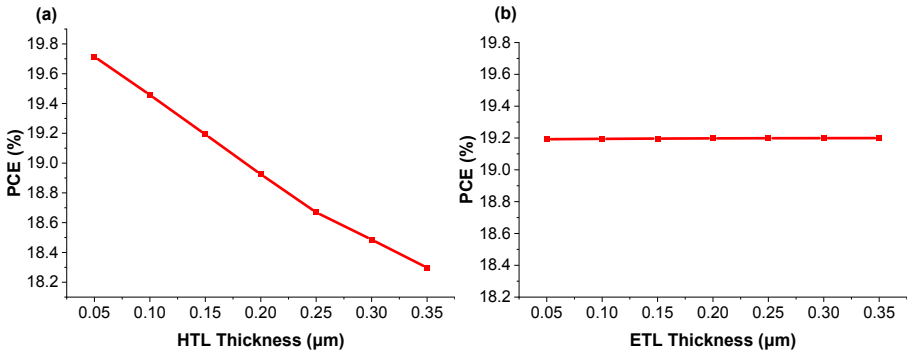

Fig. 5. (a) Influence of HTL thickness variation on PCE (b) Influence of ETL thickness Variation on PCE

Charge Transport layers thickness separates the absorber from the electrode and also facilitates the transport of charge carriers. In P-I-N structures, the variation in HTL thickness decreases the performance of solar cells because of an increase in series resistance at Absorber/HTL interface as shown in Fig. 5(a). As for ETL, the thickness variation has a negligible effect on performance as can be seen in Fig. 5(b). Optimized thickness for both HTL and ETL is found to be 100nm (0.1μm) as.

3. CONCLUSION

The ITO/CuI/$FASnI_3$/PCBM/Al PSC structure was successfully modelled in SCAPS-1D with Voc=0.87V, Jsc=28.7mA/cm^2, FF= 83.22, PCE= 16.6%. It was concluded that increasing the thickness of the absorber up to saturation point improves the PSC performance, after which it declines. The absorber was optimized at 700nm. Increasing the thickness of the CTL reduced the PCE efficiency because it increased the resistance of the cell. The charge transport layer optimized thickness was found to be 100nm. After Optimization, the PSC performance was enhanced to Voc of 0.8V Jsc 28.8 mA/cm^2, FF of 83.7, and PCE 19.45%.

4. ACKNOWLEDGEMENT

We would like to thank Prof. Dr. Marc Burgelman at the University Of Ghent, Belgium for providing us with the SCAPs simulation software.

5. REFERENCES

[1] S. Tariq Jan and M. Noman, “Influence of layer thickness, defect density, doping concentration, interface defects, work function, working temperature and reflecting coating on lead-free perovskite solar cell,” *Sol. Energy*, vol. 237, no. December 2021, pp. 29–43, 2022, doi: 10.1016/j.solener.2022.03.069.

[2] M. S. G. Hamed and G. T. Mola, “Mixed Halide Perovskite Solar Cells : Progress and Challenges,” *Crit. Rev. Solid State Mater. Sci.*, vol. 0, no. 0, pp. 1–28, 2019, doi: 10.1080/10408436.2018.1549976.

[3] N. G. Park, M. Grätzel, and T. Miyasaka, “Organic-inorganic halide perovskite photovoltaics: From fundamentals to device architectures,” *Org. Halide Perovskite Photovoltaics From Fundam. to Device Archit.*, pp. 1–366, 2016, doi: 10.1007/978-3-319-35114-8.

[4] R. Kour, S. Arya, S. Verma, J. Gupta, and P. Bandhoria, “Potential Substitutes for Replacement of Lead in Perovskite Solar Cells : A Review,” vol. 1900050, 2019, doi: 10.1002/gch2.201900050.

[5] T. M. Koh *et al.*, “Formamidinium tin-based perovskite with low Eg for photovoltaic applications,” *J. Mater. Chem. A*, vol. 3, no. 29, pp. 14996–15000, 2015, doi: 10.1039/c5ta00190k.

[6] P. Roy, S. Tiwari, and A. Khare, “An investigation on the influence of temperature variation on the performance of tin (Sn) based perovskite solar cells using various transport layers and absorber layers,” *Results Opt.*, vol. 4, no. February, p. 100083, 2021, doi: 10.1016/j.rio.2021.100083.

[7] T. R. Lenka *et al.*, “Device modeling for high efficiency lead free perovskite solar cell with Cu2O as hole transport material,” *2019 IEEE 14th Nanotechnol. Mater. Devices Conf. NMDC 2019*, pp. 14–17, 2019,

doi: 10.1109/NMDC47361.2019.9084004.

[8] D. Jayan K. and V. Sebastian, "Comparative Study on the Performance of Different Lead-Based and Lead-Free Perovskite Solar Cells," *Adv. Theory Simulations*, vol. 4, no. 5, pp. 1–11, 2021, doi: 10.1002/adts.202100027.

[9] N. Singh, A. Agarwal, and M. Agarwal, "Performance evaluation of lead–free double-perovskite solar cell," *Opt. Mater. (Amst).*, vol. 114, no. February, pp. 1–11, 2021, doi: 10.1016/j.optmat.2021.110964.

[10] S. allah Khelifi *et al.*, "Quantum efficiency improvement depending on the oxygen doping density, temperature, and layer thicknesses of an intermediate band solar cell based on ZnTe:O: Numerical analysis," *Optik (Stuttg).*, vol. 224, no. May, p. 165432, 2020, doi: 10.1016/j.ijleo.2020.165432.

[11] K. Kearney, G. Seo, T. Matsushima, C. Adachi, E. Ertekin, and A. Rockett, "Computational Analysis of the Interplay between Deep Level Traps and Perovskite Solar Cell Efficiency," *J. Am. Chem. Soc.*, vol. 140, no. 46, pp. 15655–15660, 2018, doi: 10.1021/jacs.8b06002.

[12] J. Haddad *et al.*, "Analyzing Interface Recombination in Lead-Halide Perovskite Solar Cells with Organic and Inorganic Hole-Transport Layers," *Adv. Mater. Interfaces*, vol. 7, no. 16, 2020, doi: 10.1002/admi.202000366.

[13] A. Bag, R. Radhakrishnan, R. Nekovei, and R. Jeyakumar, "Effect of absorber layer, hole transport layer thicknesses, and its doping density on the performance of perovskite solar cells by device simulation," *Sol. Energy*, vol. 196, no. November 2019, pp. 177–182, 2020, doi: 10.1016/j.solener.2019.12.014.

Numerical Modeling and Analysis of Inorganic Germanium Perovskite Solar Cell with ZnSe and CMTS Charge Transport Layer

Asfand Yar Ali Khan[1*], Muhammad Noman[1], Shayan Tariq Jan[1]
[1] U.S.-Pakistan Center for Advanced Studies in Energy, University of Engineering & Technology, Peshawar, Pakistan
[*]asfandyar.uspcase@uetpeshawar.edu.pk

***Abstract*—** Perovskite are organic-inorganic hybrid materials. The organic component of the perovskite decomposes rapidly due to humidity and moisture exposure. Cesium (Cs) has successfully been proposed as the alternate A-cation in the perovskite material. Cs is purely organic material that has comparatively low degradation due to humidity. In this work nontoxic gallium-based cesium perovskite absorber is used in the PSC. The Cs-PSC is numerically modelled through solar cell capacitance simulator (SCAPS-1D). ZnSe has been chosen as ETL in the structure due to having large band gap and transmittivity. While kesterite CMTS material has been used as the HTL due to its high electric conductivity. The effect of Cs-perovskite and the CTL on the photovoltaic cell's performance are analyzed in detail though using continuity and Poisson equations. The IV characteristics, electric potential, recombination, band alignment, power conversion and quantum efficiency are studied. Moreover, the effect of increasing absorber defect density on optimized thickness of the layer has also been found. The optimized thickness at defect density of E13 was found to be 0.9 µm with PCE of 19.66%, for E14 0.8 µm with 19.54% PCE and for E15 0.8 µm with 19.34% PCE

Keywords—Charge transport layer, $CsGeI_3$, Non-toxic, Perovskite solar cell, SCAPS

1. INTRODUCTION

Perovskite became famous in PV technologies due to its outstanding light absorbing properties [1][2]. Perovskite solar cell (PSC) are hybrid mixture of A (organic, inorganic) materials with metal B which are cations whereas X (halide) is anions forming a structure known as ABX_3 crystal structure [3]. Perovskite being hybrid and having exceptional properties give advantage to bandgap which is tunable and having efficient carrier mobility, longer diffusion length results in ideal PSC [4]. The most popular are lead base PSC with power conversion efficiency (PCE) 23% and above but these solar cells were fabricated in labs. As these solar cells were toxic in nature due to lead (Pb) used in it and instability made them restricted to commercialization [5]. For that an alternate lead free, non-toxic material that is germanium (Ge) which belongs from same family tree as tin (Sn) and Pb with same photovoltaic properties and light absorption is used in this research with non-organic cesium (Cs) A-cation [6][7]. It is also important to mention that according to studies that (Ge) PSC has ability to achieve more than 15% PCE [7][8]. which is less than Pb but Ge remove the toxic issue, on other hand Ge PSC are more stable than Sn based PSC. Moreover, Ge based PSC has high defect density due to which lower PSC have lower PCE but there is lot space available to progress in terms of efficiency, for that simulation tool can be utilized to optimize the cell structure to get better PCE [9].

2. METHODOLOGY

In this research SCAPS-1D software which is 1-Dimentional simulation tool is used. The analysis of SCAPS-1D is based on Continuity and Poisson's equation [10] The software helps researcher to design and simulate different cell structures. Several research articles have been published on this software exploring its application in finding efficiencies of solar cells [11]. In this research, the n-i-p structure is numerically modeled in SCAPS to analyze the I-V characteristics, band gap, carrier density and other parameters of cell. The Zinc Selenide (ZnSe) is used as the n-doped electron transport layer (ETL) because of having large conductivity and band gap. The $CsGeI_3$ is the perovskite i-layer used in the structure. Its function is to produce charge carriers by absorbing the photons. The last layer is Kesterite base material (CMTS) used as p-doped hole transport layer (HTL) having high electric conductivity. The layers form the structure ZnSe/$CsGeI_3$/CMTS. The material parameters extracted from literature are given below in table-1 [9][7][12]. To obtain realistic results defect density (Nt) were added in each layer that is Nt of $1x10^{15}$ cm^{-3} for absorber and Nt of $1x10^{14}$ cm^{-3} for ETL/HTL. Furthermore, Interface defects were also added between the layers (HTL/Perovskite and Perovskite/ETL). The simulations were performed taking Air Mass (AM) 1.5, Temperature 300k and 1000 W/m^2 of irradiance.

TABLE I: Layers Parameters

Parameters	Thickness (nm)	Eg (eV)	Electron Affinity (eV)	Dielectric Permittivity	Electron Mobility (cm^2/Vs)	Hole Mobility (cm^2/Vs)	Nt (cm^{-3})
ZnSe	100	2.8	4.09	8.6	400	110	1E+15
$CsGeI_3$	400	1.6	3.9	18	20	20	1E+14
CMTS	100	1.6	4.35	9	0.16	0.16	1E+15

In this work the defect density of $CsGeI_3$ has been varied and optimized thickness for each defect density has been identified. The IV curve obtained of initial structure ($ZnSe/CsGeI_3/CMTS$) is shown in Fig. 1. Based on simulation results, PCE of 18.35% is achieved with 20.99 mA/cm^2 short circuit current (JSC), 1.145 V open circuit voltage and fill factor (F.F), 76.29%.

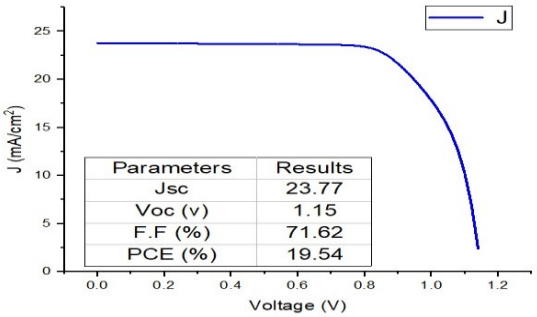

Fig. 1. I-V curve

3. RESULTS AND DISCUSSION

ENERGY BAND ALIGNMENT AND ELECTRIC FIELD

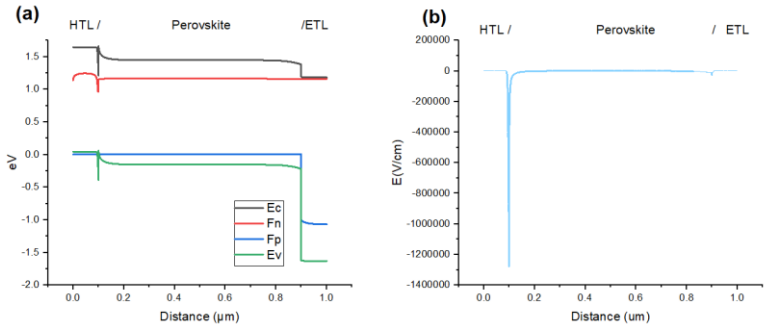

Fig. 2. Energy band alignment & Electric field

The Fig. 2a. shows that there is good alignment between ETL and perovskite, having little offset in conduction band and large offset is seen in valance band which results in good electron flow and holes being blocked. On the other hand, the HTL and Perovskite valance band for smooth flow of holes, but due to the conduction band having small offset there will be chances of recombination. From Fig. 2b it can be observed that the HTL/Perovskite has large electric potential. This is due to the spike formed in the energy band alignment of HTL/Perovskite. This high electric potential will have larger influence and separate the charge carriers more efficiently.

Recombination and Quantum Efficiency

Figure 3A shows the recombination occurring in the cell structure. It can be observed that due to the high electric field at HTL/Perovskite minimum recombination occurs there as the field efficiently separates and transports the holes. On the hand due to the low electric field at

ETL/Perovskite interface and the conduction band offset, majority recombination occurs here. Figure 3B shows the quantum efficiency of the structure

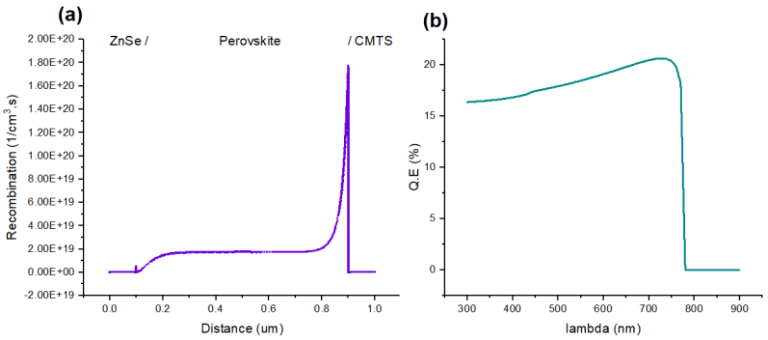

Fig. 2. Recombination & Quantum efficiency

Defect Density

When defect density is increased than trap state and defects also increase in layer which hinder the electron movement and results in more recombination due to which optimized thickness is reduced, effecting the current and finally drastic reducing the PCE. The effect of defect density on the optimized thickness and PCE are shown in Fig. 4.

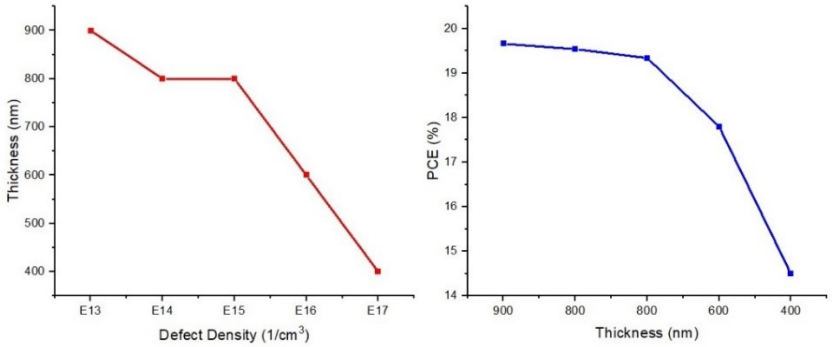

Fig. 4 Defect density vs Thickness

From the results it can be seen that the optimized thickness reduces from 900nm to 400nm as the defect density is increased from E13 to E17 cm^{-3}. Due to the reduced optimized thickness the efficiency also reduces from 19.8% to 14.4%.

4. CONCLUSION

In this work, CsGeI3 based PSC is simulated using Scaps-1D simulator. The output parameters depict that optimum efficiency is achieved by varying the defect density with respect to thickness of absorber material. On lower defect density with optimized thickness the PSC gives maximum PCE and also improve the QE. The optimized thickness at defect density of E13 was found to be 0.9 µm with PCE of 19.66%, Jsc of 24.02 mA/cm^2, Voc of 1.15 V and FF 71.26%, for E14 0.8 µm with 19.54% PCE, Jsc of 23.77 mA/cm^2, Voc of 1.15 V, FF of 71.62 and for E15 0.8 µm with 19.34% PCE, Jsc of 23.72 mA/cm^2, Voc of 1.15 V and FF 71.15%. The results can useful for fabrication but some other parameters need to be inspected in further studies.

ACKNOWLEDGMENT

The authors would like to thank Renewable energy department, U.S-Pakistan Center of Advance Studies U.E.T Peshawar for the support of this work and would like to thank SCAPS-1D developer who are behind this simulation tool which made it easy to obtain the results.

5. REFERENCES

[1] F. De Angelis, D. Meggiolaro, E. Mosconi, A. Petrozza, M. K. Nazeeruddin, and H. J. Snaith, "Trends in Perovskite Solar Cells and Optoelectronics: Status of Research and Applications from the PSCO Conference," *ACS Energy Lett.*, vol. 2, no. 4, pp. 857–861, 2017, doi: 10.1021/acsenergylett.7b00217.

[2] J. Qiu *et al.*, "Toward a New Energy Era: Self-Driven Integrated Systems Based on Perovskite Solar Cells," *Sol. RRL*, vol. 3, no. 11, pp. 1–26, 2019, doi: 10.1002/solr.201900320.

[3] Q. Chen *et al.*, "Under the spotlight: The organic-inorganic hybrid halide perovskite for optoelectronic applications," *Nano Today*, vol. 10, no. 3, pp. 355–396, 2015, doi: 10.1016/j.nantod.2015.04.009.

[4] M. Girtan, "On the electrical and photoelectrical properties of CH3NH3PBI3 perovskites thin films," *Sol. Energy*, vol. 195, no. September 2019, pp. 446–453, 2020, doi: 10.1016/j.solener.2019.11.096.

[5] U. Krishnan, "Factors affecting the stability of perovskite solar cells: a comprehensive review," *J. Photonics Energy*, vol. 9, no. 02, p. 1, 2019, doi: 10.1117/1.jpe.9.021001.

[6] X. Wu, W. Song, Q. Li, X. Zhao, D. He, and Z. Quan, "Synthesis of Lead-free CsGeI3 Perovskite Colloidal Nanocrystals and Electron Beam-induced Transformations," *Chem. - An Asian J.*, vol. 13, no. 13, pp. 1654–1659, 2018, doi: 10.1002/asia.201800573.

[7] A. Raj, M. Kumar, H. Bherwani, A. Gupta, and A. Anshul, " Evidence of improved power conversion efficiency in lead-free CsGeI 3 based perovskite solar cell heterostructure via scaps simulation ," *J. Vac. Sci. Technol. B*, vol. 39, no. 1, p. 012401, 2021, doi: 10.1116/6.0000718.

[8] A. Hima and N. Lakhdar, "Enhancement of efficiency and stability of CH3NH3GeI3 solar cells with CuSbS2," *Opt. Mater. (Amst).*, vol. 99, no. December 2019, p. 109607, 2020, doi: 10.1016/j.optmat.2019.109607.

[9] Y. H. Khattak, F. Baig, A. Shuja, S. Beg, and B. M. Soucase, "Numerical analysis guidelines for the design of efficient novel nip structures for perovskite solar cell," *Sol. Energy*, vol. 207, no. July, pp. 579–591, 2020, doi: 10.1016/j.solener.2020.07.012.

[10] S. Tariq Jan and M. Noman, "Influence of layer thickness, defect density, doping concentration, interface defects, work function, working temperature and reflecting coating on lead-free perovskite solar cell," *Sol. Energy*, vol. 237, no. December 2021, pp. 29–43, 2022, doi: 10.1016/j.solener.2022.03.069.

[11] N. Singh, A. Agarwal, and M. Agarwal, "Numerical simulation of highly efficient lead-free all-perovskite tandem solar cell," *Sol. Energy*, vol. 208, no. August, pp. 399–410, 2020, doi: 10.1016/j.solener.2020.08.003.

[12] S. Abdelaziz, A. Zekry, A. Shaker, and M. Abouelatta, "Investigating the performance of formamidinium tin-based perovskite solar cell by SCAPS device simulation," *Opt. Mater. (Amst).*, vol. 101, no. January, p. 109738, 2020, doi: 10.1016/j.optmat.2020.109738.

Numerical study of a steam methane reformer integrated membrane system for 250 kg/day hydrogen production

[1]Khalid Saif Ullah, [2]Naeem Ur Rehman, [1]Muhammad Muqaddam Javaid, [1*]Kashif Rashid
[1]khalidsaifullah543@gmail.com Department of Chemical Engineering, Pakistan Institute of Engineering and Applied Sciences (PIEAS), Lehtrar Road, P.O. Nilore, 45650, Islamabad, Pakistan.
[2]College of Earth and Environmental Sciences (CEES), Quaid-e-Azam Campus, University of the Punjab, Lahore, Pakistan.
Corresponding author (Kashif Rashid, PhD): kashifrashid@pieas.edu.pk

***Abstract*—** Steam methane reforming is one of the most used methods for hydrogen generation. The use of a membrane in the conventional steam methane reforming process is an encouraging technology to enhance the performance of the reactor. The challenge in designing and scaling up the membrane steam methane reforming reactor lines in the suitable selection of operating conditions. In this investigation, a 3-D CFD model was developed for a 250 kg/day hydrogen generation unit. The Xu and Froment kinetic model for reforming reactions was coupled with CFD by user-defined function (UDF) and the membrane permeation flux was included by using Sievert's law as a source and sink term in the species transport equations. The model was validated with the experimental results, and then the effect of the membrane on the reforming process was analyzed. The results predicted that the methane conversion increased to 97 % by using a membrane. The effect of the sweep gas flow pattern was also investigated on the overall performance.

Keywords— CFD modeling; hydrogen production; steam methane reforming; membrane separation.

1. INTRODUCTION

Hydrogen, 75% of the universe, is a key energy carrier. Reduced pollutant and greenhouse gas emissions when oxidized as fuel, various storage forms (unlike electricity), and multiple modes of transportation make H_2 an ideal energy carrier [1]. Hydrogen must be extracted from hydrocarbons, water, and biomass because there is none in nature [2]. Hydrocarbons (natural gas (NG) and petroleum) produce 78% of the world's hydrogen. Water electrolysis produces about 4% of hydrogen, and coal produces about 18%. There are several methods for producing hydrogen, including thermochemical, electrochemical, photobiological, and photochemical. Steam reforming (SR) of methane is the most used thermochemical method in hydrogen production [3].

Even though steam methane reforming is a fully developed technology for producing hydrogen, it's still being improved. Researchers are interested in using hydrogen-selective membranes in steam methane reforming. Using a membrane in the reactor to remove hydrogen from the product side increases methane conversion and hydrogen yield. Low-temperature membrane reactors reduce CO content [4–6].

In recent years, several researchers worked on membrane reactors. Kim et al. [7] performed the experimentations to investigate the effects of membrane on the steam reforming process. The results predicted the greater methane conversion in the membrane reactor. Wei-Hsin Chen et al. [8] developed a model for hydrogen separation by using Sievert's law. The model predicted higher hydrogen separation with counter-current configuration. Coroneo et al. [9] analyzed three different types of membrane in a steam reforming reactor through CFD model

and validated the model with experimental results. Chibane et al. [10] developed a numerical model to predict the effect of Palladium-based membrane on reforming reactions. The results showed high methane conversion in a membrane reactor based on to Le Chatelier's principle. Although a variety of research has done in this field, but all the developed models were based on very simplified domains. Moreover, they did not consider reaction and separation simultaneously in the reforming zone. The hydrogen distribution on the retentate side was also considered uniform. The novelty of this work was to take variable hydrogen profile by writing a user-defined function (UDF). Moreover, the CFD analysis was performed on an actual experimental setup of 250 kg/day hydrogen production capacity. The comparison of conventional and membrane reactor was also performed.

2. METHODOLOGY

T. System description and operating conditions

The geometry of membrane steam reforming reactor is designed based on the experimental setup of Rahimipetroudi et al. [11].The setup is consisted of one burner and twelve reforming tubes. The reforming tubes have two zones: (a) reaction zone (retentate) and (b) permeate zone separated by Pd-Ru-based membrane. Fig. 5 shows the symmetrical part of membrane reactor used for simulation.

Ni/Al_2O_3 commercial catalyst is packed in reforming tube retentate. Pd-Ru membranes separate hydrogen. A metal fiber burner in the reactor's center generates heat for reforming. Methane and steam enter from the bottom, and reforming occurs on the porous retentate side. Reforming creates H_2, CO_2, and CO. Permeate-side sweep gas drives permeated hydrogen.

U. Mathematical model

The membrane reactor was modeled based on mathematical equations given in [11] and [12]. The steam methane reforming process consists of three reactions: (a) steam reforming reaction (SR), (b) water gas shift reaction (WGSR) and direct steam reforming reaction (DSR). In this work, a widely accepted global kinetics expressions given by Xu and Froment [13] are used for reforming reactions.

Steam reforming reaction (SR):

$$CH_4 + H_2O \leftrightarrow 3H_2 + CO \quad (1)$$

Water gas shift reaction (WGSR):

$$CO + H_2O \leftrightarrow H_2 + CO_2 \quad (2)$$

Direct steam reforming reaction (DSR):

$$CH_4 + 2H_2O \leftrightarrow 4H_2 + CO_2 \quad (3)$$

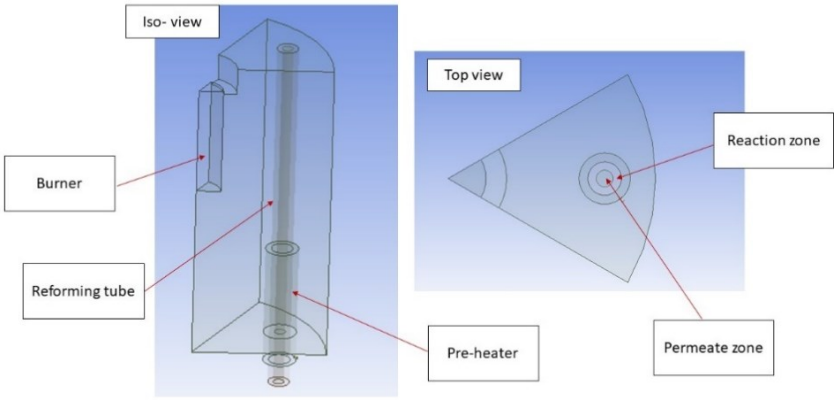

Fig. 5. Schematic diagram of membrane reactor used in the simulation

Sievert's Law:

The Sieverts' law-based equation is widely accepted and used for hydrogen permeation rate across the dense metallic membranes [14]. In this work, the hydrogen flux is incorporated as a source and sink term in the species transport equation. The overall permeation flux was calculated by:

$$\varphi = \beta . M_{w,H_2} . \frac{A_c}{V_c} . \frac{P_e}{l} . exp\left(-\frac{E_a}{RT}\right)\left(P^{0.5}{}_{r,H_2} - P^{0.5}{}_{p,H_2}\right) \quad (4)$$

Where, A_c and V_c are cell area and cell volume respectively. The hydrogen permeation rate is function of difference partial pressure of hydrogen in retentate and permeates sides.

V. Computational scheme

We used a three-dimensional computational domain to model the membrane reactor. ANSYS-Fluent 21 was used to find the solutions to the above governing equations. UDFs were developed in C to incorporate reforming reactions and hydrogen permeation. The calculations used a pressure based CFD solver, and the governing equations were solved using an upwind scheme of the second order. The energy equation has a convergence criterion of 10^{-8}, while the momentum and continuity equations have 10^{-6}.

3. RESULTS AND DISCUSSION

W. Grid sensitivity analysis

The grid sensitivity analysis was performed by using three different element sizes. The methane conversion along the reformer catalyst bed was the judging parameter. The mesh with 8 mm element size was selected for future simulations because it was appropriate in terms of computational cost and accuracy of results.

X. Model validation

Before going to further analysis of system, the model was validated first with experimental results of Kim et al. [15]. The simulations were performed at four different operating pressures and the model results was in good agreement with experimental data.

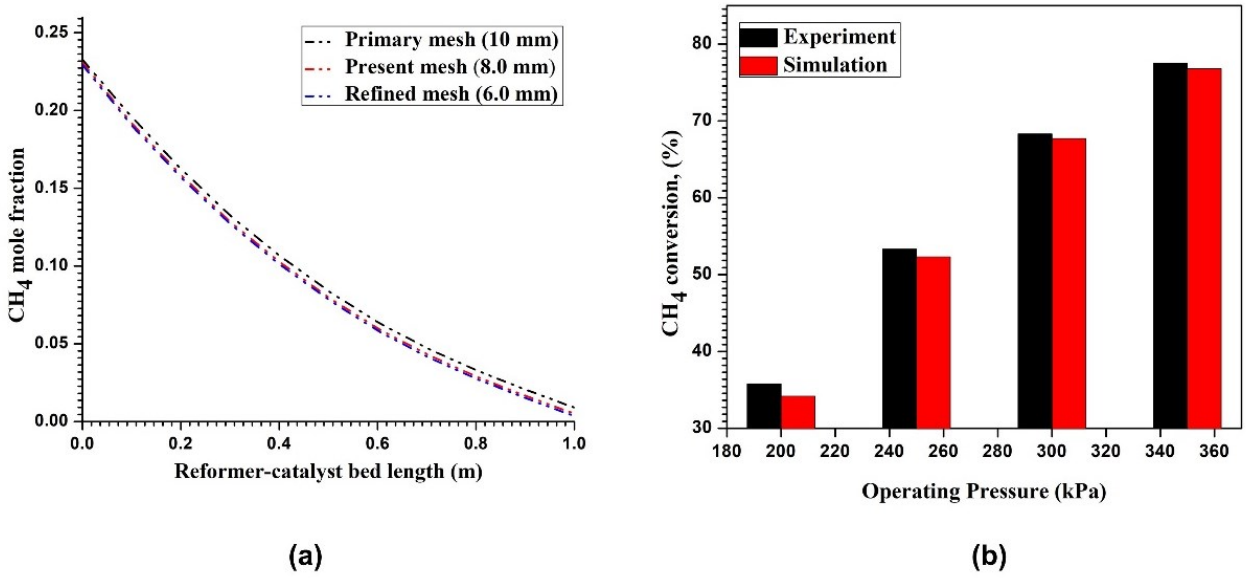

Fig. 6. (a) Grid sensitivity analysis with three different grid sizes (b) Comparison with experimental results

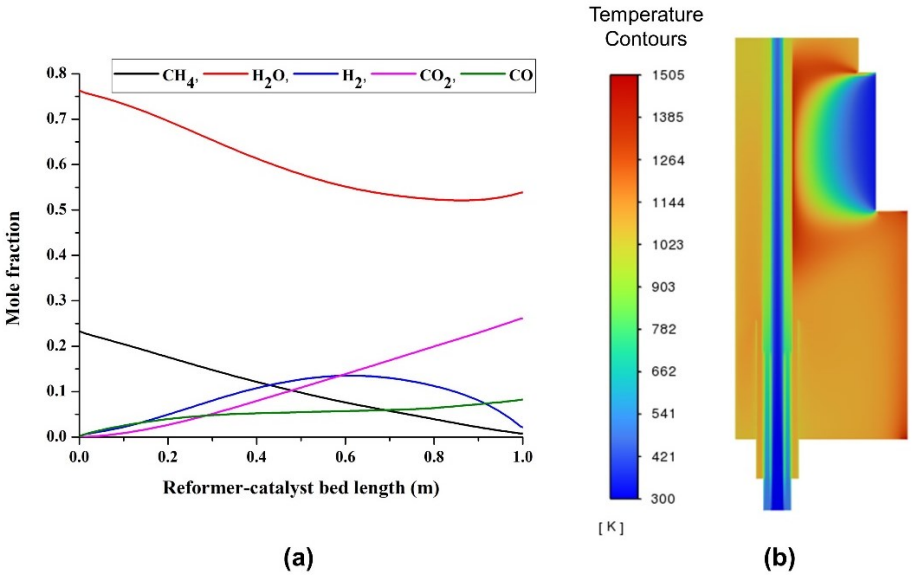

Fig. 7. (a) Distribution of species along the reformer length on the retentate side (b) Temperature distribution contours in the reactor

Y. Model results

The calculation conditions for hydrogen production (250 Kg/day) were: operating pressure = 8.5 bar, reactants inlet temperature = 550 K, gas hourly space velocity (GHSV) = 4103 h^{-1}, steam to carbon ratio = 3.25 and membrane material was Pd-Ru. In the Fig. 7 (a), the behavior

of mole fraction of methane, steam, hydrogen, carbon dioxide and carbon monoxide in the retentate side were plotted against the length of reformer catalyst bed. The mole fraction of methane decreased along the length of catalyst bed from 0.23 to 0.002. The concentration of steam in the retentate side decreased till half of the bed and then increased due to removal of hydrogen. The mole fraction of carbon monoxide and carbon dioxide increased along the catalyst bed. In the retentate side, the hydrogen produced by reforming reactions and moved to permeate side by passing through membrane.

TABLE *VII* shows the dry mole fraction of species with (co-current and counter-current sweep gas flow) and without membrane. The mole fraction of CO was lower in membrane because the system was operated at low temperature, which accelerated the water gas shift reaction. In both operations, membrane increased methane conversion (co-current and counter-current). Continuous hydrogen removal from the reaction zone product stream caused this increase.

TABLE VII. Comparison of conventional SMR with membrane SMR

Parameter	Unit	With membrane (Co-current)		With membrane (Counter-current)		Without membrane
		Retentate side	Permeate side	Retentate side	Permeate side	
X_{H_2}	(mole %, dry)	4.10	37.33	3.33	37.37	75.31
X_{CO}	(mole %, dry)	23.18	0	27.35	0	14.05
X_{CH_4}	(mole %, dry)	1.566	0	0.79	0	2.35
X_{CO_2}	(mole %, dry)	71.15	0	68.53	0	8.29
X_{N_2}	(mole %, dry)	0	62.67	0	62.63	0
$CH_{4,conv}$	(%)	92.32		96.7		92.9

4. CONCLUSION

The system was operated at limited variation in operating conditions. The main objective was to observe the effect of membrane on the overall performance of the system. The obtained results predicted the higher efficiency of the process at moderate operating conditions by using membrane. The process can be optimized in future by performing detailed parametric study on membrane SMR.

ACKNOWLEDGMENT

This research was supported by Pakistan Institute of Engineering and Applied Sciences, (PIEAS), Islamabad, Pakistan.

5. REFERENCES

[1] H. Abdi, N. Pourmahmoud, and J. Soltan, "A novel CFD simulation of H2 separation by Pd-based helical and straight membrane tubes," *Korean Journal of Chemical Engineering*, vol. 37, no. 11, pp. 2041–2053, 2020, doi: 10.1007/s11814-020-0657-4.

[2] C. J. Winter, “Hydrogen energy - Abundant, efficient, clean: A debate over the energy-system-of-change,” *Int J Hydrogen Energy*, vol. 34, no. 14 SUPPL. 1, pp. 1–52, 2009, doi: 10.1016/j.ijhydene.2009.05.063.

[3] M. Momirlan and T. N. Veziroglu, “Current status of hydrogen energy,” *Renewable and Sustainable Energy Reviews*, vol. 6, no. 1–2, pp. 141–179, 2002, doi: 10.1016/S1364-0321(02)00004-7.

[4] H. Lee, A. Kim, B. Lee, and H. Lim, “Comparative numerical analysis for an efficient hydrogen production via a steam methane reforming with a packed-bed reactor, a membrane reactor, and a sorption-enhanced membrane reactor,” *Energy Convers Manag*, vol. 213, no. April, p. 112839, 2020, doi: 10.1016/j.enconman.2020.112839.

[5] K. Ghasemzadeh, J. N. Harasi, T. Y. Amiri, A. Basile, and A. Iulianelli, “Methanol steam reforming for hydrogen generation: A comparative modeling study between silica and Pd-based membrane reactors by CFD method,” *Fuel Processing Technology*, vol. 199, Mar. 2020, doi: 10.1016/j.fuproc.2019.106273.

[6] F. Gallucci, D. A. Pacheco Tanaka, J. A. Medrano, and J. L. Viviente Sole, *Membrane reactors using metallic membranes*. Elsevier Inc., 2020. doi: 10.1016/B978-0-12-818332-8.00010-7.

[7] C. H. Kim, J. Y. Han, H. Lim, K. Y. Lee, and S. K. Ryi, “Hydrogen production by steam methane reforming in membrane reactor equipped with Pd membrane deposited on NiO/YSZ/NiO multilayer-treated porous stainless steel,” *J Memb Sci*, vol. 563, pp. 75–82, Oct. 2018, doi: 10.1016/j.memsci.2018.05.037.

[8] W. H. Chen, W. Z. Syu, C. I. Hung, Y. L. Lin, and C. C. Yang, “A numerical approach of conjugate hydrogen permeation and polarization in a Pd membrane tube,” *Int J Hydrogen Energy*, vol. 37, no. 17, pp. 12666–12679, 2012, doi: 10.1016/j.ijhydene.2012.05.128.

[9] M. Coroneo, G. Montante, J. Catalano, and A. Paglianti, “Modelling the effect of operating conditions on hydrodynamics and mass transfer in a Pd-Ag membrane module for H2 purification,” *J Memb Sci*, vol. 343, no. 1–2, pp. 34–41, 2009, doi: 10.1016/j.memsci.2009.07.008.

[10] L. Chibane and B. Djellouli, “Methane Steam Reforming Reaction Behaviour in a Packed Bed Membrane Reactor,” *International Journal of Chemical Engineering and Applications*, no. June 2011, pp. 147–156, 2011, doi: 10.7763/ijcea.2011.v2.93.

[11] I. Rahimipetroudi, J. S. Shin, K. Rashid, J. B. Yang, and S. K. Dong, “Development and CFD analysis for determining the optimal operating conditions of 250 kg/day hydrogen generation for an on-site hydrogen refueling station (HRS) using steam methane reforming,” *Int J Hydrogen Energy*, vol. 46, no. 71, pp. 35057–35076, 2021, doi: 10.1016/j.ijhydene.2021.08.066.

[12] “ANSYS Fluent Theory Guide 15”.

[13] Jianguo Xu and Gilbert F. Froment, “Methane Steam Reforming, Methanation and Water-Gas Shift: I. Intrinsic Kinetics,” *AIChE Journal*, vol. 35, no. 1, pp. 88–96, 1989, doi: 10.1177/000306516501300201.

[14] M. Upadhyay, H. Lee, A. Kim, S. hun Lee, and H. Lim, “CFD simulation of methane steam reforming in a membrane reactor: Performance characteristics over range of operating window,” *Int J Hydrogen Energy*, vol. 46, no. 59, pp. 30402–30411, 2021, doi: 10.1016/j.ijhydene.2021.06.178.

[15] C. H. Kim, J. Y. Han, H. Lim, D. W. Kim, and S. K. Ryi, “Methane steam reforming in a membrane reactor using high-permeable and low-selective Pd-Ru membrane,” *Korean Journal of Chemical Engineering*, vol. 34, no. 4, pp. 1260–1265, 2017, doi: 10.1007/s11814-016-0359-0.

Comparative analysis of chemical process simulation using open source and commercial software

Kaleem Ullah[a]*, Zeeshan ul Haq[a], Muazzam Arshad [b]
a kaleem.pse3scme@student.nust.edu.pk, School of Chemical and Materials Engineering, National University of Science & Technology, Islamabad, Pakistan.
b Department of Chemical Engineering, Faculty of Mechanical, Chemical & Industrial Engineering, University of Engineering & Technology, Peshawar, KPK, Pakistan.
Corresponding author (lead presenter): kaleem.pse3scme@student.nust.edu.pk

Abstract— Different process simulation softwares are used by researchers for process design and simulation in both academia and industry. In market, we have the availability of both open source and commercial softwares. The commercial softwares are expensive and require an annual license renewal, which may impose a financial strain on institutions or colleges with restricted budgets. In this paper, some of case studies have been simulated using both DWSIM (an open-source chemical process simulator) and Aspen HYSYS (Proprietary software). Three case studies of steady state processes which are mixer & separator, shortcut distillation column and shell & tube heat exchanger, have been simulated in both DWSIM and Aspen HYSYS using same input data. Simulation results of both softwares are presented and compared for analysis. The simulation results show that both softwares gave us nearly precise results with each other with less than 5% difference. Also, DWSIM is easy to use, easy to report, and convergence times are good. This work suggests that open-source software like DWSIM without any investment for license can be used as a process simulation tool for the systems studied in this work in academia and industries for hands on experience.

Keywords— Aspen HYSYS, DWSIM Process Simulator, Simulation software

1. INTRODUCTION

Calculation tools and software packages are constantly evolving in the field of chemical engineering as experiments at laboratory are time consuming and expensive to perform. Chemical engineers face a significant issue in determining which tool is most appropriate for a given problem in today's fast-paced world. Process engineering is primarily concerned with simulating, designing, and optimizing a chemical processing plant that consists of several processing units linked together by process streams. As part of these activities, you'll need to undertake material and energy balancing, equipment selection, and cost estimation. A computer-aided process design package or just a process simulator can do these tasks. ASPEN Plus, ASPEN HYSYS, ProSim Plus, and UniSim are proprietary softwares that must be purchased from market with a substantial license fee [1-3]. Students and small businesses may not be able to afford the high licence fee, and the fact that the model is closed source makes it hard to study how it works and fix problems and false simulation cases. Daniel Wagner Oliveira de Medeiros has fixed these two major problems by making DWSIM, a free open-source sequential modular CAPE-OPEN compliant

process simulator [4-6]. Some simulators, like the COCO simulator and the ALSOC/EMSO simulator, are free in the public domain even though they are not fully open source. These simulators can only be used for academic or non-commercial purposes [7-9]. Researchers have done mostly publications using proprietary softwares while paying high price for it. Aspen HYSYS and DWSIM are under discussion in this work.

Aspen HYSYS is worldwide accepted commercial software that can be used for simulating chemical processes. Aspen HYSYS requires a valid software license in order to model complex chemical processes involving chemical reactions and raw materials. Due to proprietary file formats and data compression algorithms, simulation models built using commercial software cannot be easily exported to any other software; instead, they must be opened, updated and run using the commercial software itself. Such restrictions could impede research collaboration among multiple organizations because they would require them to first purchase the software to build on previously produced process models. To work on previously generated process models, various organizations would have to first purchase the software, which could inhibit cross-organizational research collaboration.

In this work, by comparing the simulation results from DWSIM with those produced from commercial software such as Aspen HYSYS, aims to assess the modelling capabilities of free open-source software. Three case studies have been simulated through Aspen HYSYS and analyzed for comparison with DWSIM such as Mixer followed by separator, shortcut distillation column and shell and tube heat exchanger using same input data.

2. METHODOLOGY

Three case studies have been simulated in this section such as mixer followed by flash separator, distillation column and shell and tube heat exchanger.

1. Case 1 (Mixer and Flash Separator)

Two streams (consist of benzene and toluene) have been mixed first and then separated into liquid and vapors (consisting of both benzene and toluene). The inlet data is shown in the table 1. The simulation results have been generated using both Aspen HYSYS and DWSIM for comparison.

Table 8: Input data for Case 1

		Inlet 1	Inlet 2
ole Fractions	enzene	0.8	0.2
	oluene	0.2	0.8
olar Flow (mol/s)		100	100
emperature (C)		25	25
essure (atm)		1	1

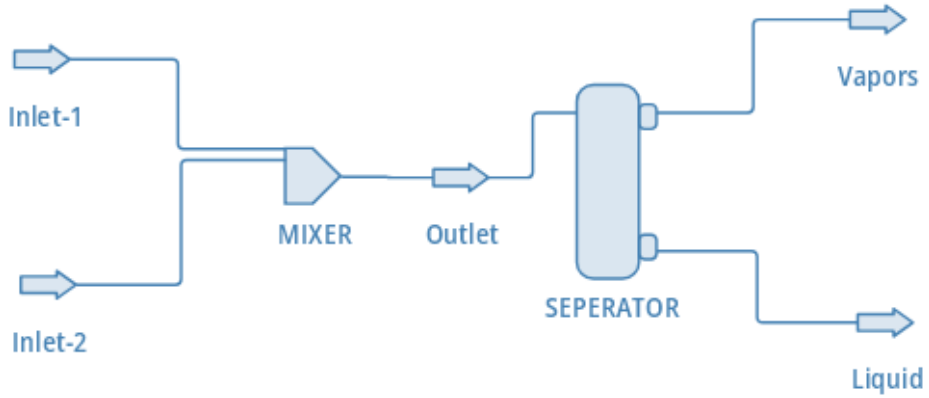

Figure 8: Case 1 flowsheet in DWSIM

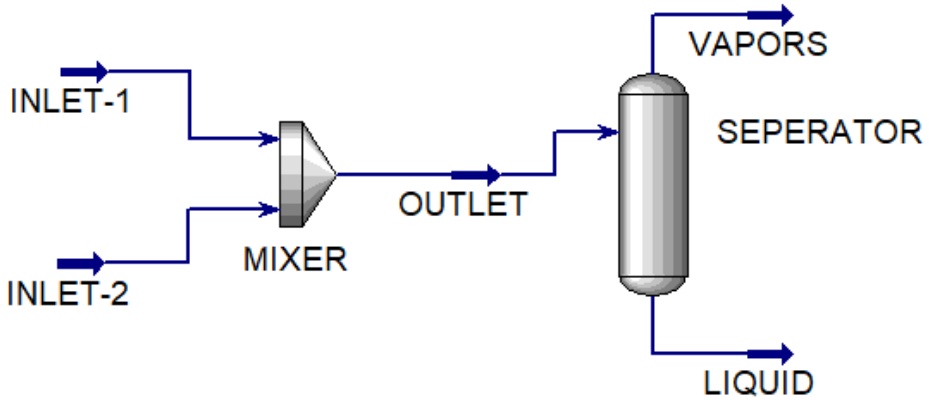

Figure 9: Case 1 flowsheet in Aspen HYSYS

2. Case 2 (Shortcut Distillation Column)

A shortcut distillation column is a tool in simulation softwares where quickly a distillation model is generated for separation of feed stream with a little information. This limited information given below is given in table 2 is inserted in both DWSIM and HYSYS to compare the design parameters such as minimum number of trays, actual number of trays, optimum feed stage etc.

Table 9: Input data for Case 2

ɔmpounds		enzene, Toluene	eflux ratio	5*Min. Reflux ratio
ıermodynamic property		eng Robinson	ght compoenent	enzene
eed	ole fractions	enzene = 0.4 oluene = 0.6	eavy component	oluene
	olar Flow (kmol/h)	0	stillate	99

essure (atm)	ottoms	01

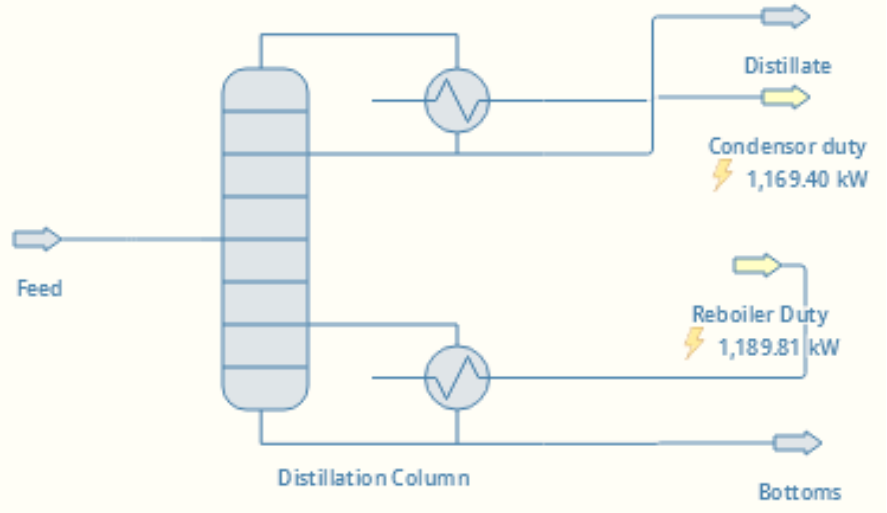

Figure 10: Case 2 flowsheet in DWSIM

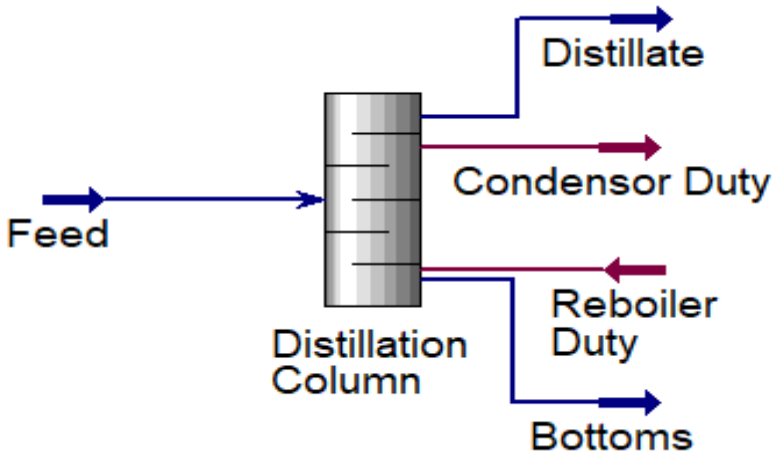

Figure 11: Case 2 flowsheet in Aspen HYSYS

3. Case 3 (Shell and Tube Heat Exchanger)

Heat exchange normally happens in every process industry where different types of heat exchangers are used. One of them i.e. shell and tube heat exchanger here simulated with the input data in table 3. The output parameters such as temperature, pressure and flow has been compared for both DWSIM and Aspen HYSYS.

Table 10: Input data for case 3

Compounds	Water	Methanol	Flow Type	Counter Current
Inlet Streams	Cold	Hot	U (W/m^2 K)	450
Mass flow (kg/h)	15000	25000	Area (m^2)	250
Mole fraction	0	1	Cold fluid ΔP (bar)	0.002
Mole fraction	1	0	Cold fluid ΔP (bar)	0.025
Temperature (C)	10	80	Property Package	Peng Robinson
Pressure (bar)	1	5		

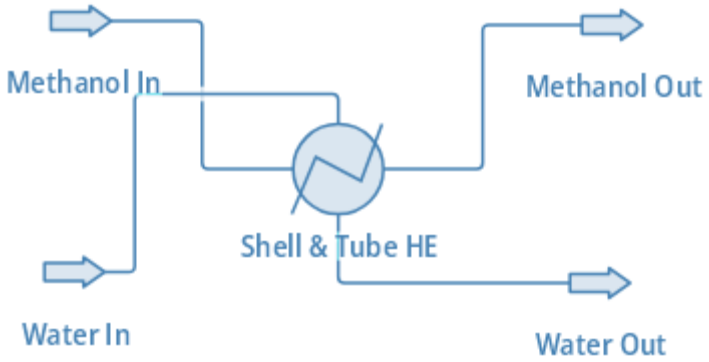

Figure 12: Case 3 flowsheet in DWSIM

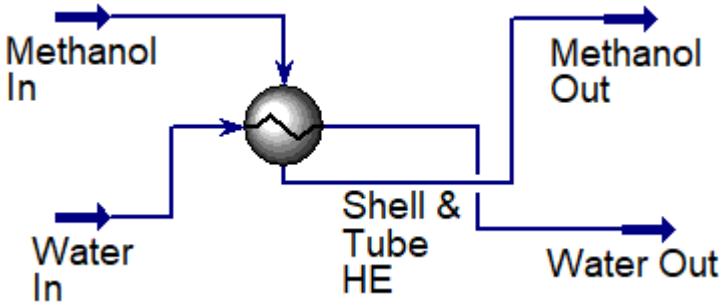

Figure 13: Case 3 flowsheet in Aspen HYSYS

.

3. RESULTS AND DISCUSSION

The comparison result has been created for both simulation tools i.e., DWSIM and Aspen HYSYS where same and critical output parameters have been compared. Following figures shows comparison of the properties of all three cases.

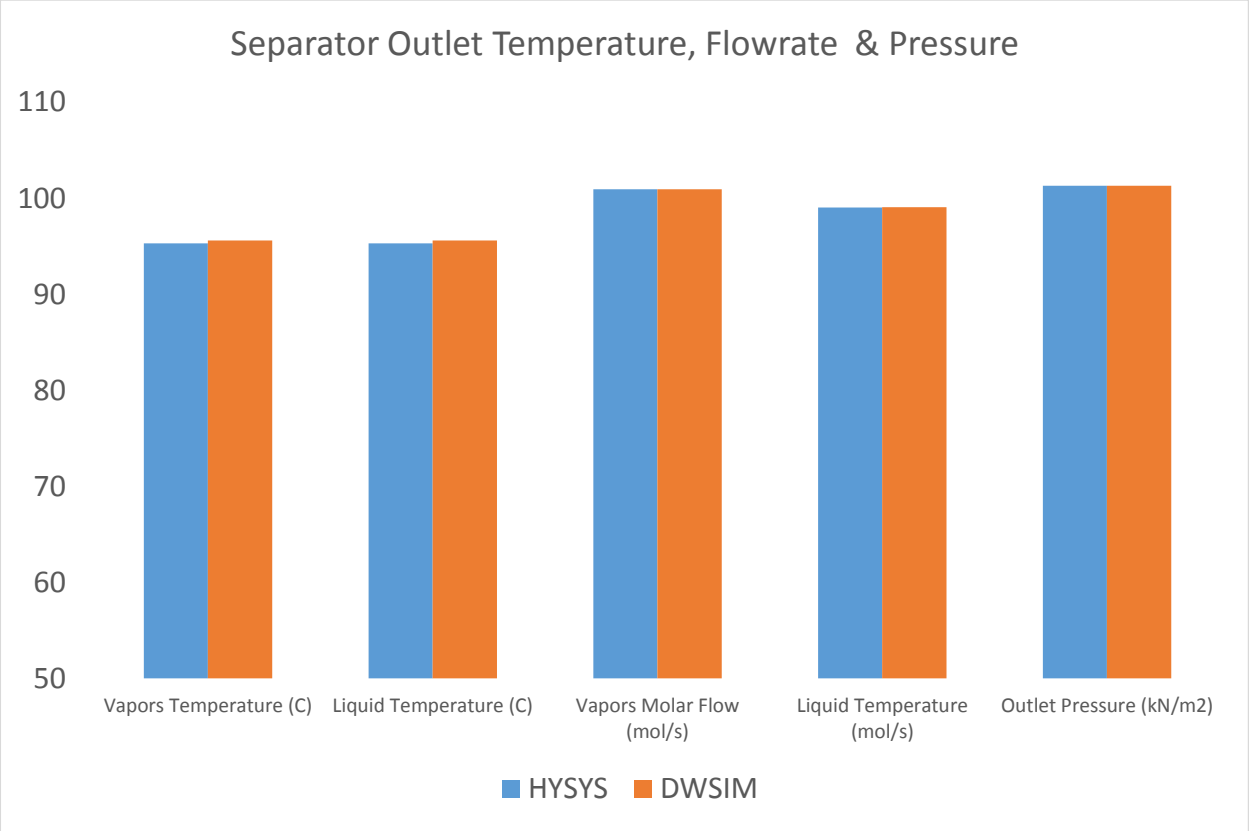

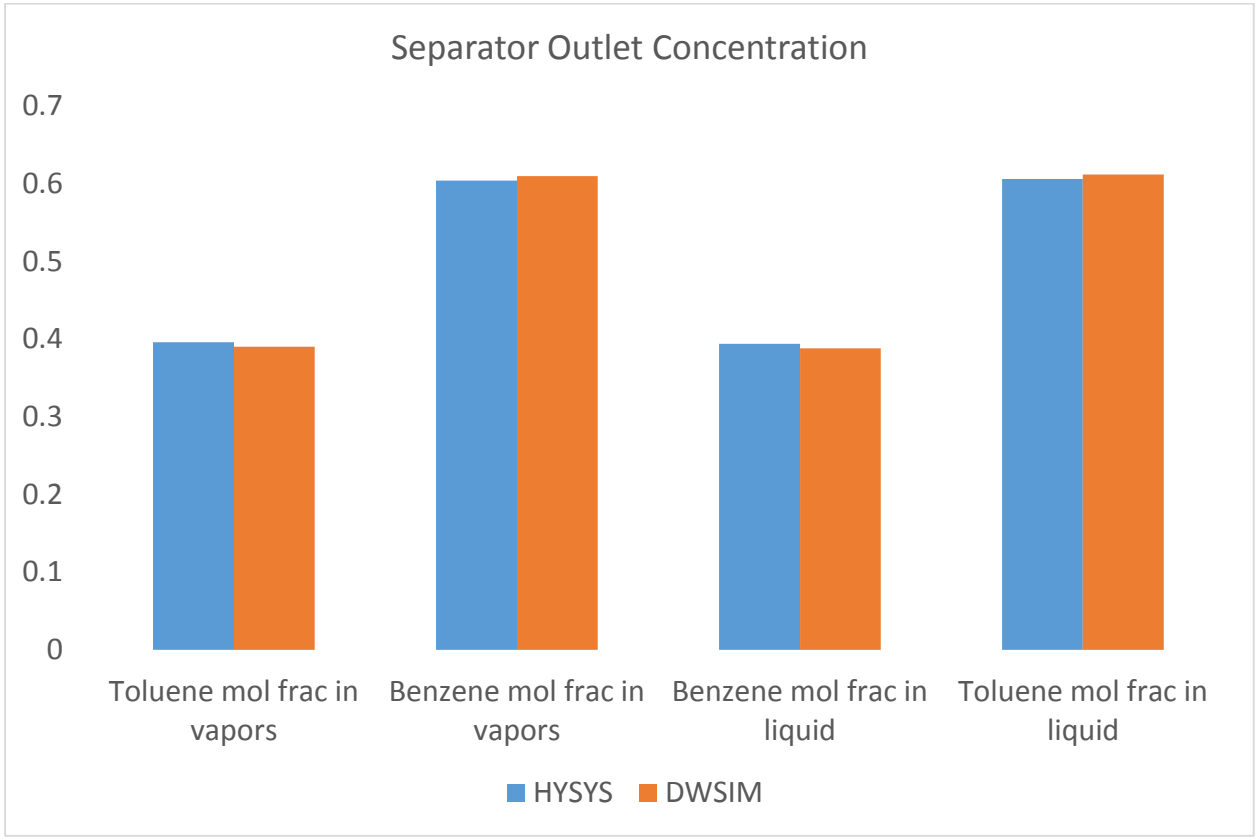
Separator Outlet Concentration
0.7
0.6
0.5
0.4
0.3
0.2
0.1
0
Toluene mol frac in vapors
Benzene mol frac in vapors
Benzene mol frac in liquid
Toluene mol frac in liquid
HYSYS
DWSIM

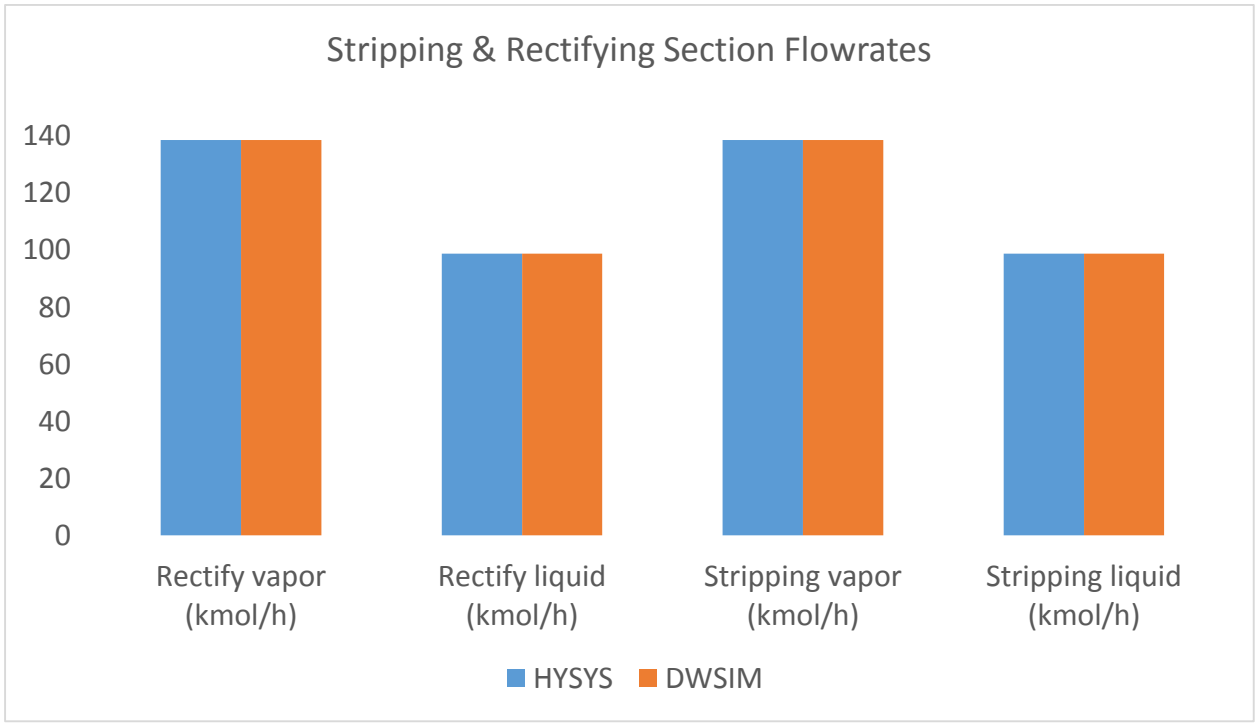
Stripping & Rectifying Section Flowrates
140
120
100
80
60
40
20
0
Rectify vapor (kmol/h)
Rectify liquid (kmol/h)
Stripping vapor (kmol/h)
Stripping liquid (kmol/h)
HYSYS
DWSIM

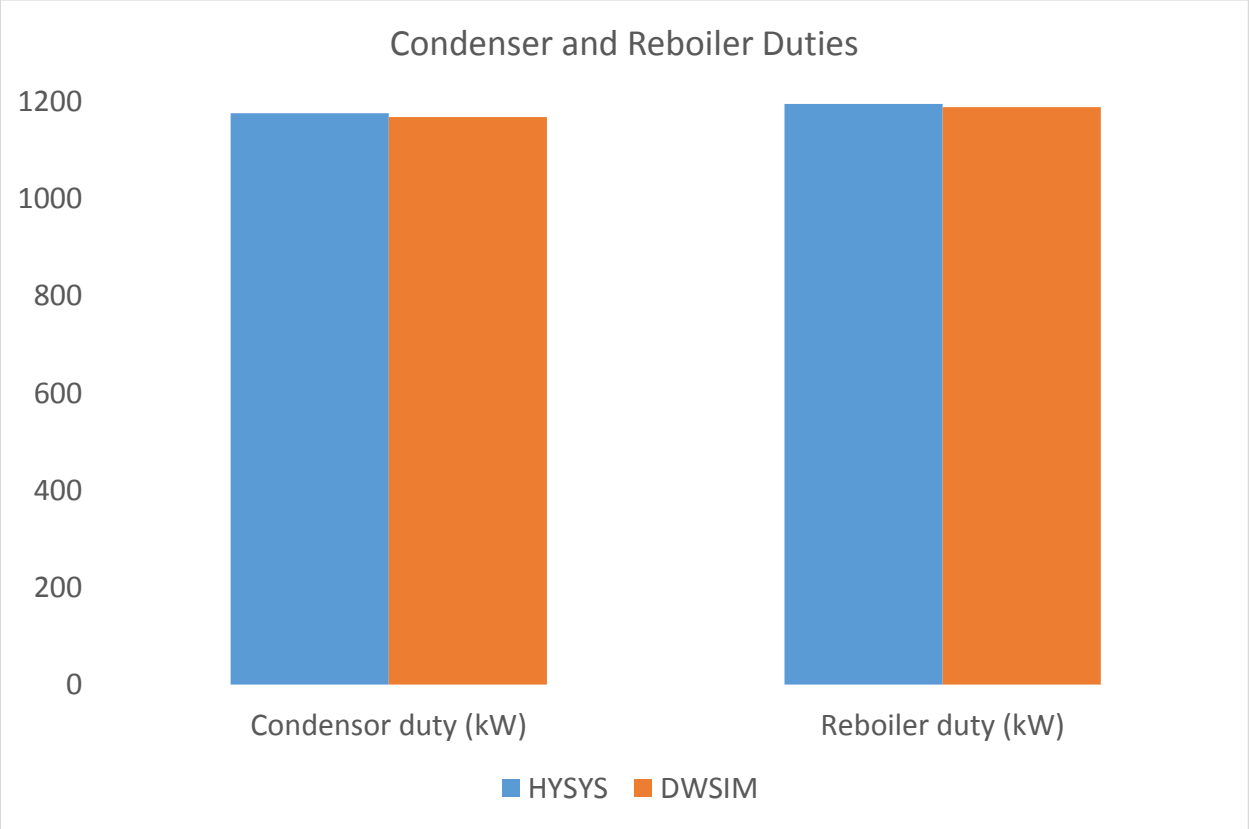
Condenser and Reboiler Duties
1200
1000
800
600
400
200
0
Condensor duty (kW)
Reboiler duty (kW)
HYSYS
DWSIM

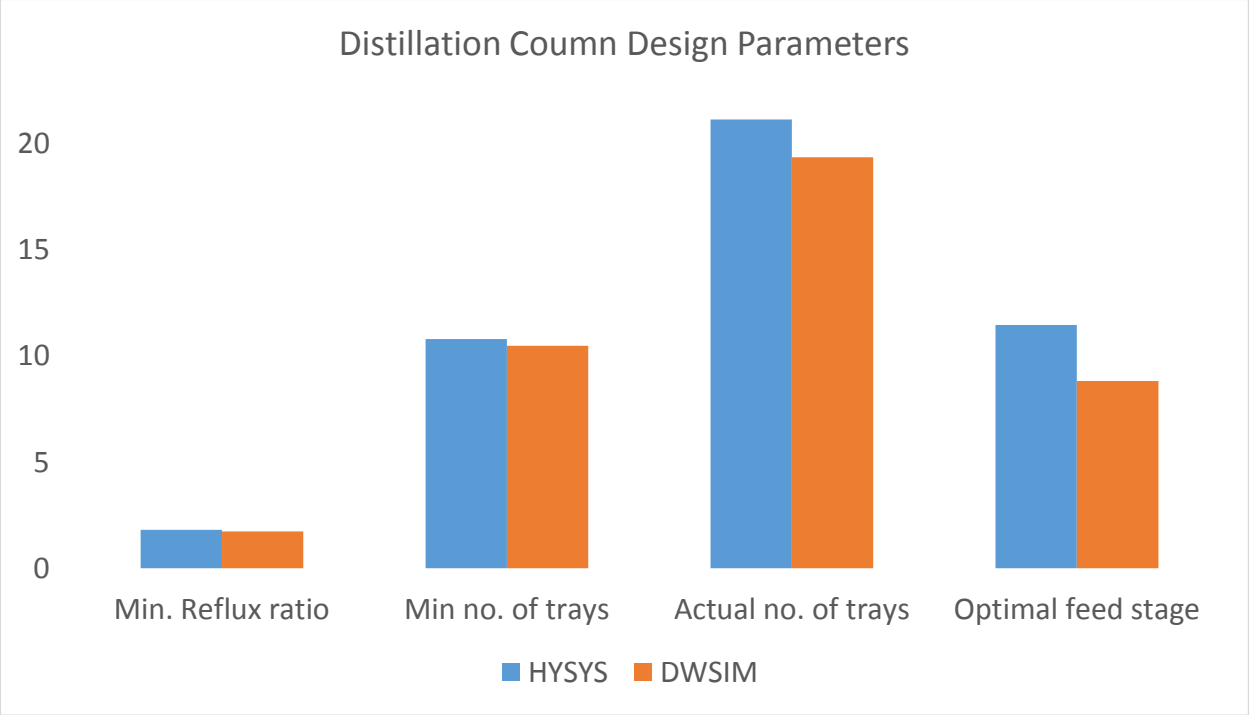
Distillation Coumn Design Parameters
20
15
10
5
0
Min. Reflux ratio
Min no. of trays
Actual no. of trays
Optimal feed stage
HYSYS
DWSIM

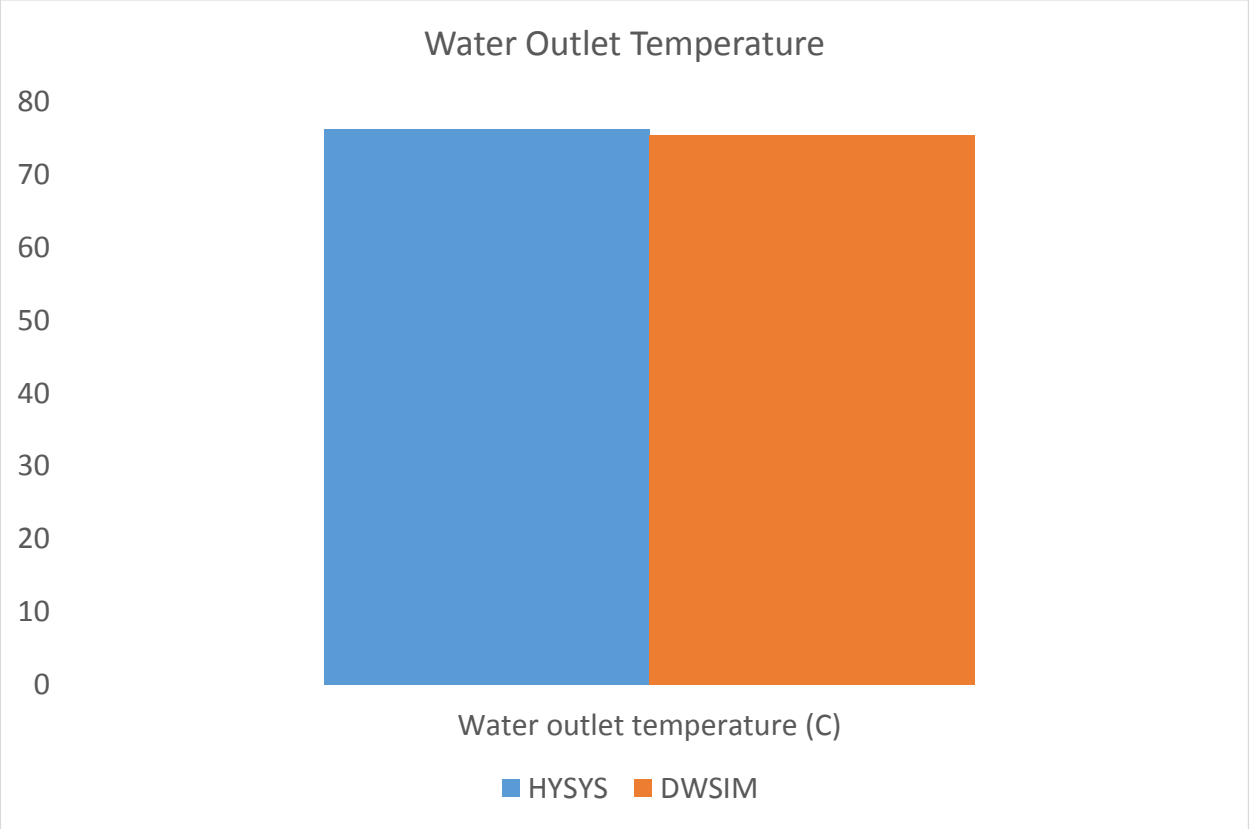

.

4. CONCLUSION

Free and open-source software like DWSIM has been shown to be capable of performing the same functions as Aspen HYSYS, a commercial product. Using DWSIM, researchers were able to correctly mimic chemical processes, as well as calculate their thermodynamic parameters and chemical composition. DWSIM's accuracy was found to be comparable to that of Aspen HYSYS in all three cases. The simulation results show that both softwares gave us nearly precise results with each other with less than 5% difference. Moreover, DWSIM is user friendly, easy to report, and convergence times are good. In conclusion, DWSIM could serve as an alternative software for process modeling and simulation.

5. REFERENCES

[1] AspenTech, “AspenTech,” 2017. .
[2] PROSIM, “PROSIM_ chemical process simulation software and services – Engineering Process Solutions and Services,” 2017. .
[3] UniSIM, “UniSim® Design Suite Customer Support Centre,” 2017.

[4] Fieg, G., Gutermuth, W., Kothe, W., Mayer, H. H., Nagel, S., Wendeler, H., Wozny, G. "A Standard Interface for Use of Thermodynamics in Process Simulation", Computers & Chemical Engineering, 19(Suppl. 1), pp. S317–S320, 1995.
https://doi.org/10.1016/0098-1354(95)87056-3

[5] Pons, M., Braunschweig, B., Irons, K., Köller, J., Kuckelberg, A. "CAPE-OPEN (CO) standards: Implementation and maintenance", In: Proceedings from the 2nd IEEE Conference on Standardization and Innovation in Information Technology, Boulder, CO, USA, 2001, pp. 335–338. https://doi.org/10.1109/SIIT.2001.968582

[6] DWSIM – The Open Source Chemical Process Simulator "Chemical Process Simulation for Everyone: DWSIM for Desktop is free and open-source", [online] Available at: https://dwsim.inforside.com.br/new/

[7] COCO "COCO: cape open to cape open simulation environment", [online] Available at: https://www.cocosimulator.org/

[8] Soares, R. de P., Secchi, A. R. "EMSO: A new environment for modelling, simulation and optimisation", Computer Aided Chemical Engineering 14, pp. 947–952, 2003.

[9] Rodrigues, R., Soares, R. P., Secchi, A. R. "Teaching chemical reaction engineering using EMSO simulator", Computer Applications in Engineering Education, 18(4), pp. 607–618, 2010.

Experimental Study of Physicochemical Properties of Aqueous Salt of Threonine blended with Mono-ethanolamine Used as a Solvent for CO2 Capture

[1]*Faiz Ahmed Abro., [1]Dr. Muhammad Shuaib Shaikh., [1]Dr. Sikandar M. Almani
[1]Mehran University of Engineering & Technology, Jamshoro, Sindh, Pakistan
Corresponding author (lead presenter): faizahmedabro07@gmail.com

***Abstract*—** The rapid growth in the world population is bringing exponential increase in consumption of energy. Looking back into the time, there is 1 billion increase in world population in time span of one decade. According to recent studies, more than 85% of energy is generated from fossil fuel, which is the main contributor in release of carbon dioxide (CO_2) in environment. The concentration of CO_2 is rapidly spreading in the atmosphere. CO_2 is responsible for more than 50% of the Greenhouse emissions. However, CO_2 can be captured using aqueous amino acid based solvents. This study is focused on solvent based on blend of Threonine ($C_4H_9NO_3$) and mono-ethanolamine (MEA), which have potential carbon capture. This research has been concentrated on understanding the physicochemical properties of these blends in terms of density, refractive index and viscosity. These physicochemical properties are very crucial in the design of CO_2 absorption. The observations illustrated a decreasing trend of properties with increase in temperature (20^OC - 70^OC). The results were compared with existing solvents available in literature, and the data found as in satisfactorily agreement with literature. Hence, the synthesized solvent can be used as a potential CO_2 capture agent.

Keywords— Aqueous amino acid blends, CO2 Capture, MEA, Physicochemical Properties, and Threonine.

1. INTRODUCTION

The Rapid Growth In World Population Is Bringing Exponential Increase In Consumption Of Energy. Looking Back Into The Time, There Is 1 Billion Increase In World Population In Time Span Of One Decade. In This Smarter World, Energy Is Utilized By Growing Population For Utilities, Transport, Appliances And Other Energy Consuming Products. According To Recent Studies, More Than 85% Of Energy Is Generated From Fossil Fuel, Which Is The Main Contributor In Release Of Co_2 In Environment. The Concentration Of Co_2 Is Rapidly Spreading

In The Atmosphere. Co_2 Is Responsible For More Than 50% Of The Greenhouse Emissions. Bearing In Mind This Issue, Researchers Developed Numerous Methods And Techniques To Limit The Production Of Co_2. Understanding The Impact Of Co_2 On Environment, Plants And Human Health, We Come To A Sum Up That Removal Or Co_2 From Fossil Fuels Before Energy Production Is The Only Solution.

The Expenditure Of Co_2 Favors The Huge Enhancement Of Greenhouse Gases [Ghg] That Causes Environmental Problems And Leads To Global Warming. The Bearable Carbon Dioxide Concentration Is 350 Ppm, Which Is Increased To 416 Ppm As Of 2021, Says Noaa. The Rapid Growth Of Co_2 Concentration Will Lead To Respiration Diseases Through Production Of Smog And Air Pollution. Recently, It Can Be Observed That Many Of The Cities In Pakistan Are Going Declined In Air Quality Index, Which Is An Alarming Sign That Development Of Co_2 In Environment Must Be Limited.

In Order To Mitigate This Increasing Carbon Dioxide Concentration, There Are Various Techniques Utilized Including; “Absorption”, In Which Solvent Is Utilized That Absorbs The Co_2 From The Mixture That Can Be Separated Later, “Adsorption”, In Which The Co_2 Is Adsorbed On The Surface Of Adsorbent Which Is Separated Later Just Like Absorption, “Membrane Technology”, In Which A Membrane Is Utilized That Has Sieve Size Smaller Than Co_2 Molecules And The Carbon Dioxide Containing Fluid Is Passed From It, All The Fluid Is Passed While, Co_2 Is Collected On Surface Of Membrane, And “Cryogenic Distillation”, In Which Capturing Is Achieved On Boiling Of Fluid On Different Temperature Ranges. Overall, The Absorption Technique Is Highly Efficient For The Capturing Of Co_2.

This study is focused on study of solvent based on blend of Threonine ($C_4H_9NO_3$) and mono-ethanolamine (MEA), which have potential carbon capture. This research has been concentrated on understanding the physicochemical properties of these blends in terms of density, refractive index (RI) and viscosity. These properties are crucial in designing carbon dioxide absorption. While conducting absorption, the density, RI and viscosity are considered as essential parameters to be put under consideration. Experimental study of these physicochemical properties is substantial for calculation of potential capture of the blend.

2. METHODOLOGY

For achieving the mentioned parameters, following methodology steps were followed:

1. **Preparation of Solutions:**
   The variety of ratios of Threonine, mono-ethanolamine (MEA) and water were considered to prepared and select the optimum aqueous amino solvent blend. As per the literature, three ratios were shortlisted to be utilized for experimental study. The selected ratios are illustrated in given table (2.1 a).

SELECTED RATIOS			
Name of Solution	**Threonine + NaOH**	**MEA**	**H_2O**
A	20%	2%	78%
B	20%	5%	75%
C	20%	10%	70%

(Table 2.1 a)

As it can be observed from the given table, the quantity of threonine was kept constant, whereas, ratio of MEA was varying, that also impacted the ratio of distilled water content in the solution.

As per the literature review, threonine has some of acidic effect on solution, for which ratio of Threonine was kept along with sodium hydroxide in an *Equimolar* manner (0.1257 moles of each). By the combination of given ratios, three solutions (A, B & C) were prepared.

2. **Determination of Density:**

Density is one of a common parameter that can be determined through variety of methods. The most frequent used method is using mass per volume ratio of the solution. The same technique was utilized to determine the density of three different solutions in temperature range of 20°C to 70°C. This temperature range was selected as per the recommendations from literature, as this is the common span of temperature focused for study of amino acid base solvent blends used in different industries. The following steps were followed for determination of density:

a. Measured and noted down the mass of solution using electronic balance.
b. Measured the volume of taken amount of solution using beaker.
c. Calculated density through mass per volume ratio.
d. Repeated the process for different temperature ranges.

The mass was measured in grams, while and volume in milliliters, so that unit of density in this study would be grams/mls.

3. **Determination of Refractive Index (RI):**

Refractive index of the solution was measured using *Abbe Refractometer* present at Department of Chemical Engineering, MUET Jamshoro. Also for this parameter, the temperature range was set from 20°C to 70°C. The following steps were followed for

determination of RI:

a. Placed the Abbe Refractometer at such place where natural light is available.
b. Cleaned the prisms with ethanol and cotton for avoiding impurities.
c. Placed 2 – 3 drops of solution maintained at certain temperature.
d. Closed the prisms and pressed the "Read" button.
e. Repeated the process for different temperature ranges.

4. **Determination of Viscosity:**

The viscosity of solutions was also measured in same temperature ranges using *Sybolt Viscometer.* The following steps were followed for determination of viscosity:

a. Placed the solution inside sybolt viscometer.
b. Took a stopwatch and calculate the amount of time taken by the solution to get out of the storage chamber.
c. Repeated the process for different temperature ranges.

3. RESULTS AND DISCUSSION

The obtained results from this experimental study depict a specific trend that can be observed in following table:

Table (3.1)

	Solution A			Solution B			Solution C		
T/K	Density	RI	Viscosity	Density	RI	Viscosity	Density	RI	Viscosity
293	0.9856	1.6691	1.175	0.9978	1.691	1.335	0.9929	1.6282	0.9781
303	0.9851	1.6662	1.085	0.9956	1.6875	1.181	0.9899	1.6262	0.9011
313	0.98	1.6653	0.9847	0.9934	1.686	1.036	0.9877	1.6251	0.8101
323	0.971	1.6502	0.8935	0.9888	1.6847	0.9578	0.9785	1.6243	0.7357
333	0.9627	1.6257	0.8122	0.9833	1.6621	0.811	0.967	1.5656	0.6698
343	0.9447	1.6114	0.7479	0.9733	1.6616	0.7481	0.9512	1.5562	0.6145

Taking under consideration density of three solutions, there is decreasing trend is observed with increasing temperature. It can be clearly observed through graph 3.1 given as following:

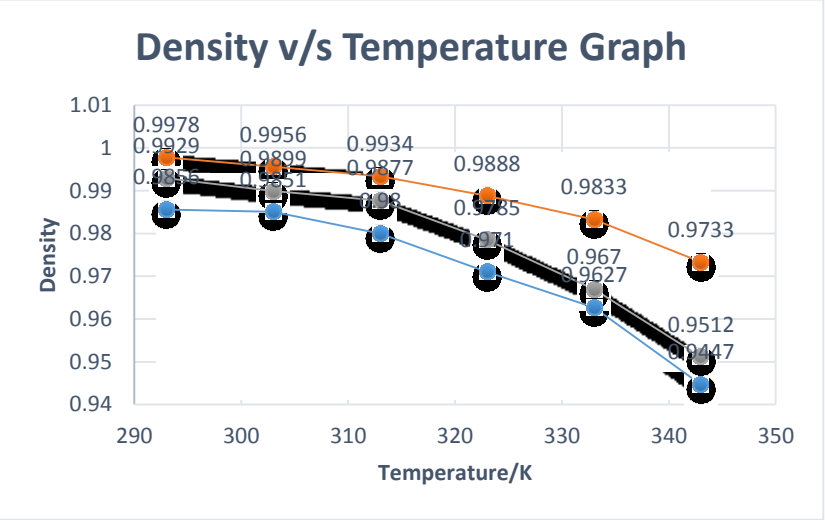

(Graph 3.1)

The similar trends can be observed in graph 3.2 and 3.3 as mentioned below:

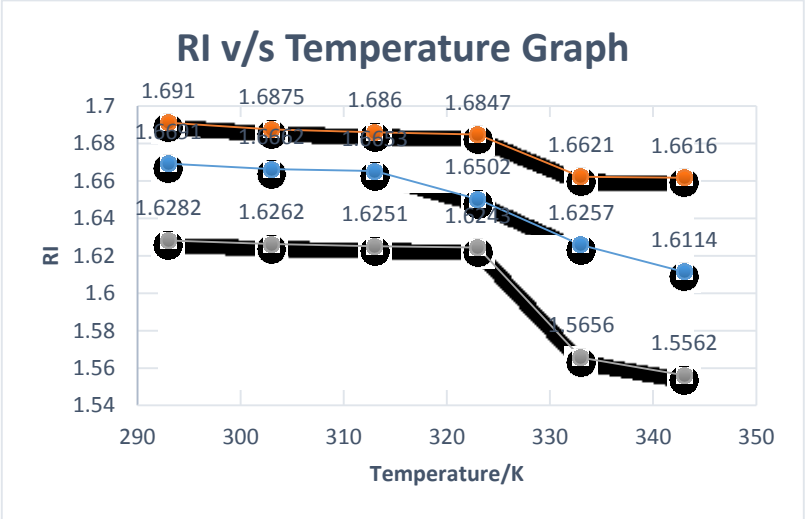

(Graph 3.2)

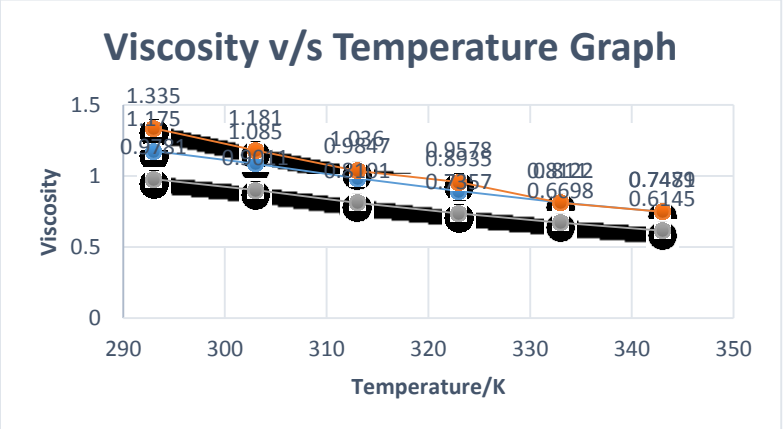

(Graph 3.3)

4. CONCLUSION

All physicochemical properties aqueous salt of Threonine blended with Mono-ethanolamine used as a solvent for CO_2 Capture have been observed showing inverse relationship with temperature as it also shares satisfactory agreement with literature as well. Looking into graphs 3.1, 3.2 and 3.3, we can observe the similar decreasing trend of densities, refractive indices and viscosity with every increase in temperature. The trend of temperature with the measured properties was consistent with the findings of other researchers. The predicted values obtained from correlation equations were in fairly good agreement with the measured values for all properties, and hence can be used in upcoming time for CO_2 removal system design.

ACKNOWLEDGMENT

The authors are pleased to acknowledge the Department of Chemical Engineering, MUET Jamshoro for providing laboratory support for utilization of equipment.

5. REFERENCES

1. Shaikh, M., et al., Measurement and prediction of physical properties of aqueous sodium l-prolinate and piperazine as a solvent blend for CO2 removal. Chemical Engineering Research and Design, 2015. 102: p. 378-388.

2. Shuaib, S.M., et al., Physical properties of aqueous solutions of potassium carbonate+ glycine as a solvent for carbon dioxide removal. Journal of the Serbian Chemical Society, 2014. 79(6): p. 719-727.

3. Shariff, A.M. and M.S. Shaikh, Aqueous Amino Acid Salts and Their Blends as Efficient Absorbents for CO 2 Capture, in Energy efficient solvents for CO2 capture by gas-liquid absorption. 2017, Springer. p. 117-151.

4. Shaikh, M., et al., Physicochemical properties of aqueous solutions of sodium l-prolinate as an absorbent for CO2 removal. Journal of Chemical & Engineering Data, 2014. 59(2): p. 362-368.

5. Dang, H. and G.T. Rochelle, CO2 absorption rate and solubility in monoethanolamine/piperazine/water. Separation science and technology, 2003. 38(2): p. 337-357.

6. Al-Ghawas, H.A., et al., Physicochemical properties important for carbon dioxide absorption in aqueous methyldiethanolamine. Journal of Chemical and Engineering Data, 1989. 34(4): p. 385-391.

7. Khan, S.N., et al. High pressure solubility of carbon dioxide (CO2) in aqueous solution of piperazine (PZ) activated N-methyldiethanolamine (MDEA) solvent for CO2 capture. in AIP Conference Proceedings. 2017. AIP Publishing LLC.

8. Bishnoi, S. and G.T. Rochelle, Physical and chemical solubility of carbon dioxide in aqueous methyldiethanolamine. Fluid Phase Equilibria, 2000. 168(2): p. 241-258.

9. Karunarathne, S.S., et al., Density, Viscosity, and Excess Properties of Ternary Aqueous Mixtures of MDEA+ MEA, DMEA+ MEA, and DEEA+ MEA. Fluids, 2020. 5(1): p. 27.

10. Mandal, B., A. Biswas, and S. Bandyopadhyay, Absorption of carbon dioxide into aqueous blends of 2-amino-2-methyl-1-propanol and diethanolamine. Chemical engineering science, 2003. 58(18): p. 4137-4144.

11. Conway, W., et al., CO2 absorption into aqueous amine blended solutions containing monoethanolamine (MEA), N, N-dimethylethanolamine (DMEA), N, N-diethylethanolamine (DEEA) and 2-amino-2-methyl-1-propanol (AMP) for post-combustion capture processes. Chemical Engineering Science, 2015. 126: p. 446-454.

12. Karunarathne, S.S., D.A. Eimer, and L.E. Øi, Physical properties of MEA+ Water+ CO2 mixtures in postcombustion CO2 Capture: A review of correlations and experimental studies. Journal of Engineering, 2020. 2020.

Investigating the optical and electrical properties of non-toxic $MASnI_3$ solar cell with kesterite and zinc-based charge transport layers

Zeeshan Khan[1*], Muhammad Noman[1], Shayan Tariq Jan[1]
[1]U.S-Pakistan Center for Advanced Studies in Energy, University of Engineering & Technology, Peshawar, Pakistan.
[*]zeeshankhan.uspcase@uetpeshawar.edu.pk

***Abstract*—** In recent years, the perovskite-based solar cell has emerged as a fast-growing photovoltaic (PV) technology due to improved performance, cost-effectiveness, and ease of use in unconventional places. In this work instead of a lead (Pb)-based, tin (Sn) based, eco-friendly N-I-P perovskite solar cell (PSC) device with methyl ammonium tin triiodide ($MASnI_3$) as an absorber layer has been proposed because of its non-toxic nature and similarity in optoelectronic properties to Pb. Based on continuity and Poisson equations, the proposed PSC has been designed by a solar cell capacitance simulator (SCAPS). Owing to the large band gap and low absorptivity, ZnSe has been chosen as ETL. While kesterite CZTSe has been selected as HTL due to its non-toxicity, cost-effectiveness, tunable band gap, and electron affinity. The effect of charge transport layers (CTLs) on the quantum efficiency (QE), band alignment diagram, electric potential, recombination, IV curve, and power conversion efficiency (PCE) of the proposed structure have been analyzed. Furthermore, the influence of defect density on the absorber layer's optimized thickness and PSC's PCE has been analyzed in detail. Based on the results the optimized thickness of the perovskite layer for defect density of E13 was found to be 1.1 µm with PCE of 30.45%, for E14 0.9 µm with 29.21%, and E15 0.7 µm with 26.21%. The results achieved in this work showed a lot of promise for further implementation of non-toxic Sn-based PSCs.

Keywords— Charge transport layer, Defect density, $MASnI_3$, Perovskite solar cell, SCAPS

1. INTRODUCTION

With the need for sustainable development and alternative energy source to fossil fuels, in the last decade and so there is extraordinary improvement in the power conversion efficiency (PCE) of the perovskite solar cells (PSCs) along with a reduction in the cost of its fabrication. A step up in PCE of PSCs from 3% to > 25% in the last ten years, makes them the perfect emerging candidate in the field of Photovoltaic (PV) technology [1], [2]. This PSC technology owing to good stability at working temperature, low material utilization, low cost, and less energy-intensive fabrication processes proves more advantageous [3]. This encourages the

researchers to employ different methods to bring about the improvement of the performance parameters of PSCs. Solar Cell Capacitance Simulator (SCAPS-1D) is utilized to boost the output performance of the solar cell before experiments owing to the high experimental costs.

2. METHODOLOGY

Proposed solar cell model

Fig.1 illustrates multiple layered N-I-P non-inverted heterojunction tin-based solar cells. It is evident from Fig.1 that the cell architecture includes TCO/ZnSe/$MASnI_3$/CZTSe where the ETL is the ZnSe and the HTL is CZTSe (kesterite material) while tin-based $MASnI_3$ is used as the absorber. Our study aims to inspect the impact of the absorber layer's defect density on its optimal thickness and performance parameters such as open circuit voltage (Voc), Open circuit current density (Jsc) Fill Factor (FF), and PCE simulated via SCAPS. The cell performance is primarily built on the material, electrical and optical parameters of each layer implemented in the simulation having methyl ammonium tin triiodide ($MASnI_3$) as an absorber layer.

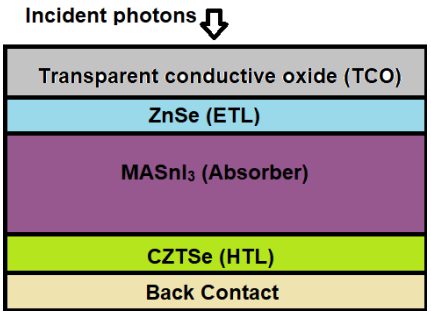

Fig.1 Proposed architecture of PSC

Simulation parameters of PSC

The proposed PSC depicted in Fig.1 was studied in detail for its output performance parameters by the SCAPS simulator. The optoelectronic parameters of all PSC layers were chosen from different literature and experiments after a thorough review [4]–[6]. All the device parameters are sorted in Table.1. Here, N_D and N_A are donor and acceptor concentrations respectively.

Table.1 Simulation parameters of PSC device and its interfacial defects

Parameters	$MASnI_3$	ZnSe	CZTSe
Thickness w (μm)	0.35	0.1	0.1
Band gap E_g (eV)	1.3	2.81	1.4
Electron affinity χ (eV)	4.17	4.09	4.1

Dielectric permittivity (ϵ_r)	8.2	8.6	9
Electron mobility ($cm^2/V.s$)	1.6	400	100
Hole mobility ($cm^2/V.s$)	1.6	110	12.5
Doping concentration (cm^{-3})	3.2×10^{15} (N_A)	1×10^{18} (N_D)	1×10^{19} (N_A)
Defect density Nt (cm^{-3})	10^{15}	10^{14}	10^{14}

To attain results as close to experimental results, the defect density N_t of all layers and the interfacial defects are introduced into the structure. Defect types of neutral and Gaussian are selected for absorber layer and CTLs respectively. All the simulations were done at 300 K working temperature under AM1.5 G standard sunlight flux.

3. RESULTS AND DISCUSSION

SCAPS numerical simulations have been done to understand the working and different properties like band energy diagram, QE, I-V curve, recombination rate, electric field, and the effects of defect density. Fig.1(a) depicts that the simulated PSC has a broader range of spectral reactions, its quantum efficiency (QE) extending from 300 nm to 970 nm wavelength. Fig.1(b) shows the plot of Voc vs Jsc. For the initial simulation, the Jsc is 30.3 mA cm^{-2} with Voc of 0.97 V giving 24.37 % PCE.

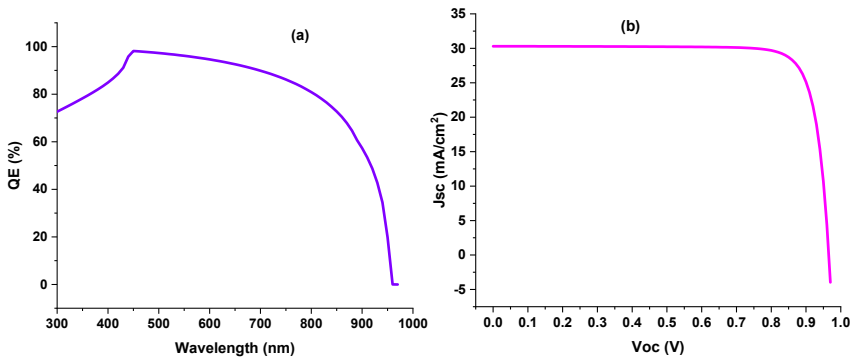

Fig.2 (a) QE of a device and (b) Jsc-Voc curve of a solar cell

The energy band energy diagram of the modeled solar cell is illustrated in Fig.3(a). This band diagram shows that the ETL forms an ideal band alignment with the perovskite material. The conduction band of the two materials aligns perfectly with the valance bands that have large offsets. This ensures the smooth flow of electrons and the blockage of holes. Similarly, the HTL also forms a good alignment of the valance bands with little offset while the conduction

band has good offsets. This ensures the smooth flow of holes and the blockage of electrons [7].

Fig.3(b) and Fig.3(c) show the recombination and electric potential inside the PSC. The recombination rate is high inside the absorber layer as illustrated in Fig.3(b). This is due to a large number of inherent traps and defects in the absorber layer owing to the perovskite material crystal growth [8]. While there is minimum recombination at the charge transport layers (CTLs) interfaces due to the good band alignment. There is an exponential rise in the electric field at the interfaces (ETL-Perovskite and Perovskite-HTL) owing to the high carrier density in the n-type ETL and p-type HTL along the depletion area. This stronger electric potential is necessary for the efficient extraction of the charge carrier from the charge-generating perovskite layer.

Further simulations were done on the PSC by varying the total defect density N_t of the perovskite active layer in a range of E13 to E17. The optimal thickness of the absorber layer for each defect density value was calculated along with other output cell parameters (Voc, Jsc, FF, and PCE) by changing its thickness from 0.05 µm to 0.12 µm with a 0.05 µm increment for each simulation. Incrementing the defect density N_t the traps centers in the material increase which ultimately increases the bulk recombination under the Shockley Read Hall model and also hamper the flow of charge carriers towards CTLs [9]. This drops the overall performance of the cell. The simulation results shown in Fig.4 illustrate that Jsc and PCE increase and then saturate while Voc and FF first decreases and then become near flat as the thickness of the absorber layer increases for each defect density. Based on the result the highest PCE of 30.45% was calculated for the optimized thickness and defect density of 1.1 µm and E13 cm^{-3} respectively for the active layer. The optimized absorber thickness and the cell output parameters for each of its defect densities are listed in Table. 2.

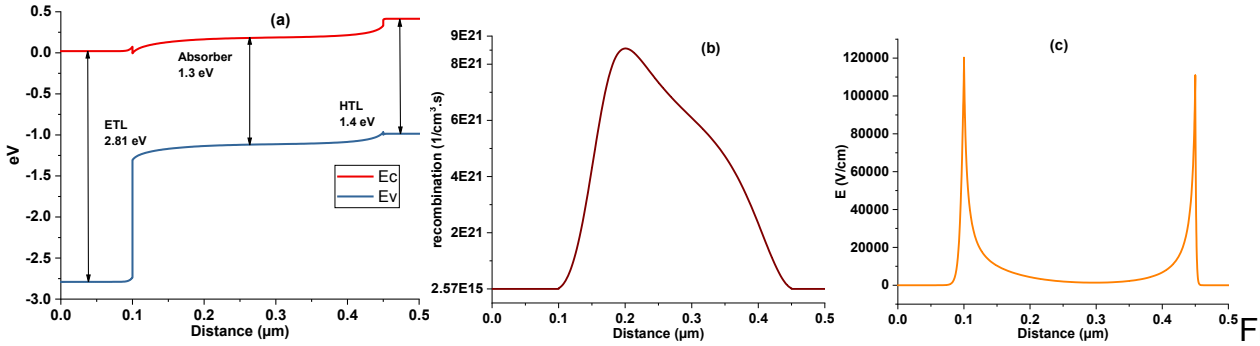

Fig.3 (a) Band energy diagram of proposed Cell, (b) Recombination rate, and (c) Electric field inside the PSC.

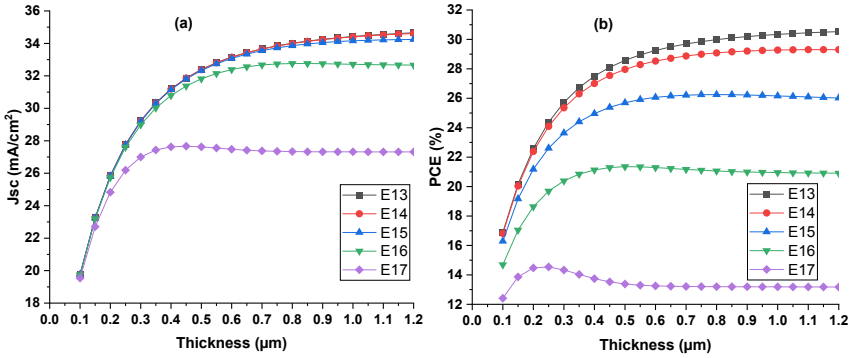

Fig.4 results of (a) Jsc and (b) PCE as an influence of thickness variation for a particular defect density

Table. 2 Optimal simulated parameters

Defect density (cm^{-3})	Thickness (μm)	Voc (V)	Jsc (mA cm^{-2})	FF (%)	PCE (%)
E13	1.1	1.011126	34.55573	87.14873	30.45
E14	0.9	0.996379	34.23218	85.63888	29.21
E15	0.7	0.947675	33.55569	82.42947	26.21
E16	0.5	0.877893	31.8158	76.44895	21.35
E17	0.25	0.794626	26.18861	69.86943	14.54

4. CONCLUSIONS

Here we used the SCAPS-1D simulator for understanding the properties which affect the conversion efficiency of $MASnI_3$-based solar cells with Zinc selenide and CZTSe as CTLs. The inspection of QE vs wavelength, Jsc-Voc curve, energy band diagram at equilibrium, recombination, and electric field curves indicate better performance. It is found that the active layer defect density and its thickness crucially raise the PCE of N-I-P PSCs. Incrementing the density of the defect decreases the optimal thickness of the active perovskite layer. our work will help grasp the working principle of PSCs along with its material characterization, stability strengthening, and efficiency enhancement.

ACKNOWLEDGEMENT

We are extending our gratitude to Professor Marc Burgelman, University of Gent, Belgium, for letting us use the SCAPS simulation software.

5. REFERENCES

[1] A. Kojima, K. Teshima, Y. Shirai, T. Miyasaka, Organometal halide perovskites as visible-light sensitizers for photovoltaic cells, J Am Chem Soc. 131 (2009) 6050–6051. https://doi.org/10.1021/ja809598r

[2] NREL National Renewable Energy Laboratory, NREL, (n.d.). https://www.nrel.gov/pv/cell-efficiency.html

[3] M.A. Rahman, Design and simulation of a high-performance Cd-free Cu2SnSe3 solar cells with SnS electron-blocking hole transport layer and TiO2 electron transport layer by SCAPS-1D, SN Appl Sci. 3 (2021). https://doi.org/10.1007/s42452-021-04267-3

[4] P. Roy, N.K. Sinha, A. Khare, An investigation on the impact of temperature variation over the performance of tin-based perovskite solar cell: A numerical simulation approach, in Mater Today Proc, Elsevier Ltd, 2019: pp. 2022–2026. https://doi.org/10.1016/j.matpr.2020.09.281

[5] T. Bendib, H. Bencherif, M.A. Abdi, F. Meddour, L. Dehimi, M. Chahdi, Combined optical-electrical modeling of perovskite solar cell with an optimized design, Opt Mater (Amst). 109 (2020). https://doi.org/10.1016/j.optmat.2020.110259

[6] Y.H. Khattak, F. Baig, H. Toura, S. Beg, B.M. Soucase, CZTSe Kesterite as an Alternative Hole Transport Layer for MASnI3 Perovskite Solar Cells, J Electron Mater. 48 (2019) 5723–5733. https://doi.org/10.1007/s11664-019-07374-5

[7] F. Baig, Y.H. Khattak, B. Marí, S. Beg, A. Ahmed, K. Khan, Efficiency Enhancement of CH3NH3SnI3 Solar Cells by Device Modeling, J Electron Mater. 47 (2018) 5275–5282. https://doi.org/10.1007/s11664-018-6406-3

[8] D. Głowienka, D. Zhang, F. di Giacomo, M. Najafi, S. Veenstra, J. Szmytkowski, Y. Galagan, Role of surface recombination in perovskite solar cells at the interface of HTL/CH3NH3PbI3, Nano Energy. 67 (2020). https://doi.org/10.1016/j.nanoen.2019.104186

[9] S. Tariq Jan, M. Noman, Influence of layer thickness, defect density, doping concentration, interface defects, work function, working temperature and reflecting coating on lead-free perovskite solar cell, Solar Energy. 237 (2022) 29–43. https://doi.org/10.1016/j.solener.2022.03.069

Emissions of black plumes from the chimneys of indigenous brick making kilns; a compositional study of the blackish particulates

Iatizaz Hassan[1], Naseer Ahmed Khan*[1], KhalidMehmood Barki[1], Najma Memon[2], NaveedulHasan Syed[1],
[1]Iatizaz_hassan@uetpeshawar.edu.pk,Department of Chemical Engineering, University of Engineering and Technology Peshawar, Pakistan
[2]National Centre of Excellence in Analytical Chemistry, University of Sindh, Jamshoro, Pakistan
Corresponding author*: naseerahmedkhan@uetpeshawar.edu.pk

Abstract—In Pakistan, bricks are processed in a fixed chimney bulls trench kiln “F.C.B.T.K.” and the fuel used to maintain high temperature is a s mixture of coal, biomass, pet-coke, motor oil, and waste rubber. In any case, the combustion of low quality fuel produces a visible portion of blackish smoke and is more hazardous when compared to typical greenhouse gases. Some of the key characterization tools were employed for assessing the physicochemical characteristics of the blackish particulates, such as the scanning electron microscope “S.E.M.,”, energy dispersive spectroscopy “E.D.S.,” unit, X-ray fluorescence “X.R.F.”, X-ray diffraction “X.R.D.,”., N_2 adsorption isotherms, and thermo-gravimetric “T.G.A.,” analytical techniques were used to provide our understanding about the chemical composition of the particulates. The SEM micrographs at a 30,000 times magnification displays the morphology of spherical objects of about different magnifications. The elements in these round particles were sulfur, oxygen, and carbon- as per the EDS analysis. These detected elements are the usual composition of the coal. Moreover, XRF analysis also underlined the presence of inorganic part of the coal. As per the adsorption curve, the specific surface area of coal particles is extremely low and by seeing “ S.E.M.,” images one may also propose that the spherical Nano objects are mostly fullerene which is one of the allotrope of carbon. Besides these, the “T.G.A.,” and “X.R.D.,” analyses were performed the inference that these emissions are fine coal particles.

Key words: Kilns, Blackish smoke, Nano coal particles, Combustion, Brick kilns

1. INTRODUCTION:

The manufacturing of bricks in Pakistan is well-known due its good physicochemical features; however, the designing method needs up-gradation because it is based on old-fashioned antique methods [1]-[4]. Since most of the buildings in Pakistan are much old, but these still made up of solid bricks [5]-[6]. In one of the provincial capital of Pakistan (Peshawar), the bricks' composition changes to some degree, i.e., homogeneous mixing of " 5 wt% ," of each (sand and coal) and " 90 wt% ," wet clay [7]. Such bricks were then dried for some days, followed by high temperature heating at "(800-1100 ^{o}C)," that delivered the strength to the employed bricks [8]-[10]. The capability of producing bricks every day of a kiln normally ranges from 25000 to 35000 bricks [11]. With the rapid growth in population and industrialization, the demand of bricks is incessantly growing. The bricks demand in the world and the construction business is assumed to cross the digit of "$10.5," trillion in future [12]-[13].

Regarding the bricks' quality, generally two key belongings are significant; composition of raw material composition such as clay etc. and the proper method of heating in orderto preserve a set temperature of "(900 ± 100 ^{o}C) "[14]. High temperature heating is needed to accomplish in a huge trench type kiln and the prerequisite kiln temperature of about "(900 ^{o}C)" is slowly achieved[14]-[15]. The supplied solid fuel is a mixture of waste polymers, coal, solid biomass, and motor oil [16]-[17]. The overall general illustration if provided in Figure 1. Presently in Pakistan, Fixed Chimney Bulls Trench Kilns "F.C.B.T.K.," is one of the most common furnace for heating the bricks [18].

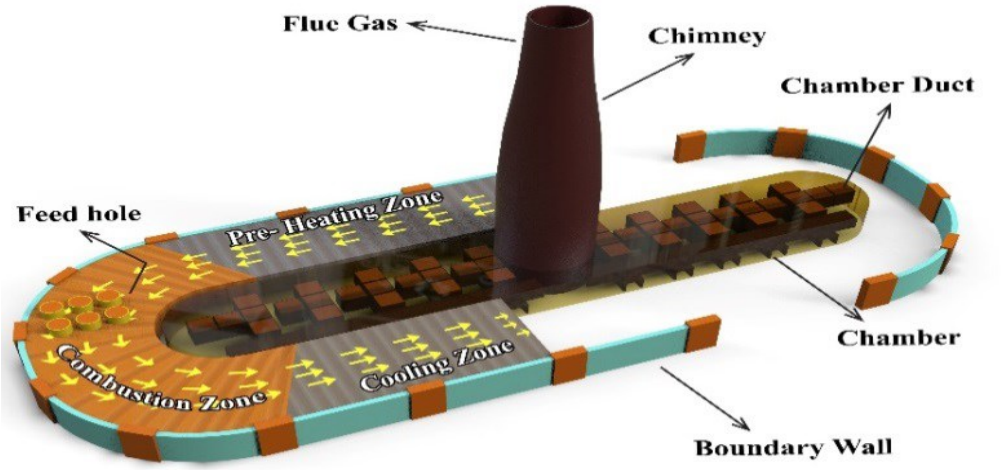

Fig.1. A layout of the fixed chimney bull's trench kiln "F.C.B.T.K.", tubular chambers connected to the main trench.

Regarding the fact that these brick kilns are also contributing to environmental risks at an alarming rate; and therefore, much effort is needed in this direction. However, the bricks manufacturing kilns on the other hand is a good opportunity to the unemployed population of a country, employing hundred-thousand of the country's population [19]. Therefore, in order to make the best use of sustainable kilns, some of the owners have either pause the usage of waste polymers as a fuel for the kilns because of its hazardous emissions, thus leading to toxic environment. But there are also some of the key hurdles in this industry such as lower finance, limited budget, and technological replacement via commercial scale which should be resolved

at the earliest in order to switch to a green brick-making industry. Parallel to this, it is very important to find out the makeup compositional analyses of the already emitted [blackish] particles in order for we could easily design an alternative and sustainable strategy so to limit the toxic emissions.

2. METHODOLOGY

Collection of samples (blackish particulates):

The collection of blackish particulates sample is one of the key stage for the experimentation to carry out. For a smooth combustion process, the kiln height should be adjusted to some "(23 m).," and the overall sample collection analysis is illustrated in "Fig.2". For the reason to climb on to the top of the kiln for capturing the sample, numerous scaffolds were thoroughly developed "Fig.2". The particulates and gases emission temperature was< "80 °C,". in a similar way, thegrade 1 type filter paper was also kept in the emission way around one hour "60 min.," wherein the particles (blackish) cohered and draw out for the instrument talanalysis.

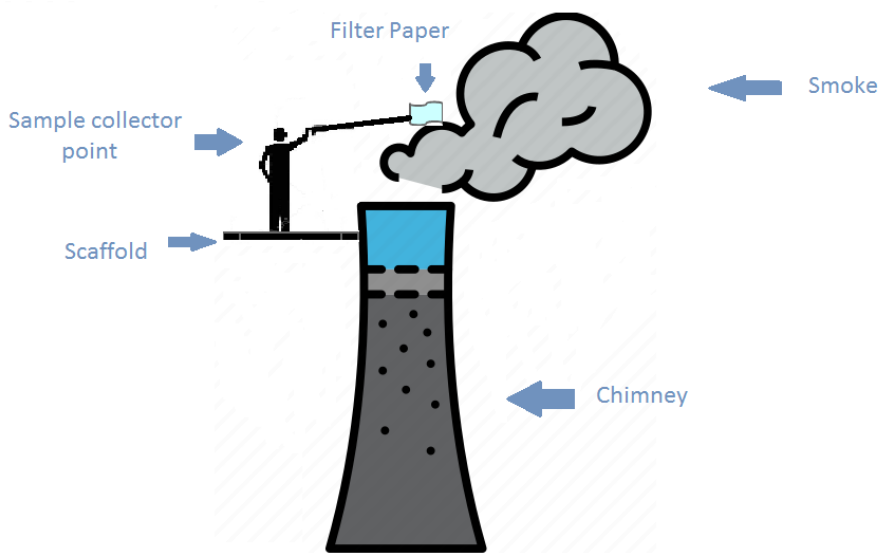

Fig. 2.Sample collection from the exhaust line.

Sample characterization:

Various characterization tools were employed for the successful testing of the captured and collected samples (blackish particulates). These include "(S.E.M., E.D.S., X.R.F., and X.R.D.)". The captured blackish particulates were assessed by using a scanning electron microscope " S.E.M.," (JSM5910, JEOL, Japan).The powdered sample was first made conducive by copper coating and laid over a conductive carbon tape meticulously and then fixed on an aluminum support. The electrons dispersed backwere also noticed to exame the surface morphological characteristics of the analyzed sample.

Similarly, Energy Dispersive X-ray Spectroscopy "E.D.S.," were employed for measuring the elemental analysis of different regions of the sample.This range of the elements was from Boron to Uranium.

In a similar analysis, the X-ray fluorescence spectroscopy "X.R.F.," was employed to judge the composition of aluminum and silicon; because, both of these are the dominant elements of the

ash content. The samples were first ground, followed by pellet pressing for the analysis. The reason to elude any possible type of complex peaks data, the binder was not even utilized.

By the same token, the samples' crystallinity and non-crystallinity was also assessed by the use of X-ray diffractometer "X.R.D.", (JDX-3532 Japan made).The copper anode produces the X-rays and filtered to monochromatic radiation of about "1.5 Å." .The range of angle of diffraction was set between "0º to 130º." . An abundant quantity of the blackish particulates was also inflexibly employed within the sample holder for the analysis of diffraction.

3. RESULTS AND DISCUSSION:

The "S.E.M.," was used for examining the structural morphology of the sample. An enlarged surface characteristic of the fine particulates was assessed with the "S.E.M.," .The display and micrographs of surface topology of the sample shows typically roundish shaped bodies, as illustrated in "Fig. 3". For a short time, the magnification of the micrographs was enhanced to 500- and1000-times so to have a detailed analysis of the structural morphology of the employed sample. The extra brightness is owed to the phenomenon of charging which specifies high concentration of organic nonconductive type of sample's composition.

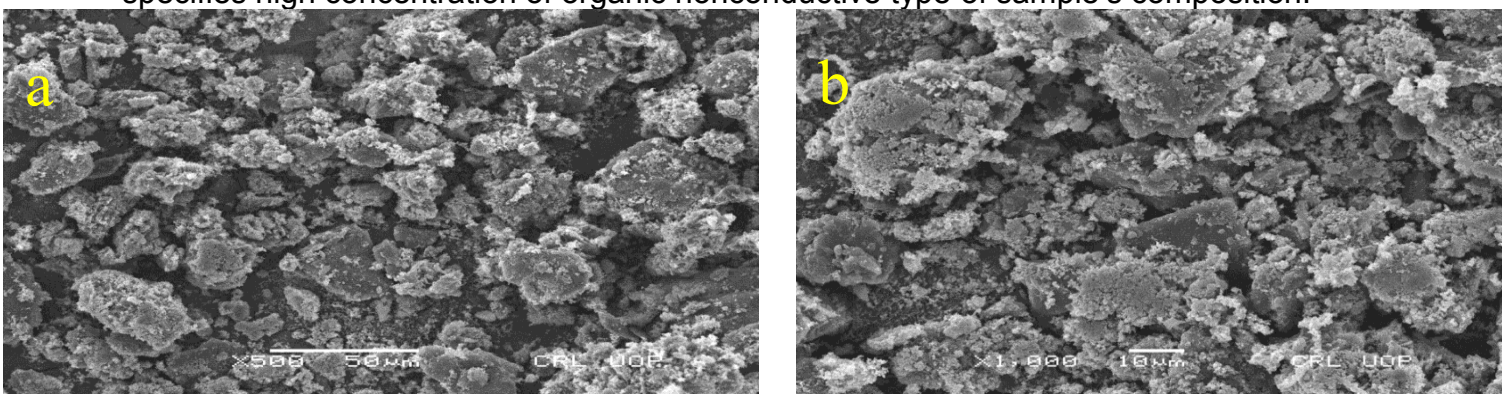

Fig.3.SEM image of the airborne particulates at a magnification of 500x 9(a), 1000x (b).

The Energy Dispersive X-ray "E.D.X.," analysis of the blackish particulates at diverse spots delivers the broad info concerning the atomic composition. The concentration of sulfur composition is typically great in the un-processed locally available coal. This characterization analysis highlights that the analyzed blackish particulates were actually the fine particles of such coal; but due to some reason not properly combusted inside the furnace.

The elemental analysis of both the carbon and oxygen element has quite lower photonic energies and therefore cannot be spotted in the spectra of "X.R.F.,". The elements which have the higher atomic number than sodium are noticeable in a conventional "X.R.F.," apparatus (such as silicon centered detector). Table.1 provides the details about the composition numbers which confirms that the collected blackish particulates are actually the fine particles of coal. Similarly, SiO_2, Al_2O_3, Fe_2O_3, and SO_3 are the main conformation of the blackish particulate sample.

Table 1:XRF analysis of the calcined sample (heating of the chimney sample to a temperature of 600 ºC) and the blackish particulates (collected from the exhaust of the chimney).

Blackish particulates		**Inorganic species, when the sample heated to (600°C)**	
Species	Oxide units (by weight)	Species	Oxide units (by weight)
SiO_2	29.06	SiO_2	41.01
SO_3	28.04	Al_2O_3	22.96
Fe_2O_3	23.98	Fe_2O_3	14.69
CaO	9.05	CaO	7.78
K_2O	3.27	SO_3	7.57
ZnO	2.72	K_2O	2.77
TiO_2	2.42	TiO_2	1.78
PbO	0.12	ZnO	1
Total	100%	Total	100%

4. CONCLUSIONS:

The combustion of fuel especially the burning of less-qualitative coal emits abundant volumes of black fumes and therefore it is very toxic for the human health and the environment. Besides, these plumes also contain different hazardous chemicals of smog formation. In Pakistan, various researchers point that such enormous volume of blackish particulates from the brick kilns is owed to the use of plastic waste as solid fuels. Here, in the present study, various high technological and innovative analytical methods are employed to find out the chemistry behind the formation of blackish particulates. The final outcomes of this research work is that the emission from brick kilns in terms of fine particles are actually the result of coal combustion; and therefore, a capturing technological efforts were employed in close vicinity of the kilns in order to get rid on these unexploited energy sources.

Acknowledgement

The authors are thankful to the Department of Chemical Engineering, UET Peshawar, for the availability of the needy and useful tools and equipment employed in the whole research work.

5. REFERENCES

[1] Achakzai, K., S. Khalid, and A. Bibi. "Determination of heavy metals in agricultural soil adjacent to functional brick kilns: a case study of Rawalpindi." *Science Technology and Development* 34 (2017): 122–129.

[2] Achakzai, Khanoranga, et al. "Air pollution tolerance index of plants around brick kilns in Rawalpindi, Pakistan." *Journal of environmental management* (Elsevier) 190 (2017): 252–258.

[3] Ali, M. Abbas, M. V. Ali, and F. Abbas. "Hidden hazardous child labor as a complex human rights phenomenon: A case study of child labor in Pakistan's brick-making industry." *Cogent Social Sciences* (Taylor & Francis) 3 (2017): 1369486.

[4] Ali, Mujahid, et al. "Assessment of local earthen bricks in perspective of physical and mechanical properties using Geographical Information System in Peshawar, Pakistan." *Structures.* 2020. 2549–2561.

[5] Ayub, Muhammad, Q. Ali, K. Shahzada, A. Naseer, and M. Shoaib. "Conservation of Islamia college building in Pakistan." *Procedia Engineering* (Elsevier) 54 (2013): 465–471.

[6] Baum, Ellen. "Black carbon from brick kilns." *Presentation for CleanAir Task Force*, 2010.

[7] Bell, S. Jonathan, and H. Böke. "Comparing the Old and New: Traditional Building Materials and the Uch Monument Complex, Pakistan." *Conservation and Management of Archaeological Sites* (Routledge) 12 (2010): 107-123.

[8] Cultrone, Giuseppe, E. Sebastián, K. Elert, M. J. D. L. Torre, O. Cazalla, and C. R. Navarro. "Influence of mineralogy and firing temperature on the porosity of bricks." *Journal of the European Ceramic society* (Elsevier) 24 (2004): 547–564.

[9] Darain, K. Mahfuz ud, et al. "Energy efficient brick kilns for sustainable environment." *Desalination and Water Treatment* (Taylor & Francis) 57 (2016): 105–114.

[10] Fiala, Jan, M. Mikolas, and K. Krejsova. "Full brick, history and future." *IOP Conference Series: Earth and Environmental Science.* 2019. 012139.

[11] Ijaz, Madiha, S. R. Ahmad, M. Akram, W. U. Khan, N. A. Yasin, and F. A. Nadeem. "Quantitative and qualitative assessment of musculoskeletal disorders and socioeconomic issues of workers of brick industry in Pakistan." *International Journal of Industrial Ergonomics* (Elsevier) 76 (2020): 102933.

[12] Johari, Izwan, S. Said, B. Hisham, A. Bakar, and Z. A. Ahmad. "Effect of the change of firing temperature on microstructure and physical properties of clay bricks from Beruas (Malaysia)." *Science of Sintering* 42 (2010): 245–254.

[13] J. John. "Archaic Technology, Social Relations and Innovations in Brick Kilns." *Centre for Education and Communication*, 2018.

[14] Kadir, Aeslina Abdul, and Abbas Mohajerani. "Effect of heating rate on gas emissions and properties of fired clay bricks and fired clay bricks incorporated with cigarette butts." *Applied Clay Science* (Elsevier) 104 (2015): 269–276.

[15] Khan, Kashif Kamran, and Amber Shezadi. "Socio-economic determinants & Dynamics of Debt Bondage: A descriptive Analysis of Brick Kiln Workers in Punjab Pakistan." 2021.

[16] Khan, Mashhood Ahmad, and Arsalan Mujahid Ghouri. "Environmental pollution: its effects on life and its remedies." *Researcher World: Journal of Arts, Science & Commerce* 2 (2011): 276–285.

[17] Khan, Muhammad Waseem, Yousaf Ali, Fabio De Felice, Aneel Salman, and Antonella Petrillo. "Impact of brick kilns industry on environment and human health in Pakistan." *Science of the Total Environment* (Elsevier) 678 (2019): 383–389.

[18] Kumar, Saten, and Muhammad Shahbaz. "Coal consumption and economic growth revisited: structural breaks, cointegration and causality tests for Pakistan." *Energy exploration & exploitation* (SAGE Publications Sage UK: London, England) 30 (2012): 499–521.

[19] Peirce, J. Jeffrey, P. Aarne Vesilind, and Ruth Weiner. *Environmental pollution and control.* Butterworth-Heinemann, 1998.

Performance evaluation of ionic liquid as adsorbent for heavy metal removal from wastewater

[1]Azfar Zaman Khattak, [2]Mansoor Ul Hassan Shah.
[1]azfarzaman.msche@uetpeshawar.edu.pk, Department of Chemical Engineering, University of Engineering & Technology Peshawar, Pakistan
[2] Department of Chemical Engineering, University of Engineering & Technology Peshawar, Pakistan
mansoorshah@uetpeshawar.edu.pk

Abstract—Heavy metals in wastewater possess a serious threat to the environment and its removal from water required significant consideration. In this regard several techniques were employed for its remediation however, the low efficiency and high toxicity of the existing adsorbents compel the researcher to investigate/develop sustainable adsorbents.Therefore, in this study the hydrophobic ionic liquid, trihexyltetradecylphosphonium dicyanamide ([PC6C6C6C14][-N(CN)2−)] is used for the removal of heavy metal, Cobalt (Co) from aqueous solution. The results showed that [PC6C6C6C14][-N(CN)2−] have the potential to adsorbed Cobalt from aqueous solution with adsorption capacity of (344mg/g). Moreover, the removal efficiency of the [PC6C6C6C14][-N(CN)2−] was also investigated and it was noticed that [PC6C6C6C14][-N(CN)2−] have the ability to remove more than 86% Cobalt from aqueous solution. Hence, the result presented in current study showed that ILs have the potential to effectively replace the conventional toxic adsorbents.

Keywords: Ionic Liquids, Heavy metal, Water treatment, Cobalt (Co)

1. INTRODUCTION

Cobalt (Co(II)) is a crucial cofactor in Vitamin B12, which is necessary for the healthy operation of the neurological system and the brain as well as for the production of blood function[1–4]. One of the most crucial transition metals for humans is Co(II), which is well known. Inadequate levels of Co(II) can cause cardiovascular disease and goiter while excessive amounts can impair thyroid activity[5–7].Co(II) is dangerous for both people and animals in excess, though. High levels of exposure to this element may have harmful effects, including nausea, problems with reproduction, hypertension (high blood pressure), lung disorders, hyperglycemia (high blood sugar), and bone deformities[8–11].It may also result in mutations (genetic alterations) in living cells. According to the Canadian Water Quality Guidelines published by the Environmental Bureau of Investigation, the acceptable limits of Co(II) in irrigation water and live-stock watering are 0.05 and 1.0 mg/L, respectively.

Several techniques like adsorption, membrane technology, photo catalytic degradation, chemical oxidation, biological treatment and ionic exchange were used to clean contaminated water containing heavy metals. However among these technologies, adsorption considered the utmost favorable technology because of its high adsorption capacity, low operational cost, high penetration and fewer slime production[12–17].

Ionic liquids got attention of many researchers from the last few years. Ionic liquids have valuable properties which make them valuable material used in separation and purification technologies. As an adsorbent, several ionic liquids were used to eliminate heavy metals from waste water. In this research IL [PC6C6C6C14][-N(CN)2−] is used to remove cobalt traces from contaminated water[18–23].

2. METHODOLOGY

1.1 *Materials*

Cobalt Salt, NaOH and HCL are bought from HAQ chemicals Ltd, Peshawar. Ionic Liquid is purchased from Queen's University, UK.

1.2 Preparation of Cobalt Solution

By dissolving 2.63 g of Cobalt Sulphate in 1 Liter of de-ionized water, a 1000 mg/L concentrated standard synthetic Cobalt contaminated wastewater was produced. A homogeneous Co contaminated water solution was produced after the system was stirred for a predetermined amount of time to completely dissolve the hazardous salt. The pH of the solution was kept at its natural pH value (6.0). The concentration of stock solution was diluted for rest of experiments.

1.3 Adsorption capacity & Removal efficiency

Standard solution of cobalt sulphate in de-ionized water was prepared at 10mg concentration of ionic liquid, pH value was 9, time taken was 20 minutes, initial concentration of standard solution was kept 40 ml, and temperature was kept 70^0C. Firstly prepared 100ml of standard solution in 250 ml of flask. The mixture was stirred and then 10 mg of IL was added to it and stirred it for 20minutes by maintaining the pH of 9 by small amount of NaOH and kept the temperature of 700C. The concentration of Cobalt heavy metal was measured using Atomic Absorption Spectrophotometer (AAS Testing). The adsorption capacity and removal efficiency of heavy metal ions could be expressed as follows

$$q\ (mg/g) = (C_i - C_0)\frac{V}{W} \quad (1)$$

$$\%\ Removal = \frac{(Ci - Co)}{Ci} \times 100 \quad (2)$$

Where q (mg/g) is the adsorption capacity, Ci and C0 represents initial and final concentration of cobalt (II) in mg/L respectively, V is the solution volume in L and W

represents the mass of IL used.

1.4 Atomic Absorption Spectrophotometer (AAS)

The concentration of Cobalt (II) ions in a permeated water after adsorption were measured by using Atomic Absorption Spectrophotometer

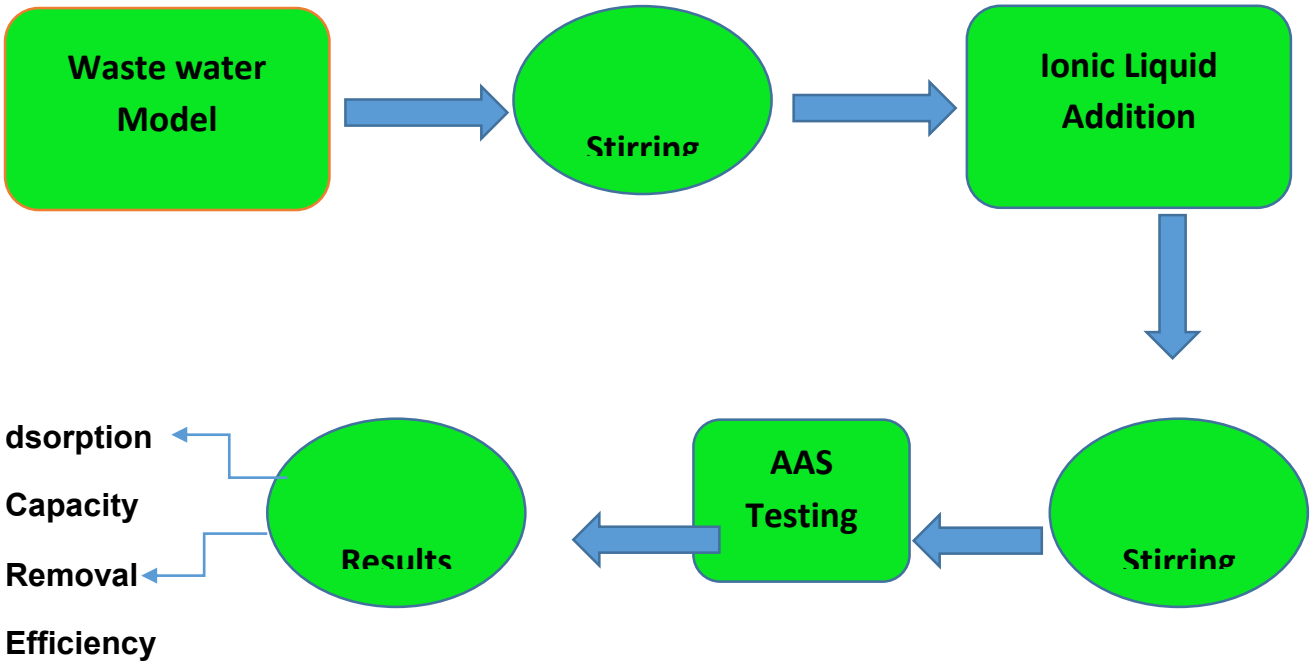

Figure 1.1 Research Methodology

3. RESULTS AND DISCUSSION

1.5 *Adsorption capacity*

Batch adsorption experiment was carried out. After optimization the adsorption capacity of Ionic Liquid (trihexyltetradecylphosphonium dicyanamide ([PC6C6C6C14][-N(CN)2−)] was found 344 mg/g for the elimination of Cobalt (II) from the wastewater.by using the following expression

$$q\ (mg/g) = (C_i - C_0)\frac{V}{W} \qquad (1)$$

1.6 Removal Efficiency

The removal efficiency of Ionic Liquid was found 86% for the elimination of Cobalt (II) from the model wastewater by using the following expression

$$\% \text{ Removal} = \frac{(Ci - Co)}{Ci} \times 100 \quad (2)$$

1.7 Comparison with Other Bio Adsorbents

Different types of ionic liquids were used to remove different types of heavy metals from contaminated water. Table 1.1 shows comparison of adsorption capacities of Co (II) onto different bio-adsorbents.

Table 1.1 Comparison of adsorption capacities of Co(II) onto different bio-sorbents.

Adsorbent	Adsorption Capacity max (mg/g)	Refs
Apricot stone activated carbon (ASAC)	111.110	[24]
Un-treated pest moss	30.030	[25]
Pest moss treated with HNO3	25.510	[25]
Pest moss treated with NaOH	35.210	[25]
Hazelnut shells	13.88	[26]
Attapulgite	0.619	[27]
Bentonite	0.560	[27]

4. CONCLUSION

At high temperature (70^{o}C), initial Concentration (40 ml), pH (9), Time (20 minutes), and IL Dosage (10mg) ionic liquid (trihexyltetradecylphosphonium dicyanamide ([PC6C6C6C14][-N(CN)2−)] was investigated for the removal of hazardous heavy metal Cobalt (II) from the model wastewater. It is found that this ionic liquid has high adsorption capacity towards cobalt removal from wastewater and also have high removal efficiency at the above mention parameters.

5. REFERENCES

[1] F.R. Adolfo, P.C. Do Nascimento, D. Bohrer, L.M. De Carvalho, C. Viana, A. Guarda, A. Nunes Colim, P. Mattiazzi, Simultaneous determination of cobalt and nickel in vitamin B12 samples using high-resolution continuum source atomic absorption spectrometry, Talanta. 147 (2016) 241–245. https://doi.org/10.1016/j.talanta.2015.09.073.

[2] M.R. Awual, Innovative composite material for efficient and highly selective Pb(II) ion capturing from wastewater, J. Mol. Liq. 284 (2019) 502–510. https://doi.org/10.1016/j.molliq.2019.03.157.

[3] P. Oustadakis, S. Agatzini-Leonardou, P.E. Tsakiridis, Nickel and cobalt precipitation from sulphate leach liquor using MgO pulp as neutralizing agent, Miner. Eng. 19 (2006) 1204–1211. https://doi.org/10.1016/j.mineng.2005.11.006.

[4] M.R. Awual, M. Ismael, T. Yaita, Efficient detection and extraction of cobalt(II) from lithium ion batteries and wastewater by novel composite adsorbent, Sensors Actuators, B Chem. 191 (2014) 9–18. https://doi.org/10.1016/j.snb.2013.09.076.

[5] M.F.A. Ahmed, V. Mahammadyunus, Microwave synthesis and antimicrobial activity of some copper (II), cobalt (II), nickel (II) and chromium (III) complexes with schiff base 2,6-pyridinedicarboxaldehyde-thiosemicarbazone, Orient. J. Chem. 30 (2014) 111–117. https://doi.org/10.13005/ojc/300114.

[6] N. V. Scheglova, T. V. Popova, A. V. Druzhinina, T. V. Smotrina, Spectrophotometric study of complexation of cobalt (II) with HEDP in aqueous solutions, J. Mol. Liq. 286 (2019) 110909. https://doi.org/10.1016/j.molliq.2019.110909.

[7] D. Citak, M. Tuzen, M. Soylak, Simultaneous coprecipitation of lead, cobalt, copper, cadmium, iron and nickel in food samples with zirconium(IV) hydroxide prior to their flame atomic absorption spectrometric determination, Food Chem. Toxicol. 47 (2009) 2302–2307. https://doi.org/10.1016/j.fct.2009.06.021.

[8] Y. Guo, H. Zhao, Y. Han, X. Liu, S. Guan, Q. Zhang, X. Bian, Simultaneous spectrophotometric determination of trace copper, nickel, and cobalt ions in water samples using solid phase extraction coupled with partial least squares approaches, Spectrochim. Acta - Part A Mol. Biomol. Spectrosc. 173 (2017) 532–536. https://doi.org/10.1016/j.saa.2016.10.003.

[9] M. He, Y. Zhu, Y. Yang, B. Han, Y. Zhang, Adsorption of cobalt(II) ions from aqueous solutions by palygorskite, Appl. Clay Sci. 54 (2011) 292–296. https://doi.org/10.1016/j.clay.2011.09.013.

[10] R. Zein, R. Suhaili, F. Earnestly, Indrawati, E. Munaf, Removal of Pb(II), Cd(II) and Co(II) from aqueous solution using Garcinia mangostana L. fruit shell, J. Hazard. Mater. 181 (2010) 52–56. https://doi.org/10.1016/j.jhazmat.2010.04.076.

[11] A.U. Karatepe, M. Soylak, L. Elci, Cobalt determination in natural water and table salt samples by flame atomic absorption spectroscopy/on-line solid phase extraction combination, Anal. Lett. 35 (2002) 2363–2374. https://doi.org/10.1081/AL-120016109.

[12] M. Soylak, E. Yilmaz, Ionic liquid dispersive liquid-liquid microextraction of lead as pyrrolidinedithiocarbamate chelate prior to its flame atomic absorption spectrometric determination, Desalination. 275 (2011) 297–301. https://doi.org/10.1016/j.desal.2011.03.008.

[13] M. Soylak, I. Narin, M.D.A. Bezerra, S.L.C. Ferreira, Factorial design in the optimization of preconcentration procedure for lead determination by FAAS, Talanta. 65 (2005) 895–899. https://doi.org/10.1016/j.talanta.2004.08.011.

[14] P. dos Santos Morales, P. Mantovani dos Santos, A. Evaristo de Carvalho, M. Zanetti Corazza, Vortex-assisted magnetic solid-phase extraction of cadmium in food, medicinal herb, and water samples using silica-coated thiol-functionalized magnetic multiwalled carbon nanotubes as adsorbent, Food Chem. 368 (2022) 130823. https://doi.org/10.1016/j.foodchem.2021.130823.

[15] S.A. El-Safty, M.R. Awual, M.A. Shenashen, A. Shahat, Simultaneous optical detection and extraction of cobalt(II) from lithium ion batteries using nanocollector monoliths, Sensors Actuators, B Chem. 176 (2013) 1015–1025. https://doi.org/10.1016/j.snb.2012.09.040.

[16] G.Z. Kyzas, E.A. Deliyanni, K.A. Matis, Activated carbons produced by pyrolysis of waste potato peels: Cobaltions removal by adsorption, Colloids Surfaces A Physicochem. Eng. Asp. 490 (2016) 74–83. https://doi.org/10.1016/j.colsurfa.2015.11.038.

[17] A. Shahat, M.R. Awual, M. Naushad, Functional ligand anchored nanomaterial based facial adsorbent for cobalt(II) detection and removal from water samples, Chem. Eng. J. 271 (2015) 155–163. https://doi.org/10.1016/j.cej.2015.02.097.

[18] C. Kokkinos, A. Economou, Microfabricated chip integrating a bismuth microelectrode array for the determination of trace cobalt(II) by adsorptive cathodic stripping voltammetry, Sensors Actuators, B Chem. 229 (2016) 362–369. https://doi.org/10.1016/j.snb.2016.01.148.

[19] M.B. Arain, E. Yilmaz, M. Soylak, Deep eutectic solvent based ultrasonic assisted liquid phase microextraction for the FAAS determination of cobalt, J. Mol. Liq. 224 (2016) 538–543. https://doi.org/10.1016/j.molliq.2016.10.005.

[20] C.Y. Cheang, N. Mohamed, M.R. Awual, N.H. Alharthi, M.M. Hasan, M.R. Karim, A. Islam, H. Znad, M.A. Hossain, M.E. Halim, M.M. Rahman, M.A. Khaleque, D. Citak, M. Tuzen, G.Z. Kyzas, E.A. Deliyanni, K.A. Matis, Removal of cobalt from ammonium chloride solutions using a batch cell through an electrogenerative process, Food Chem. Toxicol. 324 (2016) 1399–1404. https://doi.org/10.1016/j.cej.2017.05.026.

[21] Y.J. Na, Y.W. Choi, G.R. You, C. Kim, A novel selective colorimetric chemosensor for cobalt ions in a near perfect aqueous solution, Sensors Actuators, B Chem. 223 (2016) 234–240. https://doi.org/10.1016/j.snb.2015.09.098.

[22] D. Citak, M. Tuzen, A novel preconcentration procedure using cloud point extraction for determination of lead, cobalt and copper in water and food samples using flame atomic absorption spectrometry, Food Chem. Toxicol. 48 (2010) 1399–1404. https://doi.org/10.1016/j.fct.2010.03.008.

[23] M.R. Awual, T. Yaita, Y. Okamoto, A novel ligand based dual conjugate adsorbent for cobalt(II) and copper(II) ions capturing from water, Sensors Actuators, B Chem. 203 (2014) 71–80. https://doi.org/10.1016/j.snb.2014.06.088.

[24] M. Abbas, S. Kaddour, M. Trari, Kinetic and equilibrium studies of cobalt adsorption on apricot stone activated carbon, J. Ind. Eng. Chem. 20 (2014) 745–751. https://doi.org/10.1016/j.jiec.2013.06.030.

[25] C. Caramalău, L. Bulgariu, M. Macoveanu, Cobalt (II) Removal from Aqueous Solutions by Adsorption on Modified Peat Moss, Bul. Ştiinţific Al Univ. "Politehnica" Din Timisoara. 54 (2009) 13–17. http://www.ch.tuiasi.ro.

[26] E. Demirbas, Adsorption of Cobalt (II) Ions from Aqueous Solution onto Activated Carbon, Technology. (2003) 951–963.

[27] J. Hussain, N.U. Rehman, A. Al-Harrasi, L. Ali, A.L. Khan, M.A. Albroumi, Essential oil composition and nutrient analysis of selected medicinal plants in Sultanate of Oman, Asian Pacific J. Trop. Dis. 3 (2013) 421–428. https://doi.org/10.1016/S2222-1808(13)60095-X.

Copper Ore Beneficiation: Comparative study between Flotation Cell and Shaking Table

Muhammad Ibrahim*[1], Muhammad Haris Ishfaq[1], Hamza Amin[2], Subhan Aziz[1], Insiram Naveed[1], Faisal Khan[1], Naseer Ahmed Khan[1], Syed Naveed Ul Hassan*[1].
[1]University of Engineering and Technology, Pakistan. [2] Chemistry Department, University of Peshawar, Pakistan.
* Corresponding authors: engineeribrahimpakistan@gmail.com

Abstract

Copper ore depending on the grade needs to be handled because of having less desired metal which is unproductive. Copper beneficiation is carried out to increases the copper content and makes it cost effective for transport. For this there are various equipment such as hydro-cyclone, shaking table, flotation cell and fluidized bed separator etc. The purpose of this research is a comparative study of 2 of the following equipment, flotation cell and shaking table, in order to find out which one is more efficient and economically feasible. A sample of copper ore is crushed and grinded then equal amount of ore is processed through both flotation cell and shaking table. The final results are concluded based upon final copper grades, cost for materials, retention time and energy cost. This study compares and shows the importance of beneficiation in mining industry as it helps in cut down cost for transport and material handling further studies are needed for comparison of other equipment to establish the most efficient method of beneficiation.

Keywords: Copper ore, beneficiation, shaking table.

1. INTRODUCTION

The ongoing global transition to low- and zero-CO_2 energy generation and transport require more raw materials and metals than ever produced before in human history to develop the necessary infrastructure for solar and wind power generation, electric power grid distribution, and electric vehicle components, including batteries. In addition to numerous critical elements,

this transition will also require increased production of a range of other metals. This includes copper, with increased production of this metal providing the minerals industry with enhanced opportunities to secure the additional supply of associated or potential by-product elements [1] but the copper is a non-renewable resource, thus we have to use every bit of copper in mines that we can fine. Copper is one of the few minerals that can occur by itself in nature thus it is easy to obtain, process and utilize. Copper also occurs in ore form where it is the separated from unwanted material called tail, this process is known as Beneficiation of copper ore. This beneficiation can be performed in various equipment's such as shaking table, hydro-cyclone, fluidization bed and flotation cell. Shaking table separates particle based on particle density. The crushed ore is placed in feed box then the angle and frequency are adjusted. With the rapid backward movement of the table, the particles gain a forward movement thanks to momentum, so each structure is separated from the other. Separation performance in shaking tables is directly related to particle size distribution [2]. Meanwhile Flotation cell separates particle based on phobicity. By using regents, we make our desired component hydrophobic then by passing air bubble we collect the concentrate in top product as the hydrophobic particles attaches themselves to air bubbles and collects on top in form of lather which is collected by the process of skimming while the tail mostly silica settles down at the bottom of the tank [3]. This research aims to determine the most efficient way for beneficiation of copper ore by comparing the efficiency of shaking table and flotation cell.

2. Methodology

The copper ore was collected from Upper Dir Osheri Dara. The ore was crushed in jaw crusher then ball mill till all of it was able to pass through 250 mesh size. Then it was sent for testing in the lab it was found out that the ore contains 2.47% copper content in ore and the rest was mostly silicon dioxide 2 equal number of fine ore were sent to shaking table and flotation cell. The concentrate of shaking table was collected in ridges while the concentrate of flotation cell was called float and skimmed through the top both were dried out and then sent to lab for testing again.

Experimental results of copper ore before beneficiation:

The finely crushed copper ore was sent to testing to determine its components multiple tests were conducted including.

1) Atomic Absorption spectrometer (AAS)
2) Gravimetric method
3) ASTM/Robertson Research Lab UK
4) Multi Acid Digestion

The tests result showed that the ore contain almost 2.47% copper content, 0.96% sulfate, 1% phosphate and 95.57% oxide and sulfide minerals.

Table 1. Lab results before the beneficiation of the copper ore

Lab results before beneficiation of copper ore	
Ore Content	Percentage
Copper Content	2.47%
Oxides and Sulfides silicate	95.57%
Sulfate	0.96%
Phosphate	1%

Figure 2. Copper concentrate coming out in upper float of Flotation Cell.

3. Results and Discussion

Z. MATH

In Flotation Cell experiment, 1000g of copper ore was used to make a suspension solution of 70% water and 30% ore then the ore was bought to a basic pH of 9.8 because Flotation occurs in basic medium [4]. All the contents were transferred to flotation cell then a few drops of sodium amayle xanthate and floria 34 was added as a promoter and depressant. The agitator was lowered into the flotation cell and used to mix the solution for 30 minutes [5]. After that 10 ml of pine oil was added as a frothing agent and mixed well, the air bubbles were passed through the agitator; the copper particles that are hydrophobic in nature attached themselves with the air bubbles and came at the surface in the form of froth. The froth was concentrated and the product of our experiment. Some particles settled at the bottom these, were mostly silicate oxides and sulfides, they were collectively called gangue. The concentrate was collected through process called skimming, the excess water was drained concentrate and gangue was dried the final collective mass of concentrate and gangue was 996.6g the loss of

3.4g was attributed to experimental loss. The composition of both concentrates and product is as follows.

CONCENTRATE/ FLOAT: After the experiment on flotation cell the lab tests were again conducted and the results show that the total weight of concentrate was 225.6g of which copper content was found to be 27.0% the oxide and sulfide minerals were 67.2% and the rest were trace amount of minerals.
TAIL: The total mass of tail was found to be 771g of which copper 3.07% while sulfide and oxide minerals were 95.54% and the rest were trace amount of minerals.

Table 2. Lab Results For Flotation Cell

Components of ore	Concentrate		Tail		Total mass
	Percentage	Mass of component	Percentage	Mass of component	
Copper	27.0%	60.75g	3.07%	23.67g	84.42g
Sulfide, oxides silicate	67.2%	151.2g	95.54%	736.13g	887.33g
Trace minerals	5.8%	13.05g	1.39%	10.72g	23.77
	225.6 g		771 g		996.6 g

AA. Helpful Hints

During Shaking table experiment 1000g of ore was also used and a solution of 60% water and 40% ore was used the shaking table angle was set at 5° angle and the speed was set to 225 Hz the shaking table was turned on [6]. the process was and wash water valve were opened and the experiment was left to be performed for 40 minutes after that the tail, intermediate and concentrate were collected dried the total product weight was 992.2g the loss of material was attributed to experimental loss the results were as follows.

CONCENTRATE: After the shaking table experiment the total weight of concentrate was 188.7g lab tests were conducted and the results were as follows 3.47% copper content, 92.34% sulfides and oxides, 3.44% trace minerals **INTERMEDIATE**: The intermediate is an intermediate where both ore and tail can be found its weight was 302.6g. The results were as follows 2.84% copper content, 94.91% sulfides and oxides, 2.25% trace minerals.

TAIL: The total weight of tail was 500.7g and it contained 2.08% copper 95.0% sulfide and oxides and 2.92% was trace amount of minerals.

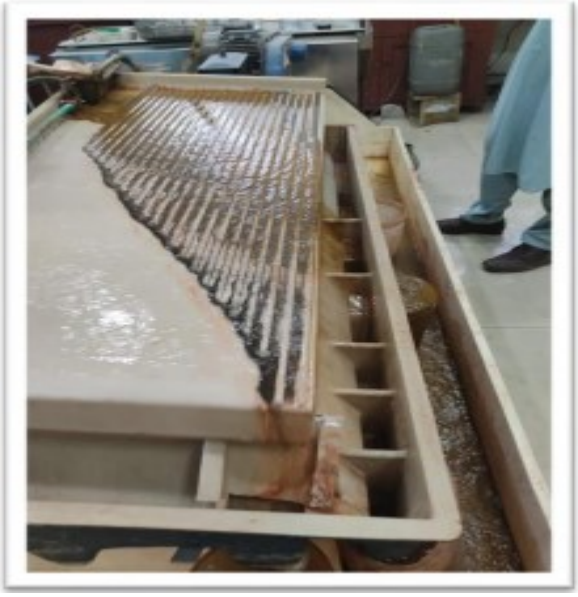

Figure 3. Shaking table used in experiment

Table 3: the above graph shows the comparison between shaking table, flotation cell and raw

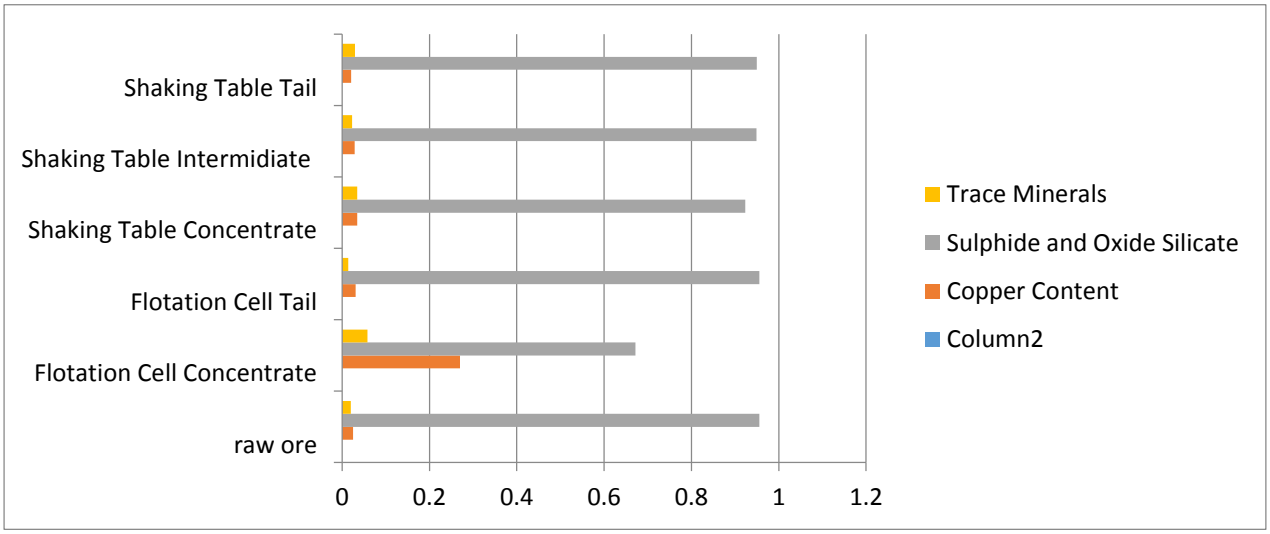

4. Conclusion

By comparing the lab results of both tests we can safely say that Flotation cell performed far better than shaking table the shaking table though shaking table did not require other reagents such as promoter or depressant but it isn't cost effective because of its power consumption and low output also it require extra step for reprocessing the intermediate part thus we can

safely conclude that flotation is a more viable option for copper ore beneficiation.

5. References

[1]. McNulty, B. A., Jowitt, S. M., & Belousov, I. (2022). The Importance of Geology in Assessing by-and Coproduct Metal Supply Potential; A Case Study of Antimony, Bismuth, Selenium, and Tellurium within the Copper Production Stream. Economic Geology.

[2]. Carvalho, M. T., Agante, E., & Durão, F. (2007). Recovery of PET from packaging plastics mixtures by wet shaking table. Waste Management, 27(12), 1747-1754.

[3]. Harbort, G. J., Jackson, B. R., & Manlapig, E. V. (1994). Recent advances in Jameson flotation cell technology. Minerals Engineering, 7(2-3), 319-332.

[4]. Nasirimoghaddam, S., Mohebbi, A., Karimi, M., & Yarahmadi, M. R. (2020). Assessment of pH-responsive nanoparticles performance on laboratory column flotation cell applying a real ore feed. International Journal of Mining Science and Technology, 30(2), 197-205

[5]. Runge, K., McMaster, J., Wortley, M., La Rosa, D., & Guyot, O. (2007, March). A correlation between Visiofroth™ measurements and the performance of a flotation cell. In Ninth Mill Operators' Conference (pp. 19-21).

[6]. Bustillo Revuelta, M. (2018). Mineral Processing. In Mineral Resources (pp. 423-530). Springer, Cham.

Economic optimization of dual effect absorption refrigeration system

[1]Muhammad Muqaddam Javaid, [1]Hira Amin, [1]Khalid Saif Ullah, [1*]Muhammad Zaman, [1]Khurram Shehzad

[1]muqaddam96@gmail.com Department of Chemical Engineering, Pakistan Institute of Engineering and Applied Sciences (PIEAS), Lehtrar Road, P.O. Nilore, 45650, Islamabad, Pakistan

Corresponding author (Muhammad Zaman, Ph.D.): zaman@pieas.edu.pk

Abstract— The world is going through an energy crisis due with soaring energy prices and related greenhouse gas emissions. Absorption refrigeration systems (ARS) can use the waste or low-grade energy, consequently reducing carbon dioxide emissions and the global energy demand. In addition to reducing fuel consumption, ARS would prevent some of the waste heat from polluting the air. However, coefficient of performance of ARS is relatively low compared to conventional compression based systems. Hence, cost reduction by optimization of ARS can improve its performance. Previously, researchers employed constant values of the heat transfer coefficient (U), during the optimization of ARS. The value of U depends on fluid properties, flow, and geometric parameters. Thus, correlations are used to prevent erroneous conclusions. In this work dual-stage, ARS series configuration system has been opted, a MATLAB model is developed, available correlations are used, and finally optimized

the ARS to minimize total annual cost. Significant changes in the design of equipment of ARS have been seen by using correlations for U compared to constant values leading to realistic and robust design of the system.

Keywords— Absorption Refrigeration System; Series Configuration; Heat Transfer Coefficients; Optimization; Total Annual Cost.

1. INTRODUCTION

Global primary energy consumption has increased by 5.8% in 2021, with fossil fuels accounting for 82% of all energy production [1]. The majority of industrial processes rely heavily on thermal energy generated by the combustion of fossil fuels to generate steam or heat [2]. This results in a significant amount of wasted, low-quality heat that is emitted into the environment. Refrigeration encompasses a wide range of fields, from the cooling of electronics to the preservation of perishable foods. Refrigeration systems like absorption refrigeration systems (ARS) can convert this surplus heat into beneficial chilling applications, negating the need to burn fossil fuels and so lowering CO_2 emissions.

Using a non-linear programming technique, Mussati et al. [3] improved the process design of the double effect ARS and decreased the total annual cost (TAC), total capital cost, and total operating cost by 9.5%, 11.1%, and 4.9%, respectively. Azhar et al. [4] optimized temperatures of generator, condenser, and solution distribution ratio for dual-stage parallel configuration ARS. A genetic algorithm (GA) based optimization tool was made for double effect series and parallel combinations of ARS. It was found that the optimum COP of the LiCl-water-based ARS system is slightly less than the LiBr-based ARS system under the same fixed conditions [5]. The thermo-economic concept was utilized by Misra et al. [6] to optimize a double-effect H_2O/LiBr ARS with the interest of reducing the overall product cost as much as possible.

During the optimization, several optimizing variables such as flow rates, temperatures of the components, pressure, composition and areas of the equipment vary to evaluate their optimal values. These variations of the optimizing variables will ultimately change the heat transfer coefficients. Hence, the correlations of heat transfer coefficients should be employed for the design calculations of the equipment of the ARS. To the author's knowledge, no prior work has optimized the entire ARS system for the minimization of total annual cost by employing correlations of heat transfer coefficients for a dual-stage series configuration. In this work, optimization was done on MATLAB using a GA and a LiBr-H_2O based system was selected. Based on criteria like reliability, applicability, and availability, various correlations for heat transfer coefficients were chosen from the published literature.

2. PROCESS DESCRIPTION

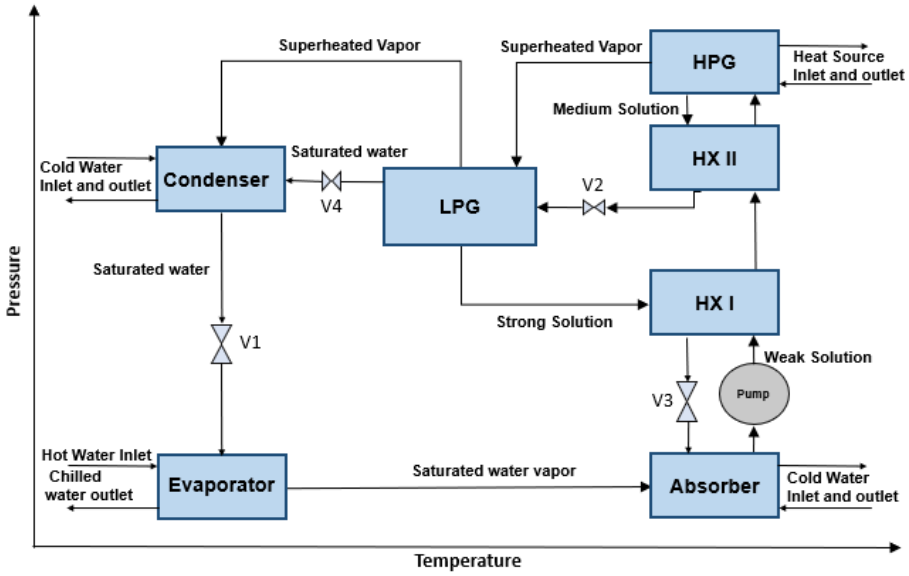

Fig. 3 Schematic of double effect series flow ARS

In Fig. 3, weak LiBr-water solution enters high pressure generator (HPG), where water becomes superheated by exchanging heat from the heat source. It then goes to low pressure generator (LPG) and heats remaining medium solution from HPG, producing more superheated steam (refrigerant). Together refrigerant goes to the condenser, becomes saturated water, then to the expansion valve and finally to the evaporator where it provides chilling to water that we want to cool down. Vapor refrigerant from evaporator, goes to the absorber where it gets absorbed in strong solution coming from LPG,by passing through heat exchangers, to become weak solution again.

3. METHODOLOGY

The methodology of this work consists of choice of correlations for heat transfer coefficients, economic analysis and optimization of the ARS by minimizing TAC. The following paragraphs present the various steps of the methodology.

BB. Correlations

Calculations of thermodynamic properties have been done using correlations from Patek et al. [7]. Rohsenow, Petukhov-Popov, and Wilke's correlations for heat transfer coefficients are used for the evaporator, solution heat exchanger, and absorber respectively. Whereas, the correlations for condenser and generator are selected from the available literature [8,9]

CC. Cost Correlations

Equation (1) calculates the TAC of ARS.

$$TAC = ACC + AOC \tag{15}$$

Where ACC and AOC represents annual capital cost and annual operating cost, respectively. Equation (2) represents the formula to calculate the ACC from total capital cost (TCC) using capital recovery factor (CRF).

$$ACC = CRF \times TCC \quad (16)$$

Equation (3) is used to find the CRF that annualizes TCC, where i shows the interest rate and n is the number of years (i =10.33% and n =25 years taken in this work).

$$CRF = \frac{i(i+1)^n}{(i+1)^n - 1} \quad (17)$$

Equation (4) shows TCC which is calculated by adding the capital costs of all the equipment of the ARS system. Equation (5) calculates the capital cost of each unit individually z_j represents the capital cost of jth component.

$$TCC = \sum z_j \quad (18)$$

$$z_j = A_j \times (10.7639 \times a_j)^{b_j} + c_j \quad (19)$$

Constants a, b, and c values for each jth component, can be obtained from Mussati et al. [3] and A represents heat transfer area. Equation (6) represents how AOC can be calculated by the utility costs of both heating (i.e., steam) and cooling utilities (i.e., water). Costs are taken as 3.0 $/ton and 0.0195 $/ton for heating and cooling utilities, respectively [10].

$$AOC = ((mass\ flow\ rate \times cost)_{heating\ and\ cooling\ utilities}) \times 3600 \times 24 \times 365 \quad (20)$$

DD. Optimization Model

The goal of optimization is to find the optimal set of decision variables that minimizes objective function, subject to certain limits. Equation (7) states the optimization problem.

$$min\ f(x) \quad \text{where,} f(x) = TAC \quad (21)$$

x is the set of decision variables. Equation (8) shows constraints, where $h(x)$ shows the set of equality constraints and $g(x)$ shows the set of inequality constraints.

$$h(x) = 0; g(x) \leq 0,\ x \in R \quad (22)$$

The equality constraints contain the mass and energy balance equations as well as constitutive relations. Equations (9) and (10) show inequality constraints that are used to avoid temperature cross-over.

$$T_{process\ unit} - T_{cold\ utility} \geq 0.5 \quad (23)$$

$$T_{evaporator} - T_{chilled\ water\ exit} \leq -0.5 \quad (24)$$

h_{min} is the minimum amount of enthalpy below which crystallization will occur [11]. Equation (11) presents that the enthalpy of any stream, in which the LiBr salt is present, should be higher than this minimum value. If not, crystals will form, and the system's efficiency would decrease.

$$h \geq h_{min} \quad (25)$$

4. RESULTS AND DISCUSSION

This section presents the validation of the model developed in this work followed by the economic optimization results based on using correlations for heat transfer coefficients.

EE. Validation

Dual stage ARS was first validated by using constant values of heat transfer coefficients and base case operating parameters by Omer et al. [12]. The results of the validation are presented in Table XI, which shows good agreement.

Table XI Validation

Components	Capacity(kW)		
	Omer et al.	This work	%Difference
HP generator	81.37	82.60	1.5
LP generator	51.45	51.55	0.2
Condenser	56.12	56.56	0.8
Evaporator	100.00	100.00	0.0
Absorber	125.44	126.26	0.7
Solution heat exchanger I/II	27.75/49.05	28.04/51.05	1.0/4.1

FF. Use of Heat transfer coefficients correlations

When heat transfer coefficients were used at conditions of Omer et al. [12], the different values of U were obtained as shown in Table XII, especially for HP generator, evaporator, and solution heat exchangers.

Table XII Comparison of constant vs correlated values at same base conditions

Components	Constant U (kW/m^2K)	U by correlations (kW/m^2K)
HP generator	1.5	1.9
LP generator	1.5	1.5
Condenser	2.5	2.1
Evaporator	1.5	3
Absorber	0.7	0.65
Heat exchanger I/II	1/1	0.41/1.48

GG. Optimization

Optimization was done by taking the initial conditions of Omer et al. [12]. The results are presented in Table XIII. The TAC had decreased from $38221 to $27820. This cost reduction was because of using optimal parameters by minimizing the TAC. Heat duty of evaporator is kept constant at 100 kW. By comparing the optimal and base case U values, it is observed that U values are variable and dependent on fluid and flow characteristics. Absorber, which covers 36.5% of the overall area, is the largest component.

Table XIII Optimization Results

Components	Parameter values ^oC	U values obtained by correlations (kW/m^2K)	Heat Duty (Q) (kW)	Area (m^2)
HP generator	134.43	1.81	92.62	1.56
LP generator	89.72	1.41	57.00	3.72
Condenser	33.16	2.18	51.65	0.99
Evaporator	5.02	3.07	100	3.93
Absorber	37.69	0.79	141.1	6.34
Heat exchanger I (effectiveness)	0.01	--	--	--
Heat exchanger II (effectiveness)	0.57	0.8	29.85	0.82
TAC ($/year)	27820	AOC/ACC ($/year)	6857/20963	

The effectiveness of heat exchanger I was nearly equal to zero which showed that it can be eliminated from the configuration. Capital cost accounts for 75.3% of the TAC.

5. CONCLUSION

In this work, correlations for heat transfer coefficients were used in the optimization model for ARS to minimize TAC. Around 27% of the TAC was reduced by the optimization strategy adopted in this work. The values of U varied considerably by using the correlations for the calculations of U. Hence, the optimal design of the components of the ARS in this work will be more realistic and robust.

ACKNOWLEDGMENT

This research was funded by the Pakistan Institute of Engineering and Applied Sciences, Islamabad.

6. REFERENCES

[1] British Petroleum, “Statistical Review of World Energy 2022.” Accessed: Sep. 18, 2022. [Online]. Available: https://www.bp.com/content/dam/bp/business-sites/en/global/corporate/pdfs/energy-economics/statistical-review/bp-stats-review-2022-full-report.pdf

[2] P. Srikhirin, S. Aphornratana, and S. Chungpaibulpatana, “A review of absorption refrigeration technologies,” 2001. [Online]. Available: www.elsevier.com/locate/rser

[3] S. F. Mussati, S. Cignitti, S. S. Mansouri, K. v. Gernaey, T. Morosuk, and M. C. Mussati, “Configuration optimization of series flow double-effect water-lithium bromide absorption refrigeration systems by cost minimization,” *Energy Convers Manag*, vol. 158, pp. 359–372, Feb. 2018, doi: 10.1016/j.enconman.2017.12.079.

[4] M. Azhar and M. Altamush Siddiqui, “Comprehensive exergy analysis and optimization of operating parameters for double effect parallel flow absorption refrigeration Cycle,” *Thermal Science and Engineering Progress*, vol. 16, May 2020, doi: 10.1016/j.tsep.2019.100464.

[5] D. Konwar, T. K. Gogoi, and A. J. Das, “Multi-objective optimization of double effect series and parallel flow water–lithium chloride and water–lithium bromide absorption refrigeration systems,” *Energy Convers Manag*, vol. 180, pp. 425–441, Jan. 2019, doi: 10.1016/j.enconman.2018.10.029.

[6] R. D. Misra, P. K. Sahoo, and A. Gupta, “Thermoeconomic evaluation and optimization of a double-effect H 2O/LiBr vapour-absorption refrigeration system,” in *International Journal of Refrigeration*, May 2005, vol. 28, no. 3, pp. 331–343. doi: 10.1016/j.ijrefrig.2004.09.006.

[7] J. Pátek and J. Klomfar, “A computationally effective formulation of the thermodynamic properties of LiBr-H2O solutions from 273 to 500 K over full composition range,” *International Journal of Refrigeration*, vol. 29, no. 4, pp. 566–578, Jun. 2006, doi: 10.1016/j.ijrefrig.2005.10.007.

[8] G. A. Florides, S. A. Kalogirou, S. A. Tassou, and L. C. Wrobel, “Design and construction of a LiBr-water absorption machine,” *Energy Convers Manag*, vol. 44, no. 15, pp. 2483–2508, Sep. 2003, doi: 10.1016/S0196-8904(03)00006-2.

[9] “475682087-Ozisik-M-Necati-Heat-Transfer-A-Basic-Approach-McGraw-Hill-Book-Company-1985-pdf - Copy”.

[10] S. F. Mussati, K. v. Gernaey, T. Morosuk, and M. C. Mussati, “NLP modeling for the optimization of LiBr-H2O absorption refrigeration systems with exergy loss rate, heat transfer area, and cost as single objective functions,” *Energy Convers Manag*, vol. 127, pp. 526–544, Nov. 2016, doi: 10.1016/j.enconman.2016.09.021.

[11] M. M. Ardehali, M. Shahrestani, and C. C. Adams, “Energy simulation of solar assisted absorption system and examination of clearness index effects on auxiliary heating,” *Energy Convers Manag*, vol. 48, no. 3, pp. 864–870, Mar. 2007, doi: 10.1016/j.enconman.2006.08.012.

[12] O. Kaynakli, K. Saka, and F. Kaynakli, “Energy and exergy analysis of a double effect absorption refrigeration system based on different heat sources,” *Energy Convers Manag*, vol. 106, pp. 21–30, Dec. 2015, doi: 10.1016/j.enconman.2015.09.010.

Investigating the effect of Charge Transport Layers on Germanium based Perovskite Solar Cell

Waqar Ahmad[1,*], Muhammad Noman[1], Shayan Tariq Jan[1, 2]
[1] U.S.-Pakistan Center for Advanced Studies in Energy, University of Engineering & Technology, Peshawar, Pakistan
[2] Department of Energy Technology, University of Technology Nowshera, Pakistan
Waqarahmad.uspcase@uetpeshawar.edu.pk*

Abstract—Perovskite material have brought revolution in the field of photovoltaics. Perovskite based solar cells have high efficiencies, low cost and good optical properties. With these properties perovskite have also some challenges like of large area fabrication, toxicity, long term stability and humidity. The toxicity of the device is because of lead. To solve the issue to toxicity, in the present study lead is replaced by germanium. Germanium also belong to the group of lead with band gap close to the lead. Cesium Germanium Tri-Iodide ($CsGeI_3$) based perovskite solar cell is simulated with electron transport layer (ETL) based on C_{60} and hole transport layer (HTL) based on CuI using SCAPS-1D simulation software. The effect of thickness and on the parameters of the solar cell are study in depth. The maximum efficiency of 15.02% is achieved with the fill factor of 85.88%. Moreover, the Voc of 0.883V and the Jsc of 19.79 $mACm^{-3}$ is obtained for the designed solar cell.

Keywords: Perovskite; $CsGeI_3$, C_{60}, SCAPS-1D

1. INTRODUCTION:

Perovskites were discovered by German Scientist, Gustav Rose in 1839 and named in honor of Russian mineralogist Lev von Perovski[1]. Perovskite have ABX_3 structure which give the advantage of tunability and excellent optical properties. In the ABX_3 structure the “A” represents the organic cation, “B” is for metal cation and “X” is the halide anion. The most common organic cations are methyl ammonium (MA) and formamidinium (FA) while Cl, Br, I are regularly used halogens. Lead (Pb) is the most popular material used as “B” cation. Due to Pb toxic nature it can be replaced with alternate cation of the same periodic group[2].

The basic structure of perovskite solar cell has multiple layers with specific functionality. The layers consists of electron transport layer (ETL), a hole transport layer (HTL), a Perovskite Layer and two electrodes. The generation of electron-hole pairs occurs in the perovskite layer. The generated ions are then separated and transported by the charge transport layers (CTLs) i.e. ETL and HTL. The function of ETL is to extract the electron efficiently from the perovskite layer and block the hole. Similarly, the function of the HTL is to block electrons and extract holes from the perovskite layer. The electrons and holes from the CTLs are then collected by the counter electrodes.

Figure 1: Layer Structure of Perovskite Solar Cell

In PV cells, the CTLs, and the counter electrodes are stacked in specific order and layer's combinations. By stacking different interfacial layers are produced. These interfaces have a key role in the power conversion efficiency (PCE) of perovskite solar cells (PSCs). The transportation of charges occurs through these interfaces. Similarly, the defects in the interfacial layers are the reason of recombination of charge carriers. Because of the mentioned factors it is of key importance that with compatible materials for solar cells we also need to have quality thin film to reduce recombination losses[3][4]. The importance and role of the interface also depends on the architecture of PSC[5].

Germanium is present richly in nature and is also a toxic free material. It is key to indicate that germanium-based perovskites face issues when dissolved in most organic solvents. There is problem of oxidation in Ge based perovskite but it can be solved if we use Ge^{4+} cations[6]. The optical properties of Ge is also well suited for photovoltaic applications. In studies [7] it is proposed that the immovability and performance of germanium based perovskite solar cell can be enhanced by changing its chemical composition using bromide ions. Ge^{+2} has higher electronegativity than lead with more covalent character and ionic radius.

HTL is fabricated under the absorber layer and the cost of perovskite solar cells is mostly depends on HTM. For that purpose number of researches are carried out to find a low-cost, stable and non-toxic hole transport material (HTM). Copper-based hole transport materials have high hole mobility, low cost, and are more stable and the most suitable alternatives of other toxic HTMs. Copper-based HTMs like $CuAlO_2$, CuO, CuOx, etc are considered most efficient for HTL[8].

In this study, the $CsGeI_3$-based perovskite material have been modelled in the PSC structure along with C_{60} ETL CuI HTL. CuI is used to increase the conductivity of the cell and C_{60} to increase the stability [9].

2. METHODOLOGY:

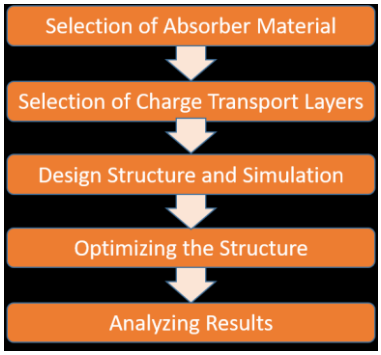

Figure 2: Research Methodology and Simulation Process

To begin the research process, the literature was studied to find out alternate absorber layer for perovskite solar cell and charge transport layers. After the detailed study it was concluded the $CsGeI_3$ can be a potential inorganic perovskite material. Germanium belongs the same group as lead and also germanium is a nontoxic material. Similarly, C_{60} is taken as electron transport layer (ETL) as carbon has good stability properties and low cost. CuI is used as hole transport layer (HTL) due to its excellent electrical conductivity. Once all the materials were defined, layer by layer structure were added and the perovskite solar cell with the structure $C_{60}/CsGeI_3/CuI$ was numerically modelled in SCAPS-1D. The performance of the solar cell structure is studied. The optimization of the different layers in the structures is carried out to enhance the cells performance. The effect of these parameters on the performance of perovskite solar cell are presented in this study.

3. RESULTS AND DISCUSSION

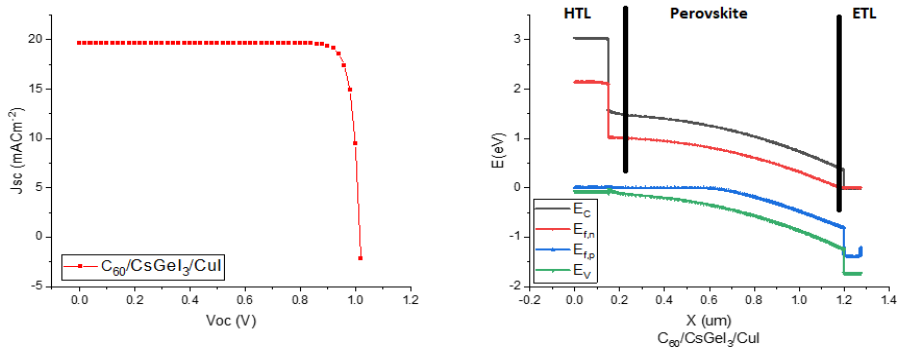

Figure 3 IV Characteristics Curve and Band Alignment of the Simulated Structure

Figure 3 represents the IV characteristics curve of the simulated structure taken under standard test conditions (STC). The PSC structure produces o Voc of 1.02 V, Jsc of 18.68 mA/cm^2 and PCE of 12.8%. On the right of the figure is the energy band alignment of the selected structure. Band alignment graph tells us about the flow of electron to the conduction band of the ETL and flow of holes to the valance band of the HTL. From figure 3 it can be clearly seen that the conduction band of ETL is aligned with the conduction band of perovskite while their valance

bands have large offsets. This indicates that C_{60} is the a suitable ETL for $CsGeI_3$. Similarly, the valance band of HTL is aligned with the valance band of Perovskite with large conduction band offsets which regulates the flow of holes easily and blocks the electrons.

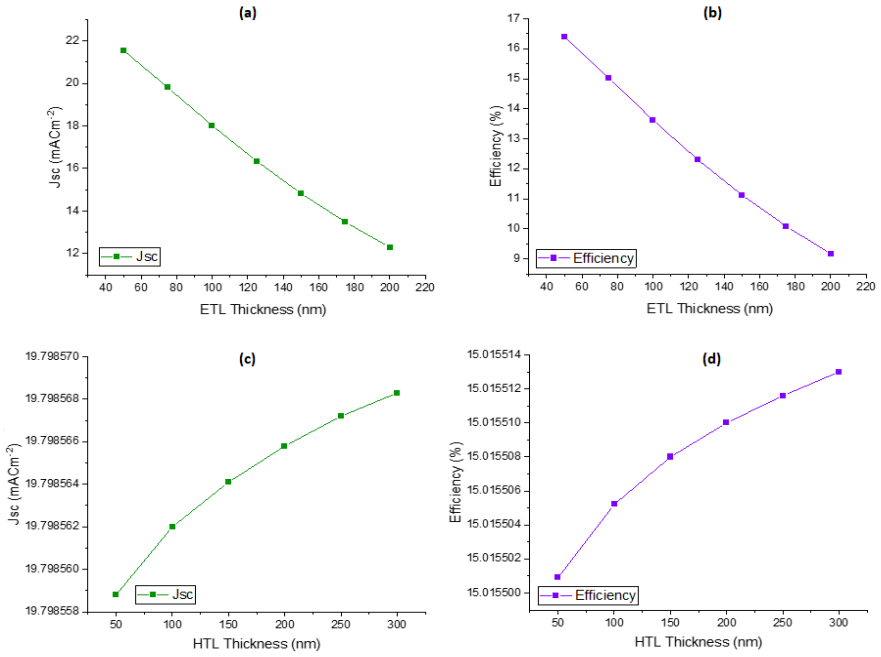

Figure 4 Effect of Thickness of CTL on Jsc and PCE

ETL and HTL has a key function in the performance and structure of perovskite solar cell. Charge transport layers (CTLs) are accountable for the separation and transportation of charge carriers from the absorber material to their respective electrodes. It also keeps the separation between holes and electrons[10][11]. Figure 4 shows the effect of layer thickness on the PSC performance. It can be noted that Jsc and PCE efficiency sharply decreases with the increase in thickness of electron transport layer. This occurs because increasing the thickness increasing the resistance of the cell. The increased resistance accelerates recombination of the charge carriers and reduce the PCE. The optimized thickness of the ETL is found to be 75nm. Similarly, increasing the thickness of CuI has very minimum effect on the PSC performance with very minute change in performance. This is because CuI is highly conductive and the increase in resistance is minimized because of it.

4. Conclusion:

From this study it can be concluded that germanium is the potential alternative to the lead. We can also tune the bandgap of Ge close to that of Pb to obtain more close results. C_{60} can be a suitable electron transport material for $CsGeI_3$ along with CuI as hole transport material. The final structure was obtained as $C_{60}/CsGeI_3/CuI$ with the maximum efficiency of 15.02% is achieved along with fill factor of 85.88%. Moreover, the Voc of 0.883V and the Jsc of 19.79 $mACm^{-3}$ is being achieved.

5. References

[1] S. Ito, “Research Update: Overview of progress about efficiency and stability on perovskite solar cells,” *APL Mater.*, vol. 4, no. 9, 2016, doi: 10.1063/1.4961955.

[2] M. Wang *et al.*, *Lead-Free Perovskite Materials for Solar Cells*, vol. 13, no. 1. Springer Singapore, 2021.

[3] J. Shi, X. Xu, D. Li, and Q. Meng, "Interfaces in perovskite solar cells," *Small*, vol. 11, no. 21, pp. 2472–2486, 2015, doi: 10.1002/smll.201403534.

[4] S. Tariq Jan and M. Noman, "Influence of layer thickness, defect density, doping concentration, interface defects, work function, working temperature and reflecting coating on lead-free perovskite solar cell," *Sol. Energy*, vol. 237, no. December 2021, pp. 29–43, 2022, doi: 10.1016/j.solener.2022.03.069.

[5] N. Marinova, S. Valero, and J. L. Delgado, "Organic and perovskite solar cells: Working principles, materials and interfaces," *J. Colloid Interface Sci.*, vol. 488, pp. 373–389, 2017, doi: 10.1016/j.jcis.2016.11.021.

[6] R. Chiara, M. Morana, and L. Malavasi, "Germanium-Based Halide Perovskites: Materials, Properties, and Applications," *Chempluschem*, vol. 86, no. 6, pp. 879–888, 2021, doi: 10.1002/cplu.202100191.

[7] I. Kopacic *et al.*, "Enhanced Performance of Germanium Halide Perovskite Solar Cells through Compositional Engineering," *ACS Appl. Energy Mater.*, vol. 1, no. 2, pp. 343–347, 2018, doi: 10.1021/acsaem.8b00007.

[8] A. Kumar, S. Singh, and A. Yadav, "Recent Development in Copper based Hole Transport Materials for Emerging Inverted Perovskite Solar Cells," *IOP Conf. Ser. Mater. Sci. Eng.*, vol. 1116, no. 1, p. 012066, 2021, doi: 10.1088/1757-899x/1116/1/012066.

[9] A. Raj *et al.*, "A computational approach to investigate the suitable ETL for lead-free CsGeI3 based perovskite solar cell," *Mater. Today Proc.*, vol. 47, no. xxxx, pp. 1564–1569, 2021, doi: 10.1016/j.matpr.2021.03.610.

[10] Y. Raoui, H. Ez-zahraouy, N. Tahiri, O. El, S. Ahmad, and S. Kazim, "Performance analysis of MAPbI 3 based perovskite solar cells employing diverse charge selective contacts : Simulation study," *Sol. Energy*, vol. 193, no. August, pp. 948–955, 2019, doi: 10.1016/j.solener.2019.10.009.

[11] E. Karimi, S. Mohamad, and B. Ghorashi, "The Effect of SnO 2 and ZnO on the Performance of Perovskite Solar Cells," 2019, doi: 10.1007/s11664-019-07804-4.

Performance Enhancement of $FAPbI_3$ perovskite solar cell with Kesterite and ZnO charge transport layer

[1]*Muhammad Aneeq, [1]Muhammad Noman, [1]Shayan Tariq Jan
[1] U.S.-Pakistan Center for Advanced Studies In Energy, University of Engineering & Technology, Peshawar, Pakistan
*maneeq.uspcase@uetpeshawar.edu.pk

***Abstract*—**Recently, methyl ammonium lead triiodide ($MAPbI_3$) perovskite solar cell (PSC) has surpassed the power conversion efficiency (PCE) of most of the established photo voltaic technologies, with PCE of 25.7%. But achieving long term structural stability still remains a hurdle in its large-scale commercialization. The methyl ammonium (MA) in perovskite material has low thermal conductivity and degrades with the built up of heat in it. This causes the leakage of the toxic lead into the environment. Research is being focused on replacing the MA with alternate thermal stable material. One such material is formamadium (FA). Formamadium lead triiodide ($FAPbI_3$) is more thermally and structurally stable than $MAPbI_3$ but has lower

efficiency. The performance of the FA-PSC can be enhanced by identifying the optimized design parameters of each layer in the PSC structure. In this work the $FAPbI_3$ is numerically modelled with CBTS and ZnO as charge transport layers in SCAPS-1D. A systematic approach is adopted to identify the optimized design parameters of each layer (hole transport layer, absorber and electron transport layer). After optimization the PCE of 24 % was achieved with Jsc of 24.271454 mA/cm2, Voc of 1.140949 V and fill factor of 86.65 %. Moreover, the effect of varying layer thickness, doping concentration, defect density and working temperature on the performance of $FAPbI_3$ is analyzed in detail.

Keywords: Perovskite solar cell, $FAPbI_3$, SCAPS-1D, Kesterite, HTL

1. INTRODUCTION

Solar energy has started growing in capturing the energy market and industry in recent times [1]. The most notable advancement is related to crystalline silicon which has captured the photovoltaic (PV) industry because of its extraordinary PCE and compelling commercialization capabilities [2]. On the other hand, the silicon's expensive and time-consuming commercialization process have prompted researchers to gaze for other potential materials for PV [3]. As a result, organic, dye-sensitized (DS) and bulk heterojunction (BHJ) PV technologies appeared as a trustworthy alternative PV cell [4]. However, their reduced PCE and short-term stability are one of their biggest drawbacks, prompting researchers to turn to further new technologies.

Recently, Hybrid organic-inorganic perovskite (HOIP) technology has emerged [5]. The word "perovskite" denotes to the $CaTiO_3$ mineral, and its name refers to a group of compounds with a stoichiometry of ABX_3, where "A" and "B" are cations and "X" an anion. Every such crystal consists of corner-sharing BX_6 octahedral. Perovskites that are used as an absorber in PV cells are often categorized as "hybrid" because they consist of organic and inorganic compounds. The "A" part in the structure is a monovalent organic compound (eg MA or FA), "B" is a Group IVa divalent cation (Sn, Pb), "X" can be a halide anion (eg I, Cl, Br) [6] [7].

In this work, the Formamadium lead triiodide ($FAPbI_3$) perovskite solar cell is numerically modelled in SCAPS-1D along with ZnO electron transport layer and CBTS hole transport layer. The effect of layer thickness, doping concentration, defect density and temperature are analyzed in detail.

2. METHODOLOGY

The FTO/ZnO/$FAPbI_3$/CBTS/Au structure was numerically modeled in SCAPS-1D simulation software. The strategy used was that initially the parameters mentioned in Table I were defined to model layers in n-i-p device structure [8]. The defects density for each layer was set as 1E15 cm^{-3} for overall simulation.

Afterwards, first the absorber thickness was varied to obtain optimized thickness. The optimized value was then used to find the thickness of both charge transport layers.

To further enhance the performance of the PSC the optimized doping concentration of each layer was also identified.

After the performance enhancement of the cell by varying thickness and doping concentration, the effect of Temperature and defect density were also analyzed to see the stability of cell.

TABLE I: Layers Parameters

Parameters		CBTS	$FAPbI_3$	ZnO
Thickness	**um**	0.1	0.1	0.1
Band Gap	**Eg (eV)**	1.9	3.05	1.4
Electron affinity	**X (eV)**	3.6	1.16	4.1
Dielectric permittivity	**Er**	5.4	10	13.6
CB effective density of states	**Nc (cm^{-3})**	2.2E18	5E18	2.2E18
VB effective density of states	**Nv (cm^{-3})**	1.8E19	5E18	1.8E19
Mobility of electrons	**Ue**	30	15	100
Mobility of holes	**Uh**	10	0.1	12.5
Donor Density	**Nd (cm^{-3})**	-	1E16	-
Acceptor Density	**Na (cm^{-3})**	1E17	-	1E17

3. RESULTS AND DISCUSSION

HH. **Thickness optimization**

The thickness of each layer plays very important role on the performance of PV cell. Increasing the thickness of absorber layer helps in absorbing more photons and producing current. The consequence of layer thickness on the performance of the PSC is presented in figure 1. The optimized value was obtained at 600nm for the perovskite layer. Further enhancing the thickness saw saturation and decline in performance because the thickness exceeds the carrier life time. Varying the thickness of HTL and ETL made negligible effect on the PSC structure so best thickness for both is selected as 100nm.

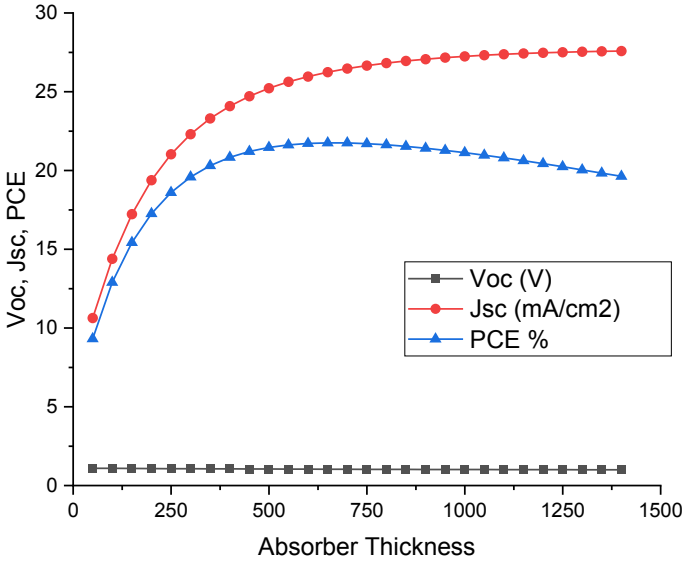

Fig 14 Optimized Thickness Curves

II. Doping Concentration Optimization

Doping concentration can be stated as the addition of charge bodies to a layer to get an improved result. The charge bodies may be of n-type charge carriers or p-type charge carriers. They help in increasing the electric potential of the cell and the current produced. For Perovskite and HTL layer the acceptor density (N_A) was varied while for ETL donor density (N_D) was varied.

It was found that the increase in doping concentration of perovskite layer resulted in enhancing the performance of the cell as can be seen in figure 2. The optimized doping concentration was found to be 1E17 cm^{-3}. Further doping reduces the cells performance because it changes the perovskites semiconductor nature to metallic. As both the charge transport layers are already highly conductive materials, increasing their doping concentration saw negligible effect on the performance of the PSC.

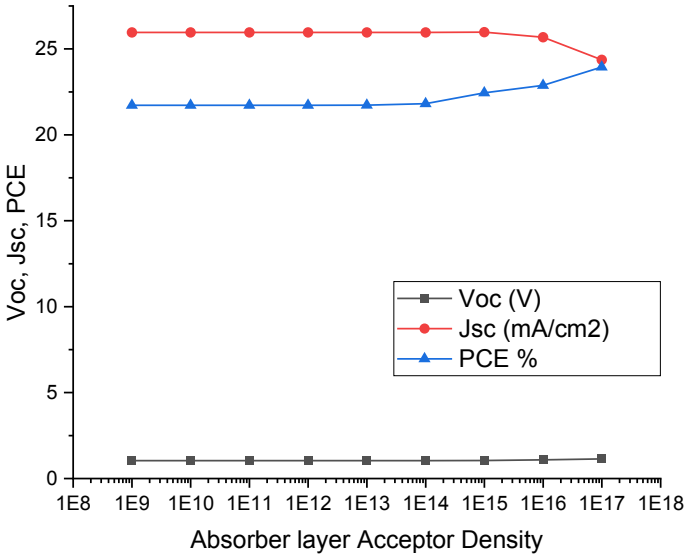

Fig 15 Optimized Doping Concentration Curves

JJ. Defect Density (N_T)

While modeling a solar cell it is necessary to add defect in the parameters to obtain results closer to experimental ones. Defect density are the trap states and defects in a material. High defect density indicated that the material has greater defects which will increase recombination and reduce PCE.

The effect of defect density on the performance of the PSC is presented in figure 3. From the results it can be seen that as the defects increase, the Jsc reduces drastically which I turn reduces the PCE. This is because the number of trap states increase in the cell which trap the charge carriers and increase recombination.

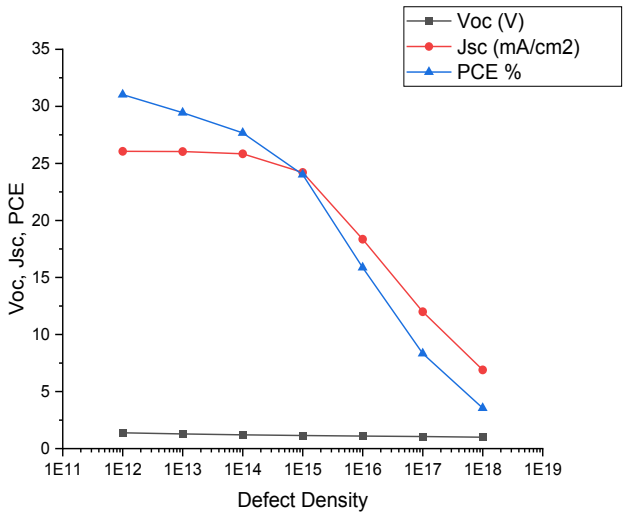

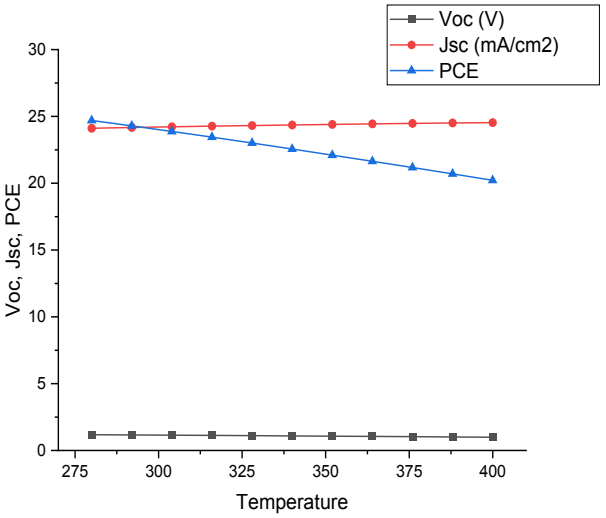

Fig 16 Effect of Defect density

Fig 17 Thermal Stability Curve

KK. Temperature

It is necessary to keep in mind the thermal stability behavior of a cell while modeling. The poor thermal stability not only results in bad performance of cell, but also causes structural degradation due to thermal stresses. Figure 4 shows the effect of temperature on the performance of the PSC. From the results it is clear that increasing the temperature reduces the Voc of the cell which in turn decreases the PCE.

4. CONCLUSION

In this work, a Hybrid organic-inorganic perovskite material $FAPbI_3$ was studied. The HOIP was modeled with a Kesterite compound as HTL and Zinc material as ETL. To enhance the performance of the cell, the thickness and doping concentration was optimized for each layer. It was found that the CTL optimization had no effect on the cell's performance, but the absorber optimization improved the performance of the cell drastically. After optimization PCE of 24 % was attained with Jsc of 24.271454 mA/cm2, Voc of 1.140949 V and fill factor of 86.65 %. It was also found that increasing the defect density and temperature reduced the PSC performance.

5. REFERENCES

[1] M. B. R. A. N. E. PezhmanDarvishzadeh, "Modeling the degradation/recovery of open-circuit voltage in perovskite and thin film solar cells," *Materials & Design,* vol. 114, pp. 339-344, 2017.

[2] T. M. ,. S. a. K. S. Takeo Oku, "Fabrication and Characterization of a Perovskite-Type Solar Cell with a Substrate Size of 70 mm," vol. 5, no. 4, 2015.

[3] N.-G. P. Hyun Suk Jung, "Perovskite Solar Cells: From Materials to Devices," vol. 11, no. 1, pp. 10-25, 2015.

[4] S. S. S. D. S. L. D. I. S. C. D. H. K. C. W. L. P. H. S. J. P. K. S. H. Dr. Dong Wook Kim, "BaSnO3 Perovskite Nanoparticles for High Efficiency Dye-Sensitized Solar Cells," *ChemSusChem,* vol. 6, no. 3, pp. 449-454, 2013.

[5] J. H. N. Y. C. K. W. S. Y. S. R. &. S. I. S. Nam Joong Jeon, "Solvent engineering for high-performance inorganic–organic hybrid perovskite solar cells," *Nature Materials,* pp. 897-903, 2015.

[6] D. H. S. S. H. I. Jin Hyuck Heo, "Planar CH3NH3PbBr3 Hybrid Solar Cells with 10.4% Power Conversion Efficiency, Fabricated by Controlled Crystallization in the Spin-Coating Process," *Advanced Materials,* 2015.

[7] Y. S. J. F. K. Farhad Fouladi Targhi, "MAPbI3 and FAPbI3 perovskites as solar cells: Case study on structural, electrical and optical properties," *Results in Physics,* vol. 10, pp. 616-627, 2018.

[8] F. B. A. S. S. B. B. M. S. Yousaf Hameed Khattak, "Numerical analysis guidelines for the design of efficient novel nip structures for perovskite solar cell," *Solar Energy,* vol. 207, pp. 579-591, 2020.

Indigenous Development of Low-Cost Electroluminescence Imaging Setup for Reliability Analysis of Photovoltaic Modules

Muhammad Noman[1]*, Muhammad Amir[1], Akif Ashraf Khan[1], Fahad Ullah Zafar[2], Umer Farooq[1], Muhammad Ali Kamran[1], Rizwan M. Gul[1]

[1]Mechanical Engineering Department, University of Engineering & Technology Peshawar, Pakistan

[2]Center for Advanced Studies in Energy, University of Engineering & Technology Peshawar, Pakistan
*Corresponding author: muhammad.noman9689@gmail.com

***Abstract*—**With the increasing use of photovoltaic (PV) modules, their reliability is a matter of keen interest for the research community as well as the manufacturers. Different techniques have been utilized for the reliability analysis of the PV modules which include the use of IV/PV curve tests, electroluminescence (EL), photoluminescence (PL), and infra-red (IR) imaging. Amongst them, EL imaging, which can effectively determine defective regions (inactive areas) in the modules, is a commonly used tool on the commercial level. This paper presents the development of a low-cost EL imaging setup for PV modules. A commercially available DSLR camera was modified into a specialized EL camera by using an IR filter. EL imaging was performed in a dark environment to avoid stray light from entering the testing area. The pre and post-processing of the images obtained by means of the setup were performed using MATLAB software. The development of the setup followed the use of standard operating conditions and international standard IEC 60904-13. The images obtained by the indigenously built setup were compared with those obtained by commercially available EL setup. The available EL setups in Pakistan are imported from abroad at high cost while this setup was developed using commercially available inexpensive components to make it economical, Furthermore, image analysis technique was applied on the EL images obtained through this setup. Cracks were detected manually as well as through image analysis in MATLAB.

Keywords: EL camera, Electroluminescence Imaging, Image Analysis, Low-cost EL Setup, Reliability Analysis.

1. INTRODUCTION

Recent research on PV module failure modes and degradation has revealed that even qualified and certified PV modules can fail or deteriorate before their projected life [1]-[2]. This is due to reliability issues, which include cell and module breakage, degradation issues, high voltage bias, delamination, and solder bond strength. These problems ought to be investigated to increase the reliability as well as the lifetime of PV modules [3]. Different techniques are used for the reliability analysis and quality inspection of PV modules such as Electroluminescence (EL), UV-Fluorescence, Photoluminescence (PL), and Infra-Red (IR) imaging. In these technologies, EL imaging is the most widely used, reliable and accurate for identifications of cracks and other defects. The reliability, durability, and performance of the PV modules output power are all affected by micro cracks, making the study and identification of these cracks extremely important [4].

Electroluminescence (EL) works on the principle of a light-emitting diode (LED) [5]; . Current is given to a solar cell and recombination of charge carriers causes light emission [6]. The radiations are sensed using a detector (EL camera), enabling us to evaluate the quality of solar cells. This paper presents the development of Indigenous and low-cost EL imaging setups according to IEC 60904-13 [7]. A CCD camera with a 950nm IR filter captures the IR radiation from the PV modules. EL images were then processed using MATLAB to extract useful data from the captured images [8]. Further details of the setup are presented below:

2. METHODOLOGY

LL. Electroluminescence Imaging

As discussed above, the setup was developed according to the IEC 60904-13 standard, using locally available components, resulting in a low-cost setup. The images were captured in a dark environment at standard temperature.

MM. Materials/Equipment Selection

An EL setup generally has the following components: A specialized camera with an IR filter and a camera lens; A DC power supply; and a dark studio environment. A camera tripod and module mount is also used for camera and module stability. Fig 1 shows the schematic diagram and the image of the EL setup components.

The first major component for the setup is the type of sensor used for capturing EL images. When the budget is constrained, the sensor selection is strictly restricted. Commercial solutions employed cutting-edge Indium Gallium Arsenide (InGaAs) sensors, which are quite costly as compared to other options available in the market. However, EL images can be acquired as long as the sensor's absorption spectrum and the module's emission spectrum overlap [9]. Generally, a Charged Couple Device (CCD) sensor is preferred over Complementary Metal Oxide Semiconductor (CMOS) sensor, because of its ability to capture high quality and low noise images. Although CMOS sensor have high capturing speed but it is more vulnerable to noise, so in this work, a CCD sensor was selected. A Nikon D3000 with a camera lens of 18-55 mm focal length range was used, as it provides high field of view in less working distance which is ideal for this type of compact setup.

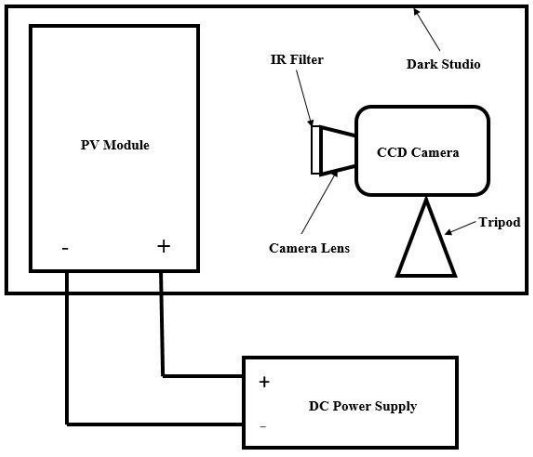

Fig 18. (a) Schematic Diagram of EL imaging setup (b) EL imaging setup

The power supply utilized to forward bias the PV module (30V and 10A) is capable of providing sufficient voltage to achieve short circuit current (I_{sc}) easily for the modules of power up to 150W. Since the IR spectrum of light is required in EL imaging and visible light must be excluded, a darkened environment is recommended for low noise and high quality EL images [9]. As a result, all EL imaging procedures are carried out in a dark room creating a dark studio environment and the temperature within this dark studio environment were kept between 20°C and 30°C.

NN. Camera Modifications

Camera sensors are equipped with an IR Cut/Blocking Filter to block out unwanted IR radiations. However, in the EL setups, IR radiations need to be collected but visible light must be blocked, therefore the IR Cut/Blocking Filter is removed from the CCD Sensor while an IR Filter with a wavelength of up to 950nm is installed on the lens to filter out visible light and allow only IR radiations.

Image Correction and Processing

Once the EL images were captured, there were some abnormalities, which include barrel distortion, in which rectangular features appear as curved barrel walls, and vignetting effect, in which the intensity of brightness falls at the image's periphery. Both abnormalities were corrected by adjusting the working distance between camera and module and capturing the module image in the center of the frame.

EL images were pre-processed before finalizing, in which stray light present in EL images and the module frame was removed/subtracted from the EL images using MATLAB image processing tool. For which two images are required; the first image is an EL image captured in a dark environment by providing the I_{sc} value mentioned on the back of the module in a temperature maintained between 20°C and 30°C, and the second image is a background image captured in the same condition with the same but unpowered module. The background image was then subtracted from the EL image as shown in Fig 2, resulting in the elimination of stray light and frames.

3. RESULTS AND DISCUSSION

A low cost electroluminescence imaging setup was developed from equipment available in market following standard IEC 60904-13. The EL imaging was performed with standard operating procedure including standard operating temperature, and dark studio/environment. The EL images were processed by different techniques to get pictorial information including image subtraction, barrel distortion and vignetting effect correction. The results are discussed below and shown in the Fig 2.

OO. Image Subtraction

Image subtraction is a technique used to remove noise present in EL image. In image subtraction, EL and background images were captured and imposed on each other to remove noise caused by stray light as shown in Fig 2. The image in the middle of Fig 2 represents the background image.

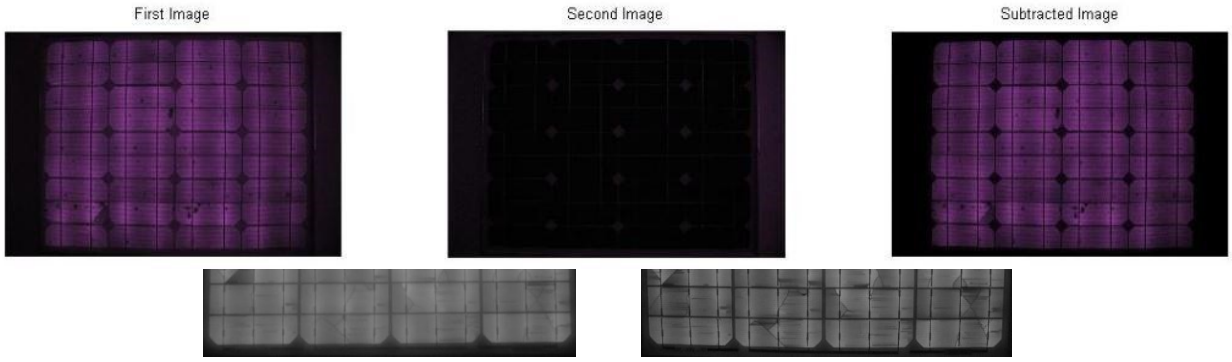

Fig 19. Image subtraction using MATLAB

PP. Comparison with Commercial setup

The EL images of the same modules are also captured from the commercial EL setup available at the PV Labs Pakistan to compare with the images from our developed EL setup, as shown in Fig 3 [10]. The result shows that our developed EL setup provides significantly clearer, sharper, brighter, and lower noise images than the commercial setup, indicating that our developed setup is not only more cost effective but is also more clear and accurate than the commercial setup.

QQ. Cracks Identification

EL images are best suited for the visualization of cracks (inactive areas) in photovoltaic modules. The cracks are easily identified in EL images as whenever there is a crack (or a defect), a difference in the color contrast on the image is seen. This difference in the contrast results from the cracked or defected region and thus providing the cracks [11]. Three modes of cracks are determined based on visual evaluation of EL images as shown in Fig 4. Mode A cracks are non-critical cracks that appear as a line defect in EL images. Because active cell areas are not destroyed or disconnected in these cracks, they do not cause cell power loss. Mode A fractures can occur in a variety of directions, including diagonal ±45, multiple directions, parallel and perpendicular to busbars [10]. The areas of the solar cell are partially electrically disconnected in Mode B cracks. High contrast regions in EL images produced with I_{sc} indicate these cracks. In Mode C types of cracks are the regions of the solar cell are completely damaged and electrically disconnected with other regions of the module circuit. These regions appear as dark (background noise only) in EL images produced with I_{sc} this mode of crack cause a significance power loss of the module. Mode C cracks are regions of the solar cell that are completely damaged and electrically

disconnected from the rest of the module circuit. In EL images obtained with I_{sc}, these regions appear as dark (background noise only). This mode of crack causes a significant power loss in the module [12]

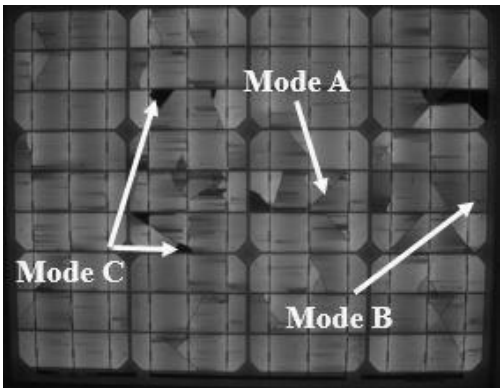

Fig 4. Modes of cracks in PV Module

4. CONCLUSION

EL imaging is a suitable method for the reliability analysis of PV modules. A low-cost EL setup was developed using the international standards. EL images of PV modules were captured in standard operating conditions and compared with commercially available setup. The results were comparable showing the reliable and better results of the developed setup while the cost of the setup was very low. For further image correction MATLAB image processing tool is used, which helps in visual identification of cracks and other defects also.

5. REFERENCES

[1] Sastry, O. S., Saurabh, S., Shil, S. K., Pant, P. C., Kumar, R., Kumar, A., & Bandopadhyay, B. (2010). Performance analysis of field exposed single crystalline silicon modules. *Solar energy materials and solar cells*, *94*(9), 1463-1468.

[2] Skoczek, A., Sample, T., & Dunlop, E. D. (2009). The results of performance measurements of field-aged crystalline silicon photovoltaic modules. *Progress in Photovoltaics: Research and applications*, *17*(4), 227-240.

[3] Dhere, N. G. (2005, January). Reliability of PV modules and balance-of-system components. In *Conference Record of the Thirty-first IEEE Photovoltaic Specialists Conference, 2005.* (pp. 1570-1576). IEEE.

[4] Muehleisen, W., Eder, G. C., Voronko, Y., Spielberger, M., Sonnleitner, H., Knoebl, K., ... & Hirschl, C. (2018). Outdoor detection and visualization of hailstorm damages of photovoltaic plants. *Renewable energy*, *118*, 138-145.

[5] Khramtchenkov, D. V., Bässler, H., & Arkhipov, V. I. (1996). A model of electroluminescence in organic double-layer light-emitting diodes. *Journal of applied physics*, *79*(12), 9283-9290.

[6] Zarrintaj, P., Vahabi, H., Saeb, M. R., & Mozafari, M. (2019). Application of polyaniline and its derivatives. In *Fundamentals and Emerging Applic ations of Polyaniline* (pp. 259-272). Elsevier.

[7] McCleland, J. C., Kwembur, I. M., Dix-Peek, R., Vorster, F., & van Dyk, E. E. (2019). Implementation of technical specifications to standardise and improve electroluminescence imaging test setups.

[8] Wu, J., Chan, E., Yadav, R., Gopalakrishna, H., & TamizhMani, G. (2018, September). Durability evaluation of PV modules using image processing tools. In *New Concepts in Solar and Thermal Radiation Conversion and Reliability* (Vol. 10759, pp. 141-156). SPIE.

[9] Nicholas Wilson. (July 2016). Low-cost Defect Detection of Solar Cells by Electroluminescence Imaging. *ENG470: Engineering Honors Thesis*

[10] Rizwan M. Gul, Muhammad Ali Kamran, Fahad Ullah Zafar, Muhammad Noman. (August 2020). The impact of static wind load on the mechanical integrity of different commercially available mono-crystalline photovoltaic modules. *Wiley*

[11] Rizwan M. Gul, Fahad Ullah Zafar, Muhammad Ali Kamran, Muhammad Noman. (October 2021). Effect of Wind Load on Performance of Photovoltaic (PV) Modules Available in Pakistan

[12] International Electrotechnical Commission (IEC) IEC 61215-2:2016 IEC 2016

Adsorption of methylene blue dye onto superabsorbent hydrogel: Synthesis, characterization, and isotherm analysis

Muhammad Umar[a], Hammad Amjad Khan[a], Sajjad Hussain[a], Muhammad Younas[b]
[a] Department of Chemical Engineering, Ghulam Ishaq Khan Institute of Engineering Sciences and Technology, Topi, Khyber Pakhtunkhwa.
[b] Department of Chemical Engineering, University of Engineering and Technology, Peshawar.

Abstract - The use of polysaccharide-based hydrogels in environmental applications is of great advantage, as they enable the removal of various noxious pollutants from the water system. An appreciable adsorption capacity towards Methylene blue (MB) was demonstrated by the development of a novel superadsorbent hydrogel synthesized by suspension polymerization technique. Maximum adsorption capacity achieved was 228 mg. g^{-1} for MB dye. The SEM images showed that grafting of itaconic acid and acrylamide onto sodium alginate backbone increased the water permeation due to the coarser and undulant surface. In conclusion, the results of the current study indicate that the synthesized superadsorbent hydrogel may be used as an efficient adsorbent for the removal of MB dye from aqueous solutions.

HIGHLIGHTS:

- **SAH WAS SYNTHESIZED BY GRAFT-COPOLYMERIZATION REACTION USING APS AND NMBA AS AN INITIATOR AND CROSSLINKER**
- **SA-G-POLY (AAM-*CO*-IA) HYDROGEL SHOWED MAXIMUM ADSORPTION CAPACITY OF 228 MG. G^{-1}.**

1. INTRODUCTION

A major category of textile dyes consists of organic dyes used in textile industries that are considered as carcinogenic. Water systems are exposed to dyestuffs with intense color and toxicity during dye production and textile manufacturing. Modern textile dyes are very stable and contain a high concentration of organics, which makes conventional treatment methods ineffective for decolorizing and destroying them [1]. In response, other effective methods were investigated. The adsorption technique has gained widespread interest due to its low cost, simplicity, and efficiency in comparison with other methods of removing dye compounds [2].
The industrial world and scientific community have shown significant interest and rapid progress since the introduction of a new concept "superadsorbent polymer" in the 1950s. Using superadsorbent hydrogels (SAHs), which are generally 3D hydrophilic networks of polymer chains, aqueous solutions can be absorbed, swelled, and retained for hundreds of times the amount of their dry weight while preserving the structural integrity of the gel [3]. Hydrogel chains contain carboxylates, amino acids, amides, hydroxyls, and sulfonic which are hydrophilic groups responsible for high swelling. The primary forces that hold together SAHs are covalent and ionic bonds, and the secondary forces are hydrogen bonds and hydrophobic interactions [4]. Since SAHs are water-loving, they are useful for agriculture, personal hygiene, building and construction, drug delivery, water purification, and in biomedical applications [5].
Synthetic SAHs are increasingly being replaced with "greener" alternatives due to their poor degradability and biocompatibility. The majority of them were used as disposable goods, which may pollute the environment. Thus, biocompatible, biodegradable, nontoxic, and renewable SAHs are needed for applications. In recent years, renewable and biodegradable polymers have gained much more attention due to their low production costs and abundant resources. A variety of natural polymers such as starch [6], cellulose [7], chitosan [8], konjac glucomannan [9], and xyloglucan [10] are synthesized recently from [11], raw bran [12, 13] and tulips [14].
Despite their limitations in reactivity and processibility, naturally abundant polymers have nevertheless been modified through cross-linking, blending with synthetic polymers, functionalizing by adding reactive groups, etc., in order to meet the specific needs of scientists and industrialists.
Sodium alginate (SA) is a highly branched and heterogeneous natural polysaccharide composed of molecular structures of mannuronate (M) and guluronate (G) [15]. Despite its limited application in drug delivery, wound dressing, food, textile, and biomedicine industries, poly (SA) hydrogels are fragile and dimensionally unstable in water medium, which makes them unsuitable for diverse prospective applications [16, 17]. Therefore, nowadays, most research focuses on synthesizing cheap semisynthetic sustainable hydrogels that are environment friendly and contain both natural and synthetic components, where synthetic components provide structural integrity, while natural components provide biodegradability and biocompatibility. A grafting approach with naturally abundant SA within synthetic polymer was used to improve the functionalities, branching, flexibility, structural integrity, biodegradability, and reusability of the polymer [18]. Several studies have been conducted on the chemical modification of SA with grafting in the past [18]. To date, no studies have examined the grafting of itaconic acid (IA) and acrylamide onto SA.
A hydrogel containing itaconic acid (IA) or containing itaconate units appear to be superior for adsorption. The synthesis of polymers containing itaconate is not only limited to their structure, but also their greater solubility in water. It normally increases the degree of swelling in hydrogels. By properly crosslinking copolymer units, a proficient network is formed for water absorption [19]. It has been shown that IA hydrogels and their esters are highly effective at adsorbing metal ions. Researchers have found that itaconic acid-containing hydrogels can

efficiently adsorb Cd^{2+}, Pb^{2+}, Zn^{2+} and Cu^{2+} ions [20]. Due to the elevated number of itaconate units, this data strongly supports their use, particularly for recovering dye from contaminated water.

Acrylamide, however, is a synthetic polymer that retains its hydrophilic nature when crosslinked and can absorb a large amount of water. Acrylamide hydrogels offer the advantages of chemical inertness, transparency, and stability over a wide range of pH, temperature, and ionic forces. A recent study has revealed that polyacrylamide hydrogels possess suitable mechanical and physical properties, including tension resistance, adequate elongation, and swelling capacity that is suitable for various applications [4].

Therefore, in this study, we have synthesized a novel and simple SAH by using minimum and low-cost precursors such as sodium alginate, itaconic acid, and acrylamide. This was achieved through facile suspension polymerization method. Due to their non-toxic nature, these can be considered environmentally friendly. The prepared SAHs were characterized by scanning electron microscope to examine the surface morphology.

2. Material and method

Chemicals and reagents

All chemicals used such as sodium alginate (C6H9NaO7), Itaconic acid (C5H6O4), acrylamide (C3H5NO), N, N′-methylene bis-acrylamide ((CH2CHCONH)2CH2), Ammonium per sulfate ((NH4)2S2O8), Methylene blue (C16H18ClN3S) dye, were of analytical grade, purchased from Merck, Sigma Aldrich and Daesung and used without any pre-treatment

Preparation of superadsorbent hydrogel

Fig. 1 shows the protocol for the synthesis of SAH. In brief, ammonium per sulfate solution will be added to the already homogenized solution of sodium alginate and stirred at 60 °C for 15 mins. Afterwards, a known amount of itaconic acid, acrylamide, and NMBA will be added to the above mixture and stirred for 1 hr at a fixed temperature of 60 °C. This will lead to the gel formation and let the gel cool at ambient temperature. It will be then dried in an air oven for 24 hrs.

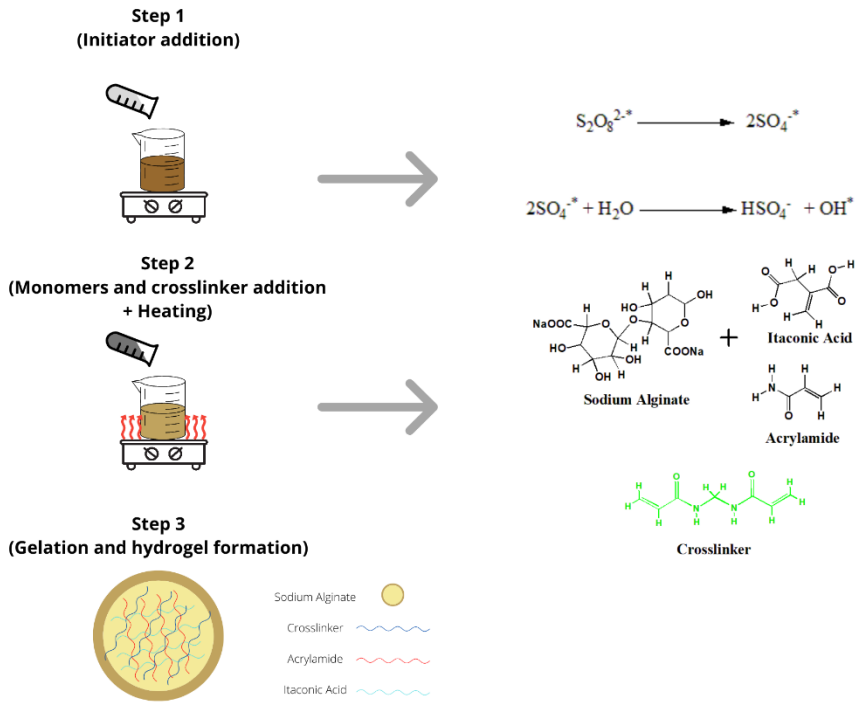

Fig. 1- *Synthesis of superadsorbent hydrogel by suspension polymerization method*

3. Results and discussion

Scanning electron microscopy (SEM)

SEM analysis was carried out to analyze the surface morphology of synthesized SAHs. Fig. a and b show the SEM micrographs of SA and SA-g-Poly(AAm-co-IA), respectively. Fig. a demonstrate the morphology of SA, which showed big rock like shape with a gradually smooth surface. However, SA-g-Poly(AAm-co-IA) hydrogel displayed a rough and undulant surface (Fig. b). It is generally believed that such coarser and undulant surface facilitates the penetration of water into polymeric networks, thus improving their capacity for water absorption [21]. Some pores were also evident at different locations which are the regions for permeation of water and provide active sites for interaction of water with the hydrophilic groups of the prepared hydrogels.

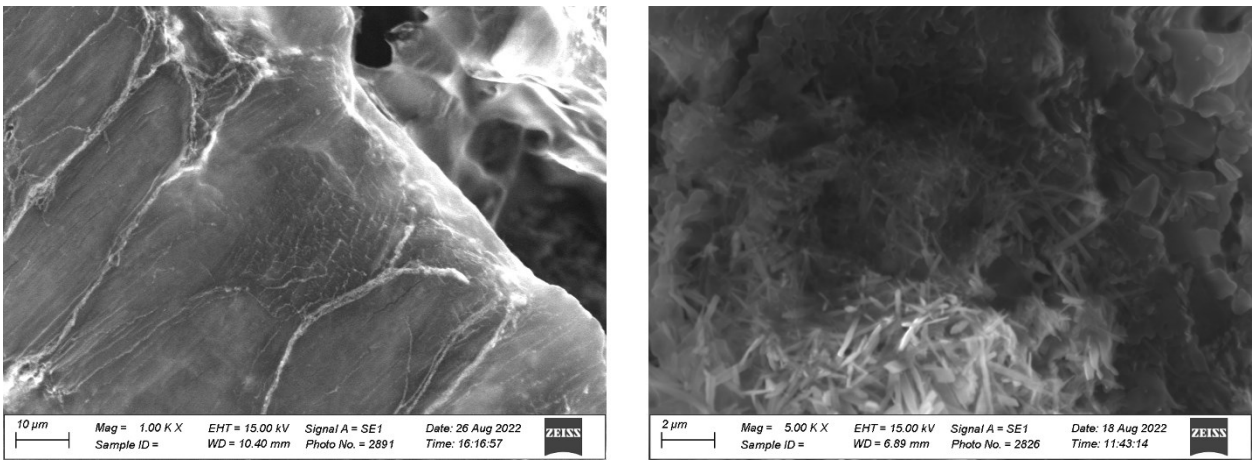

Fig. 2- SEM micrographs of **a)-** SA, **b)-** SA-g-Poly (AAm-co-IA)

Adsorption of dye

At first, an absorbance plot was used to determine dye adsorption. To conduct this study, 50 mg. L^{-1} of MB dye solution containing 10 mg SAH was stirred in a beaker for 60 minutes at room temperature. Based on **Error! Reference source not found.**, with the lapse of time, the relative concentration (C/C_o) decreased significantly, indicating that the dye had successfully adsorb on the surface. On the other hand, the adsorption capacity of 228 mg. g^{-1} was observed. As a result, this paved the way for the MB dye adsorption activity of the SAH.

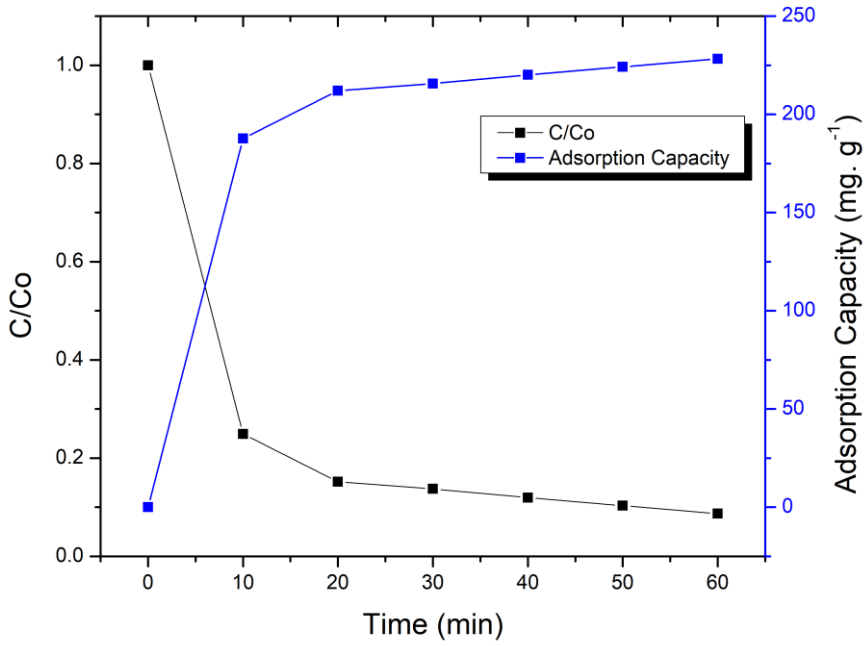

Fig. 3 *Relative concentration (C/Co) and adsorption capacity of MB dye onto SAH at various time intervals*

4. CONCLUSIONS

SA-g-Poly (AAm-co-IA) hydrogels were synthesized by graft copolymerization and were used as adsorbents for MB dye. The maximum adsorption capacity for MB dye was 228 mg. g-1. The SEM images showed that grafting of both monomers onto sodium alginate backbone increased the water permeation due to the coarser and undulant surface. In conclusion, SA-g-Poly (AAm-co-IA) hydrogel shows superb MB dye adsorption and is an excellent adsorbent for textile wastewater.

5. REFERENCES

1. Fu, F. and Q. Wang, *Removal of heavy metal ions from wastewaters: a review.* Journal of environmental management, 2011. **92**(3): p. 407-418.
2. Liu, P., et al., *Synthesis of covalently crosslinked attapulgite/poly (acrylic acid-co-acrylamide) nanocomposite hydrogels and their evaluation as adsorbent for heavy metal ions.* Journal of Industrial and Engineering Chemistry, 2015. **23**: p. 188-193.
3. Li, D., et al., *Double‐Helix Structure in Carrageenan–Metal Hydrogels: A General Approach to Porous Metal Sulfides/Carbon Aerogels with Excellent Sodium‐Ion Storage.* Angewandte Chemie International Edition, 2016. **55**(51): p. 15925-15928.
4. Baigorria, E., J.A. Galhardi, and L.F. Fraceto, *Trends in polymers networks applied to the removal of aqueous pollutants: A review.* Journal of Cleaner Production, 2021. **295**: p. 126451.
5. Darban, Z., et al., *Hydrogel-Based Adsorbent Material for the Effective Removal of Heavy Metals from Wastewater: A Comprehensive Review.* Gels, 2022. **8**(5): p. 263.
6. Motamedi, E., et al., *Synthesis and swelling behavior of environmentally friendly starch-based superabsorbent hydrogels reinforced with natural char nano/micro particles.* Journal of Environmental Chemical Engineering, 2020. **8**(1): p. 103583.
7. Huang, S., et al., *Facile preparation of biomass lignin-based hydroxyethyl cellulose super-absorbent hydrogel for dye pollutant removal.* International journal of biological macromolecules, 2019. **137**: p. 939-947.
8. Rinaudo, M., *Chitin and chitosan: Properties and applications.* Progress in polymer science, 2006. **31**(7): p. 603-632.
9. Wu, J., X. Deng, and X. Lin, *Swelling characteristics of konjac glucomannan superabsobent synthesized by radiation-induced graft copolymerization.* Radiation Physics and Chemistry, 2013. **83**: p. 90-97.
10. Mukerabigwi, J.F., et al., *Synthesis and properties of a novel ecofriendly superabsorbent hydrogel nanocomposite based on xyloglucan-graft-poly (acrylic acid)/diatomite.* RSC advances, 2015. **5**(102): p. 83732-83742.
11. Cheng, B., et al., *Advances in chitosan-based superabsorbent hydrogels.* Rsc Advances, 2017. **7**(67): p. 42036-42046.
12. Gao, J., et al., *Preparation and properties of novel eco-friendly superabsorbent composites based on raw wheat bran and clays.* Applied Clay Science, 2016. **132**: p. 739-747.
13. Ahmad, M., et al., *Biochar as a sorbent for contaminant management in soil and water: a review.* Chemosphere, 2014. **99**: p. 19-33.
14. Kollár, J., et al., *Tulips: a renewable source of monomer for superabsorbent hydrogels.* Macromolecules, 2016. **49**(11): p. 4047-4056.
15. Vásquez, A., S. Domínguez, and L.L. Dos Santos, *α-TCP cements prepared by syringe-foaming: Influence of Na2HPO4 and surfactant concentration.* Materials Science and Engineering: C, 2017. **81**: p. 148-155.
16. Lee, K.Y., *DJM (2012). Alginate: properties and biomedical applications.* Prog. Polym. Sci. **37**: p. 106-126.

17. Rocher, V., et al., *Dye removal from aqueous solution by magnetic alginate beads crosslinked with epichlorohydrin.* Journal of hazardous materials, 2010. **178**(1-3): p. 434-439.
18. Mohamadnia, Z., et al., *Ionically cross-linked carrageenan-alginate hydrogel beads.* Journal of Biomaterials Science, Polymer Edition, 2008. **19**(1): p. 47-59.
19. Karadağ, E., D. Saraydın, and O. Güven, *Radiation induced superabsorbent hydrogels. Acrylamide/itaconic acid copolymers.* Macromolecular Materials and Engineering, 2001. **286**(1): p. 34-42.
20. Soto, D., et al., *Itaconic acid grafted starch hydrogels as metal remover: Capacity, selectivity and adsorption kinetics.* Journal of Polymers and the Environment, 2016. **24**(4): p. 343-355.
21. Bao, Y., J. Ma, and N. Li, *Synthesis and swelling behaviors of sodium carboxymethyl cellulose-g-poly (AA-co-AM-co-AMPS)/MMT superabsorbent hydrogel.* Carbohydrate Polymers, 2011. **84**(1): p. 76-82.

Investigating the co-combustion characteristics of local low rank coal with Organic waste

Rovaid Khan[A], Muddasar Habib[A,*]

[A] Chemical Engineering Department, University of Engineering & Technology, Peshawar, Pakistan

Abstract- Olive waste is reflected as one of the proficient renewable energy source to replace fossil fuel and to reduce greenhouse gas emissions. Organic Olive waste and low grade coal co-combustion is a useful way to reduce energy crisis as well as to lessen the pollutant emissions. In this work proximate and ultimate analysis of low grade pure local coal, pure organic waste and their blends has been performed. The samples contained local low grade coal and olive waste and their blends having compositions of 10%, 20% and 30% .Proximate and ultimate analysis are performed and then comparison of different properties including volatile matter, fixed carbon, moisture content, ash contents, and gross calorific values are studied. Gross Calorific values of pure coals and their blends are determined using ASTM standard by using bomb calorimeter. It is concluded after experimental work that by increasing olive waste percentages, the calorific value of blended coal found increased. It was also concluded that 30% increase in the biomass content in the fuel blend would reduce cost 0f blended fuel up to 25 %.

Keywords: Organic waste, co-combustion, blended fuel, Ultimate analysis, combustion efficiency, bio mass, alternative fuel.

1. INTRODUCTION

As government of Pakistan has imposed new environmental guidelines of fossil fuels which have increase consideration to use organic waste to produce energy. Therefore Co-combustion is a choice and cost effective method to utilize biomass and wastes by power and process industry [1].Also Co firing organic waste with coal decrease net CO2 emissions from power plants and process industry. Among available energy source coal is most plentiful but produce greenhouse emission, its image can be improved by co-firing it with organic waste. Biomass helps the atmospheric carbon dioxide recycling and does not contribute to the greenhouse effect. Biomass consumes the same amount of CO2 from the atmosphere during growth as is released during combustion [2].

Combustion of biomass directly is the aged approach of utilizing biomass for energy generation. Bio waste thermo-chemical switch technologies such as paralysis and gasification

are not the mainly significant options at present; combustion is accountable for over 96% of Bio energy generation in the world [3]. The processes like gasification, paralysis, anaerobic digestion and alcohol production are far and wide used to obtain energy from Bio waste. Biomass can be directly fire into boilers but co-combustion of biomass and coal has economical, environmental and technical benefits over other available options. Single combustion of coal produces more emissions as compared to co-combustion of coal with bio waste [4].

Biomass ranks fourth as an energy resource worldwide and providing about15% of the energy requirements to the world. Biomass are wood, wastes from agricultural, bagasse, industrial residues, Olive waste, waste paper, municipal solid waste, sawdust, grass wastes, kitchen waste and Animal wastes [5]. Gross calorific value of Olive waste is greater as comparable to other organic waste therefore; it is more suitable to use olive waste with local low grade coal as a blended fuel to enhance image of low grade coal. GCV comparison is given in the below graph [6].

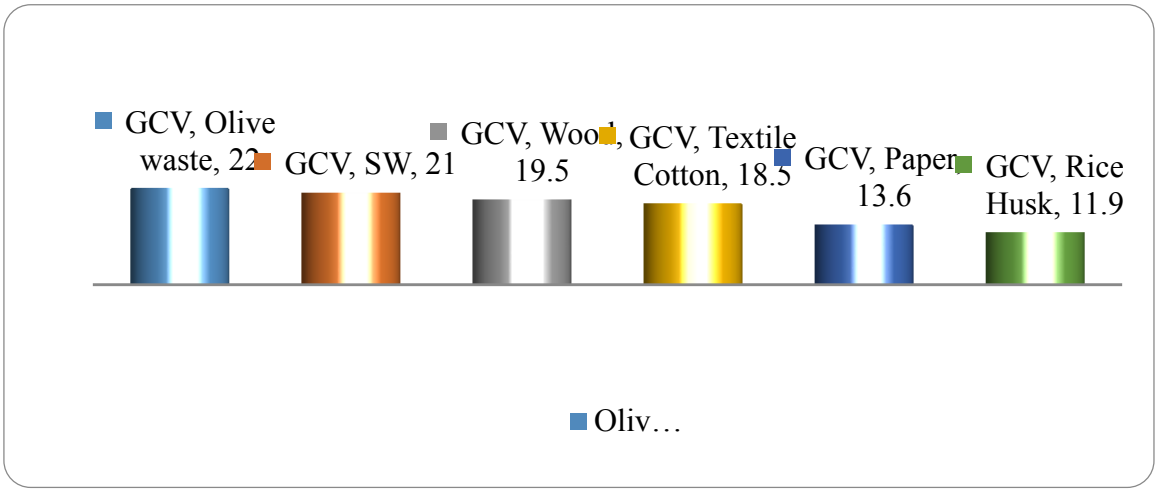

Fig 1 GCV comparison of Olive waste with other waste

Physical and Chemical characteristics of olive waste obtained for the four fractions about proximate analysis chemical analysis, ash composition and melting temperatures are given in the table 1.

Table 1: Physical and Chemical characteristics of olive waste

	Pit	Pulp	Residual Olive cake	COMWW
Ultimate Analysis (% dry basis)				
Carbon	52.270	55.205	54.895	50.075
Hydrogen	7.485	7.960	8.215	7.795
Nitrogen	0.060	1.995	2.220	2.125
Oxygen	40.097	34.042	34.386	39.752
Sulfur	<0.1	<0.1	<0.1	<0.1
Chlorine	0.088	0.798	0.284	0.253
Proximate Analysis (% dry basis)				
Volatile	80.94	79.10	77.77	69.29
Ash	0.56	5.60	4.31	18.82
Fixed Carbon	18.50	15.30	17.92	11.89
Moisture (% wet basis)	9-10	6-6.5	5.5-6	70-73
Chemical Analysis (% dry-extractive free basis)				
Cellulose	18.6	12.1	12.4	0.6
Hemicellulose	25.1	12.2	14.4	0.6
Lignin	39.3	43.3	42.8	51.3
Higher heating value (MJ/kg, dry basis)	20.61	23.39	22.42	21.36
Higher heating value (MJ/kg, dry-ash free basis)	20.70	24.35	23.27	26.29
Lower heating value (MJ/kg, dry basis)	18.96	21.64	20.61	19.64

2. METHODOLOGY

A. Raw material and sampling

Olive waste and local Pakistani coal is used as a raw material for experimentations. Olive waste is collected from Sardaryab farmhouse (District Charsada, Khyber Pukhtunkwa) and is blended with local Pakistani low grade coal. Local Pakistani low grade coal is provided by Bestway Cement Limited Farooqia plant.

Fig 2 Local low grade coal

Fig 3 Local low grade coal

B. Experimental set up

Bomb calorimeter, X Ray Spectrometer and are used for experimental work. Also Both Proximate and ultimate analysis is carried out for experimentation as per ASTM standard.

The Bomb Calorimeter is used to measure the gross calorific value of the samples. Bomb calorimeters are designed such t that they can endure the enormous pressure created within the calorimeter due to the combustion. The heating filament is made up of tungsten materials. In this method, I gm of the sample is taken in the crucible and is electrically ignited to burn in the presence of pure oxygen. During the combustion, heat is released which increases the temperature and this rise in temperature is measured.

Fig 4 Bomb Calorimeter for calculating gross calorific value (GCV)

3. RESULTS AND DISCUSSION

Both proximate and ultimate analysis are carried out and results obtained are given in the below table. Olive waste is collected from Sardaryab farmhouse (DisttCharsadda,kpk) and Local Pakistani low quality coal is provided by Bestway Cement Farooqia plant.

In this study Olive waste and Pakistani coal are used, both are Pakistani origin. Olive waste is collected as by product from Olive mill located in district Charsada, KPK. In sample preparation, bio mass were first air dried samples in open air for several days. The air dried sample were milled with shredder and then sieved to pass through screen having opening of 250 micron. The sample was kept in a air tight samples bottle to avoid more interaction with air. The proximate and ultimate analysis analysis are carried out according to ASTM standards. Gross calorific value was calculated using bomb calorimeter. Blend of coal and waste is prepared and analyzed in term of both proximate and ultimate analysis, and the parameters which are mainly focused are GCV, Ash, moisture, fixed carbon, volatile, Carbon, and hydrogen, Nitrogen, Oxygen and Sulfur.

A. Local coal vs blended fuel GCV comparison

Different Blend of Olive waste and local Coal were investigated having Olive waste ratio of (10, 20 and 30 % weight).It is showed that by increasing Olive waste waste ratio, the GCV value of blended fuel increased as shown in the below graph.

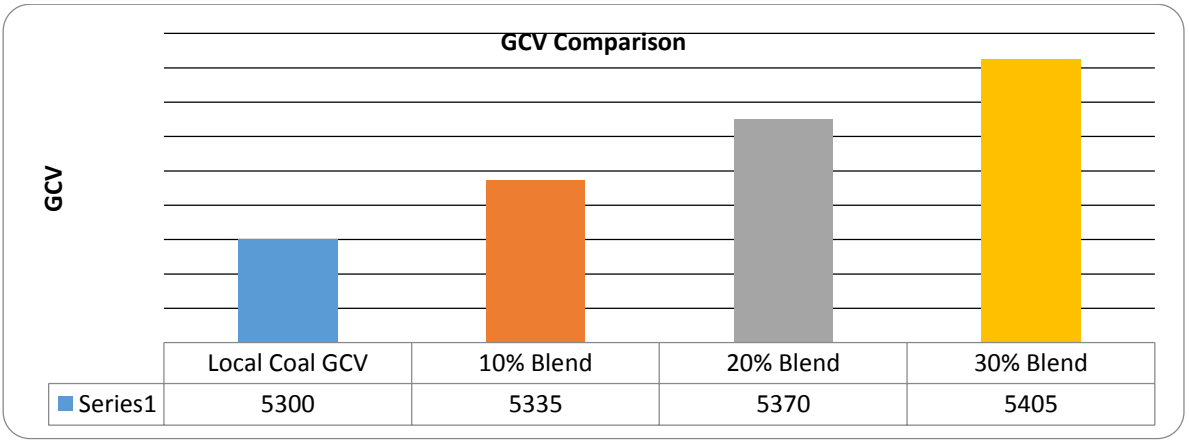

Fig 5 Local coal VS Blended fuel GCV comparison

B. Local coal vs blended fuel sulfur comparison

Local coal and blended fuel sulfur is compared as shown in the below table. It shows that blended fuel sulfur is reduced with increasing percentages of Olive waste.

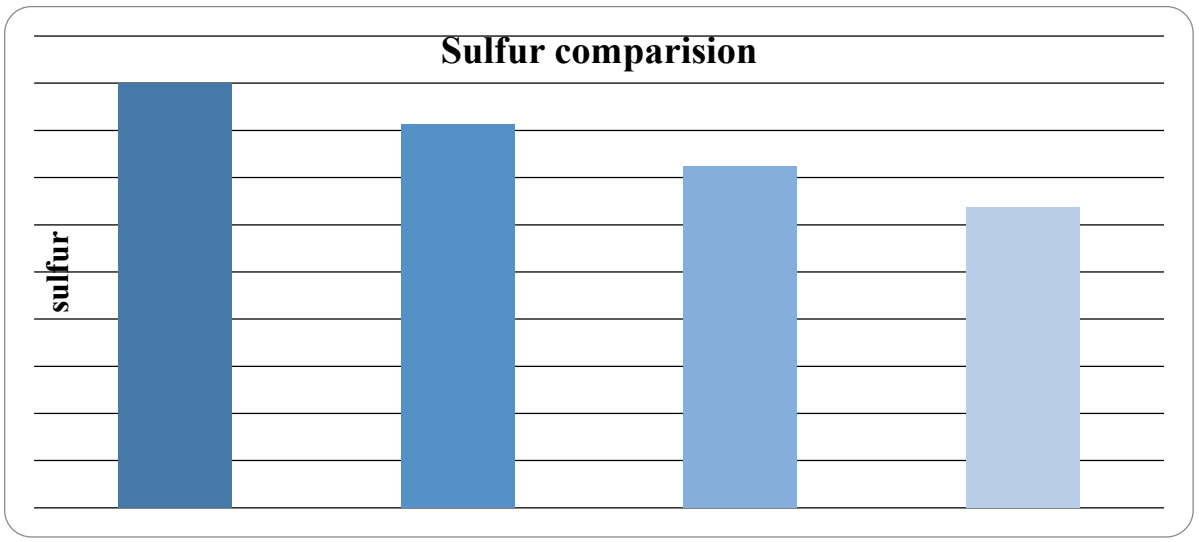

Fig 6 Local coal VS Blended fuel sulfur comparison

C. Cost comparison of local coal vs blended fuel

As the coal prices is increasing bot in Pakistan as well as in the world, which is the power sector and specially cement sector in *Pakistan* which is under stark pressure due to increased fuel cost. In Pakistan the cement sector imported around eight million tons of coal every year to meet the domestic demand for cement. Hence the use of bio mass will decrease the fuel cost of power sector as well as process industries.
In this study, different Blend of Olive waste and local Coal was investigated having Olive waste ratio of (10, 20 and 30 % weight). It is also showed that by increasing Olive waste ratio up to 30%, the cost of blended fuel decreased up to 25 %.

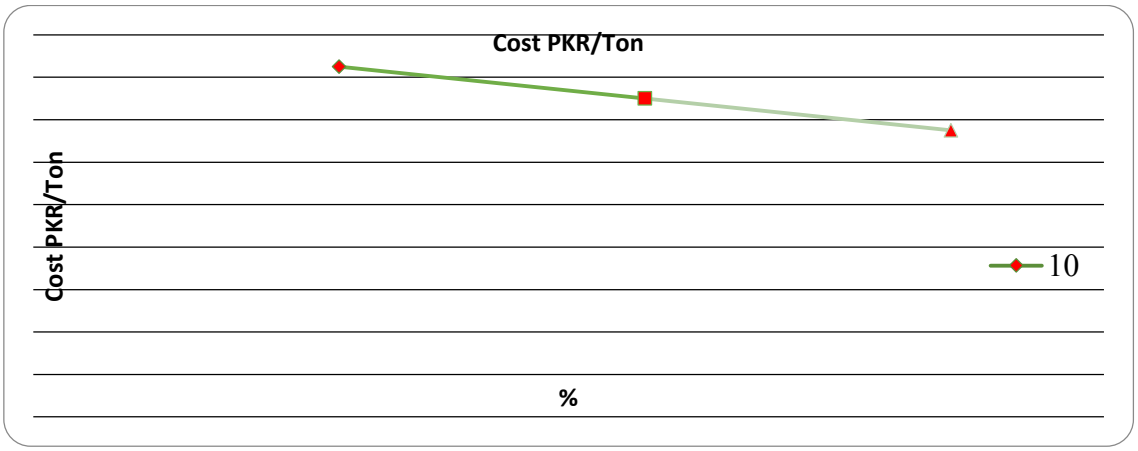

Fig 7 Cost comparison of local coal VS blended fuel

It is clear from the above graph that by increasing olive waste percentages with coal is decreasing fuel coast per ton.

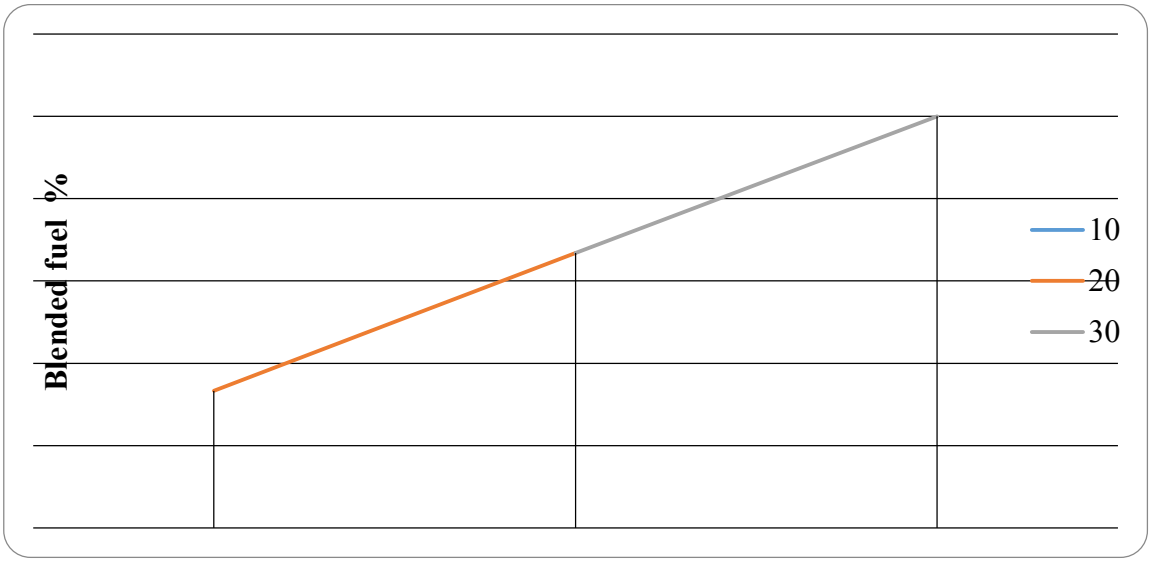

Fig 8 Cost comparisons of local Coal VS blended fuel

It is showed that by increasing blended fuel percentages up to 30 %, the fuel cost is decreased up to 25 %.

4. CONCLUSSION

This experimental study confirm that gross calorific value of Olive waste is greater as compared to other available organic waste in Pakistan and is a good choice to enhance the image of low grade local coal by co combustion of olive waste with low grade coal. It is found that by increasing olive waste percentages up to 30% in a blended fuel the gross calorific value found increased up to 6% which have reduced fuel cost of blended fuel up to 25 %.

5. REFERENCES

[1] Laboratory of Physical Metallurgy, School of Mining and Metallurgical Engineering,

[2] National Technical University of Athens (NTUA), Heroon Polytechniou 9, 15780 Zografou, Greece.

[3] Laboratory of Mineralogy, Petrology and Economic Geology, School of Mining and Metallurgical Engineering, National Technical University of Athens (NTUA), Heroon Polytechniou 9, 15780 Zografou, Greece 2017.

[4] Alkhamis TM, Kablan MM. Energy 1999;24:873.

[5] Topal H, Atimtay AT, Durmaz A. Fuel 2003;82:1049

[6] Cliffe KR, Patumsawad S. Waste Mgmt 2001;21:49.

Current practice for handling the waste lubricating oil in Pakistan, is there any improvement possible in the treatment processes, and a proposed procedure for the disposal of produced sludge

[1]Muhammad Hamza Naeem [A], Naseer Ahmed Khan*[B], and Syed Naveed Ul Hasan[C]
Email of Presenter[1]: mhamzanaeem.che@uetpeshawar.edu.pk
Corresponding author*: naseerahmedkhan@uetpeshawar.edu.pk
[A B C] University of Engineering & Technology Peshawar

Abstract

We all know that the vehicles changes oil after a certain kilometers of travelling. Collected waste oil are valuable and ideally most of it should be regenerated. In Pakistan there are a numbers of oil cleaning businesses but unfortunately almost all are reluctant to disclose their cleaning methodology. The main reason for hiding the cleaning process is because of tough governmental regulations. Usually, after heating the waste oil for few hours sulphuric acid is added slowly to remove oxidized hydrocarbons (darkish part). The sludge generated is the main environmental hazard and because this problem this simple acid cleaning process was banned in European countries. The generated sludge contains heavy metals and many other kinds of hydrogenated viscous species.

Few simple experiments were conducted to propose an alternative cleaning methodology. In short, the oil was heated till the knocking sound disappeared. After that at a room temperature the dehydrated oil was treated with the glacial acetic acid (instead of sulphuric acid) and was properly mixed for an hour. A settling time of 24 hours is provided after which reddish brownish (top) and black (bottom) layers are formed. The collected upper layer was then treated with fuller earth (Multani meti) under continuous stirring. Finally, after cooling to a room temperature the oil was filtered to a reasonably clean engine oil. This cleaning process recovers about 53.2% of the engine oil. At least theoretically the collected sludge containing acetic acid is biodegradable.

The collected sludge from both types of acid treatment was mixed with cement to prepare concrete roadblocks. The bricks were hard and had sealant property.

Key words: Used engine oil, acid cleaning, and sludge bricks.

1. INTRODUCTION

This Lubricating oil is the most important fraction of petroleum refinery and is used in almost all vehicles and machines [1] (Akilimali, 2017). Lubrication oils are used to promote the easier motion of moving parts by providing a protective layer on the metal surface. These oils also remove the heat produced due to frictional forces between metal surfaces [2] (Aljabiri, 2018). These oils are usually blended with several chemical additives to improve its lifetime and performance under sever operation conditions. However, with the passage of time the oil losses lubrication efficiency due to physical and chemical changes [3] (Alves dos Reis, 1991). These physical and chemical changes occur due to their

contamination by metals, ash, carbon residue, varnishes, water, gums, and asphaltic compounds that results out of bearing surfaces of the engine [4] (Anisuzzaman, Jumaidi, & Nasir, 2021). So, after some time the lubrication oil is needed to be replaced [5] (Audibert, 2011). The replaced oil is a waste and is called used/waste engine oil. The discarding of used lubricating oil is becoming a critical issue. This discarding of used black oil has been the reason for the mutilation of environment because of it being disposed off into the ground and water. That is the major reason of the water and soil getting polluted [6] (KAITHARI & AL-RIYAMI). A large number of valuable hydrocarbons are lost because of the discarding of black oil or waste engine oil [7,8] (Mekonnen & Ababa, 2014),(Oladimeji, Sonibare, Omoleye, Emetere, & Elehinafe, 2018). Mobil oil has great importance and value because it keeps the car engine performance at its maximum which is very important for the cars as they are a necessity in modern day existence. According to the different kinds of car engine in market there are many varieties of lubricating oil available. Mobil oil cancels the friction, wear and heating of engine parts by not letting the surfaces of moving parts contact each other [9] (Olugboji). Mobil oil also prevents corrosion, keeps certain parts of the engine cool, and cleans certain engine components don't let clogs appear as well as seal all the feasible clearances. Structural changes occur in the oil (Mobil) the reason being some external particles like dust, sand, fuel, coolant, moisture and acids. Structural changes also occur because of some components which occur internally such as soot, exhaust gases, metallic particles. These changes are the real reason behind the engine oil getting polluted. After getting polluted its properties also undergo changes that unable the lubricating oil to perform at its ideal limit [10] (Osman, Attia, & Taman, 2018). Not only it loses its ability to keep the engine at its maximum performance besides it emerges as a fatal pollutant for the environment because of its wrong discarding. This led to the apprehension that black oil is a dangerous waste which needs exceptional management policy. Many cleaning and recycling methods are being applied now to diminish its effects on environment after unusual dumping which will also help in less economic losses [11] (Pal & Nayak, 2017). Engineers tried to find worthy solutions for the cleaning of black waste oil to protect the environment and prevent the valuable loss of precious hydrocarbons. Price of the lubricating oil will also fall and decrease when the cleaning methods will be applied as well as it will have a greatrefreshing effect on environment. Acid & Clay treatment method is used to clean the waste oil but instead of sulfuric glacial acid acetic acid is used because it addresses two important problems, 1) Glacial acetic acid is organic

so it does not affect the environment 2) The sludge which is produced by this method is not harmful to the environment because of the glacial acetic acid.

2. METHODOLOGY

Three different samples of used engine oils are collected. A mixed solution of all the sample is made by mixing them. Five beakers are filled up to 100 ml. These beakers were heated at 250 °C for one hour to evaporate water and remove volatile components. These beakers were then cooled down to room temperature. The dehydrated oil was mixed with different volumes of glacial acetic acid that is 0.5 ml, 1 ml, 1.5 ml, 2 ml and 2.5 ml in the first, second, third, fourth, and fifth beaker, respectively and stirred for one hour. The mixtures were left for 24 hours at room temperature. After sedimentation the top layer was separated from that of the bottom sludge. The top layer was placed in centrifuge for one hour, which separates base oil from contaminants. In the centrifuged mixture again two layers were formed, the top reddish layer and the bottom sludge. The top reddish layer was separated in other beakers and the bottom sludge was weighed. The top layer oil was mixed with fuller earth in a ratio of 1gm per 2.5ml oil with continuous stirring and heating up to 250 °C. The fuller treated oil was again centrifuged to collect a top almost cleared oil which was then filtered to obtain clean engine oil.

3. RESULTS

After experimentation it showed that of Acid and Clay Method has more or less same kinematic viscosity as well as density as fresh oil as shown in below figure 1&2.

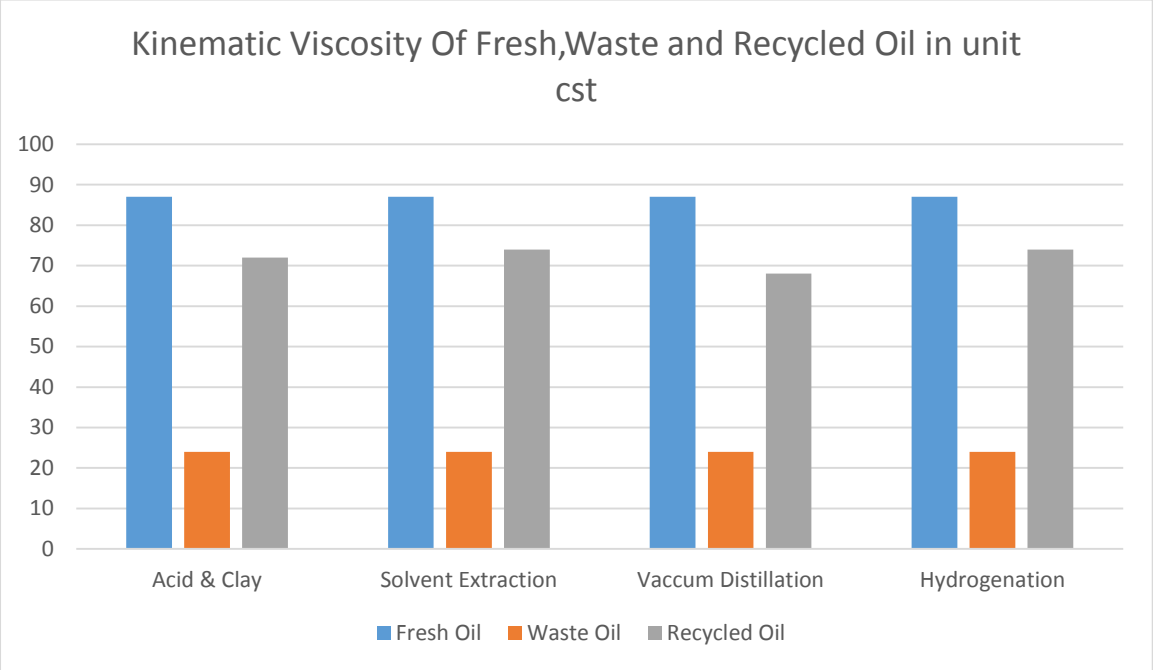

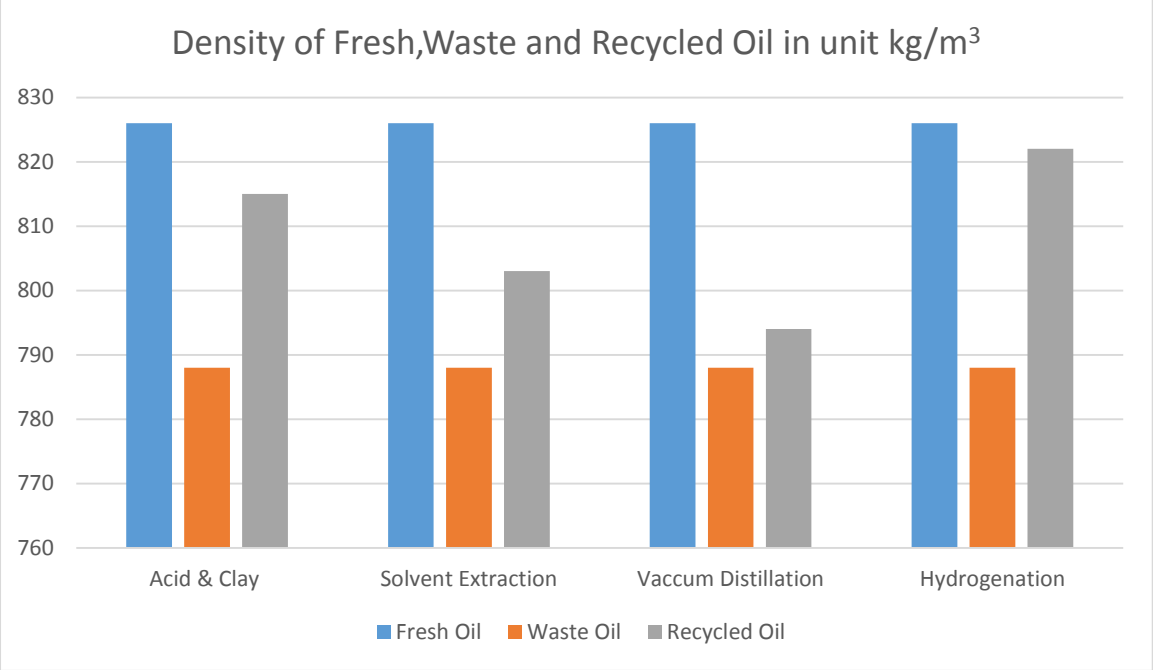

4. CONCLUSIONS

By using glacial acetic acid instead of sulfuric acid waste oil was cleaned very effectively. The product produced was comparable to that produced by conventional methods. The produced oil can be used in the vehicles as a lubricating agent. Structure of the oil is not lured at

allby the glacial acetic acid as shown by the experiments. Also glacial acetic acid does not affect the nature (environment) because it is organic in nature. The base oil recovery also turned out to be very good at 53.2%. Bricks can be made by mixing the sludge with cement.

ACKNOWLEDGEMENTS

I would like to express my heartiest gratitude to the Department of Chemical Engineering University of Engineering & Technology Peshawar. Without their continuous support it would not have been possible for me to complete the research.

5. REFERENCES

1. Akilimali, f. C. (2017). Feasibility study of recycling used lubricating oil. *A project work submitted to the department of petroleum engineering, the university of dodoma*.

2. Aljabiri, n. A. (2018). A comparative study of recycling used lubricating oils using various methods. *Journal of scientific and engineering research, 5*, 168–177.

3. Alves dos reis, m. (1991). Waste lubricating oil rerefining by extraction-flocculation. 3. A pilot plant study. *Industrial & engineering chemistry research, 30*, 2449–2456.

4. Anisuzzaman, s. M., jumaidi, m. H., & nasir, n. N. (2021). Used lubricating oil recovery process and treatment methods: a review. *Iop conference series: materials science and engineering*, *1195*, p. 012031.

5. Audibert, f. (2011). Waste engine oils: rerefining and energy recovery. Elsevier.

6. Kaithari, d. K., & al-riyami, p. K. (n.d.). Recycling of used lubricating engine oil by a solvent extraction process.

7. Mekonnen, h. A., & ababa, a. (2014). Recycling of used lubricating oil using acid-clay treatment process. *Addis ababa*.

8. Oladimeji, t. E., sonibare, j., omoleye, j., emetere, m., & elehinafe, f. B. (2018). A review on treatment methods of used lubricating oil. *International journal of civil engineering and technology, 9*, 506–514.

9. Olugboji, o. A. (n.d.). Use of spent engine oil olufemi ayodeji olugboji and oladeji akanni ogunwole.

10. Osman, d. I., attia, s. K., & taman, a. R. (2018). Recycling of used engine oil by different solvent. *Egyptian journal of petroleum, 27*, 221–225.

11. Pal, p., & nayak, j. (2017). Acetic acid production and purification: critical review towards process intensification. *Separation & purification reviews, 46*, 44–61.

Filtration of selected dyes using Ti_3AlC_2 based composite membrane

Hikmat ullah[1*], Mansoor Ul Hasan Shah[1], Waheed Ur Rehman[2], Mohammad Younas[1*]

[1] Department of Chemical Engineering, Faculty of Mechanical, Chemical and Industrial Engineering, University of Engineering and Technology, Peshawar, 25120, Pakistan

Email: * hikmatullah.che@uetpeshawar.edu.pk

Abstract

MXene is a new type of highly hydrophilic and negatively charged two-dimensional (2D) nanosheets material for the reasons especially its supernatant has good dispersibility and stability. The MXene supernatant containing several layers was treated as aqueous solvent for interfacial polymerization, consequently the prepared MXene nanocomposite membrane could maintain high perm selectivity even under low pressures required for low carbon footprint. MXene nanocomposite membrane had better hydrophilicity and higher negative charge. Na_2SO_4 rejection and the pure water flux was improved as compared with the pristine membrane. The MXene nanocomposite membrane also showed the better antifouling property and good stability [1].

Hydrophilic and negatively charged MXene supernatant had better dispersibility and stability. Substituting MXene supernatants of different concentrations for deionized water in aqueous phase, MXene nanocomposite membranes are generally prepared by interfacial polymerization. It was observed that few-layers Ti_3C_2Tx acted a crucial role in membrane surface modification, so that it improved the hydrophilicity and negative charge of membranes surface and increased surface roughness. Few-layers of MXene nanosheets with excellent hydrophilicity, negative charge and mechanical properties provided an academic basis for the preparation of low-carbon and durable NF membranes with outstanding performance [2].

Two-dimensional titanium carbides can be used to remove toxic dyes like acid blue and methylene blue, for their good adsorption contrast to other two-dimensional materials. In compared to typical adsorbents, the removal efficiencies of the use of MXene in methylene blue, methyl orange, methyl red, congo red, and Evans blue was unusually high [3].

Keywords: MXene, Nano filtration (NF) membranes, dyes,

1. INTRODUCTION

The dyes found in industrial wastewater are toxic in terrestrial life and are threats to clean water. The commonly used dyes are methylene blue, azo, aniline dyes etc. MXene are emerged as novel growing class of two-dimensional (2D) transition metal carbides or nitrides in the last decade due to their excellent morphological and capturing properties. These materials could be used in synthesis of composite membranes which can be applied for the removal of methylene blue and other dyes. Individually, Ti_3AlC_2 has defined the efficient removal and segregation of dyes and radionuclides in this research application. Firstly, MXene is prepared from MAX Phase by HF itching process. Phase inversion process will be adopted to synthesis the mixed matric composite membrane. Polyvinylidene fluoride (PVDF) will be used as membrane support. The synthesized MXene based composite membrane will first characterized through SEM, WCA. Later, the membrane sheets will be utilized to test the removal of selected dyes in a dead-end membrane filtration cell. By varying the different variables like dyes concentration, operating pressure, the pure water flux and species rejection will be measured. Stability tests will be carried out to check the long-term performance of MXene based membranes. The used membranes will be characterized and tested for antifouling and anti-aging analysis.

Clean water shortage is speedily emerging as a world crisis , threatening the future development of human society extracting clean water from wastewater , seawater and atmospheric water efficiently has become a wide challenge among the community researchers [4]. Water contamination is being hastened by human industrial activity, which is a worldwide problem. Water treatment technology which is both effective, Efficient and low-cost are urgently needed to express the problems. While, various methods have been photochemical degradation, photocatalysis, anaerobic digestion, reverse osmosis, and membrane filtering have all been created, of Membrane filtration is a cost-effective and energy-efficient method for removing a wide range of contaminants [5]. Over the previous five precipitation, membrane filtration, adsorption, solvent extraction, and photocatalytic degradation of pollutants are some of the physical, chemical, and biological procedures that have been

developed as countermeasures. Air and water pollution have increased dramatically as a result of increasing industrialization around the world, posing a severe threat to human health and biodiversity. Organic dyes and poisonous gases are examples of harmful contaminants that are commonly encountered [6]. There have been reports of research investigations on sulfonic group alteration utilizing a one-step approach. A compilation of numerous researches on Ti_3AlC_2 base composite membrane for dyes removing application. The monolayer mechanism of Ti_3AlC_2 base composite membrane interaction with dyes has been published and validated by Langmuir isotherm suitability [7]. According to recent research, the successful synthesis of different MXenes has concluded in a great potential for MXene-based membranes to be used in the sectors of organic solvent filtration and water purification technologies. In response to environmental and energy concerns, membrane separation has emerged as a viable alternative to classic liquid separation methods such as filtering,crystalisation,evaporation and distillation in recent decades [8]. Two-dimensional titanium carbides can be used to remove toxic dyes like acid blue and methylene blue, for their good adsorption contrast to other two-dimensional materials. In compared to typical adsorbents, the removal efficiencies of the use of MXene in methylene blue, methyl orange, methyl red, congo red, and Evans blue was unusually high We'll go through the latest developments in MXene-based membrane separation applications such water treatment, Nano fluidic ion transport, organic solvent purification, and osmotic energy conversion in great detail. Hydrophilicity, excellent flexibility, and a large number of surface groups, all of which are aligned with separation membranes, have an impact. MXene has gotten a lot of attention in the field of separation processes and has gotten a lot of positive feedback as a

consequence [9]. In fig.1 the structure of layers, MXenes specification and reaction of HF and shows particular the MXenes sheets.

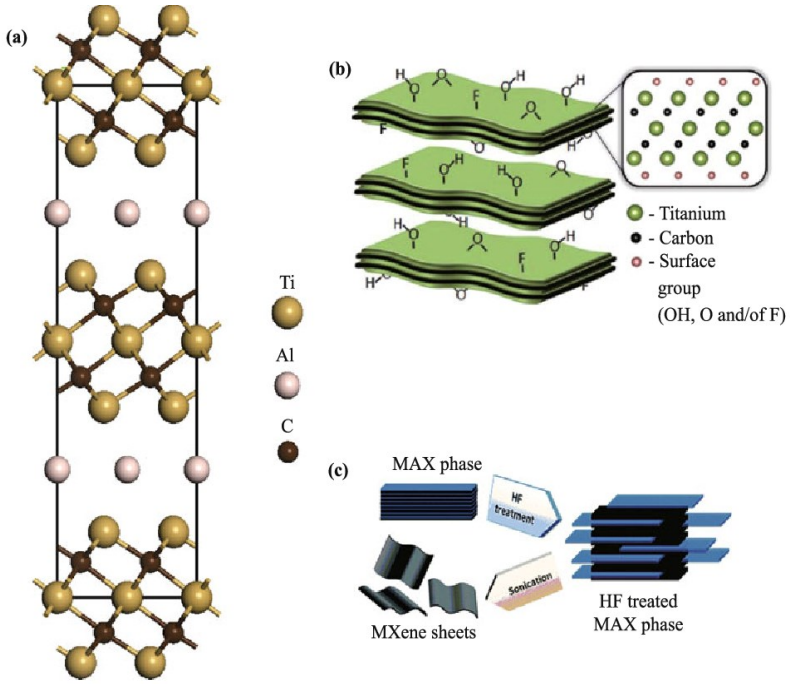

Fig. 1 (a) Ti_3AlC_2 layered Structure (b) Abandoned MXene. (c) Schematic demonstrating the creation of MXenes from MAX phases

2. Method

MXenes are a novel type of transition metal carbides, nitrides, and carbonitrides with two dimensions. having Mn+1XnTx (n = 1-3), where M signifies transition metal, X denotes Carbon or Nitrogen, and T specifies surface termination groups such as (-F), (= O), (-Cl), and (-OH), and *x* shows the number of surface functionalities. MXenes are commonly synthesized through selective etching of A-element layers from the precursor MAX ($M_{n+1}AX_n$) phase powder in HF solutions at ambient temperatures. M signifies an early transition metal, A any element from groups 12-16, X Carbon and/or Nitrogen, and n equals 1-3 in the phrase MAX.Titanium-based MXenes (such Ti_3AlC_2 and Ti_2AlC_2) are the most commonly employed in environmental applications, Adsorption of cationic dyes methylene blue (MB), gold, lead (Pb^{2+}), and chromium (Cr^{6+}), as well as intercalation of a diverse spectrum of cations (Na+, K^+, NH4+, Mg^{2+}, and Al^{3+}) between Ti_3AlC_2 layers

,From 2011 to 2019, researchers studied the manufacture of multilayered mxene flakes and nanomaterials, including via wet etching with HF, HCL-LIF, or HCL-NaF. There are three ways to make other nanomaterial-based membranes that comprise carbon nanotubes, graphene oxides, or metal-organic frameworks. (i) constructing a lamellar structure using mxene as a skeleton material (ii) different nanomaterial are add to fabricate mixed matrix membranes with mxenes (iii) mxene as a coating material to modify a membrane support Layer. The use of MXene membranes for dye removal from polluted water caused by industrial dye discharge has sparked global concern. Apart from other pollutants dyes are the most difficult pollutants to treat owing consisting of molecules and great chemical resistance, in natural water the diffusion dyes can be find while linked to aromatic molecule find cancer diseases, causes changes in the marine ecology by preventing sunlight from penetrating. MXene membrane can easily solve the treat of polluted dyes wastewater. In recent years, an elegant exfoliation procedure has been employed to create MXene, a new family of 2D transition metal carbides and nitrides produced from layered MAX phase. Contrast to traditional adsorbents, studies on Ti_3AlC_2 base composite membrane application to avoid hazardous dyes in water are utilizing particularly promising. MXenes distinctive features emerge laterally, leading to suggestions for development applications. MXene was built on a standard suction filter which could be charged the different concentration of methylene blue solution for dyes removal. Ti_3AlC_2 recognized to be one of the most effective technologies that can be implemented to treat industrial wastewater the type and nature of adsorbing materials influence efficiency of separation process. However, regeneration of Ti_3AlC_2 requires expensive and environmentally unfriendly methodologies because It is cheap, effective, easy to operate, and produces high-quality effluent, thus it is widely utilized Additionally, it is a versatile technology, that have been developed to capture organic and inorganic pollutants Such as incineration, or washing with solvents. In methodology for dyes removal application initially selecting etching from MAX phase after eteching process need to be exfoliate to ready the process to delimitation further more vacuum filtration is required to pass the liquid from MXene membrane , characterization and treatment of dyes from the relevant solution is best attempt for optimization of maximum dyes

removing Dye water flux and pure water flux both comprises with water flux, as well as dye removal, where F is the flow of water V/S*T*P = F where V is the volume (L) of the decontaminated dye solution, S is membrane area of effective , which is fixed at 13.84104 m^2, and T and P are Filtration time and pressure particular , which are both fixed at 1.0 bar for first time. we have taken 10 mg/l feed concentration while in dye water flux we have flux 16.69 liter /meter hour about dye removal percentage 98.56 in 10 ml volume will check each volume in 1& 2 different pressures and 30, 60, 80 and 720 seconds particularly and considerably check the fresh, fouled and clean membrane properties particular to comprehend how our membrane can be economically for industries.

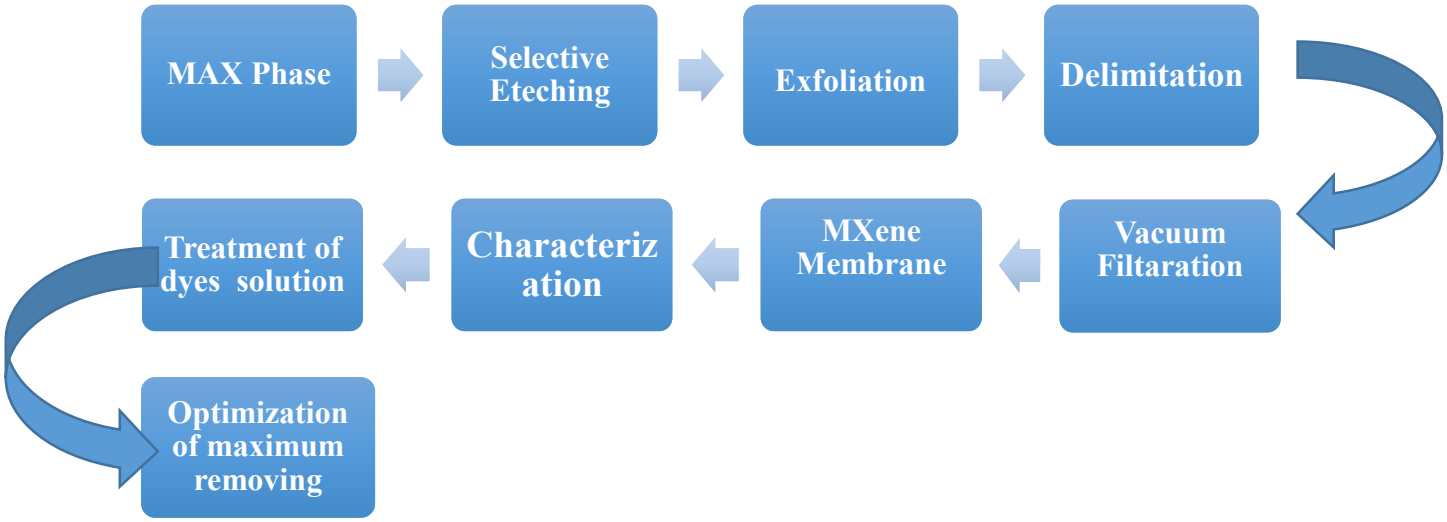

Fig. 2: Application for dyes removal

3. Results

Materials and methods

1. Materials

MAX Phase (Ti3AlC2) were purchased from the LUOYANG TONGRUN INFO TECHNOLOGY CO., LTD, China the MXenes have purity 99.5 % and mesh size -325. The amount of 100g were imported. And methylene blue and other dyes were purchased from haq chemical Peshawar kpk Pakistan All other chemicals were used without any

further purification. Deionized water was used for the preparation of all the required solution

2. Preparation of $Ti_3C_2T_x$ based composite membrane

Take 100 mg of $Ti_3C_2T_x$ MXene powder and Prepare a solution of 100 mg of TMAOH in 10 mL of deionized water in a 20-mL glass vial for Mix the $Ti_3C_2T_x$ MXene powder with TMAOH solution to Stir the mixture for 12 hours at room temperature furthermore The mixture is alkaline having pH ~10 should Wash the alkaline mixture twice via centrifugation for 5 minutes at 3500 rpm in a 50-mL tube while The pH of supernatant liquid should drop to ~7 in addition Collect the stable MXene colloidal solution after 1 hour of centrifugation at 3500 rpm so Collect the intercalated/delaminated $Ti_3C_2T_x$ MXene sediments via vacuum assisted filtration in the same way Dry the intercalated/delaminated $Ti_3C_2T_x$ MXene in a vacuum oven at 120 ^oC for 24 hours

3. Characterization of the adsorbents

The $Ti_3C_2T_x$ based composite membrane MXenes were characterized by FTIR, XPS, N2 adsorption-desorption isotherms, PXRD, SEM, EDX, HR-TEM, and TGA

4. Characterization of the filtration properties of the membrane

The membrane was cut into a wafer with appropriate size and put into a mold, then, a certain amount of the dye solution was pressed into the filterable mold with an injector and passed through the membrane.

4.1. Dead-End Filtration

The separation performance of the fabricated membranes was first assessed using a dead-end (DE) filtration setup with an effective filtration area of 9.60 cm 2. Unless stated otherwise, the filtration tests were conducted at a pressure of 1 bar and were stirred at 800 rpm and performed in duplicates.

The weight of the permeate after 1 h of filtration time was measured and the water flux (J_F) of the fabricated membrane was calculated using Equation (1): jw=v/atp

where V denotes the quantity (volume/mass) of permeation (L), A indicates the effective surface area (m 2), P is the applied pressure in bar, and t denotes the time in hours of the

prepared membranes.

A feed solution stream comprising 100 mg L−1 MG, and 150 mg L−1 BSA was utilized

to calculate the membrane rejection.
The rejection (R) equation (Equation (2)) for solutes was calculated as follows:
R(%)=CF-CP/CF*100 (2)
where C□ and C□ denote the concentration of the feed and permeate solutes in mg/L, respectively. The effective pore diameter (a) of the prepared hybrid NF membranes was measured via the Ferry equation (Equation (3)), as shown below [27], using DE filtration:
R=100[1-(1-r/a)^2]^2 (3)
R indicates the solute rejection (%) and r refers to the diameter of the solute. The MWCO of the fabricated membrane is the molar mass of the solutes which are 90% rejected by the membrane. Plotting the rejection (%) of the solutes against their corresponding molar mass in daltons the MWCO to be calculated

4. CONCLUSIONS

Environmental pollution has permanently been community panic, dyes polluted wastewater that creates from anthropogenic actions in several areas, for example agricultural activities, industries, domestic manure and others, has continuously been a hazard to human health and environment. however, dyes such as methylene blue, orange, acid, green and sunset yellow dyes etc., are usually present in trace quantities, they are considered as the greatest poisonous and extensive components in wastewater effluents. The goal of this research is to create a low-cost membrane based on MXenes that can easily and successfully remove dyes from wastewater The predictable dye removal from the waste water by the development of a low-cost MXenes-based membrane is greater than 90%.

5. REFERENCES

[1] Kwon O, Choi Y, Kang J, Kim JH, Choi E, Woo YC, et al. A comprehensive review of MXene-based water-treatment membranes and technologies: Recent progress and perspectives. Desalination 2022;522:115448. https://doi.org/10.1016/j.desal.2021.115448.

[2] Karahan HE, Goh K, Zhang C (John), Yang E, Yıldırım C, Chuah CY, et al. MXene Materials for Designing Advanced Separation Membranes. Adv Mater 2020; 32:1906697. https://doi.org/10.1002/adma.201906697.

[3] Snapshot n.d.

[4] A comprehensive review of MXene-based water-treatment membranes and technologies: Recent progress and perspectives - ScienceDirect n.d. https://www.sciencedirect.com/science/article/abs/pii/S0011916421005191#! (accessed January 5, 2022).

[5] A comprehensive review of MXene-based water-treatment membranes and technologies: Recent progress and perspectives - ScienceDirect n.d.

[6] Kwon O, Choi Y, Kang J, Kim JH, Choi E, Woo YC, et al. A comprehensive review of MXene-based water-treatment membranes and technologies: Recent progress and perspectives. Desalination 2022;522:115448. https://doi.org/10.1016/j.desal.2021.115448.

[7] Water Pollution Facts, Types, Causes and Effects of Water Pollution | NRDC n.d. https://www.nrdc.org/stories/water-pollution-everything-you-need-know (accessed January 5, 2022).

[8] Water Pollution Facts, Types, Causes and Effects of Water Pollution | NRDC n.d.

[9] Water Pollution Facts, Types, Causes and Effects of Water Pollution | NRDC n.d. https://www.nrdc.org/stories/water-pollution-everything-you-need-know (accessed January 5, 2022)

Heavy metals accumulation in soil via wastewater irrigation: analysis and possible solution

[1*] Muhammad Qasim Gul. [2] Nehar ullah.
[1*]chemicalengrss@gmail.com,
[1, 2] UET Peshawar, Pakistan

Abstract

Unplanned industrial urbanization adversely affects society and human health. Effluents from widespread industrial sectors containing harmful substances like heavy metals, whose discharge directly affecting human health via food chains. Heavy metal contamination in industrial untreated effluent water transfer to food chain via irrigation of agricultural soil. Rapid and unorganized urban and industrial developments have contributed to the elevated level of heavy metals in the urban environment of the developing countries (1; 2).

The current research work investigates the identification, characterization, and evaluation of specific heavy metals in industrial wastewater (IWW) collected from selected agricultural field irrigating canals of IWW in Haripur Hattar (Pakistan) and an economical purification technique for the IWW has been suggested. Obtained results were compared with the tube well water irrigated samples (3). Heavy metals accumulation was tested through atomic absorption spectrometry (AAS). Analysis of water samples showed that the concentration in mg l^{-1} of heavy metals in Industrial wastewater follows the trend Fe (4.25)> Pb (2.98)> Zn (0.20)> Ni (0.155)> Cr (0.068)> Cu (0.01) while Tube well water has Fe (1.70)> Zn (0.09)> Cr (0.085)> Ni (0.068)> Pb (0.029)> Cu

(0.009). Analysis of the soil samples irrigated with IWW followed the order of Fe (67.85)> Cu (12.99)> Pb (9.56)> Zn (8.95)> Ni (3.54)> Cr (1.736) and Fe (40.37)> Zn (0.712)> Pb (0.529)> Cr (0.323)> Cu (0.15)> Ni (0.068) irrigated with TWW.

Heavy metals concentration values found in soil irrigated with IWW were higher than the soil irrigated with TWW which are higher than the normal allowable WHO limits. For the purification of IWW, Carboxymethyl Guar (CMG) and Hydroxypropyl Guar (HPG), derivatives of guar gum, innovative coagulants used for the separation of heavy metals at large scale efficiently and economically (4). Experiments showed significant reduction in the metals contents of IWW after processing with coagulants. It was observed that guar gum could achieve 60% removal, at an initial Pb concentration of up to 3 mg L^{-1}. The current study suggests the continuous monitoring of soil, irrigation water and agricultural products to prevent heavy metals concentration beyond allowable limits, in the food chain.

Keywords: CMG: Carboxymethyl Guar, HPG: Hydroxypropyl Guar IWW: Industrial waste water

1. INTRODUCTION

Clean water is essential for life on earth and every living specie need water. Apart from direct needs, there is a huge indirect requirement of clean water for irrigation, food and other product manufacturing, domestic and industrial uses etc. Hygienic production of plants, food chain products and other direct life consumable items require clean water like irrigation, farming etc. (6). Due to scarcity of fresh water in developing countries and availability of large scale untreated effluent waste water from unplanned industrialization, people are using toxic wastewater effluent streams for irrigation and farming purposes.

Industries are the backbone of any country development measures. But increase in population made the urban areas more congested and reduction in fresh and clean ecosystem. Production and sales competition in developing countries caused the industrial urbanization causing no consideration of sustainable development (2). Due to which industrial effluents are directly affecting human health via food chains. These toxic pollutants gradually accumulate in agricultural soil with in turn becomes a part of food chain. Increasing level of toxic contents especially in crops due to contaminated soil possess serious health issues for the consumers. The most common heavy metals found in industrial wastewater (IWW) include arsenic (As), cadmium (Cd), chromium (Cr), copper (Cu), zinc (Zn), nickel (Ni), manganese (Mn), lead (Pb), and iron (Fe) (2). A very small amount of heavy metals such as cobalt (Co), Cu, Fe, Mn, molybdenum (Mo), vanadium (Vd), and Zn are required to run various biochemical and physiological functions for good health (3). These heavy metals and contaminants originate from industries, municipal waste, and natural disasters.

IWW contains a large proportion of toxic metals which is continuously being discharged to irrigating canals and streams ends up in the irrigated soil. Increased discharge of wastewater containing heavy metals in large quantities from industries is a matter of great concern for the survival of the ecosystem (8). Industrial applications such as Pharmaceutical, smelting, pottery, paints, battery processing, arms manufacturing, and car industries are pouring various hazardous heavy metals into the system especially Pb that is much higher in all targeted areas and has hazardous effects (2). Discharge of the untreated industrial effluents continuously increasing with the rapid and unplanned industrialization in developing countries. A large portion of the waste is dumped and discharged into nearby rivers and canals, which acts as a sink for the waste disposal of these industries. The heavy metals are continuously accumulating into the soil and being utilized for cultivation (5).

Several possible solutions are proposed for the reduction and removal of heavy metals from IWW streams. But in under developed countries like Pakistan due to the absence of Law enforcement processes, no industrialist is ready to follow un-economical separation techniques.

Guar gum is the powdered endosperm of the seeds of the *Cyanosis tetragonolobus* which is a leguminous crop (4). It contains a complex polysaccharide called galactomannan, due to its thickening, emulsifying, binding and gelling properties, quick solubility in cold water, wide pH stability, film forming ability and biodegradability, it finds

applications in large number of industries. It is a long chain polysaccharide used to remove Pb^{2+} from wastewater (9). The requirement of ultra-low amount of biopolymer in the range of 1.25 mg L^{-1} to treat the relatively high volume of waste water provides an additional financial advantage (1). So, that's why highly efficient and most economical coagulants, derivatives of Guar Gum, Carboxymethyl guar (CMG) and Hydroxypropyl guar (HPG) are suggested in this study for the reduction of HMs from IWW streams of Hattar Industrial State after successful experiments.

2. METHODOLOGY

To determine the concentration of heavy metals in contaminated water and soil, how it exceeds the permissible limit, the use of a filtration process to remove heavy metal impurities in industrial wastewater. Scientists around the world are working to save water. Therefore, one of the ways is to reuse industrial and municipal wastewater and re-use it for agriculture and other purposes. Water scarcity in some parts of the world is alarming (5).

2.1 Sample collection

Industrial waste water (IWW) and Tube Well water (TWW) samples collected in dried, clean bottles and airtight plastic bags used for soil samples collection for the analysis of toxic heavy metals (6).

Samples collected from the points where local farmers are using effluent streams directly for irrigation purposes. Soil samples were collected from selected agricultural fields with the guidance and support of local farmers. The samples were taken from canals fed by industries and are termed as IWW. Similarly, the sample of water is taken from the tube well of the study area that feeds the control sample soil and is termed as tube-well wastewater (TWW). Two different agricultural fields in the same study were chosen for the cultivation of similar agricultural produces grown with IWW fed canals and TWW, respectively (9).

2.2 Sample preparation

Water samples (50ml) taken in beaker cleaned twice with boiled water. 10ml Concentrated HNO3 added to water sample beaker and heat it up till that total solution remains 40ml. Filter the solution using whatman No.42 filter paper. Filtrate diluted by adding 10ml of distill water to it (9).

Soil samples were prepared for HM analysis in AAS after digesting in mixture of 33% HCL (Hydrochloric acid), 63% HNO3 (Nitric acid), and perchloric acid. In all experiments, deionized water was used for sample preparation.

Each sample of soil was scrubbed with distilled water to remove stones and unwanted particles. The soil samples were dried in the oven to remove the water. Aqua regia of HNO3 and HCl (1:3) were prepared in the round bottom flask. 2 g of each sample was mixed with 10 mL of aqua regia solution. Then, the samples were heated in an oven at 90˚C for 20–25 min. After cooling, the samples were filtered using Whatman 42 filter paper. The filtrate was diluted with distilled water using a volumetric flask to fill up to the 25ml volume for analysis purposes.

2.3 Spectrometric analysis

Atomic absorption spectrophotometer was used for the determination of heavy metals. After necessary set up and standardization procedures, the samples were placed and sequentially tested into the atomic absorption spectrophotometer (8). Also, after every five samples reading, standards were run to make sure that the machine is working accurately. All the readings were taken in triplicate.

2.4 Determination of heavy metals

All tests were accomplished at the CRL Laboratory, university of Peshawar. Prepared samples of industrial wastewater and soil were detected with the help of the Atomic Absorption Spectrophotometer (Perkin Elmer AAS-700) at the Centralized Resource Laboratory, Peshawar University for heavy metal analysis (8).

2.5 Waste water treatment

The adsorption process is widely used for the removal of heavy metals from wastewater because of its low cost, availability and eco-friendly nature (10). Both commercial adsorbents and bio adsorbents are used for the removal of heavy metals from wastewater, with high removal capacity. Guar gum derivatives (Carboxymethyl Guar, Hydroxypropyl Guar) used to adsorb heavy metal from the waste water stream (7). Due to its thickening, emulsifying, binding and gelling properties, quick solubility in cold water, wide pH stability, film forming ability it can be used as an adsorbent in the adsorption process.

A. Carboxymethyl Guar (CMG) as Coagulant

Very low quantity of CMG is required for adsorption HM from large amount of wastewater. 0.1% of the volume of water, Carboxymethyl Guar (0.10DS) is required for adsorption of HMs.

Add 10g of CMG powder in 10L of waste water in a clean food grade tank. Disperse the powder in the water using stirrer for 5min, then allow to swell the coagulant for 30min. After, add borax (0.2% of the total mass of the water), dissolve. Borax helps create giant coagulant molecule for easy settle down. Clean water sample collect from top for AAS analysis and heavy metals adsorbed CMG from bottom of the tank (1).

B. Hydroxypropyl Guar (HPG) as Coagulant

Same procedure repeated as for CMG, and after that clean water sample taken for the comparative analysis of CMG and HPG separation efficiency for heavy metals. Results presented in the Table (1.3).

3. RESULTS AND DISCUSSION

Water samples collected from exit streams of Volta Batteries, ICI Pharma and BAIFO industries Hattar were analyzed in AAS for determination of Heavy metals. Results compared with Tube well water sample and WHO allowable limits for clean water. The order of heavy metals concentration in IWW follows as Fe (4.25)> Pb (2.98)> Zn (0.20)> Ni (0.155)> Cr (0.068)> Cu (0.01) as shown in Table 1.1. IWW contains Pb (2.98mg/L)>TWW Pb (0.05mg/l) > WHO allowable limit Pb (0.01mg/L). The concentrations of Pb and Fe found higher than the standards of W.H.O, and Zn and Cu less compare to allowable limits (Table 1.1).

When these IWW streams are used for irrigation of soil, soil work as HM absorbent media which in turn effects the food chain directly. Soil samples irrigated with IWW found much higher concentration of Pb (170 mg/kg), Fe (928 mg/kg) and Zn (213mg/kg) specifically compare to the soil irrigated with clean tube well water having Pb (16.94mg/kg), Fe (150mg/kg) and Zn (21.63mg/kg).

The comparative analysis of waste water and tube well water given in the Table 1.1, soil irrigated both with waste water and tube well water is given in Table 1.2.

Table 14.1 Heavy metals in IWW, TWW and their comparison with WHO standards

Water Samples	Pb (mg/l)	Fe (mg/l)	Cu (mg/l)	Cr (mg/l)	Zn (mg/l)	Ni (mg/l)
W1	2.288±0.026	5.503±0.51	3±0.21	0.104±0.019	0.009±0.015	0.67±0.034
W2	3.331±0.091	4.98±0.06	0.068±0.05	0.155±0.08	0.1±0.075	0.71±0.005
W3	3.995±0.035	4.18±0.030	0±0.02	0.121±0.17	0.05±0.024	0±0.01
W4	1.148±0.17	3.21±0.044	0.05±0.01	0.229±0.047	0±0.056	0.098±0.02
W5	3.973±0.005	3.12±0.031	2.03±0.19	1.106±0.029	1.099±0.094	0±0.05
W6	3.983±0.025	5.25±0.025	1.015±0.021	0.068±0.04	0.22±0.042	0.155±0.03
TWW	0.19±0.090	1.33±0.05	1.61±0.051	0.129±0.024	0±0.01	0.057±0.09
W.H.O	0.05	0.3	1.5	0.05	5	0.1

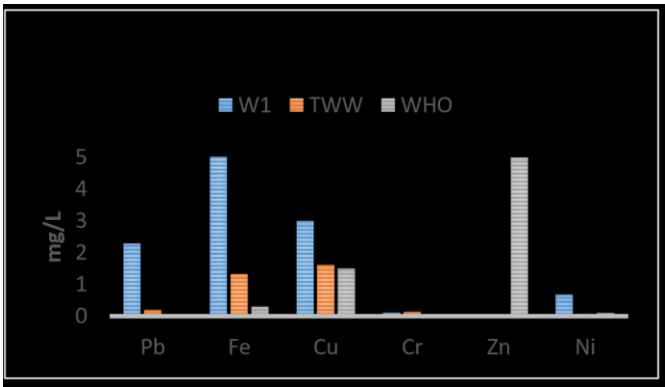

Figure 1.1 Comparison for waste water sample (50meter)

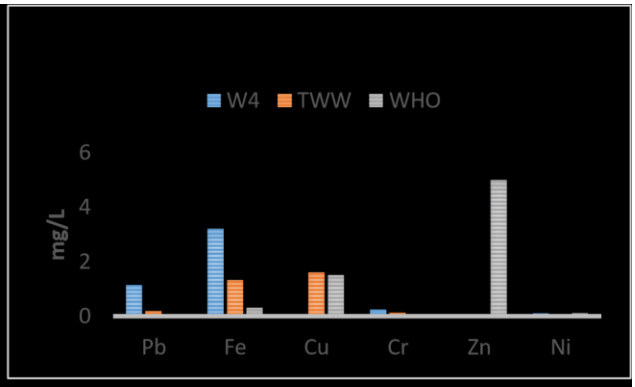

Figure 1.2 Comparison for waste water sample (400meter)

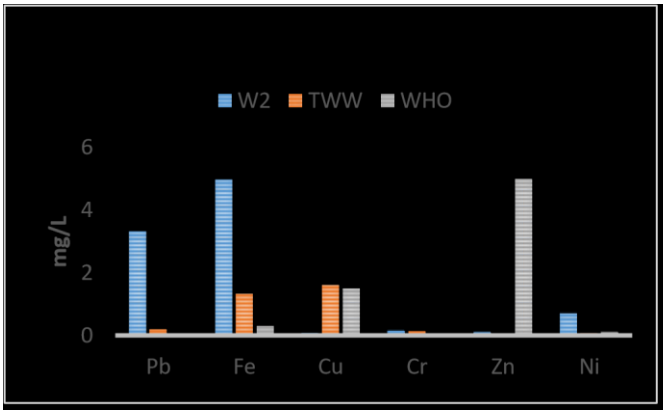

Figure 1.3 Comparison for waste water sample (200meter)

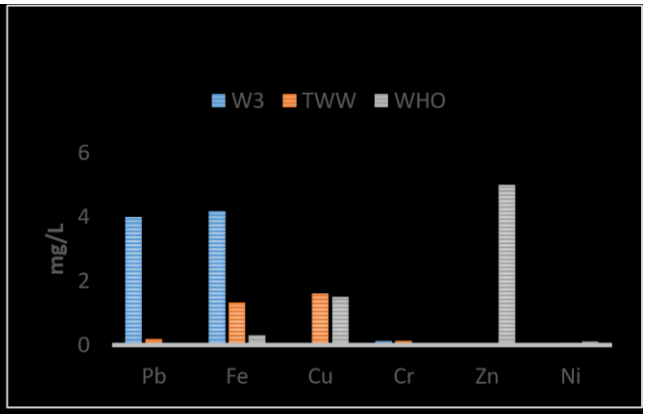

Figure 1.4 Comparison for waste water sample (200meter)

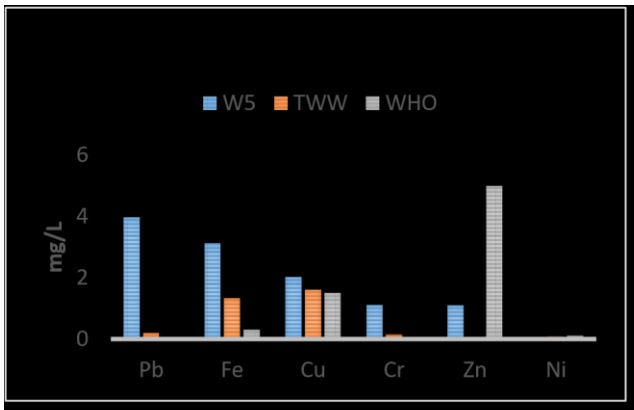

Figure 1.5 Comparison for waste water sample (200meter)

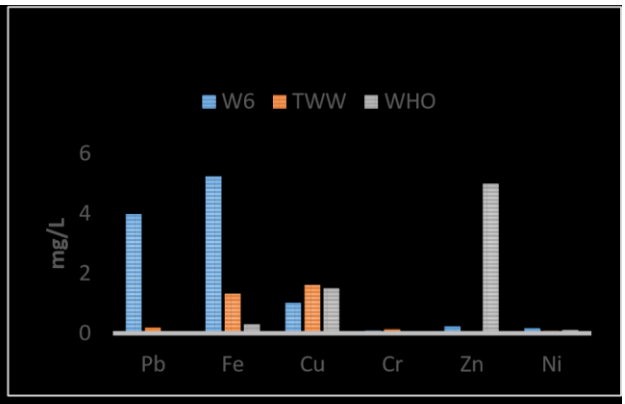

Figure 1.6 Comparison for waste water sample (200meter)

From all these comparative charts for HM in IWW, we observed that there is significant reduction in toxic contents as we go away from the source (4). At distance of 50m, highest amount of metals present while when we reach 500m away, there is more the 60% reduction the HM contents.

Table 1.15 Heavy metals concentraion in soil samples

Soil Sample	Pb (mg/kg)	Fe (mg/kg)	Cu (mg/kg)	Cr (mg/kg)	Zn (mg/kg)	Ni (mg/kg)
S1 (50m)	170	928.13	33.91	25.58	213.5	10.64
S2 (50m)	119.59	894	162.38	21.7	0	44.25
S1 (200m)	72.81	885.5	23.04	16.79	106.76	18.91
S2 (200m)	54.38	847	14.85	18.29	91.61	17.95
S1 (400m)	31.61	504.63	1.88	4.04	8.9	0.85
S2 (400m)	15.68	847	11.54	15.61	55.66	14.91
S3 (500m)	25	706.75	24.76	16.21	93.11	21.163
TWW Irrigated	16.94	150	2.875	0	21.63	1.375
W.H.O	85.00	300	36	100.00	50.00	35

Maximum samples tested were found to be high in comparison with permissible limits for an agricultural area. However, as we go away from the emitting source, because to the decrease in waste water stream contents, there is also a significant reduction in soil

heavy metal contents (9). Thus, it suggests that the soil of targeted area is severely contaminated with the studied metals and may also with the other ones.

As the tested soil samples were compared with both, the tube well irrigated soil samples and W.H.O, it is found TWW irrigated sites are much more cleaner and within the very safe limits for agricultural use (2).

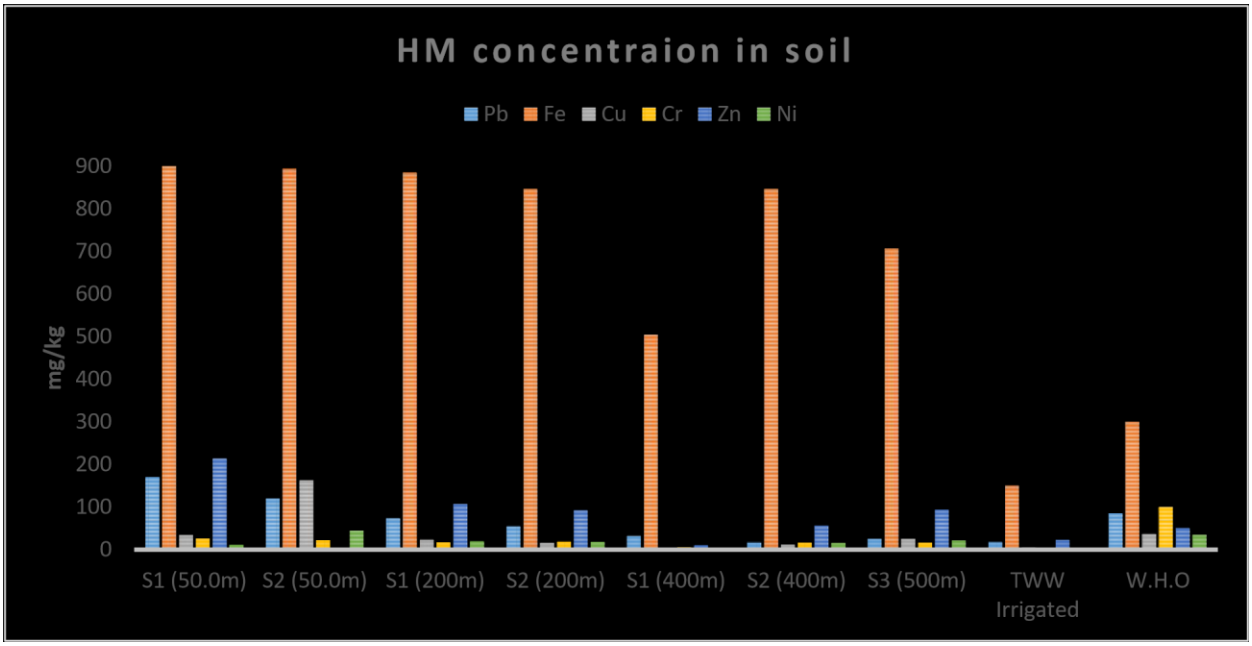

Figure 2 Heavy metals content in soil samples irrigated with IWW and TWW vs W.H.O Limits

Due to the discharge of huge streams of waste water from several industries in Hattar on daily basis, it's highly necessary to regularize their discharge stream (10). Processing waste water before discharge is costly process. However, adsorption process can widely be used due to its economic, eco-friendly and efficient reduction of HM in IWW. Bio-sorbent, Hydroxy Propyl Guar used in our experiment for the removal of HM from Waste water sample, shown up to 65% removal for the toxic contents like Pb, as show in the table 1.3. While using Carboxy Methyl Guar has given up the results up to 50% reduction in heavy metal contents (Table1.3).

Table 1.3 Heavy metals in water comparison after adsorption treatment with HPG and CMG

WATER SAMPLES	COMPARISON AFTER WATER TREATMENT WITH HPG					
	Pb	Fe	Cu	Cr	Zn	Ni
W1 (MG/L)	2.288	5.503	3.02	0.104	0.009	0.67
W-HPG (MG/L)	0.801	1.926	1.057	0.0364	0.0032	0.235
WATER SAMPLES	Comparison after Water treatment with CMG					
	Pb	Fe	Cu	Cr	Zn	Ni
W1 (MG/L)	2.288	5.503	3.02	0.104	0.009	0.67
W-CMG (MG/L)	1.18	3.082	1.691	0.058	0.005	0.375

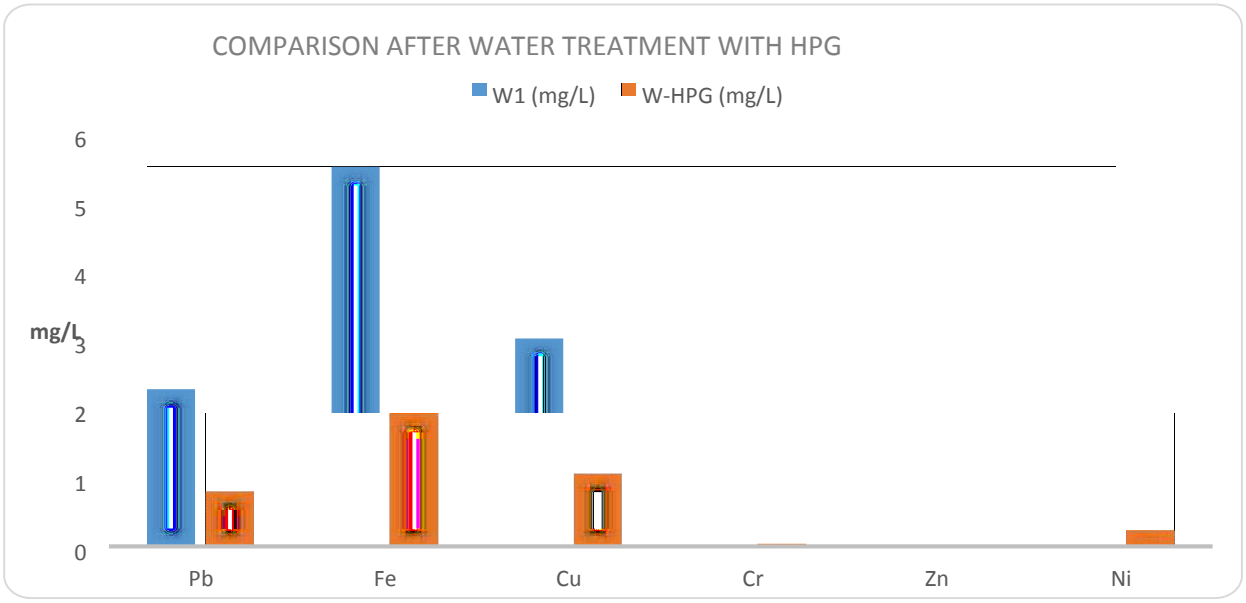

Figure 3 Comparison between treated water with HPG and waste water sample

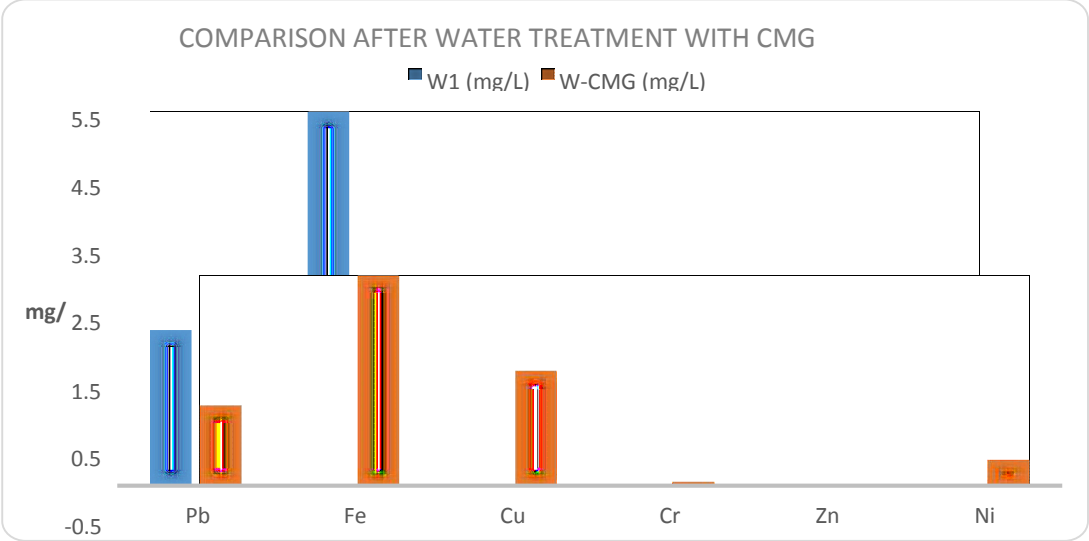

Figure 4 Comparison between treated water with CMG and waste water sample

4. CONCLUSION

From all results it is concluded that Fe and Pb are very much higher than the permissible standards for irrigating streams and also for agricultural soil. It is becoming necessary for the related authorities to plan out serious solution for the area. It doesn't matter that how low level of a toxic metal is present in the effected soil or grown crop, it totally undesirable. Therefore, regular scrutiny is required for the industries discharging unprocessed stream into open canals. Consequently, this study encourages environmentalists, administrators, and public health workers to create public awareness to avoid the consumption of vegetables grown in contaminated soils, hence reducing health risks.

5. REFERENCES

1. Market basket survey for some heavy metals in Egyptian fruits and vegetables. **Radwan, M.A., Salama, A.K.** 2006, food and chemical toxicology, pp. 1273-1278.

2. Flocculation properties of polyacrylamide guar gum (CMG-g-PAM) synthesized by conventional and microwave assisted method. **Sagar Pal, G Udayabhanu.** s.l.: Journal of Hazardous materials, 2011, Vols. pp.1580-1588.

3. Effect of waste water irrigation on vegetables in relation to bioaccumulation of heavy metals and biochemical changes. **S. Gupta, S. Satpai, S. Nayek, D.Garai.** 2010, Springer, Environ Monit Assess, pp. 165 :(169-177).

4. Human health risk assessment of heavy metals via consumption of contaminated vegetables collected from different irrigation sources in Lahore, Pakistan. **Adeel Mahmood, Riffat Naseem Malik.** 2014, Arabian Journal of Chemistry, pp. 7, (91-99).

5. Assessing risk of heavy metals from consuming food grown on sewage irrigated soils and food chain transfer. **Chary, N.S., Kamala, C.T., Raj, D.S.S.,** 2008, Ecotoxicol. Environ. Safety, pp. 69(513-524).

6. Treatment of Explosive Industrial Pollutants: A Comparative Analysis. **Uzaira Rafique, Saima Nasreen, Faiza Hussain.** 2014, International Journal of chemical and environmental engineering, WARP, pp. Volume 5, No.3.

7. Application of guar gum for the removal of dissolved lead from wastewater. **Soumyadeep, Mukhopadhyay Muhammad Zakwan Bin Zafri, Xinmin ZhanaMoh.** s.l.: Industrial Crops and Products, 2017, Vols. 111, pp.261-269.

8. Assessment of some heavy metals in vegetables, cereals and fruits in Saudi Arabian markets. **Al-Qahtani, Mohamed H.H & Khairia M.** 2012, Egyptian Journal of Aquatic Research, pp. 31-37.

9. Atomic Absorption Spectroscopic Determination of Heavy Metal Concentrations in Kulufo River, Arbaminch, Gamo Gofa, Ethiopia. **HK, Tsade.** s.l.: Journal of Environmental Analytical, 2016, Vols. Environ Anal Chem 2016, 3:1.

10. Heavy metals in agricultural soils of the European Union with implications for food safety. **G. Tóth a, T. Hermannb, M.R. Da Silva c, L. Montanarella.** 2016, Environment International, ELEVIER, pp. 88, (299-309).

11. Water purification using different waste fruit cortexes for the removal of heavy metals. **Al-Qahtani, Khairia M.** 2016, Journal of Taibah University for Science, pp. 10 (700–708).

12. Accumulation of heavy metals in edible parts of vegetables irrigated with waste water and their daily intake to adults and children, district Mardan, Pakistan. **Noor-ul-amin, Anwar Hussain, Sidra Alamzeb, Shumaila Begum.** 2012, ELSEVIER, pp. 1515-1523.

13. **https://www.researchgate.net/publication/345038819_Application_of_guar_gum_for_the_removal_o f_dissolved_lead_from_wastewater.**

14. Dietary intake of pollutant aerosols via vegetables influenced by atmospheric deposition and wastewater irrigation. **Pandey, R., Shubhashish, K., Pandey, J.,** 2012, Ecotoxicology and Environmental Safety, ELSEVIER, pp. 200-208.

15. The effect of long-term irrigation using wastewater on heavy metal contents of soils under vegetables in Harare, Zimbabwe. **F. Mapandaa, E.N. Mangwayanaa, J. Nyamangaraa, K.E. Giller.** 2005, Agriculture, Ecosystems and Environment, ELSEVIER, pp. 107, (151-165).

16. Water purification using different waste fruit cortexes for the removal of heavy metals. **M.Al-Qahtani, khairia.** 2016, Journal of Taibah University for Science, pp. 700-708.